U.S.NRC
United States Nuclear Regulatory Commission
*Protecting People and the Environment*

**Technical Letter Report**

**TLR-RES/DE/REB-2021-09**

# *Probabilistic Leak-Before-Break Evaluation of Westinghouse Four-Loop Pressurized-Water Reactor Primary Coolant Loop Piping using the Extremely Low Probability of Rupture Code*

Date:

August 13, 2021

Prepared in response to Task 3 of User Need Request NRR-2014-004, by:


*C. J. Sallaberry*
Engineering Mechanics Corporation of Columbus

*R. Kurth*
Engineering Mechanics Corporation of Columbus

*E. Kurth-Twombly*
Engineering Mechanics Corporation of Columbus

*F. W. Brust*
Engineering Mechanics Corporation of Columbus


NRC Project Manager:


*Matthew Homiack*
Materials Engineer
Reactor Engineering Branch

**Division of Engineering**
**Office of Nuclear Regulatory Research**
**U.S. Nuclear Regulatory Commission**
**Washington, DC 20555–0001**

**DISCLAIMER**

# EXECUTIVE SUMMARY

This report presents the results of a study using the Extremely Low Probability of Rupture (xLPR) Version 2 probabilistic fracture mechanics code to analyze a representative primary coolant loop piping system in a Westinghouse four-loop pressurized-water reactor (PWR). The objective of the study was to assess whether such systems exhibit an extremely low probability of rupture consistent with the requirements of Title 10 of the *Code of Federal Regulations*, Part 50, Appendix A, General Design Criterion (GDC) 4, when subject to the effects of primary water stress-corrosion cracking (PWSCC). GDC 4 states the following:

> Structures, systems, and components important to safety shall be designed to accommodate the effects of and to be compatible with the environmental conditions associated with normal operation, maintenance, testing, and postulated accidents, including loss-of-coolant accidents. These structures, systems, and components shall be appropriately protected against dynamic effects, including the effects of missiles, pipe whipping, and discharging fluids, that may result from equipment failures and from events and conditions outside the nuclear power unit. However, dynamic effects associated with postulated pipe ruptures in nuclear power units may be excluded from the design basis when analyses reviewed and approved by the Commission demonstrate that the probability of fluid system piping rupture is extremely low under conditions consistent with the design basis for the piping.

Under this regulation, many PWR licensees eliminated the use of certain equipment, such as pipe whip restraints and jet impingement barriers, that was designed to protect against the failure of piping systems based on the U.S. Nuclear Regulatory Commission (NRC) staff's approval of the licensees' deterministic leak-before-break (LBB) analyses. These analyses were used to demonstrate that the primary coolant loop piping had an extremely low probability of rupture, and thus, the protective equipment was no longer necessary. Following its guidance, such as in Standard Review Plan Section 3.6.3, the NRC staff approved the licensees' LBB analyses because, at the time, the PWR primary coolant loop piping systems were not known to be subject to any active degradation mechanisms that can be potential sources of piping rupture. Later, however, the degradation mechanism PWSCC was discovered to be active in certain nickel-based dissimilar metal welds in the primary coolant loop piping of PWRs. Since PWSCC had not been addressed in the original LBB analyses, a regulatory question remained as to whether the primary coolant loop piping systems with PWSCC in PWRs continue to demonstrate an extremely low probability of rupture consistent with the requirements of GDC 4, especially when considering the latest inservice inspection requirements and industry PWSCC management strategies.

The study had two focus areas: (1) use the xLPR code to generate numerical failure frequency estimates with uncertainties for welds in a representative PWR piping system considering the effects of PWSCC and other key parameters, such as leak rate detection, inservice inspection, mitigation, and seismic events; and (2) aggregate the numerical estimates from multiple welds

to generate an annual, piping system failure frequency to determine whether the requirements of GDC 4 are met. The Westinghouse four-loop PWR primary coolant loop piping system was selected for the study because it is the predominant piping system for which the NRC staff has granted approvals for LBB. The system typically contains eight welds that are susceptible to PWSCC: four welds that connect the reactor vessel outlet nozzles (RVONs) to the hot leg piping and four additional welds that connect the cold leg piping to the reactor vessel inlet nozzles (RVINs). The simulated period was 80 effective full-power years to bound plant operation as would be authorized by an original 40-year operating license and up to two renewed operating licenses.

The probability of rupture with leak rate detection served as the quantity of interest (QoI) used to assess whether such piping systems demonstrate an extremely low probability of rupture consistent with the requirements of GDC 4. The xLPR code uses an indicator function to calculate this QoI. The function takes on either: (a) a value of zero for each realization without rupture and each realization that had a leak rate greater than the leak rate detection threshold before rupture, and (b) a value of one for each realization that ruptured before the leak was detected. Mean estimates for the QoI were generated for representative RVON and RVIN welds. The individual weld estimates were then aggregated at the piping system level. The system-level rupture probability estimate was considered acceptable if it was less than $1 \times 10^{-6}$ ruptures per year, which is comparable to a frequency of $1 \times 10^{-6}$ ruptures per reactor-year consistent with the basis for the GDC 4 rulemaking. Uncertainties were considered in the convergence of the statistical solution and through a host of sensitivity studies used to investigate the effects of specific analysis parameters and assumptions.

Several other QoIs were also calculated to provide additional insights into the behavior of these piping systems. These QoIs included the probabilities of first crack, first leak, and rupture without leak rate detection. They form the basic set of outputs from the xLPR code. The probabilities of LBB time lapse, LBB ratio, and leak rate jump were also calculated. The LBB time lapse QoI estimates the distribution of time between detectable leak rates and ruptures. The LBB ratio estimates the distribution of the ratios between the critical crack lengths at rupture and the lengths of cracks that result in detectable leakage. This QoI is the probabilistic analog to the current deterministic LBB acceptance criteria. The leak rate jump QoI estimates the probability of a sudden jump in leakage that would indicate fast and potentially unstable crack growth that could lead to rupture or a loss-of-coolant accident.

All the RVON and RVIN weld analyses showed zero probability of rupture with a 1 gpm leak rate detection capability. The RVIN weld analyses also showed zero probabilities for all the other QoIs because no cracks initiated in the simulations, due to a lower operating temperature. The RVON weld probability of rupture with no inspection or leak rate detection considering crack initiation was estimated to be $1.1 \times 10^{-3}$, which is equivalent to an annual frequency of $1.5 \times 10^{-5}$ for the base case. In the most conservative sensitivity study case focusing on the normal operating loads, it was estimated to be $5.4 \times 10^{-3}$, which is equivalent to an annual frequency of $6.7 \times 10^{-5}$. The mean LBB time lapse for the RVON weld was between 50 and 60 months with a 1 gpm leak rate detection capability and typically around 30 months with a 10 gpm leak rate detection capability. The case that had the lowest LBB time lapse was a sensitivity study that

investigated the impacts of fatigue. Here, the mean LBB time lapse was considerably lower at 14 and 10 months with 1 and 10 gpm leak rate detection capabilities, respectively. All such timeframes would provide ample opportunities to identify a degraded weld before it fails. The mean LBB ratio for the RVON weld was around 9 or 10 with a 1 gpm leak rate detection capability and around 4 with a 10 gpm leak rate detection capability. All these values are well above the deterministic acceptance margin of 2.0 from SRP Section 3.6.3. The probabilistic results thus highlight conservatisms present in the deterministic LBB approach, which may be reduced using probabilistic approaches. Only two of the RVON weld analyses had non-zero probabilities of leak rate jump given the sample sizes used for the analyses. The analysis that had the highest probability of leak rate jump was a sensitivity study that investigated the impacts of more severe welding residual stresses. However, further investigation revealed that the results were due to instances where unrealistically high values were sampled for one of the input distributions (i.e., the minimum distance between two circumferential cracks before they coalesce). The use of a more realistic input distribution would thus eliminate these leak rate jump events.

The individual RVON and RVIN weld results with zero probabilities of rupture with leak rate detection demonstrate that a typical primary loop piping system in a Westinghouse four-loop PWR continues to meet with requirements of GDC 4 when subject to the effects of PWSCC. In addition, an analysis was performed using the other QoIs to illustrate how the results from multiple welds can be aggregated for system-level safety assessment. Only the results for the four RVON welds were considered in this aggregation, however, as the RVIN weld results were small enough to not have an impact on the system-level failure probability. The approach used to aggregate the results considered each RVON weld independently, which is reasonably conservative. Since the individual RVON weld probabilities were small, their combination only increased the system-level estimate by roughly a factor of 4 corresponding with the number of RVON welds in the piping system. Thus, the system-level results do not affect the conclusions drawn on an individual weld basis and remain below the $1 \times 10^{-6}$ annual frequency acceptance threshold considered in the study.

This study represented the first comprehensive application of the xLPR code to support risk-informed regulatory decisionmaking. As such, it provided an excellent opportunity to build experience applying the xLPR code and to interpret the results to resolve a safety-significant problem. The analysts identified best practices during the process of defining the analysis cases, inputs, and outputs, and in running the analyses and analyzing the results. The breadth of sensitivity studies and QoIs considered also led to many observations on the impacts of various factors that influence the behavior of dissimilar metal welds in PWR primary coolant loop piping systems. The methods and results presented in this report may be used as the basis for performing probabilistic LBB analyses for other nuclear power plant piping systems.

# ACKNOWLEDGEMENTS

This study was facilitated, in part, through a collaborative effort between the NRC's Office of Nuclear Regulatory Research and the Electric Power Research Institute under an addendum to their general memorandum of understanding on cooperative nuclear safety research. The authors benefited from the experience, knowledge, and work of many individuals supporting both organizations. The authors would particularly like to thank Mr. Matthew Homiack of the NRC staff and Dr. Craig Harrington of EPRI for their efforts in leading the effort. The authors would also like to thank Mr. Markus Burkardt of Dominion Engineering, Inc. as he was a major force in running companion analyses cases from the EPRI side. All the fruitful discussions and exchanges with him over the course of the project were much appreciated. Finally, the authors would like to thank Mr. Bruce Bishop from Phoenix Engineering Associates, Inc., who was a constant and reliable source of historical information on both deterministic and probabilistic approaches and the associated rationale. He reviewed most of the analyses performed and his insights led to many improvements.

# TABLE OF CONTENTS

# LIST OF TABLES

# LIST OF FIGURES

# ACRONYMS

| | |
|---|---|
| a | crack depth |
| ADAMS | Agencywide Documents Access and Management System |
| c | half-crack length |
| cc | cubic centimeter |
| C | Celsius |
| CB | confidence bound |
| CDF | cumulative distribution function |
| CFR | *Code of Federal Regulations* |
| CI | confidence interval |
| cm | centimeter |
| COD | crack opening displacement |
| DM1 | Direct Model 1 |
| EDF | Électricité de France |
| EFPY | effective full-power years |
| EPRI | Electric Power Research Institute |
| g | gravity |
| GDC | general design criterion |
| gpm | gallons per minute |
| hrs | hours |
| ISI | inservice inspection |
| K | thousand |
| KAPL | Knolls Atomic Power Lab |
| kg | kilogram |
| kN | kilonewton |
| L | leak |
| LBB | leak-before-break |
| LCB | lower confidence bound |
| LOCA | loss of coolant accident |
| LR | leak rate |
| LRD | leak rate detection |
| m | meter |
| MC | Monte Carlo |
| mm | millimeter |
| mon | month |
| MPa | megapascal |
| MSIP | Mechanical Stress Improvement Process |
| NRC | Nuclear Regulatory Commission |
| OD | outside diameter |
| P | probability |
| Pa | pascal |
| PDI | Performance Demonstration Initiative |

| | |
|---|---|
| PFM | probabilistic fracture mechanics |
| PNNL | Pacific Northwest National Laboratory |
| POD | probability of detection |
| ppb | parts per billion |
| ppm | parts per million |
| psi | pounds per square inch |
| PWR | pressurized-water reactor |
| PWSCC | primary water stress-corrosion cracking |
| QoI | quantity of interest |
| R | ratio |
| RVIN | reactor vessel inlet nozzle |
| RVON | reactor vessel outlet nozzle |
| SC | surface crack |
| SRM | staff requirements memorandum |
| SRP | standard review plan |
| SSE | safe shutdown earthquake |
| T | time |
| TWC | through-wall crack |
| UCB | upper confidence bound |
| WRS | weld residual stress |
| xLPR | Extremely Low Probability of Rupture |
| yr | year |
| YS | yield strength |

# 1 INTRODUCTION

## 1.1 Leak-Before-Break History

In 1975, the U.S. Nuclear Regulatory Commission (NRC) staff was informed of newly defined asymmetric blowdown loads that result by postulating rapid-opening, double-ended ruptures of pressurized-water reactor (PWR) piping at the most adverse location in the primary piping system. The topic was designated as Unresolved Safety Issue A-2. In response to a conclusion based on analyses in 1980 that some plants might require extensive modifications to address this safety issue, Westinghouse Electric Corporation undertook a deterministic fracture mechanics evaluation to demonstrate that the assumed double-ended rupture is not a credible design-basis event for PWR piping base and weld metals. Westinghouse Electric Corporation reports WCAP-9570, "Mechanistic Fracture Evaluation of Reactor Coolant Pipe Containing a Postulated Circumferential Through-Wall Crack," Revision 2, issued June 1981 [1], and WCAP-9788, "Tensile and Toughness Properties of Primary Piping Weld Metal for Use in Mechanistic Fracture Evaluation," issued June 1981 [2], document the fracture mechanics evaluations for piping base and weld metals, respectively.

Around the same time, the NRC published the results of a probabilistic PWR piping fracture study in NUREG/CR-2189, "Probability of Pipe Fracture in the Primary Coolant Loop of a PWR Plant," Volume 5, "Probabilistic Fracture Mechanics Analysis, Load Combination Program, Project I Final Report," issued August 1981 [3]. The Westinghouse Electric Corporation and NRC-sponsored studies used different methodologies; however, both supported the conclusion that double-ended ruptures in PWR primary system piping are extremely low probability events. The results of these studies were submitted to the NRC's Advisory Committee on Reactor Safeguards. In a June 14, 1983, letter to the NRC's Executive Director for Operations, the Advisory Committee on Reactor Safeguards stated that:

> Fracture mechanics analysis clearly indicates that in PWR primary piping a substantial range of stable crack sizes exists between those which give detectable leaks and the much larger size that results in sudden failure… However any relaxation of requirements to cope with double-ended guillotine break should be preceded by rigorous reexamination of the integrity of heavy component supports under all design conditions.

As a result, in 1985 [4] the NRC proposed to modify General Design Criterion (GDC) 4, "Requirements for Protection of Dynamic Effects of Postulated Pipe Ruptures," in Title 10 of the *Code of Federal Regulations* (10 CFR), Part 50, Appendix A. These requirements ensure that structures, systems, and components important to safety are protected against the dynamic effects of postulated large piping ruptures. GDC 4 had been conservatively applied to require all nuclear power reactors to employ massive pipe whip restraints and jet impingement shields to mitigate the dynamic effects of a postulated guillotine rupture in the largest piping in the reactor coolant system. It was also demonstrated through research performed by the NRC and industry, coupled with operating experience, that the protective devices degrade overall safety

because they reduce the effectiveness of inservice inspection (ISI) and present difficulties and potential errors in their installation or reinstallation.

The resulting amendment to GDC 4 in 1987 [5] allows for analyses to serve as the basis for excluding dynamic effects associated with certain piping system ruptures from the design basis of a nuclear power plant. These analyses constitute what is commonly referred to as the leak-before-break (LBB) concept. The deterministic and probabilistic analyses showed that, for the primary loop piping in PWRs, double-ended guillotine or longitudinal ruptures are extremely unlikely. The analyses depend on advanced fracture mechanics techniques and include investigations of potential indirect failure mechanisms which could lead to piping rupture. The objective of the LBB approach is to demonstrate by analysis that the detection of small flaws, either by ISI or by leakage monitoring systems, is assured long before the flaws could grow to critical or unstable sizes and lead to large breaks, such as the double-ended guillotine pipe rupture. Acceptable analytical procedures are outlined in NUREG-1061, "Report of the U.S. Nuclear Regulatory Commission Piping Review Committee," Volume 3, "Evaluation of Potential Pipe Breaks," issued November 1984 [6].

The general design criteria in 10 CFR Part 50, Appendix A [7], require that the emergency core cooling systems of nuclear power plants be capable of tolerating a double-ended guillotine break. Specifically, GDC 4 states that:

> Structures, systems, and components important to safety shall be designed to accommodate the effects of and to be compatible with the environmental conditions associated with normal operation, maintenance, testing, and postulated accidents, including loss-of-coolant accidents. These structures, systems, and components shall be appropriately protected against dynamic effects, including the effects of missiles, pipe whipping, and discharging fluids, that may result from equipment failures and from events and conditions outside the nuclear power unit. However, dynamic effects associated with postulated pipe ruptures in nuclear power units may be excluded from the design basis when analyses reviewed and approved by the Commission demonstrate that the probability of fluid system piping rupture is extremely low under conditions consistent with the design basis for the piping.

LBB technology was applied to commercial nuclear power plant piping beginning in the 1980's in the U.S. GDC 4 requires mitigation against the potential dynamic events from a postulated dynamic piping break (i.e., use of pipe whip restraints and jet impingement shields), unless it can be shown there is an extremely low probability of rupture. The NRC staff developed a deterministic LBB procedure documented in NUREG-1061, Volume 3 [6], which is based on a stringent set of screening criteria and a deterministic fracture mechanics flaw tolerance evaluation.

In 1987, the NRC solicited public comments on Standard Review Plan (SRP) Section 3.6.3 [8], which incorporated the screening criteria and deterministic fracture mechanics review procedures. Per this guidance, for a piping system to be eligible for LBB analysis, it should, among other factors, satisfy the following:

- have no active degradation mechanisms (e.g. erosion, corrosion, and fatigue) that can be a potential source of pipe rupture
- use materials of construction with high toughness (i.e., not be susceptible to brittle fracture)
- have a low potential for water hammer events and negligible impact from indirect sources of pipe rupture defined in the plant's design basis (e.g., seismic events)

The failure mode of concern for PWR primary loop reactor coolant system piping is circumferential cracking in butt-welds, although axial cracking can lead to leaks.

Following the procedures in SRP Section 3.6.3, a leakage crack size in the reactor coolant system piping is calculated for a leak rate equal to the plant leakage detection system threshold (e.g., 1 gpm) multiplied by a safety factor of 10 to account for uncertainties. Once the leakage crack size is determined at normal operating conditions, the critical crack size at normal and transient loading (typically seismic) conditions is determined by limit load or elastic-plastic fracture mechanics analysis. This includes a margin of 2 on the crack length or 1.4 on the stresses. Therefore, an extremely low probability of rupture is demonstrated deterministically by having a piping system with high fracture toughness, low stresses, an analytical flaw tolerance evaluation, and no active degradation mechanisms.

## 1.2 A New Degradation Mechanism

Around 2000, a new degradation mechanism was identified in PWR piping systems that were previously approved for LBB. The new mechanism was termed primary water stress-corrosion cracking (PWSCC). It is characterized by a long crack initiation time and a relatively fast crack growth rate. It occurs in the dissimilar metal welds (i.e., Alloy 82/182 filler weld metals) between stainless and ferritic steel piping components. The susceptible welds were not stress-relieved, and the normal operating stresses were low, so subcritical crack growth was primarily driven by the weld residual stresses (WRS). From a deterministic viewpoint, there are two primary scenarios: (1) when the combined WRS and normal operating stresses produce a crack that grows quickly through the pipe wall thickness, and (2) when a surface crack grows a long distance around the inside circumference before becoming a through-wall crack (TWC). The first scenario represents LBB behavior; however, the second has the opposite effect (i.e., represents undesirable break-before-leak behavior) unless more complicated analytical evaluations are performed which consider the effects of ISI.

Various industry events prompted greater NRC and industry emphasis on effectively managing PWSCC. For example:

- The NRC issued several generic communications [9] [10] [11] to underscore the significance of PWSCC.
- EPRI completed a comprehensive butt weld safety assessment [12] followed by issuing inspection and evaluation guidelines [13] [14]. Industry voluntarily implemented these guidelines under the Nuclear Energy Institute's materials aging management initiative [15], an action which the NRC staff viewed positively and which facilitated the NRC staff's decision to pursue the deliberative process of codifying requirements involving all stakeholders rather than initiating other reactive regulatory actions [16].
- At the request of the NRC staff [17], ASME developed improvements to the ASME Code Section XI requirements on inspection frequencies for reactor coolant system butt welds containing Alloy 82/182 [10]. ASME Code Case N-770-1 was subsequently developed and approved by ASME [18], and the NRC incorporated it directly into 10 CFR 50.55a in 2011 as an augmented examination requirement [19].
- Significant advances were made to increase the effectiveness of ultrasonic testing through actions to incorporate lessons learned from operating experience into examination planning and implementation of ASME Code, Section XI, Appendix VIII, Supplement 10 requirements for dissimilar metal weld examinations.

From a deterministic viewpoint, there are two primary scenarios: (1) when the combined WRS and normal operating stresses produce a crack that grows quickly through the pipe wall thickness, and (2) when a surface crack grows a long distance around the inside circumference before becoming a through-wall crack (TWC). The first scenario represents LBB behavior; however, the second has the opposite effect (i.e., represents undesirable break-before-leak behavior) unless more complicated analytical evaluations are performed which consider the effects of ISI. A revision to SRP Section 3.6.3 in 2007 [20] clarified that the NRC staff considers PWSCC to be an active degradation mechanism in Alloy 600/82/182 materials in PWRs. As such, SRP Section 3.6.3 does not allow LBB applications for piping systems with active degradation mechanisms, such as PWSCC, unless the NRC staff confirms that these mechanisms are not potential sources of pipe rupture. Even though the piping systems experiencing PWSCC have been shown to be compliant with the regulations through qualitative arguments, neither the NRC staff nor the industry has prepared a thorough quantitative assessment of the impacts of PWSCC in LBB analyses. Such an initial assessment is the focus of the study presented herein.

## 1.3 The xLPR Code

In 2008, the NRC Office of Nuclear Regulatory Research signed a memorandum of understanding addendum with EPRI to initiate a pilot study to cooperatively develop a new probabilistic fracture mechanics (PFM) code to analyze the risks associated with nuclear power plant piping systems subject to active degradation mechanisms. The motivation for code development stemmed in part from NRC staff and industry interests in effectively managing

PWSCC and its implications for prior LBB analyses. The code was intended to be comprehensive with respect to known challenges, vetted with respect to scientific adequacy of the models and inputs, flexible enough to permit analysis of a variety of inservice situations, and adaptable to accommodate evolving and improving knowledge. The resultant PFM code was called "xLPR" for extremely low probability of rupture, which is the language used in GDC 4. For a summary of the xLPR Pilot Study, the reader is referred to NUREG-2110, "xLPR Pilot Study Report," issued May 2012 [21].

xLPR Version 2, which was used for the present study, incorporates a set of state-of-practice deterministic models to evaluate both fatigue and PWSCC degradation mechanisms from crack initiation and growth until rupture. It also models WRS, leak rate detection, ISI, and seismic events. Additionally, it can model the various techniques employed in nuclear power plants to mitigate PWSCC, such as water chemistry changes and the application of inlays, overlays, and mechanical stress improvement. The various models are implemented in a modular form and linked together by a central probabilistic framework that contains the logic for code execution, exercises the individual modules as required, and performs the necessary administrative and bookkeeping functions. This version of the code was developed under a rigorous quality assurance program and independently reviewed by a panel of experts.

## 1.4 Objectives of This Study

The present study represents the first comprehensive application of xLPR Version 2 to support risk-informed regulatory decisionmaking. As such, the xLPR code was the primary tool for both generating the probabilistic results and assessing the validity of the methodologies considered. The primary objectives of the study were twofold:

1. Use the xLPR code to generate numerical failure frequency estimates with uncertainties for welds in a representative PWR piping system considering the effects of PWSCC and other key parameters, such as leak rate detection, ISI, mitigation, and seismic events.
2. Combine the estimates from multiple welds to generate an annual, piping system-level failure frequency to determine whether the requirements of GDC 4 are met.

To support the first objective, several quantities of interest (QoIs) were considered as follows:

- Rupture with Leak Rate Detection – This QoI directly estimates the occurrence of ruptures with consideration of the leak rate detection capability. It is represented as a cumulative probability over the simulated period of plant operation.
- Leak Rate Jump – This QoI estimates the probability of a sudden jump in leakage from below a lower leak rate threshold value to above an upper leak rate threshold value from one simulation timestep to the subsequent time step. The probabilistic result is expressed as a time-dependent probability over the simulated period of plant operation. It is based directly on the recommendations in the technical basis document on acceptance criteria [22].

- LBB Time Lapse – This QoI estimates the time between a detectable leak rate and a rupture. The probabilistic result is a distribution of the LBB time lapse over the simulated period of plant operation conditional on having cracks that both leak and rupture the pipe. It provides useful insights by capturing the time-dependent behavior of the system, which cannot be captured in a deterministic LBB analysis.
- LBB Ratio – This QoI estimates the ratio between the critical crack length at rupture and the length of a crack that results in detectable leakage. It is the probabilistic analog to the SRP Section 3.6.3 deterministic LBB acceptance criterion. The probabilistic result is a distribution of the LBB ratio over the simulated period of plant operation conditional on having cracks that both leak and rupture the pipe.

Since the LBB ratio and LBB time lapse are conditional on having cracks, leaks, and ruptures, the associated results must be interpreted considering the likelihood of those events occurring as applicable to the analysis. The time-dependent probabilities of first crack, first leak, and rupture without leak rate detection provide additional insights. These are the standard indicator outputs from the xLPR code and were also considered.

A comprehensive base analysis was prepared for each weld susceptible to PWSCC in the selected piping system. The base analyses were then supported by alternative scenarios or sensitivity studies selected by a team of industry and NRC staff experts. Each sensitivity study was a probabilistic analysis with many inputs considered uncertain. However, the sensitivity study cases differed from the base cases as “what if” scenarios, where a specific input or set of inputs were selected differently to test important input assumptions. These assumptions could increase or decrease the probabilities of failure and may also vary depending on the applicable QoIs. They also demonstrate defense in depth from an analytical perspective.

The second objective of the study was established because the xLPR code by design can only consider one weld in each simulation. However, analyses used to demonstrate that the probability of rupture is extremely low consistent with the requirements of GDC 4 require estimating the probability of adverse events for the entire plant or piping system. Thus, a mathematical methodology was developed to aggregate the results from single weld analyses to draw system-level estimates. The probability of rupture with leak rate detection served as the QoI used to assess whether such piping systems demonstrate an extremely low probability of rupture consistent with the requirements of GDC 4 when subject to the effects of PWSCC. Results from the other QoIs were considered for information purposes.

Finally, an ancillary objective of the study was to build experience in applying the xLPR code and develop associated best practices. Potential areas for improvement were outlined during the process of defining the analysis cases, inputs, and outputs, and in running the analyses and analyzing the results. The breadth of sensitivity studies and QoIs considered also allowed the analysts to make many observations on the impacts of various factors that influence the behavior of dissimilar metal welds in PWR primary coolant loop piping systems. The results of the completed study may serve as the basis for developing a standardized and comprehensive approach for probabilistic LBB assessment.

# 2 ANALYSIS APPROACH

## 2.1 Piping System Selection

The piping system selected for this study is the primary, or main loop, piping in a Westinghouse four-loop PWR design. Such a system is illustrated in Figure 2-1. This design was selected because it is the predominant piping system for which the NRC staff has granted LBB approvals. It also has multiple dissimilar metal welds and, therefore, could support the second objective of the study to combine the estimates from multiple welds to generate an annual, piping system-level failure frequency. Finally, much of the input data needed to analyze this system was already available and conveniently assembled in the required xLPR input set format.

In this study, the analyses were prepared generically to bound the RVON and RVIN welds and operating stresses in the primary loop piping in the following PWRs:

- Braidwood Station, Units 1 and 2
- Byron Station, Units 1 and 2
- Callaway Plant, Unit 1
- Catawba Nuclear Station, Units 1 and 2
- Comanche Peak Nuclear Power Plant, Units 1 and 2
- Donald C. Cook Nuclear Plant, Units 1 and 2
- McGuire Nuclear Station, Units 1 and 2
- Millstone Power Station, Unit 3
- Salem Nuclear Generating Station, Units 1 and 2
- Seabrook Station, Unit 1
- Sequoyah Nuclear Plant, Units 1 and 2
- South Texas Project, Units 1 and 2
- Vogtle Electric Generating Plant, Units 1 and 2
- Watts Bar Nuclear Plant, Units 1 and 2
- Wolf Creek Generating Station, Unit 1

Although licensed to operate when this study was conducted, Diablo Canyon Nuclear Power Plant, Units 1 and 2, and Indian Point Nuclear Generating, Units 2 and 3 were not explicitly included because their licensees had announced plans to cease operations.

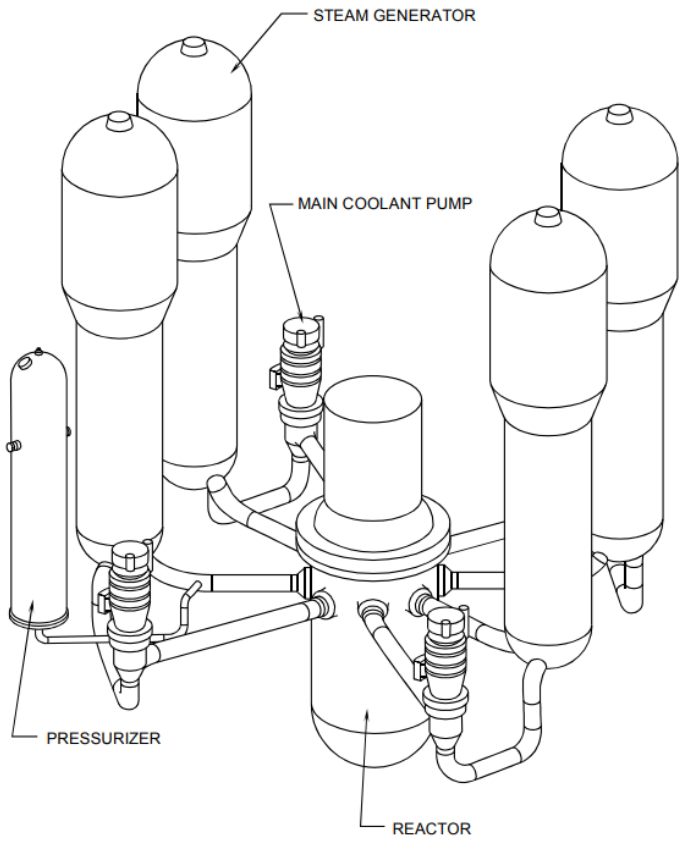


**Figure 2-1 Schematic of a four-loop Westinghouse PWR**

As PWSCC is the primary degradation mechanism of interest, only the Alloy 82/182 dissimilar metal welds were analyzed. In the subject piping system, these welds are located at the connections between the primary loop piping and the reactor vessel outlet nozzles (RVONs) and the reactor vessel inlet nozzles (RVINs). Thus, there are total of 8 welds in the piping system that are susceptible to PWSCC. Mitigation of PWSCC in these welds by application of the mechanical stress improvement process (MSIP) is common.

## 2.2 Quantities of Interest

The QoIs considered in this study were selected on the basis that they could provide information to a decisionmaker to determine whether a piping system has an extremely low probability of rupture consistent with the requirements of GDC 4. The period of interest for all the QoIs was 80 effective full-power years (EFPY) to bound plant operation as would be authorized by an original 40-year operating license and up to two renewed operating licenses. The evaluated period of 80 EFPY assumes a plant capacity factor of 100 percent throughout the entire period of licensed operation. Thus, as presented in this report, 80 EFPY is equivalent to 80 calendar years of operation. This assumption is conservative as it subjects the piping components to the most amount of degradation in the simulation.

Sections 2.2.1 through 2.2.4 describe the primary QoIs in detail (i.e., probability of rupture with leak rate detection, leak rate jump, LBB time lapse, and LBB ratio). In general, two leak rate detection capabilities were considered in this study: 1 and 10 gpm. The latter was chosen because many licensees had demonstrated a 1 gpm leak rate detection capability for approval of their original, deterministic LBB analyses. However, per SRP Section 3.6.3, a safety factor of 10 was applied, giving the 10 gpm value. This safety factor was meant to address many of the uncertainties that the xLPR code addresses directly; therefore, the former, 1 gpm leak rate detection capability was also examined.

The other QoIs considered included the probabilities of first crack, first leak, and rupture without leak rate detection. These QoIs were considered for informational purposes to support the general LBB concept, and because they can be more useful when analyzing the results of a sensitivity study. Moreover, they are useful in assessing the level of convergence of the Monte Carlo (MC) method. The approach taken to demonstrate adequate convergence for this study is described in Section 2.3.

### 2.2.1 Rupture with Leak Rate Detection

The probability of rupture is one of the standard xLPR indicator results. With consideration of the offsetting effects of leak rate detection, it was used in this study as the decisionmaking QoI for probabilistic LBB assessment because it directly addresses the language in GDC 4 (i.e., "demonstrate that … piping rupture is extremely low"). The probability of rupture with leak rate detection is the average of an indicator function that takes on: (a) a value of zero for each realization without rupture and for each realization that had a leak rate greater than the leak rate detection threshold before rupture, and (b) a value of one for each realization that ruptured before the leak was detected. The probabilistic result is expressed as a time-dependent probability of occurrence over the 80 EFPY simulated period of plant operation.

### 2.2.2 Leak Rate Jump

The leak rate jump and associated thresholds are based directly on the recommendations in the technical basis document on acceptance criteria [22]. It was considered as an informative QoI in this study because it estimates the probability of a sudden jump in leakage from below a lower threshold value (defined as 10 gpm) to above an upper threshold value (defined as 50 gpm) from one simulation timestep (defined as 1 month) to the subsequent time step. Several conservatisms are present in this approach as detailed in [22]. This QoI can be used to support probabilistic LBB assessment because a quickly increasing leak rate would indicate fast and potentially unstable crack growth that could lead to rupture or a loss of coolant accident (LOCA). Ruptures are also counted in the leak rate jump results if they occur before the lower leak rate jump threshold is reached. An advantage of this QoI is that it accounts for the temporal aspects of the problem. As such, it provides greater insights as compared to deterministic LBB analyses prepared following the guidance in SRP Section 3.6.3, which do not account for such aspects. Additionally, as explained in [22], this QoI is tied to the NRC's risk-informed decisionmaking framework. The main factors that affect the leak rate jump are the crack growth rate and crack

opening displacement (COD). The probabilistic result is expressed as a time-dependent probability of occurrence over the simulated 80 EFPY period of plant operation.

### 2.2.3 LBB Time Lapse

The LBB time lapse estimates the time between a detectable leak rate and a rupture. It was considered as an informative QoI in this study because, when a TWC is experiencing subcritical crack growth, the time between when the TWC is detected by a plant's leakage detection system and when the TWC becomes unstable and leads to rupture provides insights into the time-dependent behavior of the system. The main factors that affect the LBB time lapse are the crack growth rate and uncertainties in the leak rate models. The probabilistic result is a distribution of the LBB time lapse conditional on having cracks that both leak and rupture the pipe. It is expressed as a cumulative distribution function (CDF) reflecting the entire 80 EFPY period of simulated plant operation.

### 2.2.4 LBB Ratio

The LBB ratio estimates the ratio between the critical crack length at rupture and the length of a crack that results in detectable leakage. It was considered as an informative QoI in this study because it is the probabilistic analog to the current deterministic LBB acceptance criteria. In accordance with SRP Section 3.6.3, the deterministic LBB analysis should demonstrate that there is a margin of at least two between the leakage crack size and the critical crack size. The leakage crack size represents the size of the TWC under normal operating loading that will produce a leak rate 10 times greater than the reactor coolant system leak rate detection capability. The critical crack size represents the size of the crack at the onset of instability under normal operating plus SSE loading. Both 1 and 10 gpm leak rate detection capabilities were chosen to define the LBB ratio in the probabilistic study, however. The main factors that affect the LBB ratio are the crack size, COD, leak rate, and crack stability models. The probabilistic result is a distribution of the LBB ratio conditional on having cracks that both leak and rupture the pipe. It is expressed as a CDF reflecting the entire 80 EFPY period of simulated plant operation.

## 2.3 Statistical Approach

### 2.3.1 Separation of Uncertainties

xLPR is a PFM code that uses sampling-based MC methods. It allows the user to split uncertainty into two types: (1) epistemic (in the outer loop) and (2) aleatory (in the inner loop). The separation between aleatory and epistemic uncertainties is applied when a distinction needs to be made between the risk (represented by aleatory uncertain quantities) and uncertainty over the risk (represented by epistemic uncertain quantities). However, a drawback of splitting the uncertainty is that it requires a larger total sample size, because the total sample size is equal to the epistemic sample size multiplied by the aleatory sample size. As a result, when only mean values are considered for a QoI, a single loop analysis provides a more efficient way to reach statistical convergence. In the present study, which considered the QoIs described in Section 2.2, a single loop was used for most of the analysis cases. A sensitivity

study was conducted to analyze the impact of using a dual loop approach and to show the additional information generated. Section 3.2.2.17 presents the results from this sensitivity study.

### 2.3.2 Sampling Method and Sample Sizes

To benefit from the dense stratification of Latin hypercube sampling, only the epistemic (outer) loop was generally used. An analysis using only the aleatory (inner) loop was also performed as describe in Section 3.2.1.1.3 to demonstrate that the choice of either loop does not affect the results beyond what would be expected from using a different random seed for the simulation.

The accuracy level of the MC method was expected to conform with the basis for the GDC 4 rulemaking [5], which states that, for reactor coolant loop piping, a representative value which would qualify as "extremely low" would be of the order of $10^{-6}$ per reactor year when all rupture locations are considered in the fluid system piping or portions thereof. This is comparable to an annual system failure frequency as low as 1 in a million (i.e., 1 x $10^{-6}$ events per year). In the xLPR code, the sample size is functionally limited by the computational time required to run a simulation, the amount of data saved (a GoldSim model file is limited to 3 gigabytes), and the ease of post-processing the results. To work within these constraints, the xLPR code's GoldSim model file was optimized in terms of the data it recorded to accommodate the sample sizes needed for this study.

The sample size selected when an analysis case used one of the crack initiation models was typically 105,000 realizations (a composite of 7 runs each of 15,000 realizations). With 105,000 realizations run over a period of 80 EFPY, it is expected that the annual frequency of an any event in the range of 1 x $10^{-6}$ would be detected. For example, 1 event in 105,000 trials over an 80-EFPY period leads to a probability of occurrence of 9.5 x $10^{-6}$ over that period. With such low numbers, the frequency and probabilities are about the same, and the annual frequency can be estimated by dividing the probability by the period (i.e., 80 EFPY). This equates to an approximate annual frequency of 1 in 8 million (i.e., $1.2 \times 10^{-7}$). When a case included axial cracks, the sample size was reduced to 70,000 (a composite of 7 runs each of 10,000 realizations), which corresponds to an annual frequency of roughly $1.8 \times 10^{-7}$.

The initial flaw density option was used in addition to the crack initiation models. This option seeds pre-existing crack(s) at the beginning of a simulation. In certain cases, the results using the initial flaw density approach were also more accurate than results when using the crack initiation models For instance, comparisons of the RVON weld results show that the distributions for the LBB ratio and LBB time lapse are similar between use of the crack initiation model and use of the initial flaw density option. Considering that the probability of having a circumferential crack over an 80 EFPY simulated period of plant operation using one of the PWSCC initiation models is around $3 \times 10^{-3}$, a sample of size 5,000 for any case using the initial flaw density option was considered large enough to provide accurate results.

As described in Section 3.2.1, stability analyses were performed for the RVON weld base cases with the generation of confidence intervals to graphically and numerically assess the accuracy

of the various QoIs. The results demonstrate that the selected sample sizes are adequate for generating stable results at 80 EFPY and appropriate for making the conclusions to support the objectives of the study.

### 2.3.3 Probability to Annual Frequency

Several outputs presented in this report are probabilities of occurrence of an adverse event over a period of *T* years. These probabilities need to be expressed as annual frequencies for comparison against the threshold of 1 x $10^{-6}$ ruptures per reactor-year. Using the assumption that these events follow a Poisson process, it is possible to estimate relative annual frequencies from the probabilities. The equation used to estimate that at least one event occurs over a period of *T* years for a homogeneous Poisson process of annual frequency $\lambda$ is as follows:

$$P(event \geq 1)_T = p = 1 - e^{-\lambda T}$$

This equation can be reversed to estimate $\lambda$ as a function of $p$ and $T$ as follows:

$$\lambda = -\frac{\ln(1-p)}{T}$$

The latter equation was used whenever a frequency is given relative to a probability in this report.

Important caveats are that the resulting annual frequency is (a) still relative to the period considered (i.e., from 0 to T years), and (b) based on the assumption of homogeneity. If the rate of probability of the event under consideration changes over time, then the annual frequency would also change. For instance, the annual frequency over the period of 0 to 80 EFPY may be different than the annual frequency over the period of 50 to 80 EFPY.

A Taylor series expansion of the logarithmic function gives the following estimate for $\lambda$:

$$\lambda = -\frac{\ln(1-p)}{T} = \frac{p + \frac{p^2}{2} + \frac{p^3}{3} + \cdots + \frac{p^n}{n} + o(p^n)}{T} \cong \frac{p}{T} + o(p)$$

For low probability values (e.g., 1 x $10^{-3}$ or less), the higher order terms provide a negligible contribution. While this simple estimate is faster and is sufficient in most cases, only the former was used for consistency since it can be applied to higher probabilities.

### 2.3.4 Confidence Intervals

The stability of the MC approach (i.e., adequacy of the sample size to produce stable statistics), can be assessed graphically and quantitatively using confidence intervals. A confidence interval at level $q$ over a statistic of interest is an interval in which the true value of the statistic should lie with a probability $q$. Larger sample sizes would lead to tighter confidence intervals and, therefore, increase confidence in the estimate. In this report, the traditional centered confidence level of 95 percent between the 2.5$^{th}$ and 97.5$^{th}$ percentiles was used.

Over the last two decades, confidence intervals on statistics of interest have been estimated using bootstrapping methods. These approaches consist of sampling $N$ times with replacement from the original distribution of $N$ results and then estimating the statistic from this new sample. The operation is then repeated many times to produce a distribution of statistics. In the present study, the confidence intervals were estimated on the probabilities of events $p$, which are estimated as the mean statistics of occurrences, which can be equal to either 0 (no event) or 1 (event). Applying a bootstrap to such data sets means sampling a 1 with a probability $p$ and 0 with a probability $(1-p)$ every time resampling occurs. This approach is essentially equivalent to performing a Bernoulli trial $N$ times, and thus equivalent to a binomial distribution. Using the inverse of the cumulative distribution function of a binomial distribution provides (a) a simple way to calculate the confidence intervals without having to use resampling techniques, and (b) greater accuracy than a traditional bootstrap approach.

## 2.4 Computational Platforms and Simulation Execution Strategy

All the analyses were executed on the computational platforms described in Table 2-1. Nearly all the simulations used GoldSim Pro with its parallel processing capabilities to decrease run times.

**Table 2-1 Computational platforms**

| | Platform 1 | Platform 2 |
|---|---|---|
| **Random-access memory** | 32 GB | 16 GB |
| **Central Processing Unit** | Intel® Core™ i9-9920X @ 3.5GHz | Intel® Core™ i5-8350U @ 1.70 GHz |
| **Operating System** | Microsoft Windows 10 Pro | Microsoft Windows 10 Enterprise, 64-bit |
| **Disk Drive** | Solid state drive | Solid state drive |
| **GoldSim License** | GoldSim Pro | GoldSim Player |
| **GoldSim Version** | 11.1.7 | 11.1.7 |

## 2.5 Project Team

This study was facilitated in part through a collaborative effort between the NRC Office of Nuclear Regulatory Research and EPRI under an addendum to their general memorandum of understanding on cooperative nuclear safety research [23]. Separate NRC and EPRI analysis teams were formed, which included NRC staff, EPRI staff, and their contractors. Case definition and data collection activities necessary to gather sources for inputs were largely a cooperative effort; however, the analyses were performed independently.

Independence was achieved using a graded approach. First, the input values and distributions for the base cases were discussed between the teams until a consensus was reached. The

base cases were then run by each team using the same input set but with different random seeds and sampling approaches. The results were then compared and deemed similar enough to be used as the basis for all the subsequent analyses. The sensitivity study cases were coordinated to avoid unnecessary duplication of efforts, but key input choices were left to the analysts to define separately. The teams generally adopted two approaches for the sensitivity studies. The NRC team took a generally more conservative approach to demonstrate defines in depth. The EPRI team also took a conservative approach, but to a lesser degree, to support plant operational considerations. All the results were shared between the teams, but their ultimate presentation and the conclusions drawn were strictly an independent exercise. This report presents the NRC team's results and conclusions.

## 2.6 Necessary Code Corrections and Modifications

This effort represented the first comprehensive application of the xLPR Version 2.0 code. Although this version was rigorously tested, as is common with all software, increased use often identifies minor bugs or areas for enhancement not revealed to the developers through prior review and testing. Such was the case in this effort. In addition, the analysts identified the need for minor modifications that were necessary to extract the desired results and to optimize the code for memory and run-time considerations. As a result, incremental beta versions of the code were developed to implement and exercise the necessary corrections and modifications. Each impacted case was then re-executed using the appropriate beta version. The specific versions used to analyze each case are listed in Appendix A.

A protocol for developing, reviewing, and testing the beta versions was developed for use by the NRC and EPRI project teams. The protocol followed quality assurance measures like, but more flexible than, the ones ultimately set forth in the official xLPR software maintenance process, which was being developed in parallel with this effort. Major versions were reserved for corrections or modifications, whereas, minor versions were used primarily to optimize the amount of data saved without affecting the results. While implementation of these changes was not a primary goal of the study, the teams considered it important to develop and apply such a protocol because the increased traceability and documentation would simplify the process of incorporating the changes into a future release of the code. Furthermore, the process increases confidence in the validity of the results and conclusions. All the changes in the major versions have been referred to the maintenance process and approved by the xLPR Maintenance Control Board for official implementation.

A brief description of each version of the code used in this study is as follows:

- Major Version 2.0a – This version corrects errors that impact the circumferential COD, circumferential surface crack stability, and circumferential TWC stability calculations. It served as the basis for the following versions:
    - Minor Version 2.0a_001 – This minor version was used to check the changes implemented and validate their adequacy.
    - Minor Version 2.0a_002 – This minor version was abandoned.

    - Minor Version 2.0a_003 – This minor version suppressed the number of outputs saved by default to provide additional memory overhead for efficiency purposes. It also implemented some additional outputs necessary for calculating the QoIs selected for the study and other useful parameters determined by consensus reached between by the NRC and EPRI project teams.

- Major Version 2.0b – This version extended the range of the axial COD module for low values of $\rho$, which represent the area of interest for the large pipes considered. It resulted in lower leak rate estimates, which are considered more realistic and more representative of inservice conditions. It served as the basis for the following version:
    - Minor Version 2.0b_001 – This minor version adjusted the output information saved consistent with the modifications implemented in Minor Version 2.0a_003.
- Major Version 2.0c – This version implements an optimized algorithm for Direct Model 1 for PWSCC initiation as described by Sallaberry and Kurth [24]. This method estimates the minimum value for the proportionality constant that will lead to a circumferential crack occurrence within the simulation and then samples a value from the distribution conditioned by this minimum. A weight based on this conditional distribution is applied to the corresponding realizations accordingly, which leads to faster convergence. It was only used by the NRC team as a proof of concept and in one case to generate non-zero estimates that were not otherwise possible to generate.
- Major Version 2.0d – This version corrects errors that result when a crack occurs in the same timestep as an inservice inspection. This version builds upon Major Version 2.0b and thus does not include the optimized algorithm for Direct Model 1. It served as the basis for the following version:
    - Minor Version 2.0d_001 – This minor version adjusted the output information saved consistent with the modifications implemented in Minor Version 2.0a_003.

# 3 ANALYSES

## 3.1 Scope

The scope of analyses performed is summarized in the case matrix shown in Table 3-1. The cases were selected and defined by the NRC and EPRI project teams. Cases 1.1.0 and 1.1.1 serve as the base cases for the RVON weld, with the only difference being in whether a crack initiation model was used in the analysis. The analyses for these cases used many of the inputs from Case 1, Scenario 2 as documented in the xLPR Inputs Group report [25], which is also aligned with the RVON weld in a Westinghouse four-loop PWR. The need for specific changes to that set of inputs was reached by consensus of the teams; however, the final input values were determined by the individual analysts as appropriate. The base cases were then supplemented with sensitivity studies to investigate factors that were not considered in the base case inputs and that could affect key aspects of the analyses. These studies focused on aspects such as the effects of the PWSCC initiation models, WRS, seismic events, crack growth models, leak detection models, rupture models, mitigation, and ISI. As these aspects were treated as sensitivity study cases, their effects were not assessed in each case. The focus of theses analyses was on those factors that are known to or could potentially affect PWSCC, which is the degradation mechanism of concern in Westinghouse four-loop PWR main coolant piping systems. Information from the U.S. PWR fleet on the geometry, loading, and operating conditions was collected from a variety of sources to determine the appropriate analysis inputs. Some sensitivity study cases were also included to study the potential contributions of fatigue. Two additional cases were included to study the RVIN weld. Appendix A summarizes the results for each case; the analysis inputs are listed in Appendix B.

**Table 3-1 Summary of RVON and RVIN weld analysis cases**

| Weld | Case No. | Crack Orientation | Crack Initiation Method | Crack Growth Mechanism | Objective |
|---|---|---|---|---|---|
| RVON weld | 1.1.0 | Circumferential | PWSCC (Direct Model 1) | PWSCC | Assess the base likelihood of failure caused by PWSCC initiation and growth with no ISI, mitigation, or seismic effects |
| | 1.1.1 | Circumferential | Initial Flaw Density | PWSCC | Assess the sensitivity of the likelihood of failure due to whether the crack initiation process is modeled in the analysis |
| | 1.1.2 | Circumferential | PWSCC (Direct Model 1) | PWSCC | Assess the sensitivity of the likelihood of failure due to severe, yet plausible, WRS |
| | 1.1.3 | Circumferential | PWSCC (Direct Model 2) | PWSCC | Assess crack initiation model uncertainty using Direct Model 2 |
| | 1.1.4 | Circumferential | PWSCC (Weibull Model) | PWSCC | Assess crack initiation model uncertainty using the Weibull model |
| | 1.1.5 | Circumferential | Initial Flaw Density | PWSCC | Assess the sensitivity of the likelihood of failure due to SSE |
| | 1.1.6 | Circumferential and Axial | PWSCC (Direct Model 1) | PWSCC | Assess the sensitivity of the likelihood of failure due to inclusion of axial cracks |
| | 1.1.7 | Circumferential | PWSCC (Direct Model 1) | PWSCC | Assess the sensitivity of the likelihood of failure due to the normal operating loads |
| | 1.1.8 | Circumferential and Axial | PWSCC (Direct Model 1) | PWSCC | Assess the impacts of leak detection on the likelihood of failure |
| | 1.1.9 | Circumferential | PWSCC (Direct Model 1) | PWSCC | Assess the impacts of MSIP on the likelihood of failure |
| | 1.1.10 | Circumferential | Initial Flaw Density | PWSCC | Assess the impacts of ISI on the likelihood of failure |
| | 1.1.11 | Circumferential | Initial Flaw Density | PWSCC | Assess the impacts of ISI model parameter uncertainty |
| | 1.1.12 | Abandoned | | | |
| | 1.1.13 | Abandoned | | | |

| Weld | Case No. | Crack Orientation | Crack Initiation Method | Crack Growth Mechanism | Objective |
|---|---|---|---|---|---|
| | 1.1.14 | Circumferential | Initial Flaw Density | PWSCC | Assess the impacts of hydrogen water chemistry on the likelihood of failure |
| | 1.1.15 | Circumferential and Axial | PWSCC (Direct Model 1) and Fatigue | PWSCC and Fatigue | Assess the impacts of the combined effects of PWSCC and fatigue |
| | 1.1.16 | Circumferential | Fatigue | N/A | Assess the likelihood of fatigue crack initiation |
| | 1.1.17 | Circumferential | Initial Flaw Density | Fatigue | Assess the sensitivity of the likelihood of failure due to fatigue crack growth from a large initial flaw size |
| | 1.1.18 | Abandoned | | | |
| | 1.1.19 | Circumferential | Initial Flaw Density | PWSCC | Assess the sensitivity of the likelihood of failure due to weld width and weld thickness |
| | 1.1.20 | Circumferential | Initial Flaw Density | PWSCC | Assess the sensitivity of the likelihood of failure due to operating temperature |
| | 1.1.21 | Circumferential | Initial Flaw Density | PWSCC | Assess the sensitivity of the likelihood of failure due to the initial flaw dimensions |
| | 1.1.22 | Circumferential | PWSCC (Direct Model 1) | PWSCC | Assess the sensitivity of the likelihood of failure due to the time step |
| | 1.1.23 | Circumferential | Initial Flaw Density | PWSCC | Assess the impacts of separating aleatory and epistemic uncertainties |
| RVIN weld | 1.2.0 | Circumferential | PWSCC (Direct Model 1) | PWSCC | Assess the base likelihood of failure caused by PWSCC initiation and growth with no ISI, mitigation, or seismic effects |
| | 1.2.1 | Circumferential | PWSCC (Direct Model 1) | PWSCC and Fatigue | Assess the impacts of the combined effects of PWSCC and fatigue |

## 3.2 Reactor Vessel Outlet Nozzle Weld

The RVON weld analyses consisted of two base cases followed by a suite of sensitivity studies. The base case analyses are presented in Section 3.2.1. The sensitivity study analyses are presented in Section 3.2.2.

### 3.2.1 Base Cases

#### *3.2.1.1 PWSCC Initiation with Direct Model 1*

3.2.1.1.1 Case Description

The objective of Case 1.1.0 was to assess the base likelihood of failure caused by PWSCC initiation and growth with no ISI, mitigation, or seismic effects. It served as the reference case for the RVON weld analysis and was used as a basis of comparison for many of the sensitivity study cases.

Most of the inputs used to analyze this case came from Case 1, Scenario 2 as detailed in [25]. Direct Model 1 was used for circumferential crack initiation with the parameters recommended in the technical report on PWSCC initiation model parameter development, confirmatory analyses, and validation [26]. A separate study presented in Appendix C was used to confirm the appropriateness of these parameters by developing new model parameters calibrated strictly to laboratory crack initiation data.

The case also used the RVON weld no-repair WRS profile as documented in the xLPR WRS Subgroup report [27] and shown in Figure 3-1. This WRS profile was selected over the 15 percent and 50 percent RVON weld depth repair profiles because it was the most tensile on the inside diameter and would thus favor PWSCC initiation, which has been shown through prior sensitivity analyses to have a large influence on the probability of rupture as documented in TLR-RES/DE/CIB-2021-000, “Sensitivity Studies and Analyses Involving the Extremely Low Probability of Rupture Probabilistic Fracture Mechanics Code,” issued Month 2021 [28]. Furthermore, there was no data available to support the choice of one WRS profile over another.

The normal operating stresses used in this case were representative of design-basis values, which adds a degree of conservatism. The effects of ISI and seismic events were excluded as they were considered as part of the supporting sensitivity studies. The hydrogen concentration in the reactor coolant system was set to 37 cc/kg, which is the median, unmitigated concentration from EPRI Report 1022852, “Materials Reliability Program: Probabilistic Assessment of Chemical Mitigation of Primary Water Stress Corrosion Cracking in Nickel-Base Alloys (MRP 307), Zinc Addition and Hydrogen Optimization to Mitigate Primary Water Stress Corrosion,” issued 2011 [29].

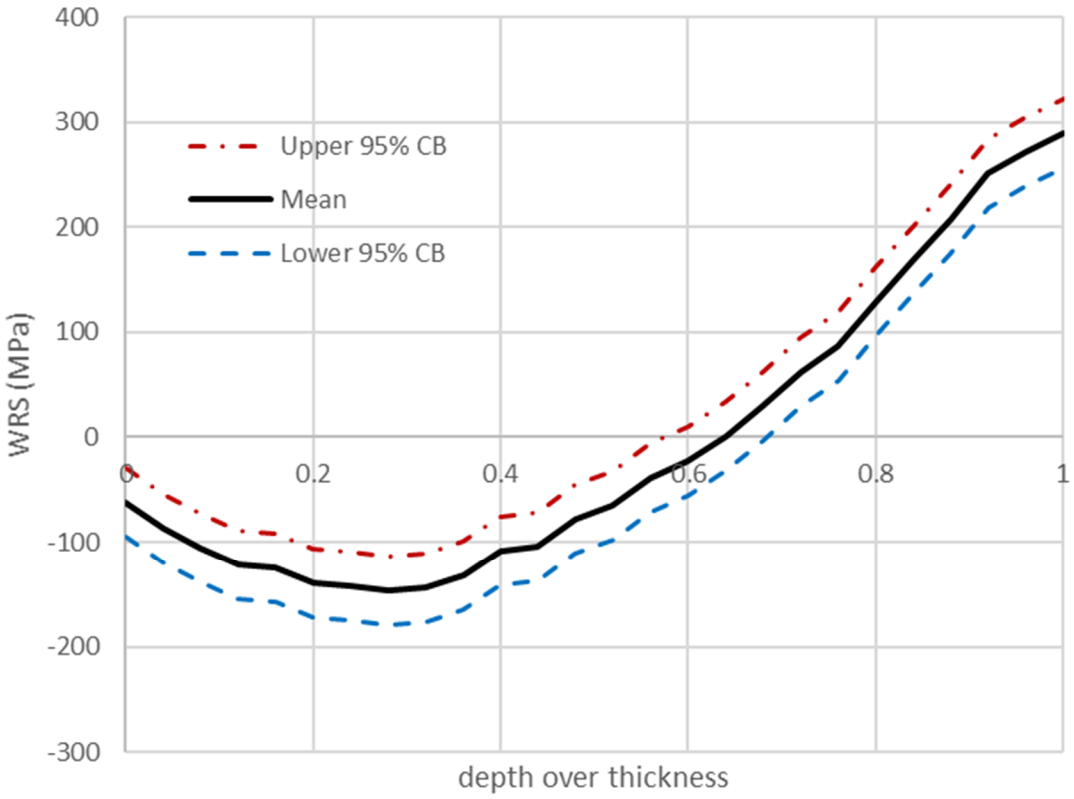


**Figure 3-1 Representation of RVON weld no-repair WRS profile with uncertainties**

Several different simulations were performed for Case 1.1.0 to validate the overall sampling approach outlined in Section 2.3. They included the following:

- The first simulation placed all uncertain inputs on the aleatory (inner) loop. A sample of size of 100,000 realizations was expected to provide converged results, so 4 simulations each with 25,000 realizations were performed. Each sample was split into 250 epistemic (outer) by 100 aleatory (inner) realizations. Since all the uncertainties were set to aleatory, this approach generated 25,000 different values for each uncertain input.
- The second simulation placed all uncertain inputs on the epistemic (outer) loop with only this loop used (i.e., the aleatory (inner) loop sample size was set to 1). The results were expected to be the same as with the prior approach. Each sample size was limited to 15,000 as this approach stores more information in memory. As a result, a total of 7 runs were performed to generate an aggregate sample of size 105,000.
- The third simulation used an optimized Direct Model 1 as described in [24] with a sample size of 2,000 and all uncertain inputs placed on the aleatory (inner) loop with only this loop used (i.e., the epistemic (outer) loop sample size was set to 1). It greatly reduced the required sample size and gave more accurate solutions in about 4.2 and 2.2 percent of the total time of the two previous approaches, respectively.

Section B1 describes the specific inputs and other simulation details used to analyze this case.

3.2.1.1.2 Results and Analysis

Rupture with Leak Rate Detection

There were no ruptures with a 1 gpm leak rate detection capability for this case.

Leak Rate Jump

There were no leak rate jump events for this case.

LBB Time Lapse

The mean LBB time lapses and standard errors with a 1 gpm leak rate detection capability were as follows:

- 48.5 ± 1.7 months (minimum observed: 14 months) from 100,000 realizations on the aleatory (inner) loop
- 50 ± 2.2 months (minimum observed: 15 months) from 105,000 realizations on the epistemic (outer) loop
- 49 ± 0.8 months (minimum observed: 12 months) from 2,000 realizations using the optimized Direct Model 1

With a 10 gpm leak rate detection capability they were as follows:

- 33.7 ± 1.1 months (minimum observed: 13 months) from 100,000 realizations on the aleatory (inner) loop
- 35.4 ± 1.7 months (minimum observed: 9 months) from 105,000 realizations on the epistemic (outer) loop
- 34.2 ± 0.6 months (minimum observed: 9 months) from 2,000 realizations using the optimized Direct Model 1

The standard errors are reported to provide an indication of the uncertainty in the mean estimates. All LBB time lapses beyond 12 EFPY were conservatively excluded as they were found to strongly influence the mean. Such a long period of time is also not of practical interest. For example, if the LBB time lapse is greater than 12 EFPY, it is typically due to a slow-growing crack, an arrested crack, or a crack that has been mitigated, if mitigation is included. Considering all the results, the mean LBB time lapse was between 33 and 50 months, and the minimum observed was 9 months with no ISI or leak rate detection, excluding seismic effects.

LBB Ratio

The mean LBB ratios and standard errors with a 1 gpm leak rate detection capability were as follows:

- 9.37 ± 0.09 (minimum observed: 6.5) from 100,000 realizations on the aleatory (inner) loop
- 10.10 ± 0.3 (minimum observed: 7.26) from 105,000 realizations on the epistemic (outer) loop
- 9.93 ± 0.08 (minimum observed: 6.21) from 2,000 realizations using the optimized Direct Model 1

With a 10 gpm leak rate detection capability they were as follows:

- 4.59 ± 0.02 (minimum observed: 4.09) from 100,000 realizations on the aleatory (inner) loop
- 4.62 ± 0.03 (minimum observed: 3.99) from 105,000 realizations on the epistemic (outer) loop
- 4.62 ± 0.01 (minimum observed: 3.99) from 2,000 realizations using the optimized Direct Model 1

Figure 3-2 and Figure 3-3 show the LBB ratio CDF plots with 1 and 10 gpm leak rate detection capabilities, respectively, based on 100,000 realizations on the aleatory (inner) loop.

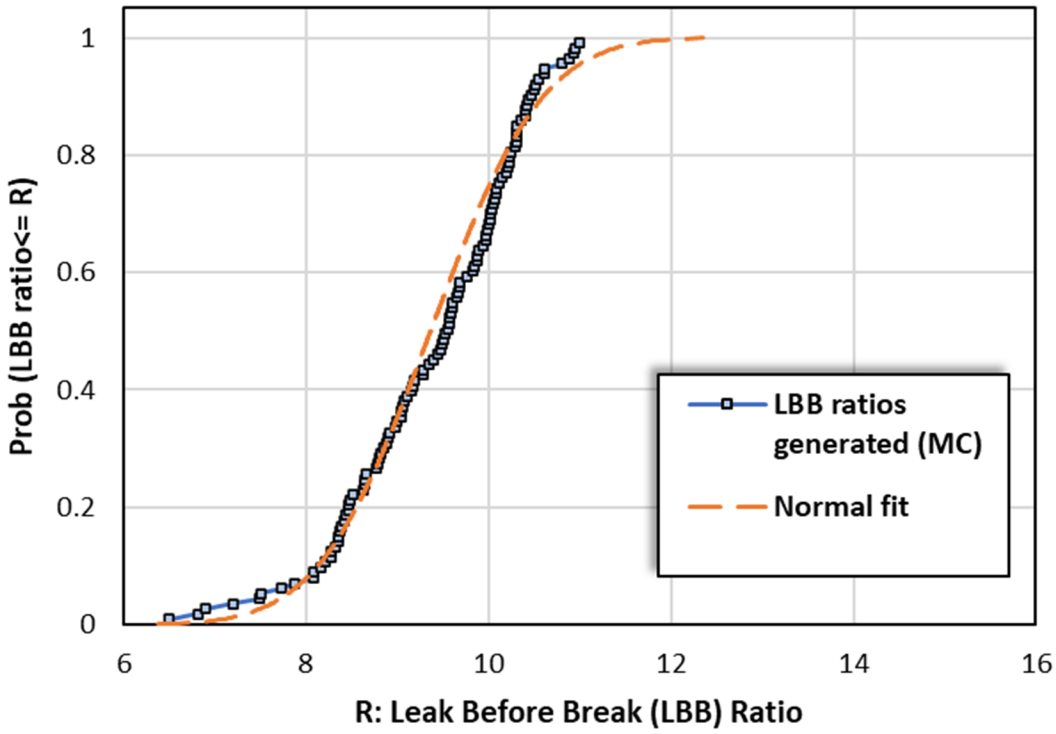


**Figure 3-2** **Case 1.1.0 distribution of LBB ratio with a 1 gpm leak rate detection capability**

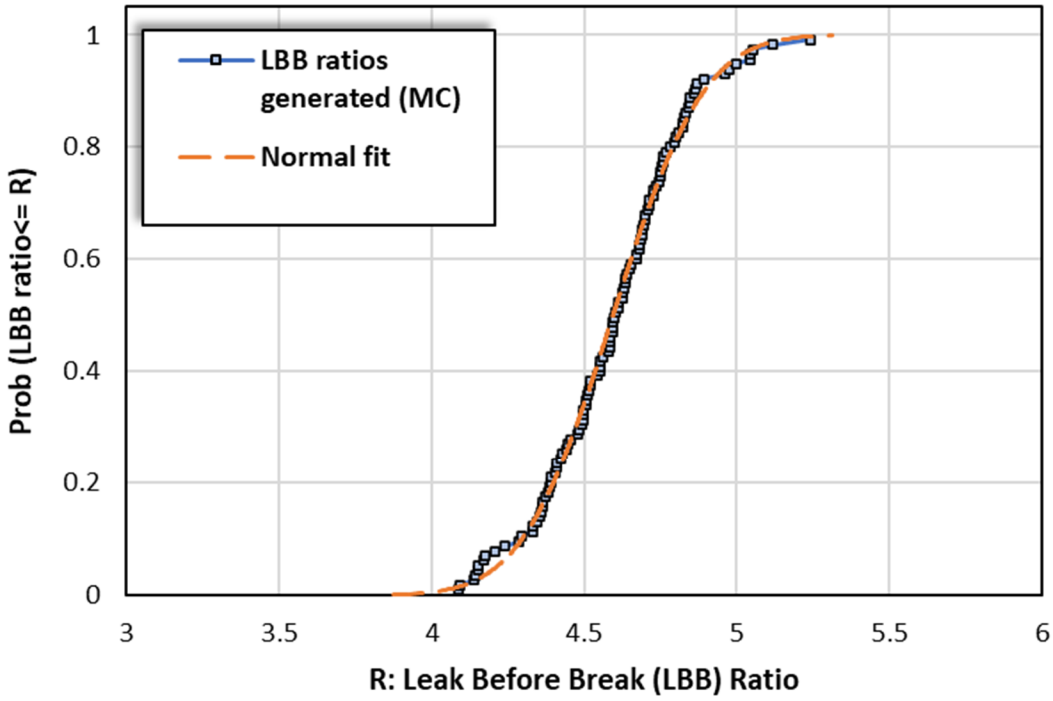


**Figure 3-3 Case 1.1.0 distribution of LBB ratio with a 10 gpm leak rate detection capability**

The LBB ratio represents the crack size at rupture divided by the crack size that leaks at a rate of either 1 or 10 gpm (i.e., the leakage crack size). A deterministic LBB analysis performed in accordance with SRP Section 3.6.3 typically uses a 10 gpm leakage crack size, which is the result of safety factor of 10 applied to a 1 gpm detectable leak rate. The safety factor accounts for uncertainties in the leak rate detection capabilities and leak rate models. Since the xLPR code can directly account for uncertainties in the leak rate models, it is useful to compare the mean value and CDF of the LBB ratio using both leak rate detection thresholds. The mean LBB ratio is almost reduced in half using a 1 gpm leak rate detection capability. However, the CDF is much tighter with a 10 gpm leak rate detection capability, which indicates less uncertainty about the mean. In both cases, the mean value is well above the SRP Section 3.6.3 acceptance margin of 2. In fact, the minimum value observed over all simulations is nearly twice as high. Results including seismic loads, which are more akin to the SRP Section 3.6.3 approach, are presented in Section 3.2.2.3.

Standard Indicators

Figure 3-4 shows a comparison of the standard indicators for the different simulations. The first observation from these results is that the probabilities of first crack compare quite well. The composite 100,000- and 105,000-realization simulation results fall on top of each other. The 2,000-realization simulation results using the optimized Direct Model 1 show higher probabilities of crack initiation at early times due to more realizations with cracks and is thus more accurate in this region. The results then quickly converge with those from the other two simulations.

These results demonstrate that the sample sizes selected for all three approaches were large enough to generate similar results and that use of the epistemic (outer) loop versus the aleatory (inner) loop to sample the inputs does not affect the mean values.

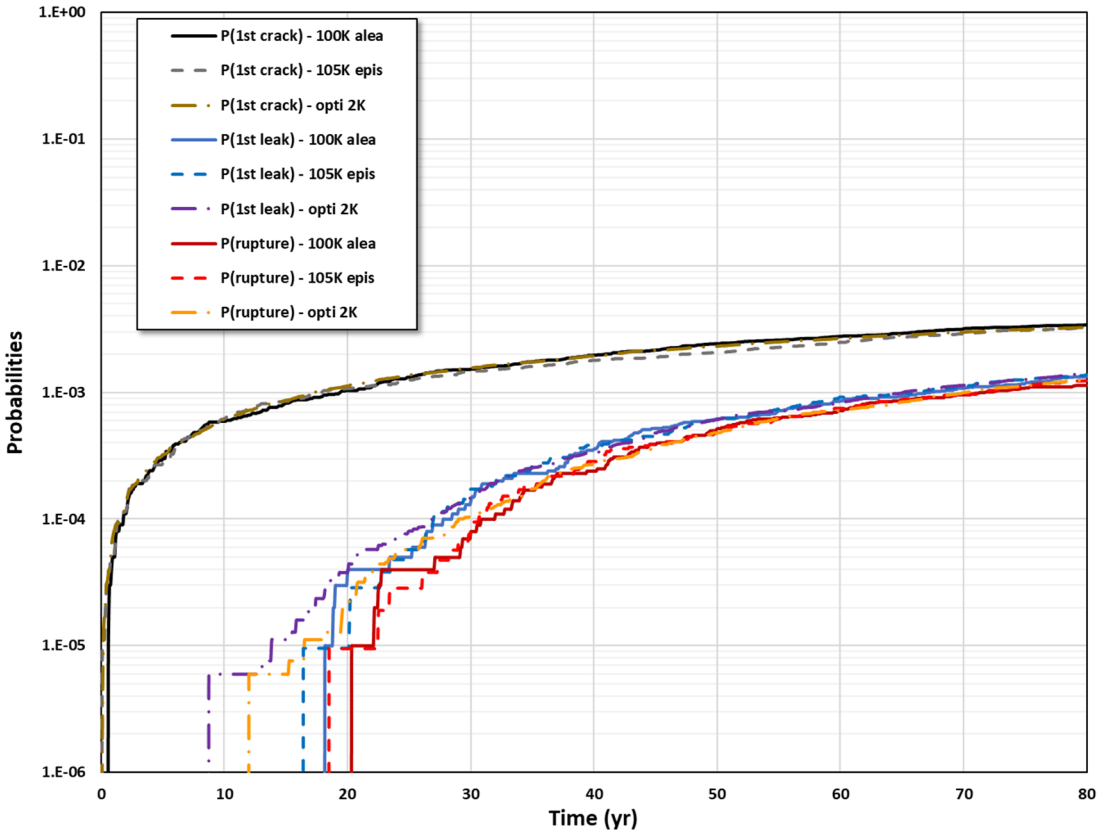


**Figure 3-4 Comparison of Case 1.1.0 time-dependent mean probabilities of first crack, first leak, and rupture using different simulation approaches**

The probabilities of first leak shows some differences up to about 30 EFPY, and then the results from all three simulations converge. Figure 3-5 shows only the probabilities of first leak from the three different simulations. This figure shows that the 2,000-realization simulation using the optimized Direct Model 1 results converge earlier as compared to the other simulations. Convergence occurs when the curves become smooth, and Section 3.2.1.1.3 provides the more detailed convergence analysis results. This outcome is expected because the optimized model ensures that each simulation initiates a crack, which is not the case in the other simulations.

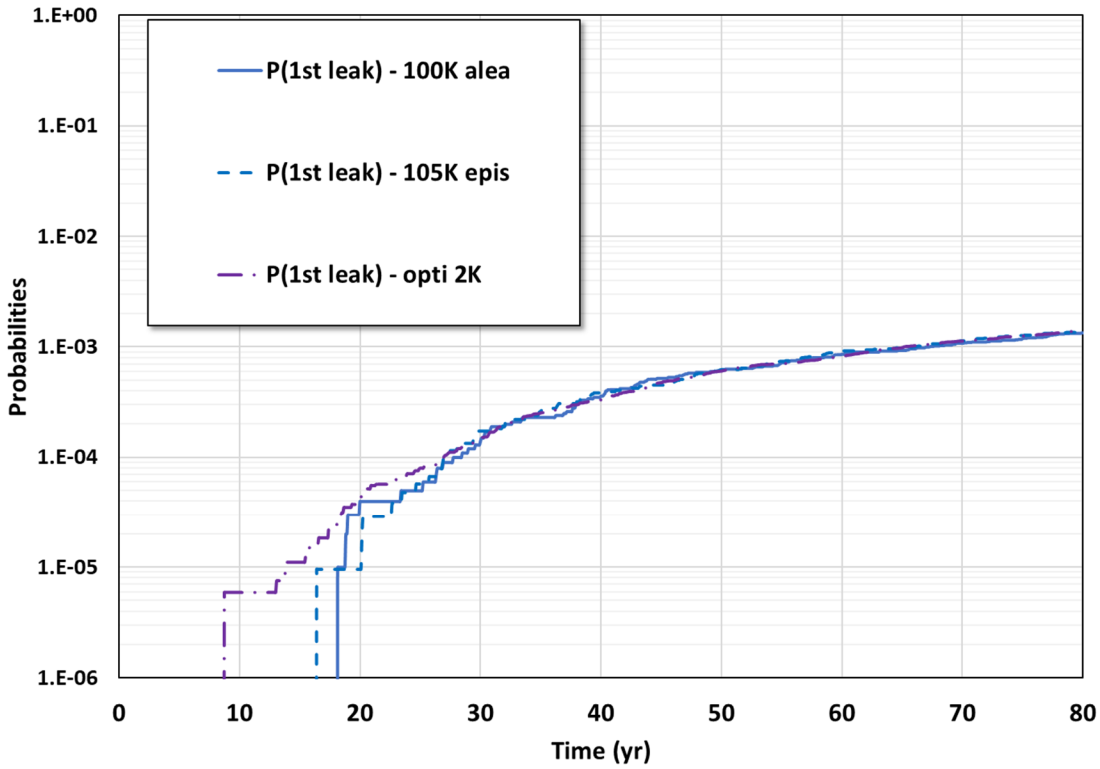


**Figure 3-5 Comparison of Case 1.1.0 time-dependent probabilities of first leak using different simulation approaches**

Figure 3-6 shows only the probabilities of rupture for the three different simulations. This figure also shows that the 2,000-realization simulation using the optimized Direct Model 1 results become smooth earlier when compared to the other two simulations. The reason for this behavior is the same as noted previously for the probabilities of first leak. All the simulations converge to the same probability at 80 EFPY.

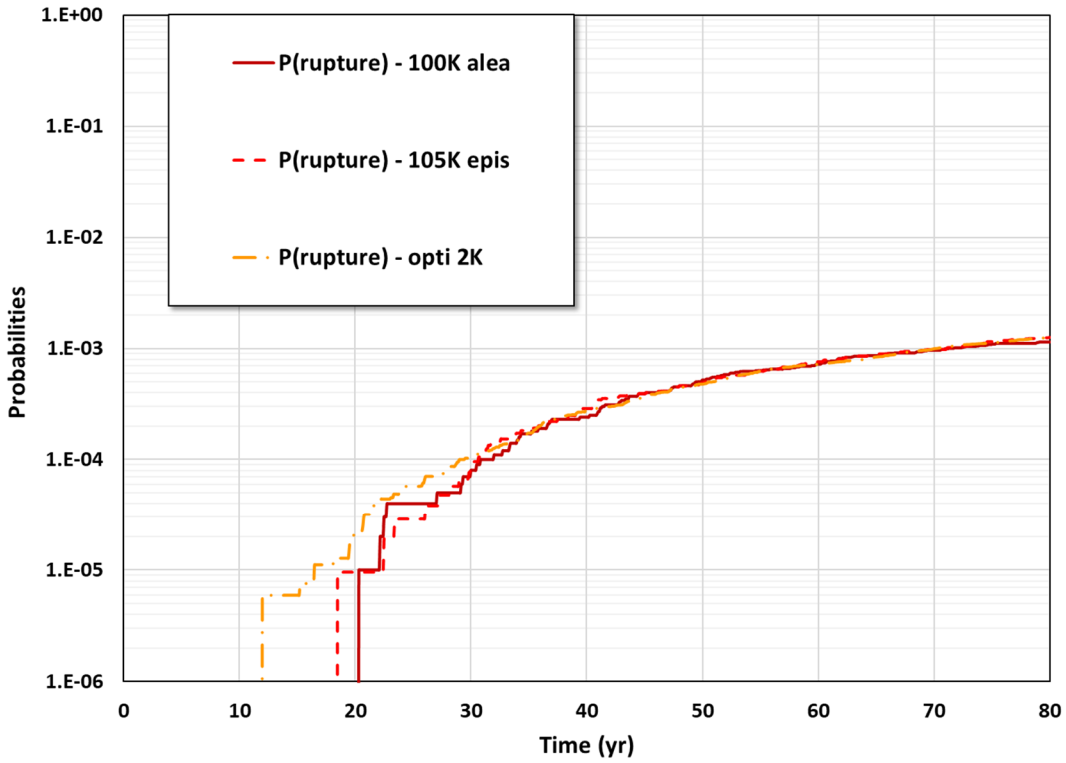


**Figure 3-6 Comparison of Case 1.1.0 time-dependent probabilities of rupture using different simulation approaches**

3.2.1.1.3 Supplemental Analyses

Confidence Intervals

To assess the stability of the Case 1.1.0 results, 95 percent centered confidence intervals between the 2.5$^{th}$ and 97.5$^{th}$ percentiles were estimated for all three standard indicators across all three simulations. Figure 3-7, Figure 3-8, and Figure 3-9 show the results.

The confidence intervals for the 100,000- and 105,000-realization composite simulations were estimated using a binomial distribution to emulate a bootstrap estimate. For the 100,000-realization composite simulation, the confidence intervals start to reduce once a minimum probability of $2 \times 10^{-4}$ is reached, which means that the event of interest occurs in 20 or more realizations. This point is also when the two simulations begin to reach agreement in the results.

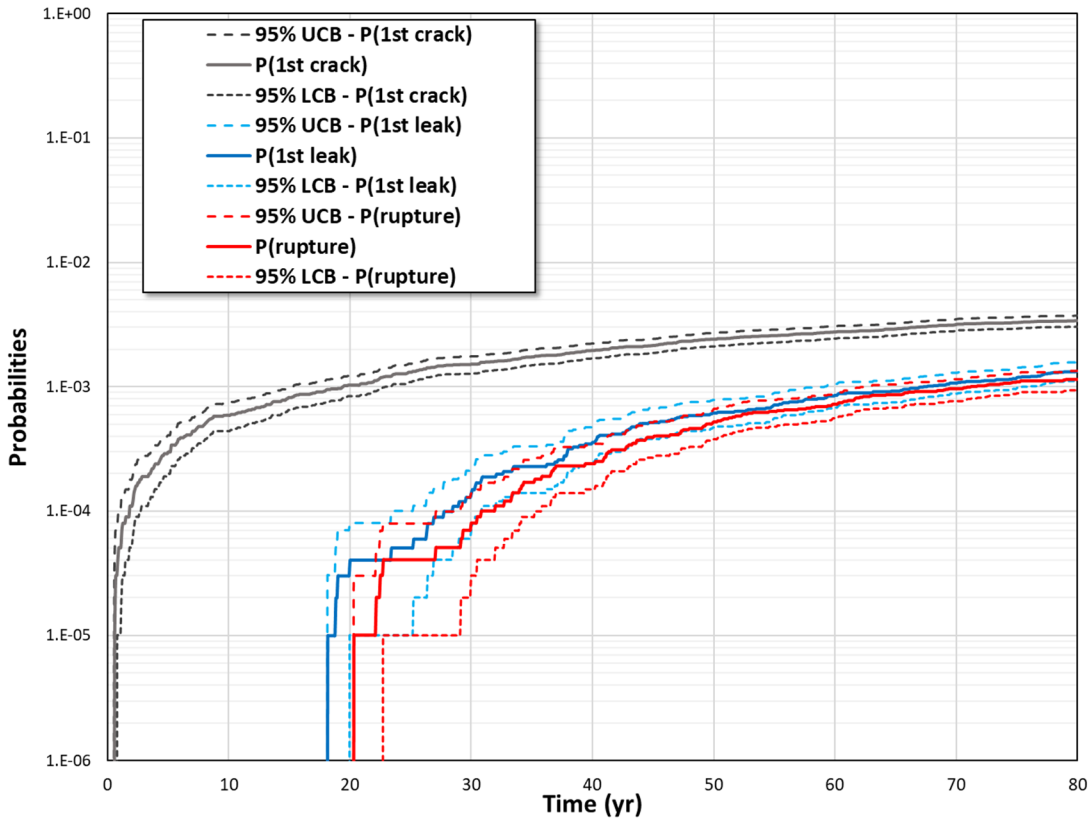


**Figure 3-7 Comparison of Case 1.1.0 time-dependent probabilities of first crack, first leak, and rupture with 95 percent confidence intervals from 100,000 realizations on the aleatory (inner) loop**

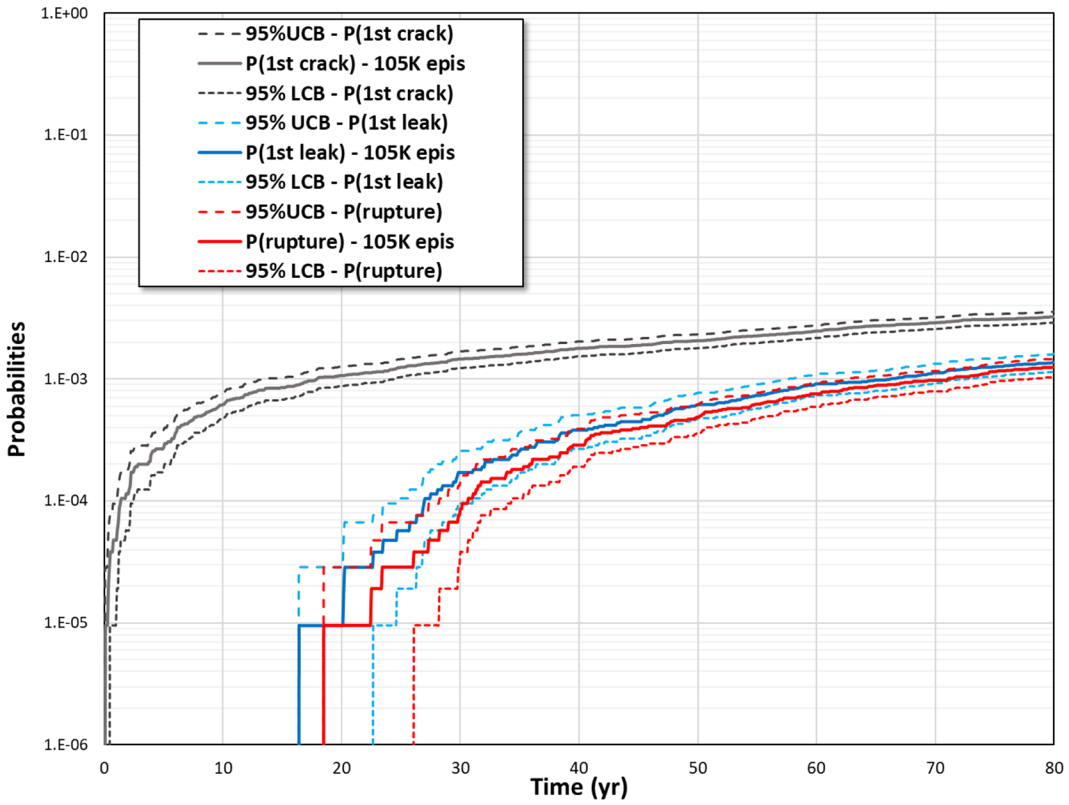


**Figure 3-8 Comparison of Case 1.1.0 time-dependent probabilities of first crack, first leak, and rupture with 95 percent confidence intervals from 105,000 realizations on the epistemic (outer) loop**

The binomial distribution cannot be used to estimate the confidence intervals for the 2,000-realization simulation using the optimized Direct Model 1 because of the weights associated with each realization, so instead a classical q-bootstrap method was used following the 1994 *An Introduction to the Bootstrap* [30]. This method uses resampling with replacement many times and finds the corresponding quantile. The q-bootstrap in this case was estimated using Microsoft Excel with a resampling size of 10,000. The results show tighter confidence intervals compared to the 100,000- and 105,000-realization composite simulations.

By comparing the smoothness of the curves representing the probabilities of first leak and rupture, it appears that use of the optimized Direct Model 1 provides between 4- and 5-times greater accuracy. Put differently, 500,000 realizations using the non-optimized Direct Model 1 would be required to produce an equivalent level of accuracy. Although, this is an extrapolation based on qualitative observations, the variance for the 2,000-realization simulation using the optimized Direct Model 1 was estimated at other timesteps, and it appears that similar accuracy with the 100,000- and 105,000-realization composite simulations is reached at around $5 \times 10^{-4}$. This result indicates an equivalent accuracy to between 400,000 and 500,000 realizations.

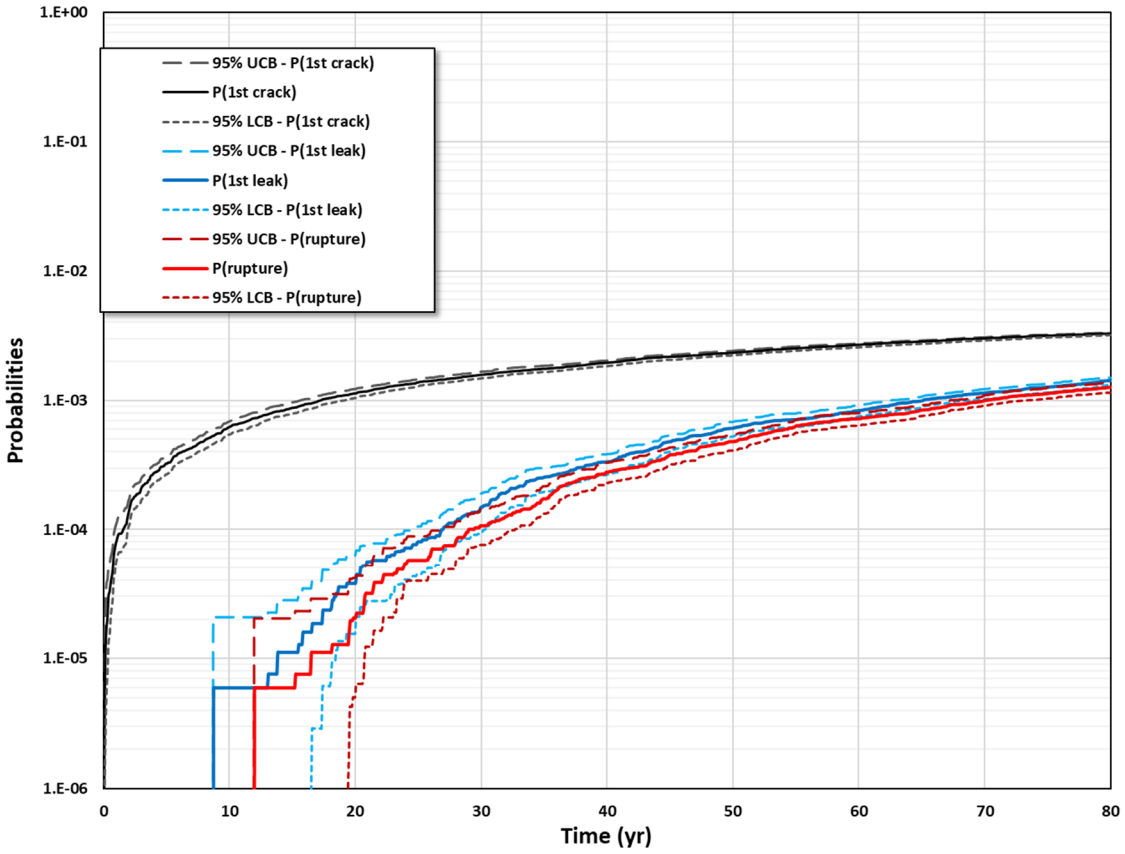


**Figure 3-9 Comparison of Case 1.1.0 time-dependent probabilities of first crack, first leak, and rupture with 95 percent confidence intervals from 2,000 realizations using the optimized Direct Model 1**

Table 3-2 reports the confidence bounds on the probabilities of first leak and rupture from the three different simulations. For the 100,000- and 105,000-realization composite simulations, the 95 percent confidence bounds are within 15 to 22 percent of the calculated mean at 80 EFPY. These results demonstrate adequate statistical convergence for the purposes of this study. For the 2,000-realization simulation using the optimized Direct Model 1, the confidence bounds are between 5 and 10 percent.

**Table 3-2 Variation between confidence bounds and estimated mean values**

| | 100,000 Realizations on the Aleatory (Inner) Loop | | 105,000 Realizations on the Epistemic (Outer) Loop | | 2,000 Realizations with Optimized Direct Model 1 | |
|---|---|---|---|---|---|---|
| | Probability of First Leak | Probability of Rupture | Probability of First Leak | Probability of Rupture | Probability of First Leak | Probability of Rupture |
| **Lower Confidence Bound** | -16.4 % | -21.3 % | -16.0 % | -16.8 % | -8.2 % | -9.0 % |
| **Upper Confidence Bound** | 17.2 % | 15.6 % | 14.3 % | 17.5 % | 5.1 % | 9.4 % |

Distribution Fitting on Leak Rate Increase

Since there was no leak rate jump event in any of the Case 1.1.0 simulations, the estimated probability of such an event is zero. For additional insights, lognormal distributions were fit to the leak rate gains obtained over a 1-month time step after reaching a 10 gpm leak rate. These lognormal distributions were then used to estimate the theoretical likelihood of having a leak rate gain greater than 40 gpm (i.e., 50 gpm minus 10 gpm, the thresholds used to define the leak rate jump QoI). Both a moment-matching fit and a conservatively biased fit were included based on calculations in Microsoft Excel. The biased fit is conservative in that it will over-predict 40-gpm or greater leak rate increases. Such a change in the leak rate jump definition would make it more informative for large diameter piping, and it would provide for more insightful comparisons and potential risk rankings among the base and sensitivity study cases.

Results based on the 100,000-realization composite simulation data are shown in the next set of figures. The moment-matching fit is shown in Figure 3-10 and Figure 3-11 for the whole set of data and the region of interest, respectively. Figure 3-12 shows the conservatively biased fit in the region of interest. The moment-matching lognormal fit gives an estimate of $1.05 \times 10^{-12}$, whereas, the biased fit gives an estimate of $4.09 \times 10^{-9}$. Both results are conditional on having a 10 gpm leak rate, which has a probability of occurrence around $1 \times 10^{-3}$.

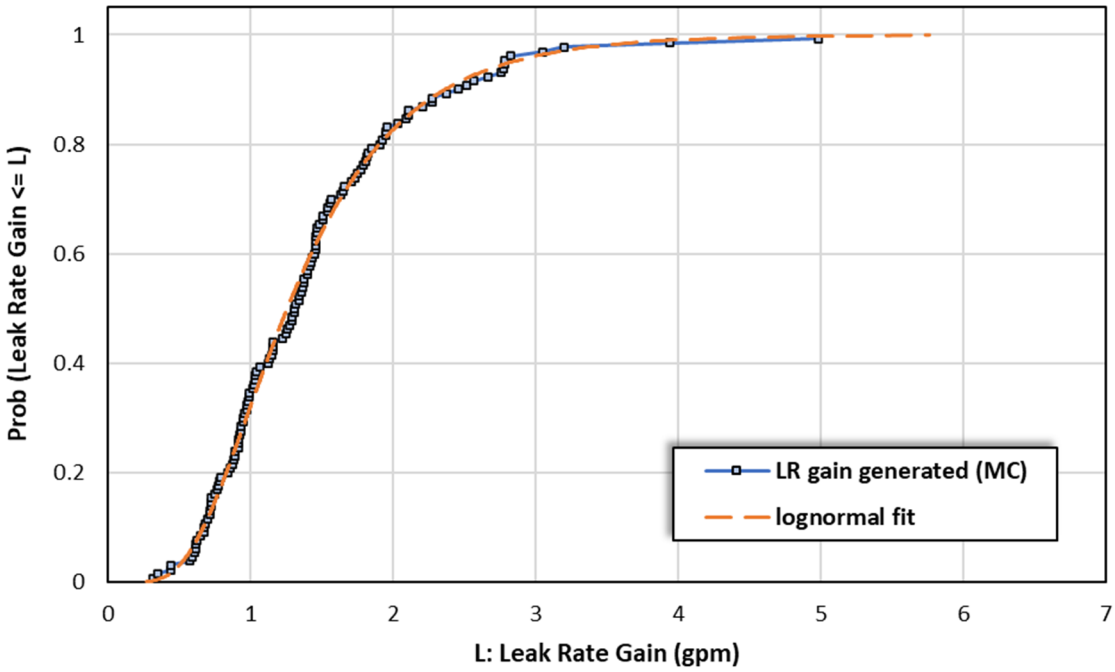


**Figure 3-10 Moment-matching lognormal distribution fit to Case 1.1.0 leak rate increase one month after occurrence of 10 gpm leak from 100,000 realizations on the aleatory (inner) loop**

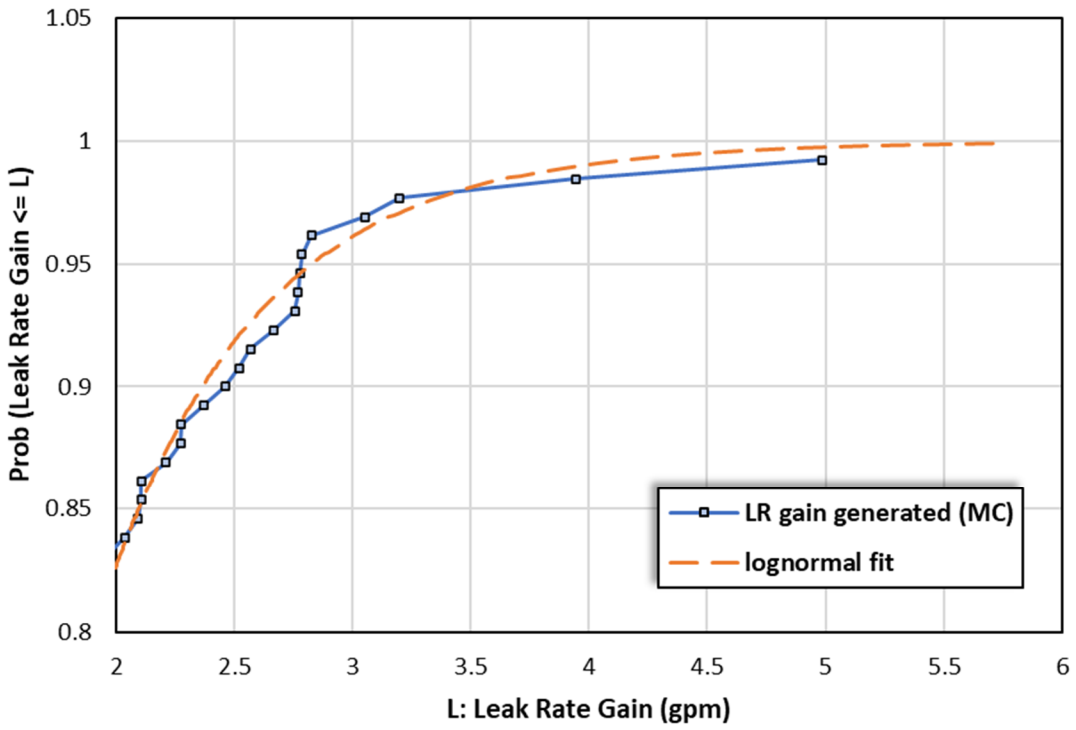


**Figure 3-11 Moment-matching lognormal distribution fit in the region of interest to Case 1.1.0 leak rate increase one month after occurrence of 10 gpm leak from 100,000 realizations on the aleatory (inner) loop**

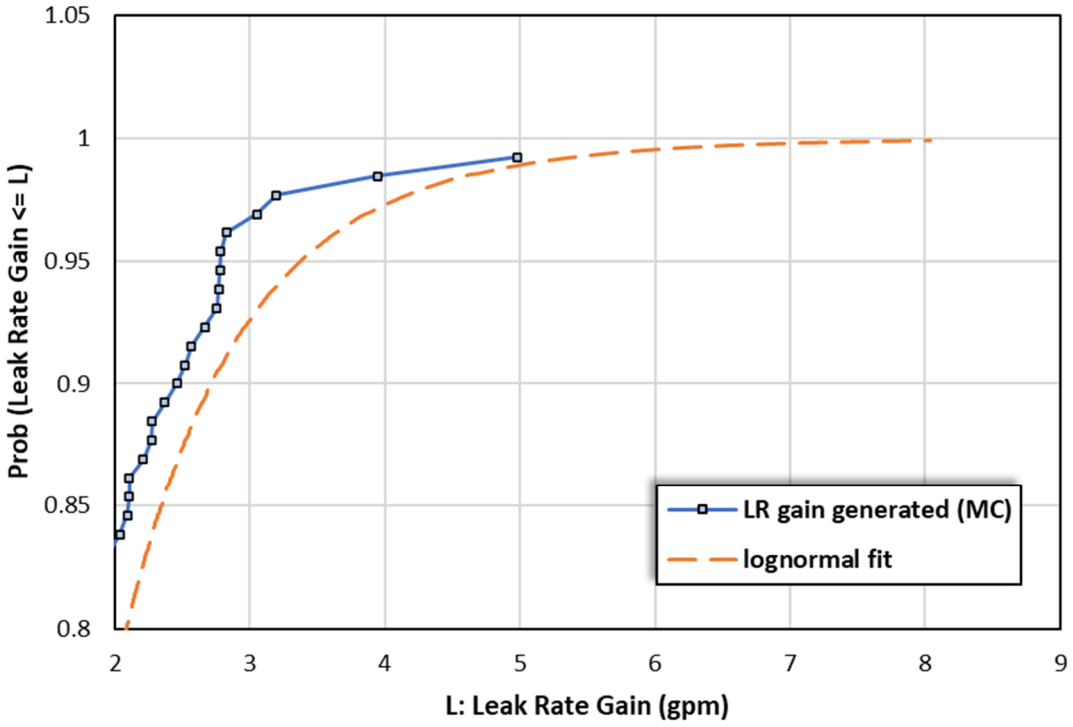


**Figure 3-12 Conservatively biased lognormal distribution fit in the region of interest to Case 1.1.0 leak rate increase one month after occurrence of 10 gpm leak from 100,000 realizations on the aleatory (inner) loop**

Similar results based on the 105,000-realization composite simulation data are shown in Figure 3-13. The moment-matching lognormal distribution, which is already conservative for high values, gives an estimate of $1.94 \times 10^{-11}$. Again, the results are conditional on having a 10 gpm leak rate, which has a probability of occurrence around $1 \times 10^{-3}$.

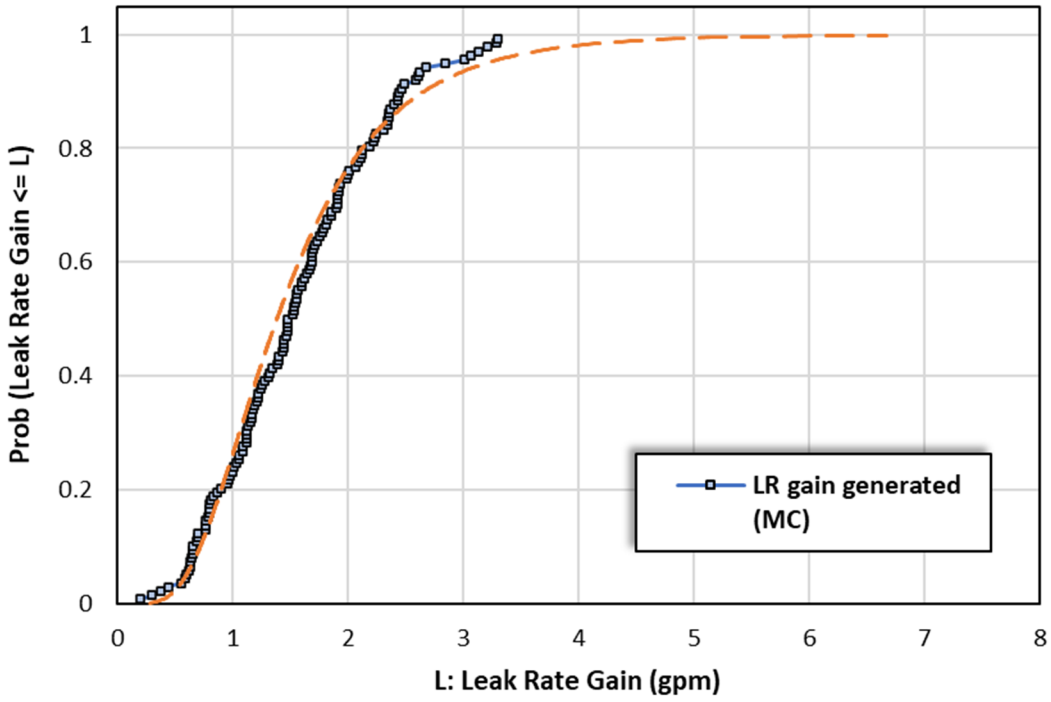


**Figure 3-13 Moment-matching lognormal distribution fit to Case 1.1.0 leak rate increase one month after occurrence of 10 gpm leak from 105,000 realizations on the epistemic (outer) loop**

Finally, Figure 3-14 shows a comparison of the leak rate gain distributions based on data from the 100,000- and 105,000-realization composite simulations and the 2,000-realization simulation using the optimized Direct Model 1. The latter dataset has more realizations with TWCs (i.e., 690 versus 129 and 137, respectively); therefore, the resulting distribution is smoother and more accurate.

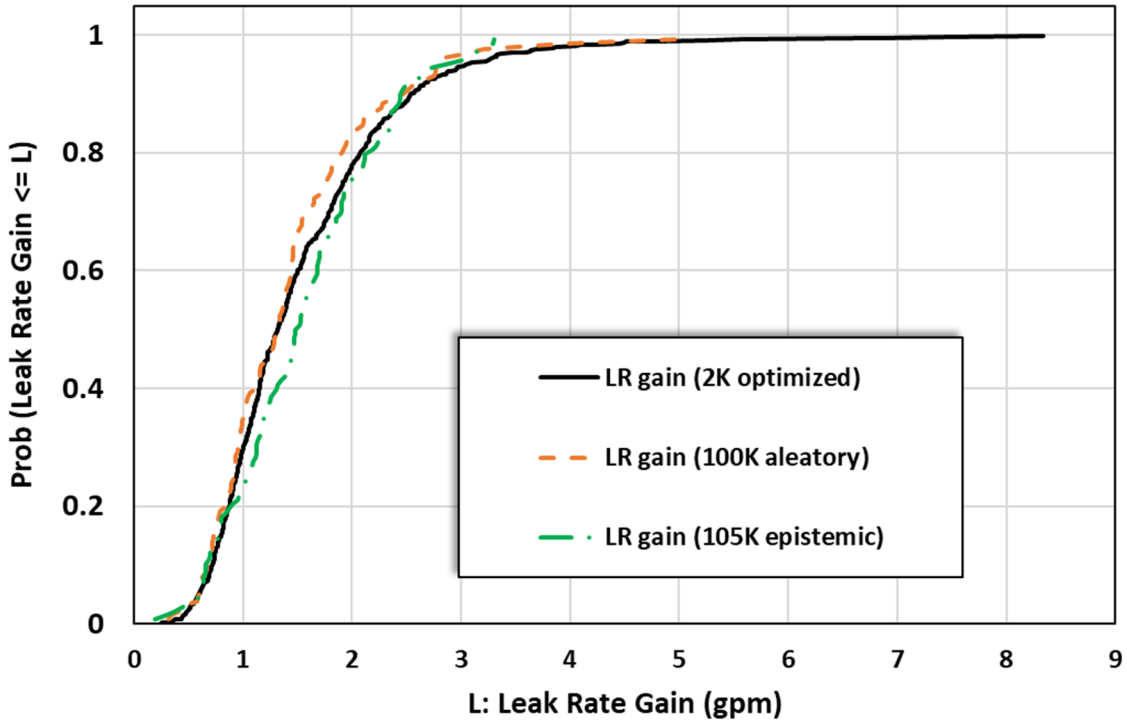


**Figure 3-14 Comparison of Case 1.1.0 leak rate increase one month after occurrence of 10 gpm leak using different simulation approaches**

Comparison of LBB Ratio with Deterministic LBB Analysis

To provide context, the probabilistic results from Case 1.1.0 were compared with results from a deterministic LBB analysis prepared following the guidance in SRP Section 3.6.3. The guidance states that a deterministic fracture mechanics and leak rate evaluation should be performed, and the acceptance criteria for the analysis are as follow:

- The through-wall flaw size should be large enough so that leakage from the flaw during normal operation would be 10 times greater than the minimum leakage the detection system is capable of sensing.
- Using fracture mechanics stability or limit load analysis, the critical crack size for the postulated TWC using loads from the normal plus SSE should have a margin of at least 2 on the leakage crack size.
- The size of the leaking cracks should not become unstable if 1.4 times the normal plus SSE loads are applied. This margin should be reduced to 1.0 if the normal plus SSE loads are combined based on the absolute sum method.

The deterministic LBB analysis was approached like a vendor would when preparing a licensing submittal for NRC staff review. Accordingly, a circumferential TWC in the weld was assumed.

The detectable leak rate was assumed to be 1 gpm and, to meet the SRP Section 3.6.3 acceptance criterion, a factor of 10 was then applied.

Using 10 gpm as the target leak rate, the SQUIRT4 module of the "SQUIRT" code, as documented in NUREG/CR-4599, "Short Cracks in Piping and Piping Welds—Semiannual Report October 1992 – March 1993, Vol. 3, No. 2," issued March 1994 [31], was used to determine the leakage crack size. The inputs for the SQUIRT4 module are listed in Section B1. The material property data used was for 316 stainless steel. The crack was assumed to be in the weld close to the stainless steel base metal; therefore, the material property data for the SA-508 carbon steel was not used in the analysis. In addition, although not a direct input into SQUIRT4, the J-R curve of form $J_{mat} = J_{Ic} + C(\Delta a)^m$, with $J_{Ic} = 524.3\ N/mm$, $C = 586.3$, and $m = 0.661$, values which are representative of Alloy 82/182 materials, was used for the weld metal. Neither crack face pressure nor WRS were applied in the analysis because these stresses are not taken into consideration in SRP Section 3.6.3 guidance.

The leakage crack size calculated by SQUIRT4 was 135.94 millimeters (mm), which represents about 5 percent of the circumference. Next, the "NRCPIPE" code using the "LBB.ENG2" method, also as documented in NUREG/CR-4599 [31], was used to determine crack instability. The inputs to the analysis included the leakage crack size, applied bending moment of4593.5 kilonewton-meters (kN-m), and total axial force of 6401.0 kN (i.e., 6805.8 kN from the operating pressure and -404.79 kN from the normal operating loads) converted to an equivalent pressure. For the NRCPIPE analysis, the base metal Ramberg-Osgood material properties and weld metal J-R curve were used as described previously.

SRP Section 3.6.3 provides two methods to combine the loads: algebraic sum and absolute sum. If the algebraic sum method is used to combine the deadweight, thermal expansion, pressure, SSE, and seismic anchor motion loads, then a factor of 1.4 should be applied to their sum. The critical crack size calculated using this method should be greater than the leakage crack size by a margin of at least 1.0 to meet the margin on load. In addition, to meet the margin on crack size, the critical crack size is determined using a factor of 1.0 on stress in the algebraic sum method, and it must be greater than the leakage crack size by a margin of at least 2.0. If the absolute sum method is used to combine the loads, then the safety factor is reduced to 1.0. The critical crack size using this method should be greater than the leakage crack size by a factor of 2.0 to meet the margin on both load and crack size. Both methods were used to determine the critical crack sizes for this analysis.

Using the absolute sum method, the critical crack size was determined to be 515.69 mm. Since the leakage crack size is 135.94 mm, the margin between the two is 3.79. Therefore, the SRP Section 3.6.3 margins on both load and crack size are met. Using the algebraic sum method, the critical crack size was determined to be 352.1 mm. This crack size was determined using a safety factor of 1.4 on the loads and is larger than the leakage crack size; therefore, the SRP Section 3.6.3 margins on load are met. In addition, the crack size using a factor of 1.0 on loads (515.69 mm) is greater than 2 times the leakage crack size; therefore, the SRP Section 3.6.3 margins on crack size are also met. The margin between the algebraic sum method critical crack size and leakage crack size is 2.59.

The preceding results were calculated using COD-dependent crack morphology parameters. However, most traditional LBB analyses did not use this approach; therefore, a separate set of results was generated using COD-independent crack morphology parameters. In this case, the leakage crack size changes from 135.94 mm to 178.2 mm, and the margins are reduced from 3.79 to 2.89 for the absolute sum method and from 2.59 to 1.98 for the algebraic sum method.

Table 3-3 summarizes the results of the deterministic LBB analysis using 316 stainless steel material properties, which is a more conservative approach. The same analysis was also performed used an equal mixture of the 316 stainless steel and SA-508 carbon steel base metal material properties, like the approach used in the xLPR code analyses. Higher margins were calculated in all cases as shown in Table 3-4. The range of results is presented to illustrate that there can be different interpretations of the same inputs or different calculation techniques, which could lead to different conclusions. However, the results highlight the importance of the leakage crack size and the ability to accurately calculate the leak rate. The next subsection compares the deterministic LBB analysis results with the probabilistic LBB ratios.

**Table 3-3 Case 1.1.0 deterministic LBB analysis results using only 316 stainless steel material properties**

| | Leakage Crack Size (mm) | Critical Crack Size (mm) | Margin |
|---|---|---|---|
| **Using Non-COD-Dependent Crack Morphology Absolute Sum Method** | 178.2 | 515.69 | 2.89 |
| **Using Non-COD-Dependent Crack Morphology Algebraic Sum Method** | 178.2 | 352.1 | 1.98 |
| **Using COD-Dependent Crack Morphology Absolute Sum Method** | 135.94 | 515.69 | 3.79 |
| **Using COD Dependent Crack Morphology Algebraic Sum Method** | 135.94 | 352.1 | 2.59 |

**Table 3-4 Case 1.1.0 deterministic LBB analysis results using an equal mixture of the base metal material properties from 316 stainless steel and SA-508 carbon steel**

| | Leakage Crack Size (mm) | Critical Crack Size (mm) | Margin |
|---|---|---|---|
| **Using Non-COD-Dependent Crack Morphology Absolute Sum Method** | 231.59 | 702.13 | 3.30 |
| **Using Non-COD-Dependent Crack Morphology Algebraic Sum Method** | 231.59 | 587.79 | 2.54 |
| **Using COD-Dependent Crack Morphology Absolute Sum Method** | 176.17 | 702.13 | 3.99 |
| **Using COD Dependent Crack Morphology Algebraic Sum Method** | 176.17 | 587.79 | 3.00 |

Distribution Fitting on LBB Ratio Results

The results from the deterministic LBB analysis prepared following the guidance in SRP Section 3.6.3 were compared to the probabilistic analysis results using the LBB ratio QoI. To perform this comparison, normal distributions were fit to the LBB ratio data based on a 10 gpm leak rate detection capability. These normal distributions were then used to estimate the likelihood of not meeting the minimum margins in SRP Section 3.6.3. Both a moment-matching fit and a conservatively biased fit were included. The bias is conservative in that it will under-predict the LBB ratio.

Results based on the 100,000-realization composite simulation data are shown in the next set of figures. The moment-matching fit is shown in Figure 3-15 and Figure 3-16 for the whole set of data and the region of interest, respectively. Figure 3-17 shows the conservatively biased fit in the region of interest.

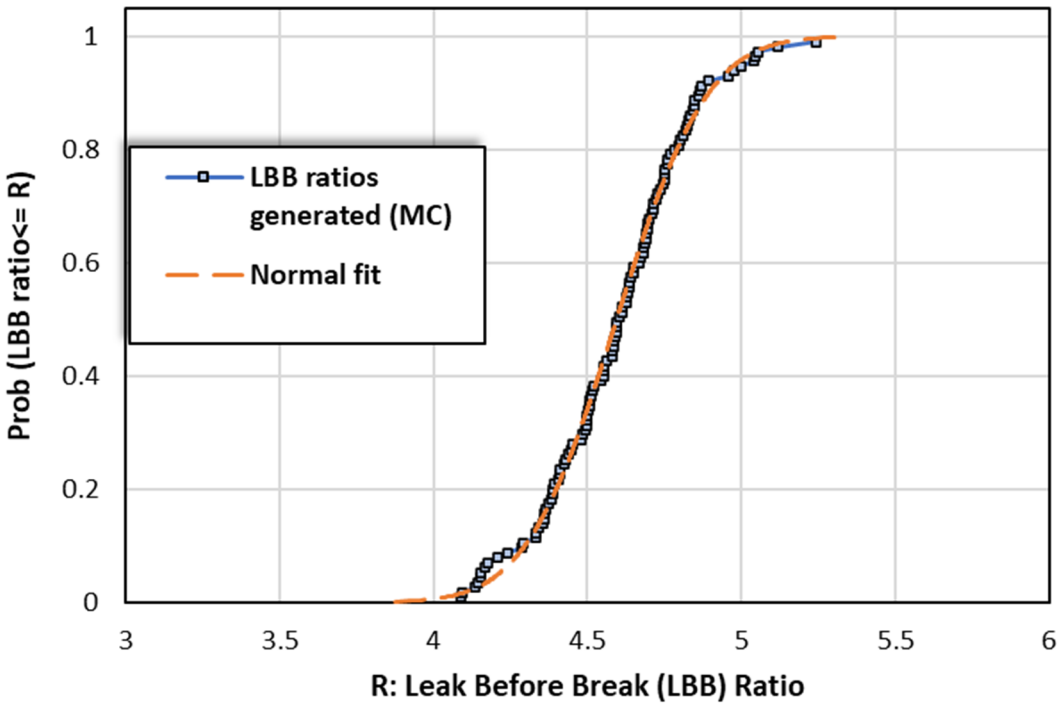


**Figure 3-15 Moment-matching normal distribution fit to Case 1.1.0 LBB ratio with a 10 gpm leak rate detection capability from 100,000 realizations on the aleatory (inner) loop**

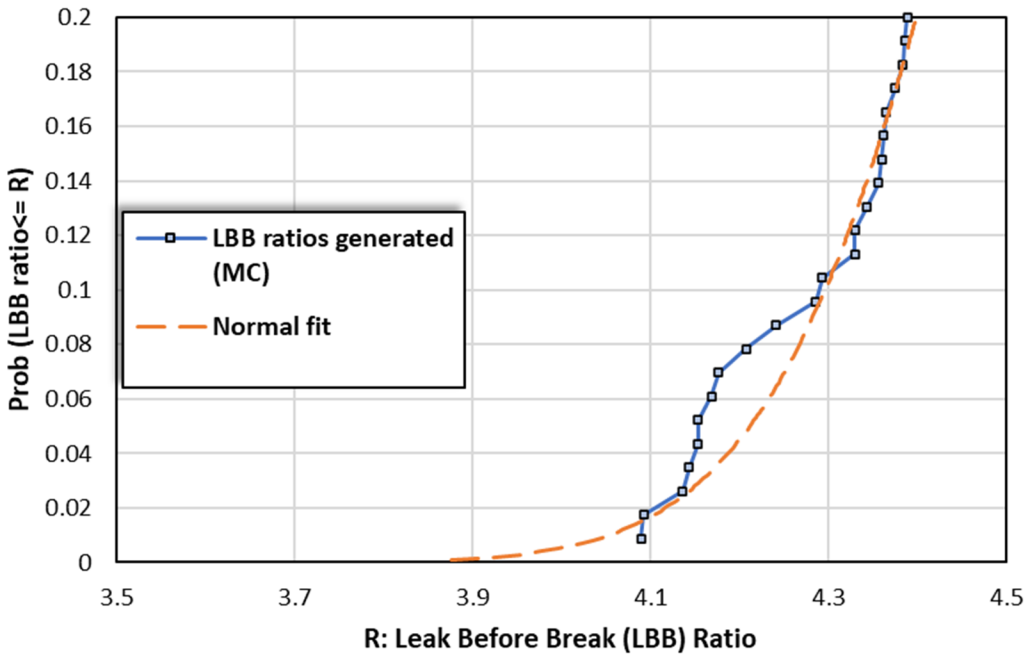


**Figure 3-16** **Moment-matching normal distribution fit in region of interest to Case 1.1.0 LBB ratio with a 10 gpm leak rate detection capability from 100,000 realizations on the aleatory (inner) loop**

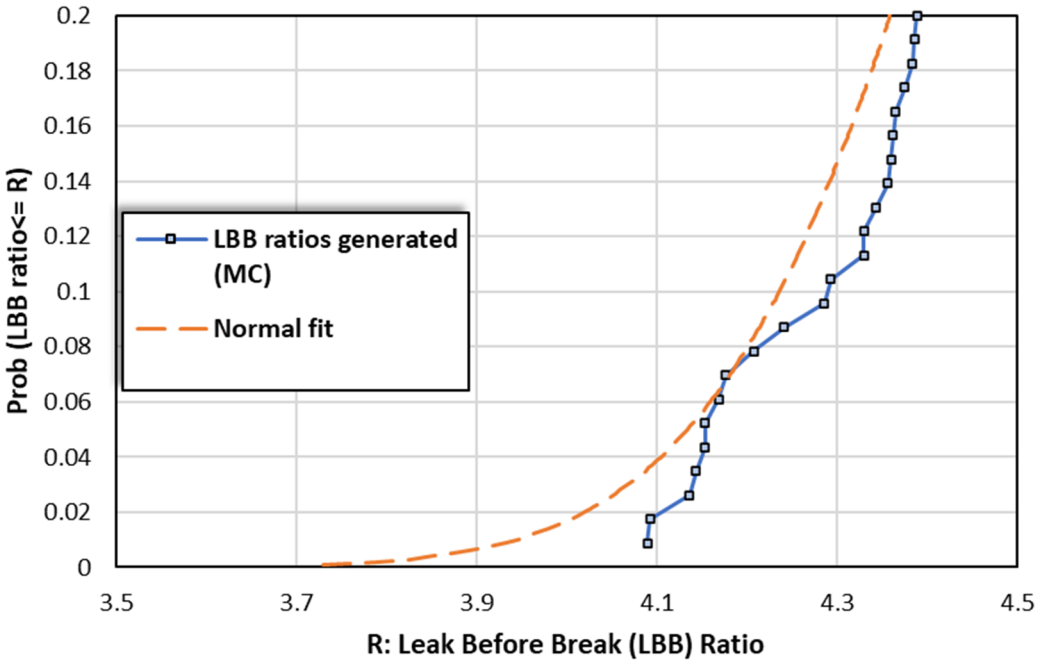


**Figure 3-17** **Conservatively biased normal distribution fit in region of interest to Case 1.1.0 LBB ratio with a 10 gpm leak rate detection capability from 100,000 realizations on the aleatory (inner) loop**

Similar moment-matching results based on the 105,000-realization composite simulation data are shown in Figure 3-18.

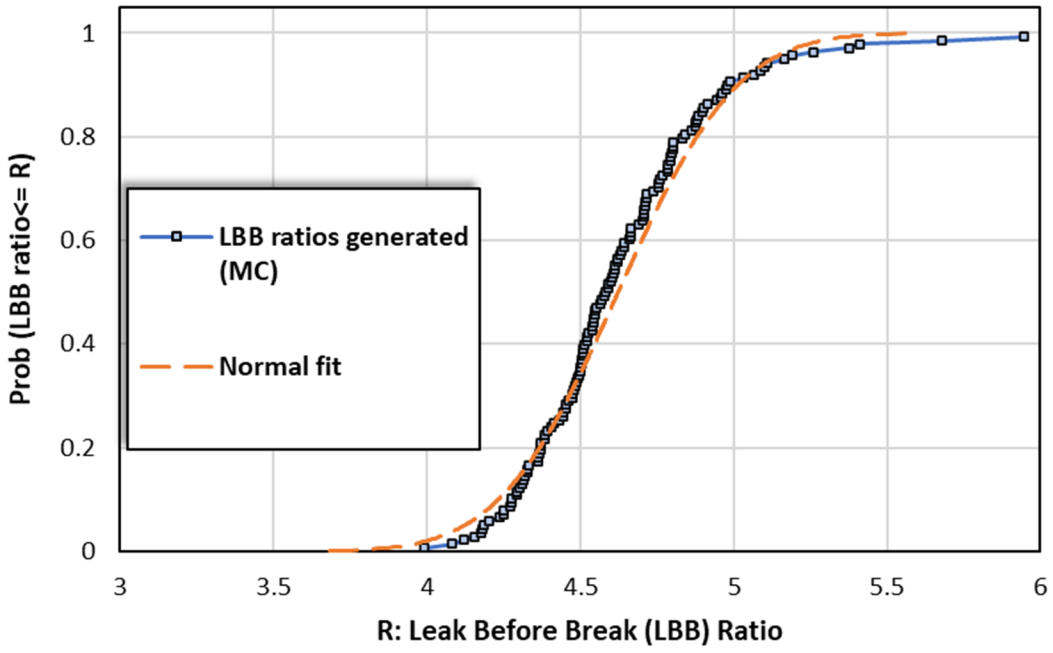


**Figure 3-18 Moment-matching normal distribution fit to Case 1.1.0 LBB ratio with a 10 gpm leak rate detection capability from 105,000 realizations on the epistemic (outer) loop**

Finally, Figure 3-19 shows the moment-matching results based on the 2,000-realization simulation using the optimized Direct Model 1. The result is smoother, yet still consistent with the results from the 100,000- and 105,000-realization composite simulations.

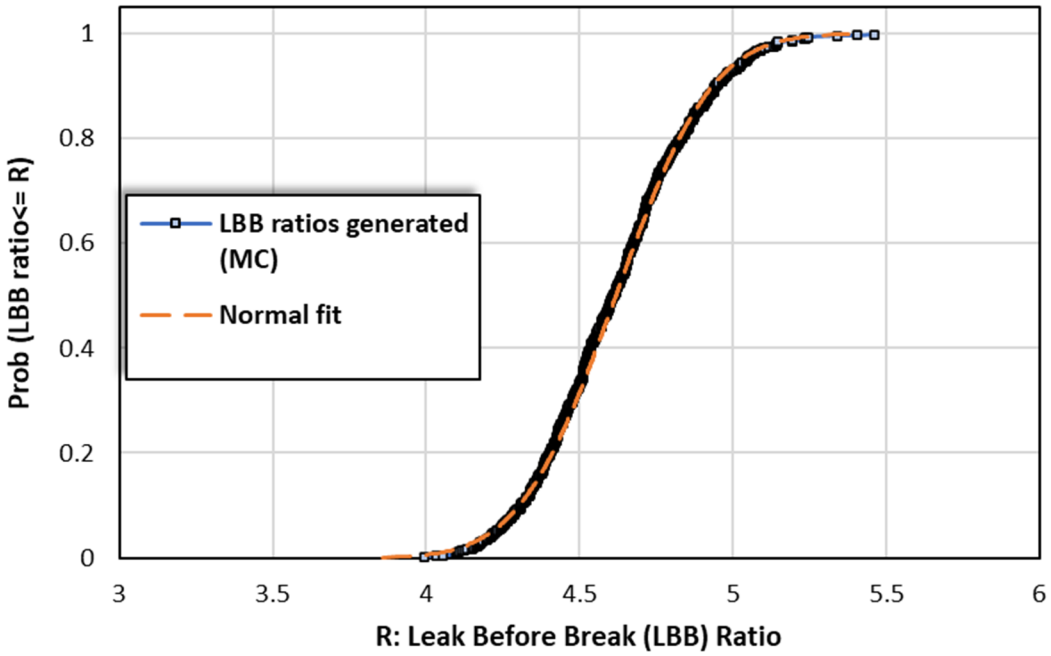


**Figure 3-19 Moment-matching normal distribution fit to Case 1.1.0 LBB ratio with a 10 gpm leak rate detection capability from 2,000 realizations using the optimized Direct Model 1**

SRP Section 3.6.3 states that ratio between the critical and leakage crack sizes should be at least 2.0. The normal distributions fits based on the preceding figures were used to estimate the likelihood of having a ratio smaller than 2.0. With the moment-matching normal distribution fit, the probability of such an event is estimated to be around $3.44 \times 10^{-29}$ (i.e., essentially 0). With the conservatively biased fit, the probability is estimated to be $9.54 \times 10^{-21}$ and $3.88 \times 10^{-18}$ for the 100,000-and 105,000-realiztion composite simulations, respectively. The estimated probability of having an LBB ratio less than or equal to 2.0 is $9.31 \times 10^{-27}$ based on the moment-matching normal distribution fit to the data from the 2,000-realization simulation using the optimized Direct Model 1. The probabilistic results thus highlight conservatisms present in the deterministic LBB approach as applied to the RVON weld.

Distribution Fitting on LBB Time Lapse Results

The LBB time lapse data based on a 10 gpm leak rate detection capability can also be represented by fitting a lognormal distribution. These lognormal distributions were then used to estimate the likelihood of having an LBB time lapse less than a certain length of time. Both a moment-matching fit and a conservatively biased fit (i.e., one that bounds all the data points) were prepared. The bias is conservative in that it will underpredict the amount of time between leakage and rupture.

Results based on the 100,000-realization composite simulation data are shown in the next set of figures. The moment-matching fit is shown in Figure 3-20 and Figure 3-21 for the whole set of

data and the region of interest, respectively. Figure 3-22 shows the conservatively biased fit in the region of interest.

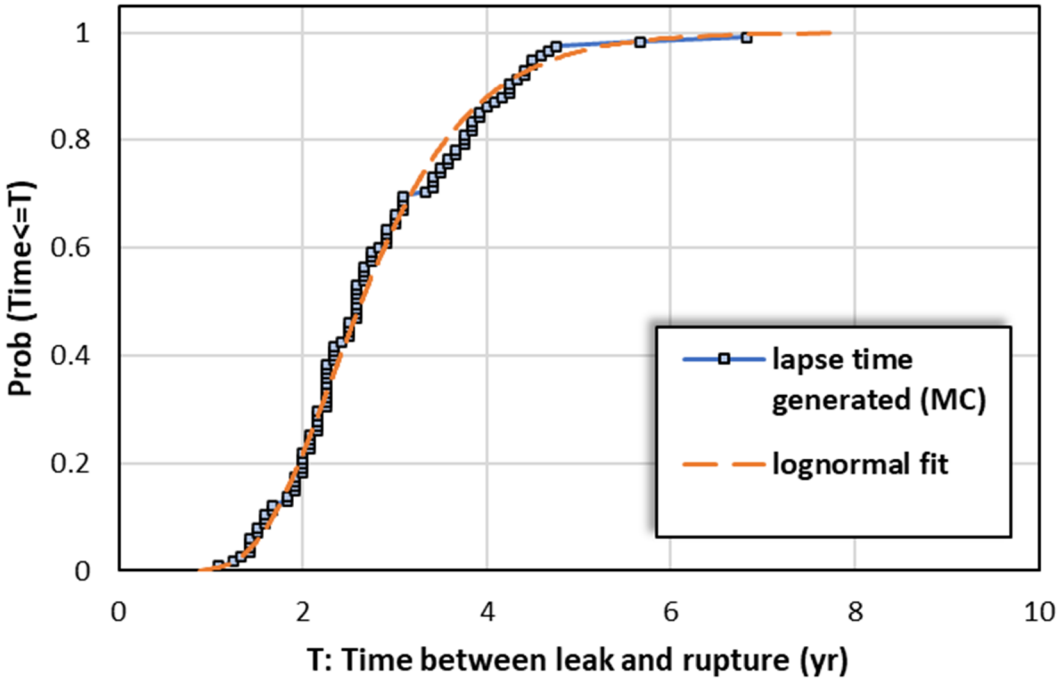


**Figure 3-20 Moment-matching lognormal distribution fit to Case 1.1.0 LBB time lapse with a 10 gpm leak rate detection capability from 100,000 realizations on the aleatory (inner) loop**

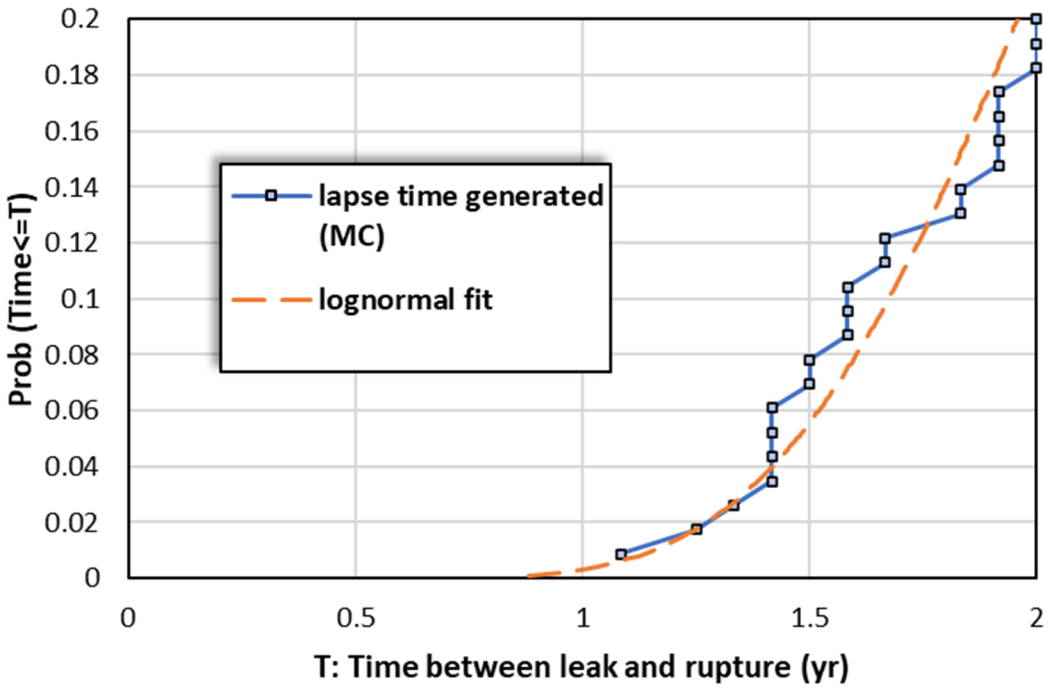


**Figure 3-21 Moment-matching lognormal distribution fit in region of interest to Case 1.1.0 LBB time lapse with a 10 gpm leak rate detection capability from 100,000 realizations on the aleatory (inner) loop**

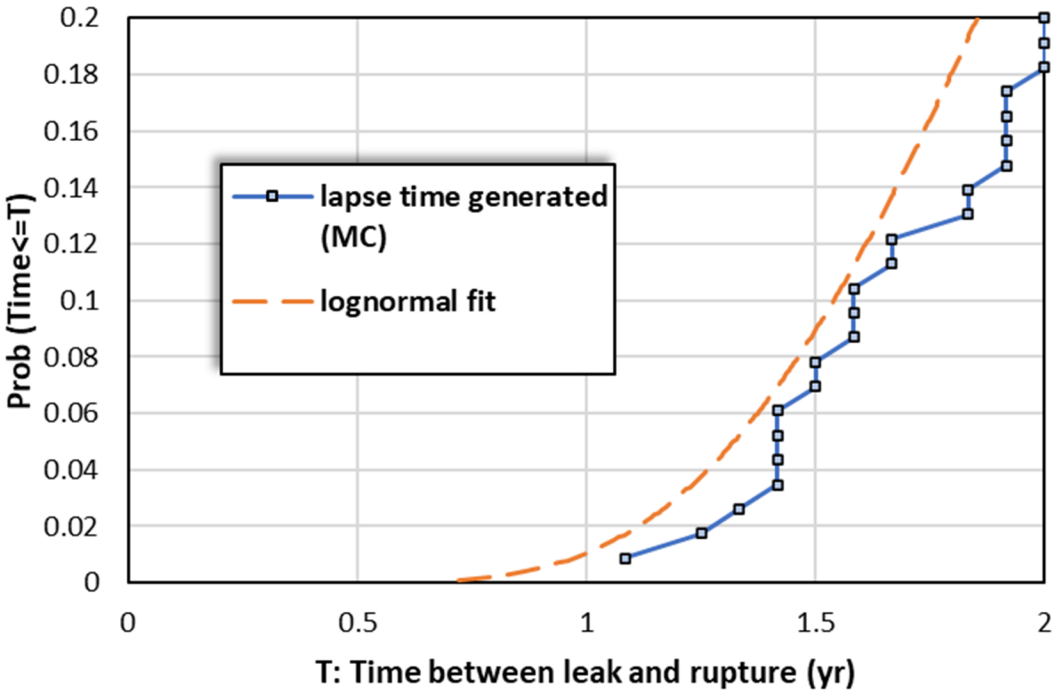


**Figure 3-22 Conservatively biased lognormal distribution fit in region of interest to Case 1.1.0 LBB time lapse with a 10 gpm leak rate detection capability from 100,000 realizations on the aleatory (inner) loop**

Similar moment-matching results based on the 105,000-realization composite simulation data are shown in Figure 3-23. Figure 3-24 shows that the moment-matching lognormal fit is conservative in the lower tail of the distribution.

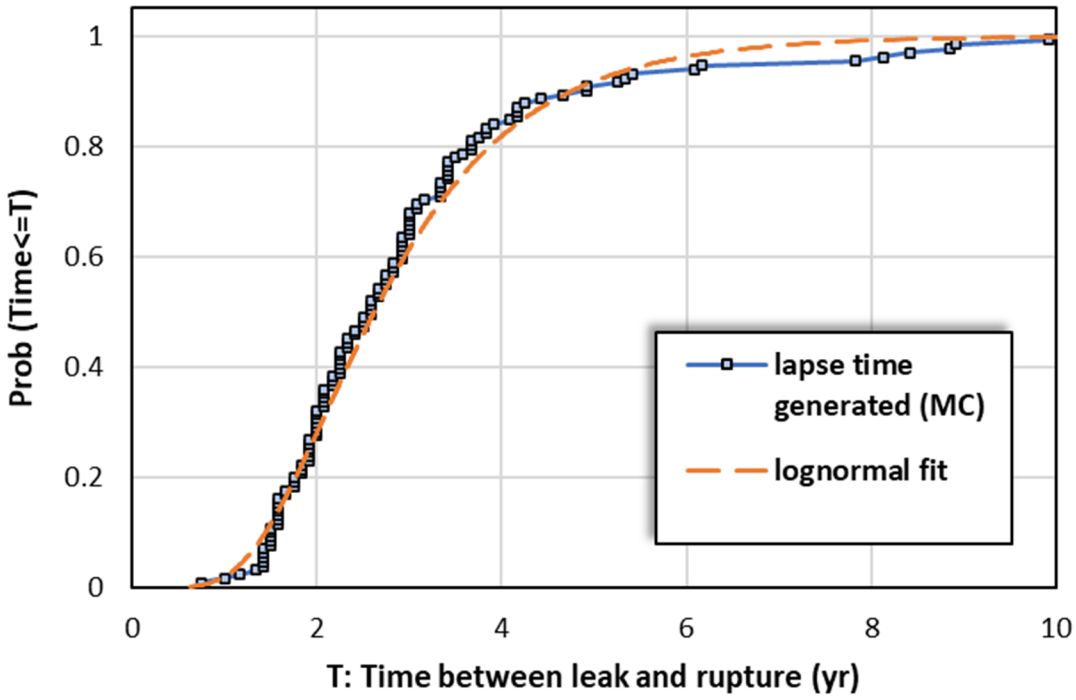


**Figure 3-23 Moment-matching lognormal distribution fit to Case 1.1.0 LBB time lapse with a 10 gpm leak rate detection capability from 105,000 realizations on the epistemic (outer) loop**

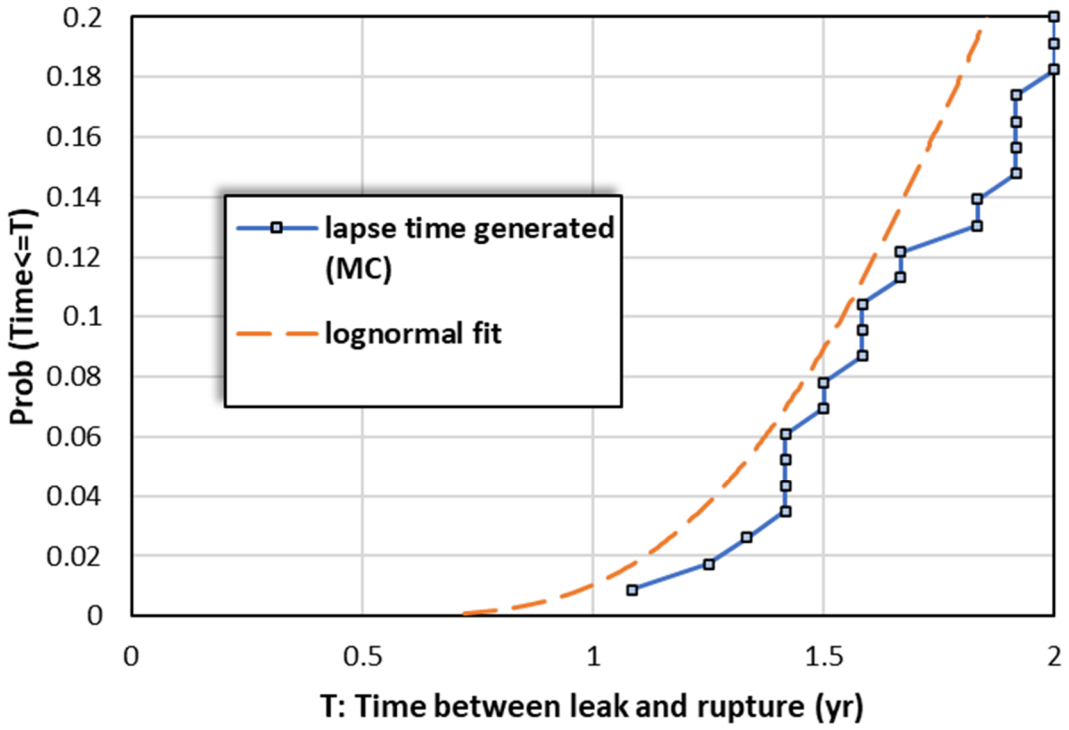


**Figure 3-24 Conservatively biased moment-matching lognormal distribution fit in region of interest to Case 1.1.0 LBB time lapse with a 10 gpm leak rate detection capability from 105,000 realizations on the epistemic (outer) loop**

Finally, Figure 3-25 shows the moment-matching results based on the 2,000-realization simulation using the optimized Direct Model 1. The resulting distribution is a lot smoother than the other simulations and matches closely with the lognormal distribution fit.

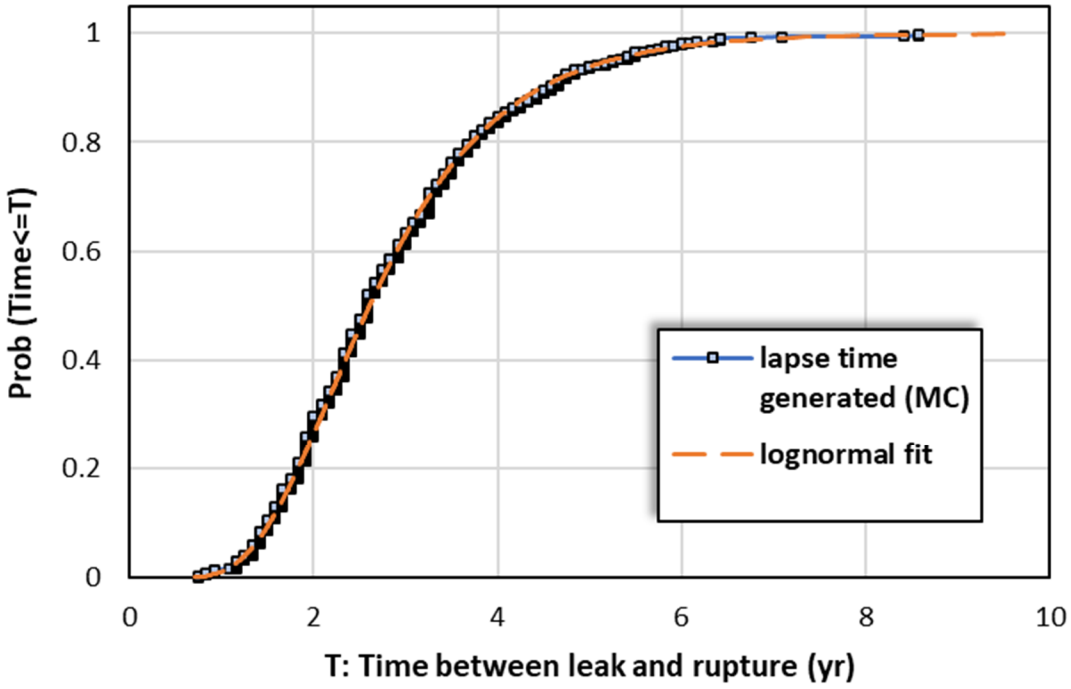


**Figure 3-25 Moment-matching lognormal distribution fit to Case 1.1.0 LBB time lapse with a 10 gpm leak rate detection capability from 2,000 realizations using the optimized Direct Model 1**

The lognormal distributions based on the preceding figures were used to estimate the probabilities of two events occurring over 80 EFPY of plant operation: (1) an LBB time lapse less than or equal to 1 month, which represents the time step used in the simulation, and (2) an LBB time lapse less than or equal to 4 months. The latter is a more conservative threshold for the minimum LBB time lapse that was selected for comparison purposes. With the moment-matching fit based on the 100,000-realization composite simulation results, the probability of the LBB time lapse being less than or equal to 1 month is estimated to be $9.7 \times 10^{-23}$, and the probability of it being less than or equal to 4 months is estimated to be $2.7 \times 10^{-9}$. Using the conservatively biased fit, the probabilities increase to $9.7 \times 10^{-17}$ and $4.2 \times 10^{-7}$, respectively. The moment-matching lognormal distribution fit to the data from the 2,000-realization simulation using the optimized Direct Model 1 is conservative on the lower tail. Using this distribution, the estimated probability of an LBB time lapse being less than 1 month is $5.31 \times 10^{-14}$, and the probability of it being less than 4 months is $4.39 \times 10^{-6}$. With the moment-matching fit based on the 2,000-realization simulation using the optimized Direct Model 1, the probability of the LBB time lapse being less than or equal to 1 month is estimated to be $1.32 \times 10^{-16}$, and the probability of it being less than or equal to 4 months is estimated to be $4.97 \times 10^{-7}$. All these probabilities are conditional on having ruptures, which is around $1 \times 10^{-3}$ over 80 EFPY of plant operation.

#### *3.2.1.2 Initial Flaw*

3.2.1.2.1 Case Description

The objective of Case 1.1.1 was to assess the sensitivity of the likelihood of failure based on whether the crack initiation process is modeled in the analysis. It is like Case 1.1.0 except that it uses the initial flaw density option instead of Direct Model 1. The hydrogen concentration in the reactor coolant system was set to 37 cc/kg, which is the same value as used in Case 1.1.0. Case 1.1.1 was also used as a basis of comparison for many of the sensitivity studies.

In the xLPR code, the initial flaw density option can be used to seed pre-existing crack(s) at the beginning of the simulation. Case 1.1.1 was analyzed using a single circumferential crack because the likelihood of having 2 or more cracks occurring over 80 EFPY of plant operation is estimated to be around $9.5 \times 10^{-5}$ based on the number of realizations with 2 or more circumferential cracks. This estimate equates to an annual frequency of $1.2 \times 10^{-6}$. Furthermore, it is likely that the time between the occurrences of these cracks will be large enough such that they would not interact most of the time. The depth and length of the initial crack were sampled from lognormal distributions with median values of 1.5 and 4.8 mm, respectively. These distributions are the same ones used in Case 1.1.0 for PWSCC-initiated cracks.

A single loop was used with all uncertain inputs placed on the epistemic (outer) loop. A sample size of 5,000 realizations was used, which was considered adequate given that each realization begins with a crack. Section B2 describes the specific inputs and other simulation details used to analyze this case.

3.2.1.2.2 Results and Analysis

<u>Rupture with Leak Rate Detection</u>

There were no ruptures with a 1 gpm leak rate detection capability for this case.

<u>Leak Rate Jump</u>

There were no leak rate jump events for this case.

<u>LBB Time Lapse</u>

The mean LBB time lapses and standard errors with 1 and 10 gpm leak rate detection capabilities were respectively as follows:

- 56.3 ± 0.4 months (minimum observed: 11 months)
- 39.7 ± 0.3 months (minimum observed: 7 months)

Note that, as with Case 1.1.0, all results beyond 12 EFPY were excluded as they strongly influence the mean. Section 3.2.1.1.2 provides the rationale for this approach. In both cases,

the mean LBB time lapse was well over 3 years. The minimum LBB time lapse based on a 10 gpm leak rate detection capability was 7 months.

LBB Ratio

The mean LBB ratios and standard errors with 1 and 10 gpm leak rate detection capabilities were respectively as follows:

- 9.88 ± 0.01 (minimum observed: 7.81)
- 4.63 ± 0.004 (minimum observed: 3.97)

Figure 3-26 and Figure 3-27 show the LBB ratio CDF plots. The mean LBB ratio based on a 10 gpm leak rate detection capability is 4.63, which is more than twice the SRP Section 3.6.3 deterministic margin of 2.0. In fact, the minimum from all 5,000 realizations was 3.97, which is nearly twice as high.

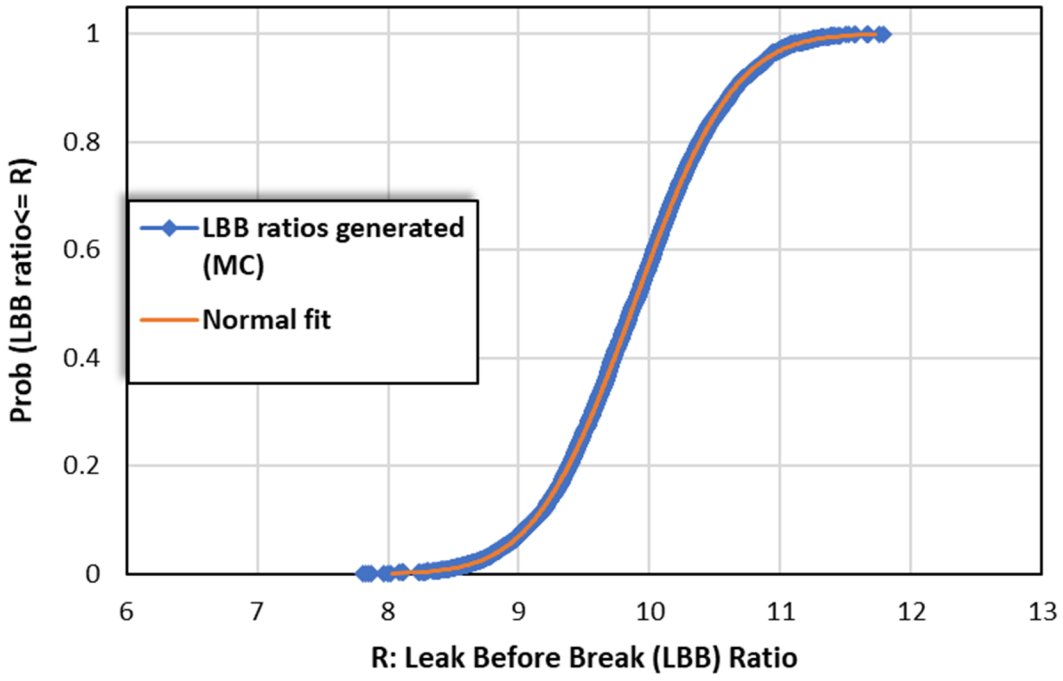


**Figure 3-26 Case 1.1.1 distribution of LBB ratio with a 1 gpm leak rate detection capability**

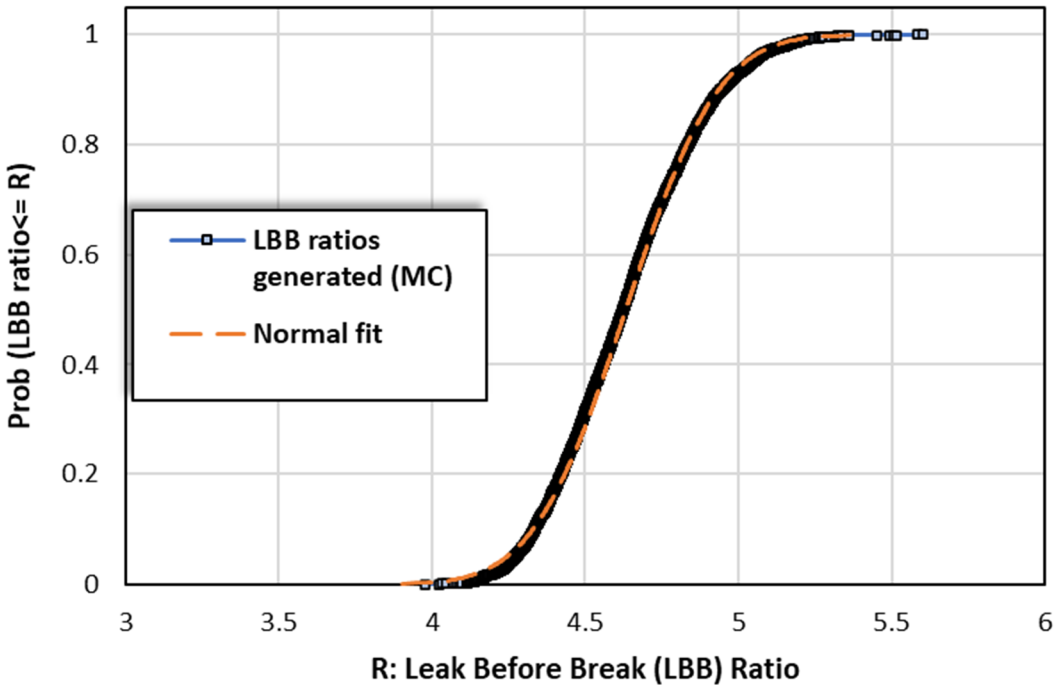


**Figure 3-27 Case 1.1.1 distribution of LBB ratio with a 10 gpm leak rate detection capability**

Standard Indicators

Figure 3-28 shows the probabilities of first leak and rupture along with their 95 percent confidence intervals. The confidence intervals are close to the mean in log-space and demonstrate that the results are sufficiently converged using the sample size of 5,000. Compared to Case 1.1.0, the difference between first crack and first leak at 80 EFPY is higher; however, these results are expected considering that all the cracks have the full 80 EFPY of plant operation to grow in Case 1.1.1.

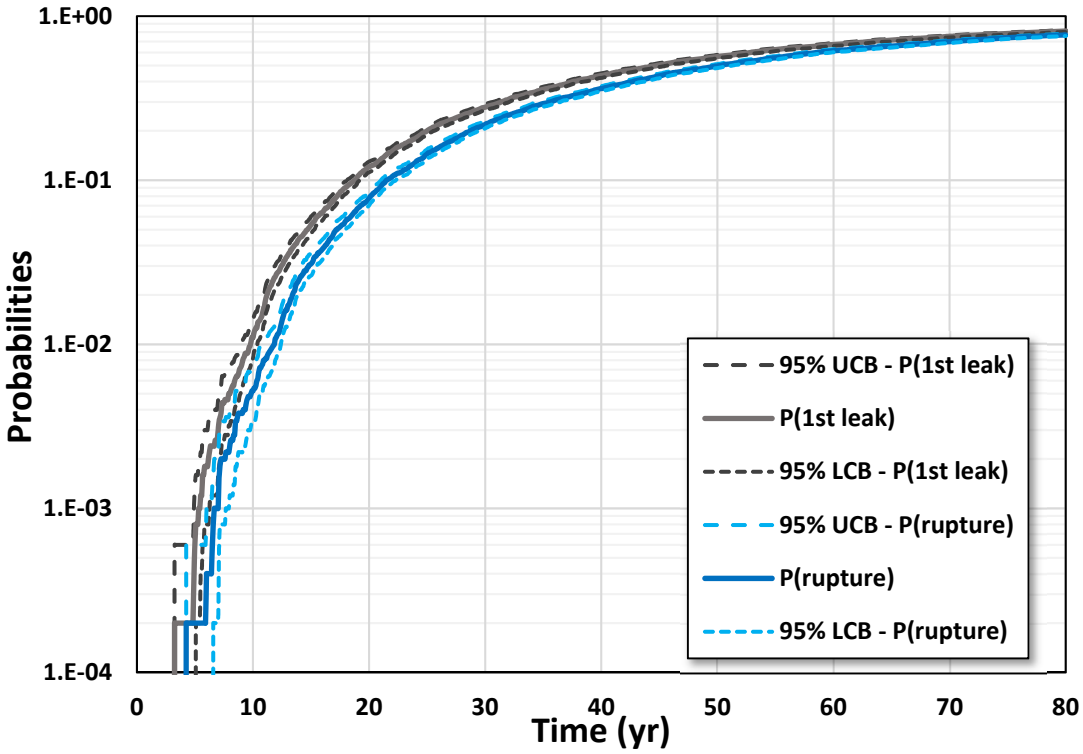


**Figure 3-28 Case 1.1.1 time-dependent probabilities of first leak and rupture with 95 percent confidence intervals**

3.2.1.2.3 Supplemental Analyses

Distribution Fitting on Leak Rate Increase

As was done in the supplemental analyses for Case 1.1.0, distributions were fit to the leak rate increase results for Case 1.1.1 to estimate the likelihood of having a leak rate gain greater than 40 gpm after reaching a 10 gpm leak rate. Figure 3-29 displays the results with a moment-matching lognormal distribution fit. Using this distribution, the probability of having a leak rate increase greater than or equal to 40 gpm is estimated to be $1.08 \times 10^{-13}$.

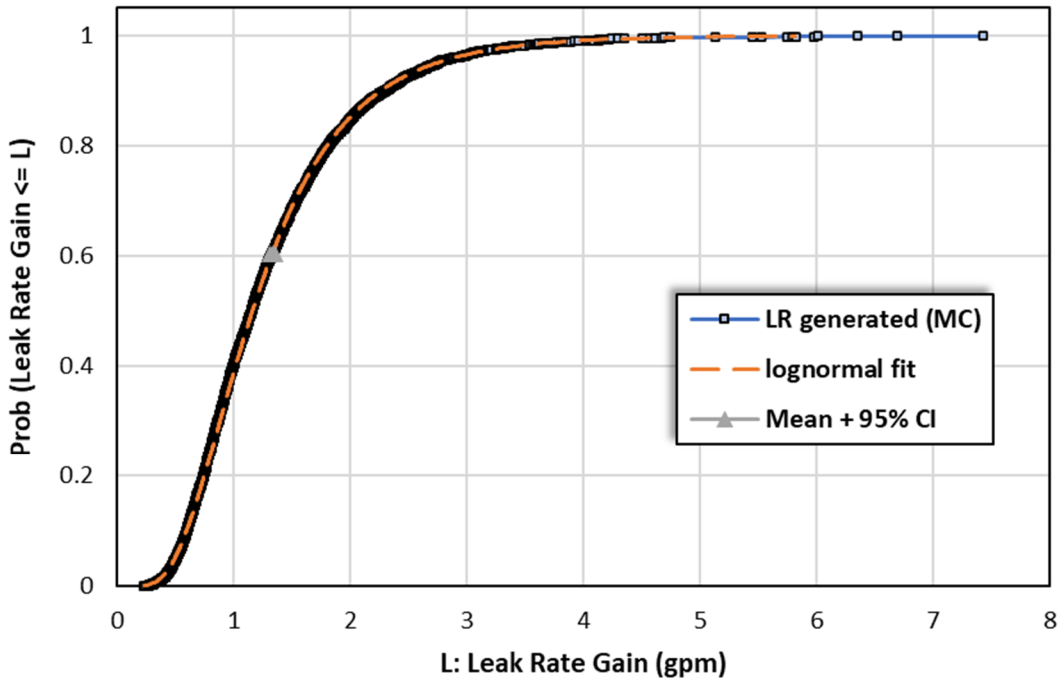


**Figure 3-29 Moment-matching lognormal distribution fit to Case 1.1.1 leak rate increase one month after occurrence of 10 gpm leak**

It was expected that the leak rate jump distribution would be minimally affected by the crack initiation model. To confirm this expectation, the CDFs from Cases 1.1.0 and Case 1.1.1 were compared as shown in Figure 3-30. The results show good agreement between the two distributions. The Case 1.1.1 CDF leads to slightly lower values because all the sampled WRS values are included. However, in Case 1.1.0 the lowest sampled WRS values are not included in the CDF, and these values may lead to later or no crack initiations.

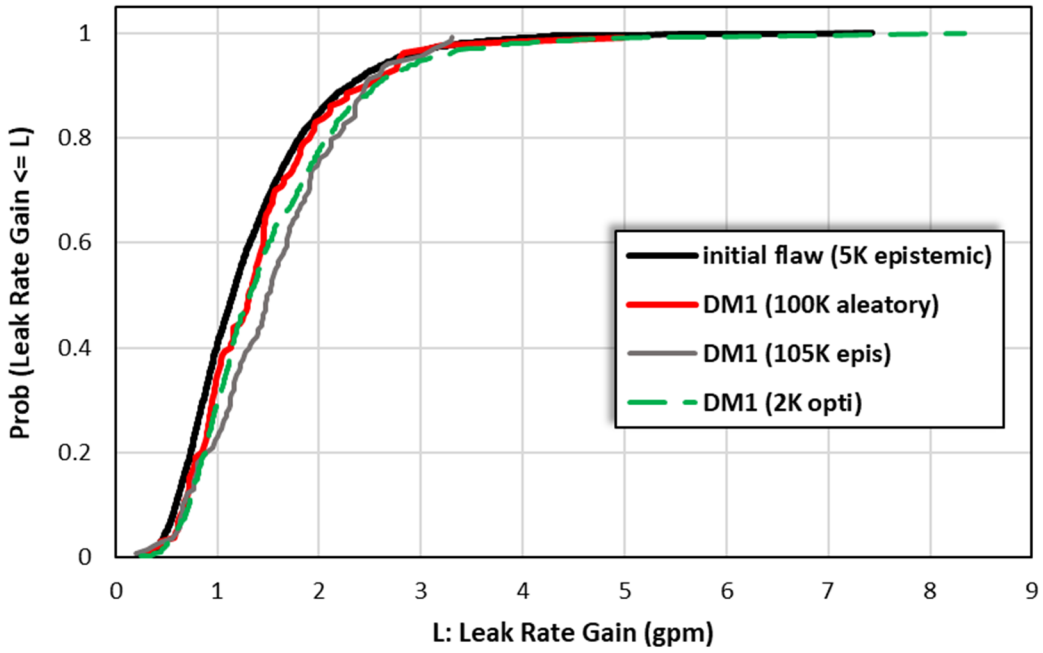


**Figure 3-30 Comparison of Case 1.1.1 distribution of leak rate increase one month after occurrence of 10 gpm leak with Case 1.1.0**

Distribution Fitting on LBB Ratio Results

As was done in the supplemental analyses for Case 1.1.0, a distribution was fit to the LBB ratio results from Case 1.1.1 to estimate the likelihood of not meeting the minimum margins stated in SRP Section 3.6.3. Figure 3-31 displays the Case 1.1.1 LBB ratio results based on a 10 gpm leak rate detection capability with a moment-matching normal distribution fit. Using this distribution, the probability of having an LBB ratio less than or equal to 2.0 is estimated to be $3.98 \times 10^{-29}$ (i.e., essentially zero).

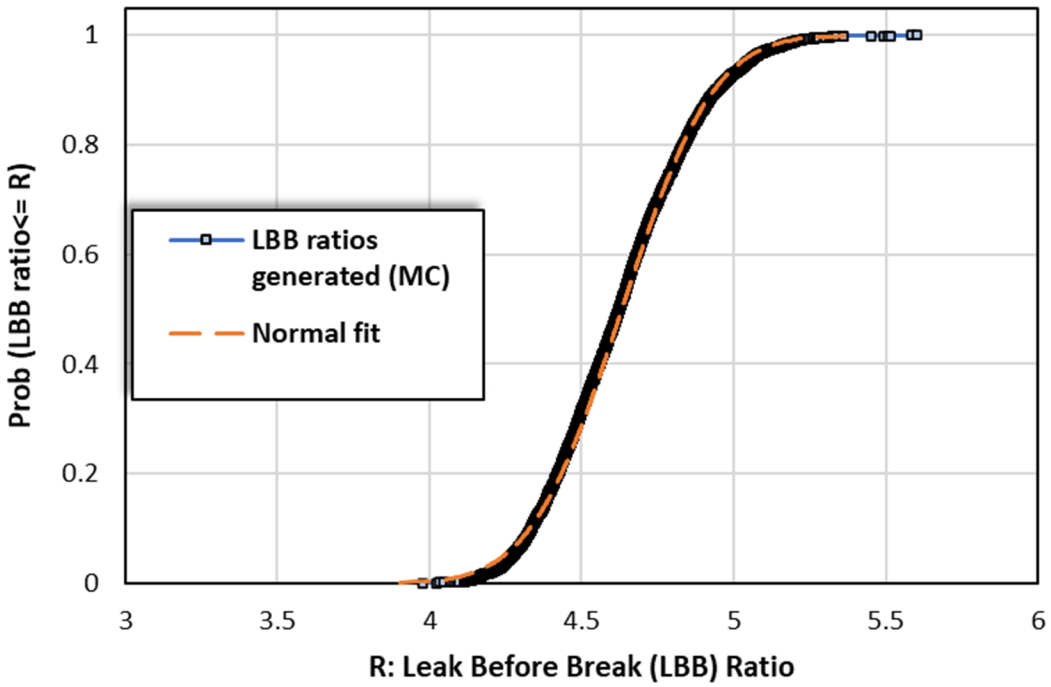


**Figure 3-31 Case 1.1.1 distribution of LBB ratio with a 10 gpm leak rate detection capability**

It was also expected that the LBB ratio distribution would be minimally affected by the crack initiation model. To confirm this expectation, the CDFs from Cases 1.1.0 and Case 1.1.1 were compared as shown in Figure 3-32. The results show good agreement consistent with the expectation.

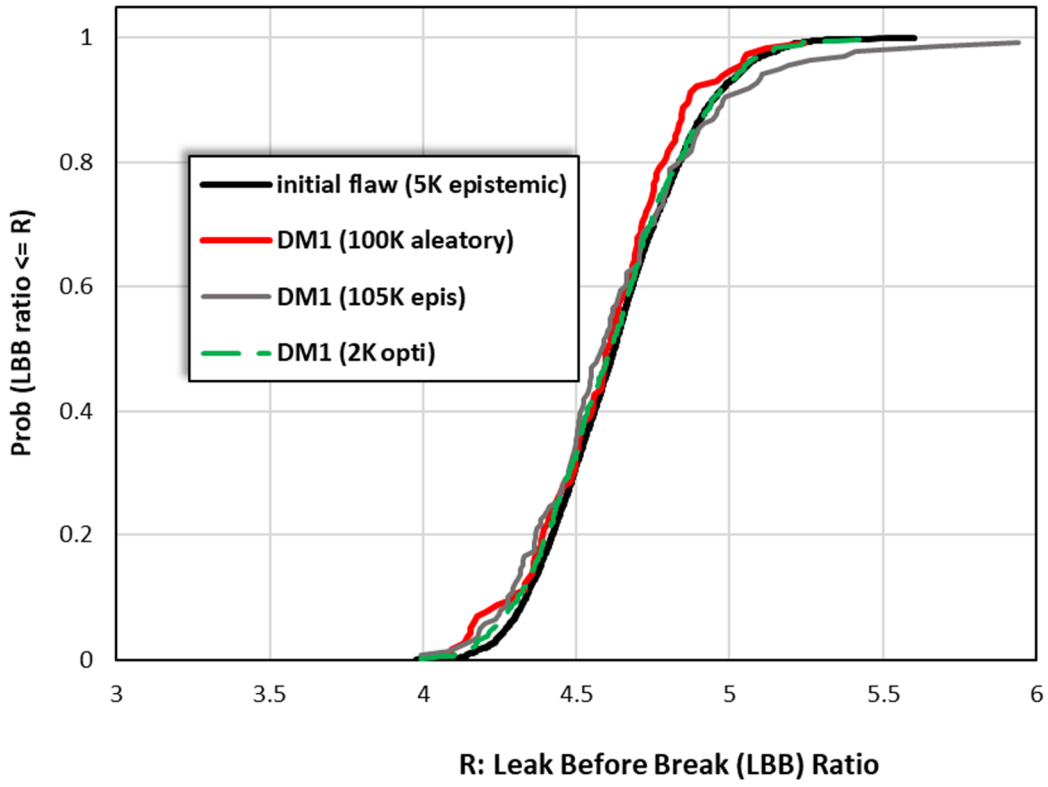


**Figure 3-32 Comparison of Case 1.1.1 LBB ratio distribution with a 10 gpm leak rate detection capability with Case 1.1.0**

Distribution Fitting on LBB Time Lapse Results

As was done in the supplemental analyses for Case 1.1.0, a distribution was fit to the LBB time lapse results from Case 1.1.1 to estimate the likelihood of an LBB time lapse. Figure 3-33 displays the Case 1.1.1 LBB time lapse results based on a 10 gpm leak rate detection capability with moment-matching lognormal distribution fit. The fit is slightly offset compared to the leak rate increase and LBB ratio results, but it is still close to the distribution based on the data from xLPR code simulations. Using this distribution, the probability of having an LBB time lapse of 1 month or less is estimated to be $9.28 \times 10^{-12}$, and the probability of it being less than or equal to 4 months is estimated to be $1.78 \times 10^{-5}$.

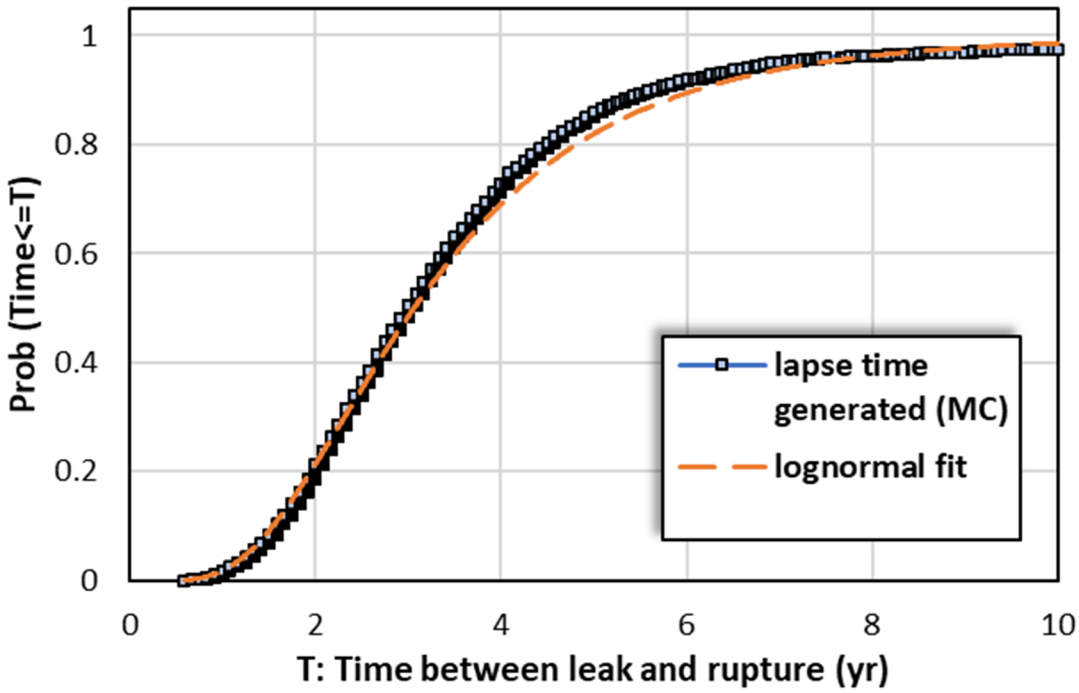


**Figure 3-33 Moment-matching lognormal distribution fit to Case 1.1.1 LBB time lapse with a 10 gpm leak rate detection capability**

It was expected that the LBB time lapse distribution would vary somewhat with the crack initiation model. The LBB time lapse results are conditional on the occurrence of rupture. Rupture is more likely to occur in Case 1.1.1 because the cracks are present at the beginning of the simulation, whereas, in Case 1.1.0 they could be present at any time up to 80 EFPY, or not at all. Therefore, the distributions for Case 1.1.0 were expected to be biased for larger values, representing the realizations that had detectable leakage but did not rupture during the simulation time of 80 EFPY. This bias can be observed in Figure 3-34, which plots the CDFs from Cases 1.1.0 and 1.1.1.

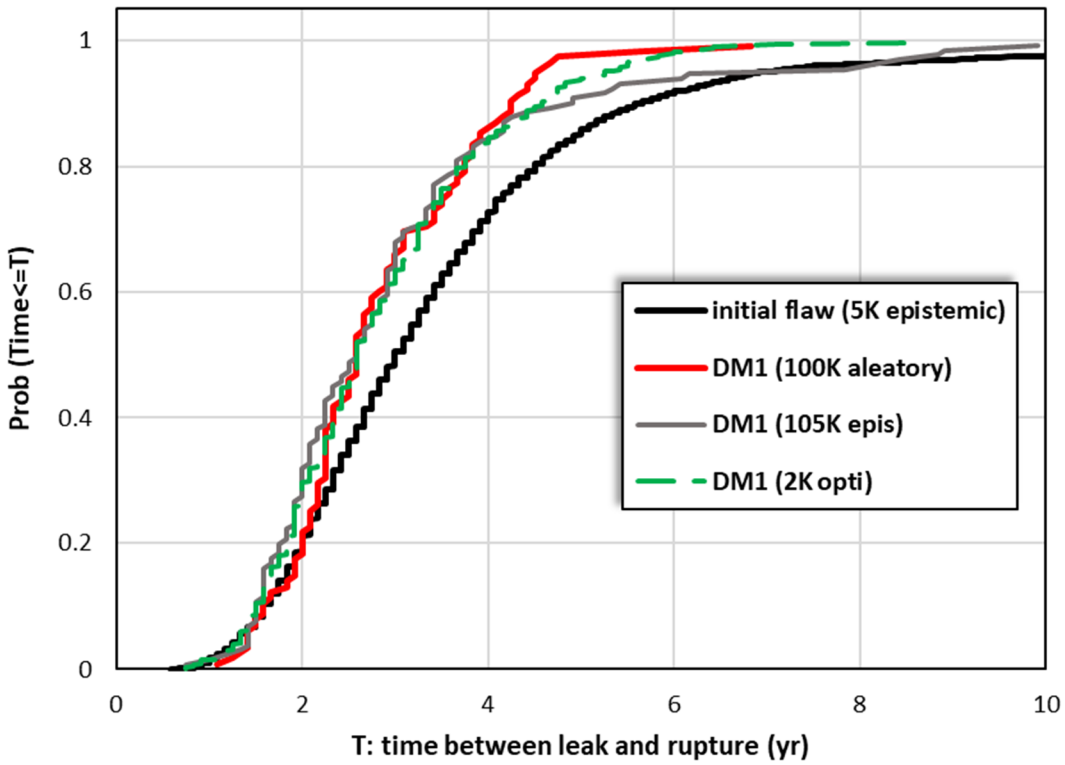


**Figure 3-34 Comparison of Case 1.1.1 LBB time lapse distributions with Case 1.1.0**

#### *3.2.1.3 Summary*

Based on the analyses of the Cases 1.1.0 and 1.1.1 results, the probability of failure of the RVON weld is extremely low. There were no ruptures with leak rate detection in either case. No leak rate jump events were observed in either case as well. Based on the sample sizes considered, these results give similar estimates beyond a $1 \times 10^{-7}$ annual frequency. The probability of a leak rate increase that is greater than 40 gpm, a value derived from the leak rate jump thresholds, was conservatively estimated to be on the order of $1 \times 10^{-9}$. In addition, the LBB ratio results demonstrate that the likelihood of not meeting the deterministic margins from SRP Section 3.6.3 is on the order of $1 \times 10^{-18}$. Furthermore, the probability of an LBB time lapse of 1 month or less was estimated to be on the order of $1 \times 10^{-12}$. These results are the highest probabilities between the two cases. Finally, Case 1.1.1 confirms that the RVON weld has an extremely low probability of failure even without modeling the crack initiation process.

### 3.2.2 Sensitivity Study Cases

To supplement the RVON weld base cases, sensitivity studies were conducted to assess defense-in-depth considering the following areas:

- WRS (Section 3.2.2.1)
- crack initiation model uncertainty (Section 3.2.2.2)
- SSE (Section 3.2.2.3)
- axial cracks (Section 3.2.2.4)
- normal operating loads (Section 3.2.2.5)
- detectable leak rate (Section 3.2.2.6)
- mechanical stress improvement (Section 3.2.2.7)
- ISI (Section 3.2.2.8)
- hydrogen concentration in the reactor coolant system (Section 3.2.2.9)
- combined effects of PWSCC and fatigue (Section 3.2.2.10)
- fatigue crack initiation (Section 3.2.2.11)
- large initial flaw with fatigue crack growth (Section 3.2.2.12)
- weld geometry (Section 3.2.2.13)
- operating temperature (Section 3.2.2.14)
- initial PWSCC flaw size (Section 3.2.2.15)
- time step (Section 3.2.2.16)
- separation of aleatory and epistemic uncertainties (Section 3.2.2.17)

Sections 3.2.2.1 through 3.2.2.17 describe these sensitivity studies and present the results.

#### *3.2.2.1 Weld Residual Stress*

3.2.2.1.1 Case Description

The objective of Case 1.1.2 was to assess the sensitivity of the likelihood of failure due to a more severe, yet plausible, WRS profile. It is like Case 1.1.0 with only a change in the mean WRS profile (i.e., the same standard deviation was assumed). This more severe WRS profile was developed from the geometry of a Babcock and Wilcox PWR used for a previous analysis effort by Rudland, et al. [32]. That analysis was for an inlay, so for the present study the finite element analysis was rerun using the same mesh, but with no inlay and with Alloy 82/182 material properties. The average of the isotropic and nonlinear kinematic hardening results was then taken following the approach of the xLPR WRS Subgroup [27]. The more severe WRS profile is primarily a result of the greater distance between the dissimilar metal weld and the stainless steel weld. This configuration produces a more tensile WRS field at the inside

diameter, which would increase the probability of crack initiation. The crack initiation model has been shown through prior sensitivity analyses to have a large influence on the probability of rupture [28]. The configuration also increases the severity of the compressive zone, which in turn may favor the chances of the extremely unlikely event of a long, thin crack that could lead to an undesirable break-before-leak scenario. A comparison between the mean WRS profiles used in Cases 1.1.0 and 1.1.2 is shown in Figure 3-35. Section B3 describes the specific inputs and other simulation details used to analyze this case.

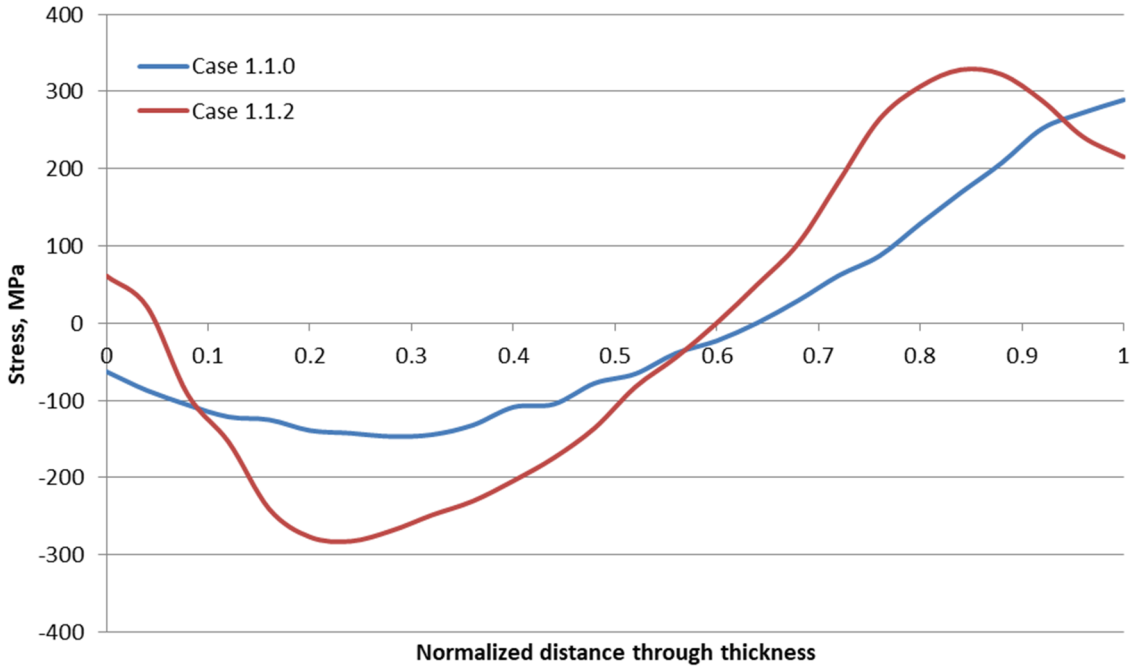


.

**Figure 3-35 Comparison of WRS profiles used for Cases 1.1.0 and 1.1.2**

3.2.2.1.2 Results and Analysis

Rupture with Leak Rate Detection

There were no ruptures with a 1 gpm leak rate detection capability for this case.

Leak Rate Jump

The probability of leak rate jump for Case 1.1.2 was estimated to be around 1 x $10^{-4}$ after 80 EFPY of simulated plant operation as shown in Figure 3-36. With an increase of 100 megapascals (MPa) at the inside diameter, the more severe WRS profile led to more realizations with multiple cracks that could then coalesce and produce faster crack growth after the cracks penetrated through-wall. However, it is important to note that this probability may be overestimated due to the overly conservative input used for the coalescence of two TWCs as discussed in Section 3.2.2.5.2.

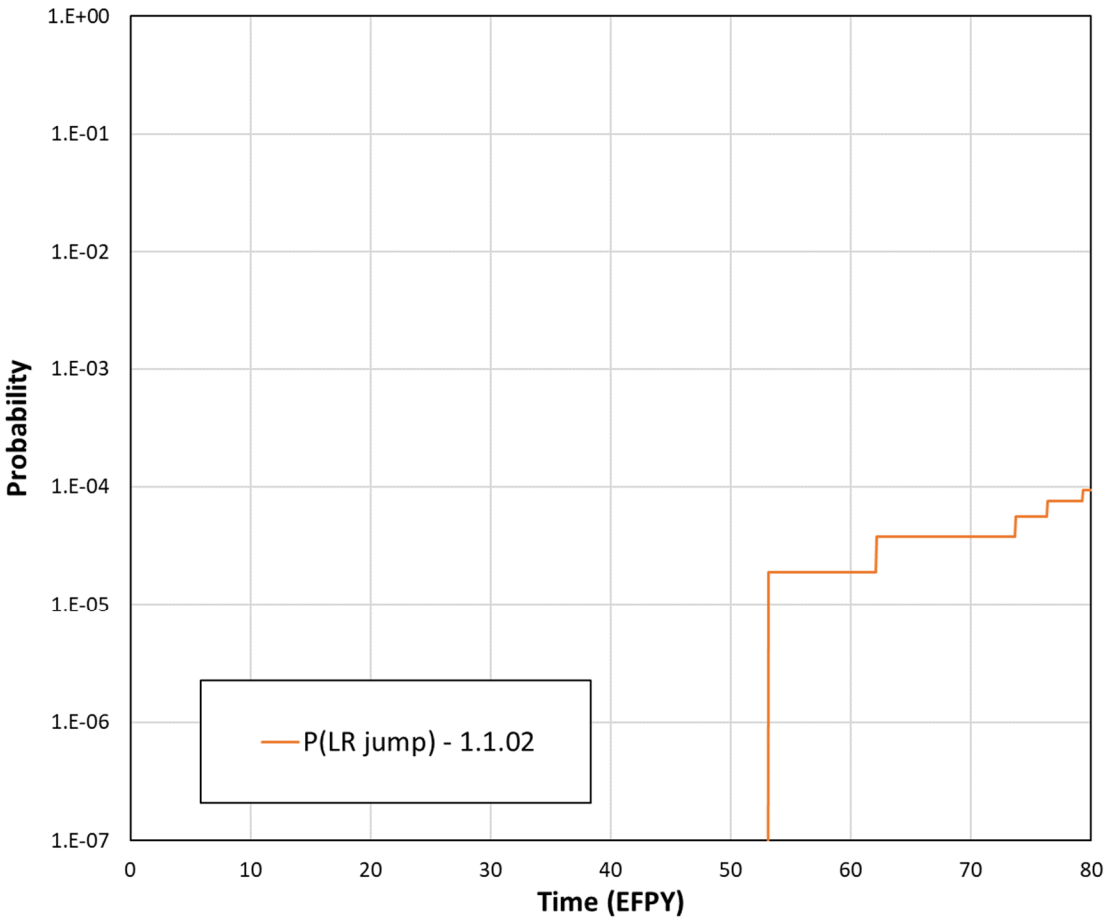


**Figure 3-36 Case 1.1.2 time-dependent probabilities of leak rate jump**

LBB Time Lapse

The mean LBB time lapses and standard errors with 1 and 10 gpm leak rate detection capabilities were respectively as follows:

- 34.8 ± 2.7 months (minimum observed: 2 months)
- 30.7 ± 2.5 months (minimum observed: 2 months)

Note that, as with Case 1.1.0, all results beyond 12 EFPY were excluded as they strongly influence the mean.

Figure 3-37 shows the CDF plots for the LBB time lapse. Overall, the LBB time lapses in Case 1.1.2 were shorter than in Case 1.1.0. This result is expected, however, because of the more severe WRS profile used in Case 1.1.2. With either a 1 or a 10 gpm leak rate detection capability, the minimum LBB time lapse was 2 months, which was the shortest among all the cases examined in this study. This result indicates that the WRS profile has a significant impact on the LBB time lapse.

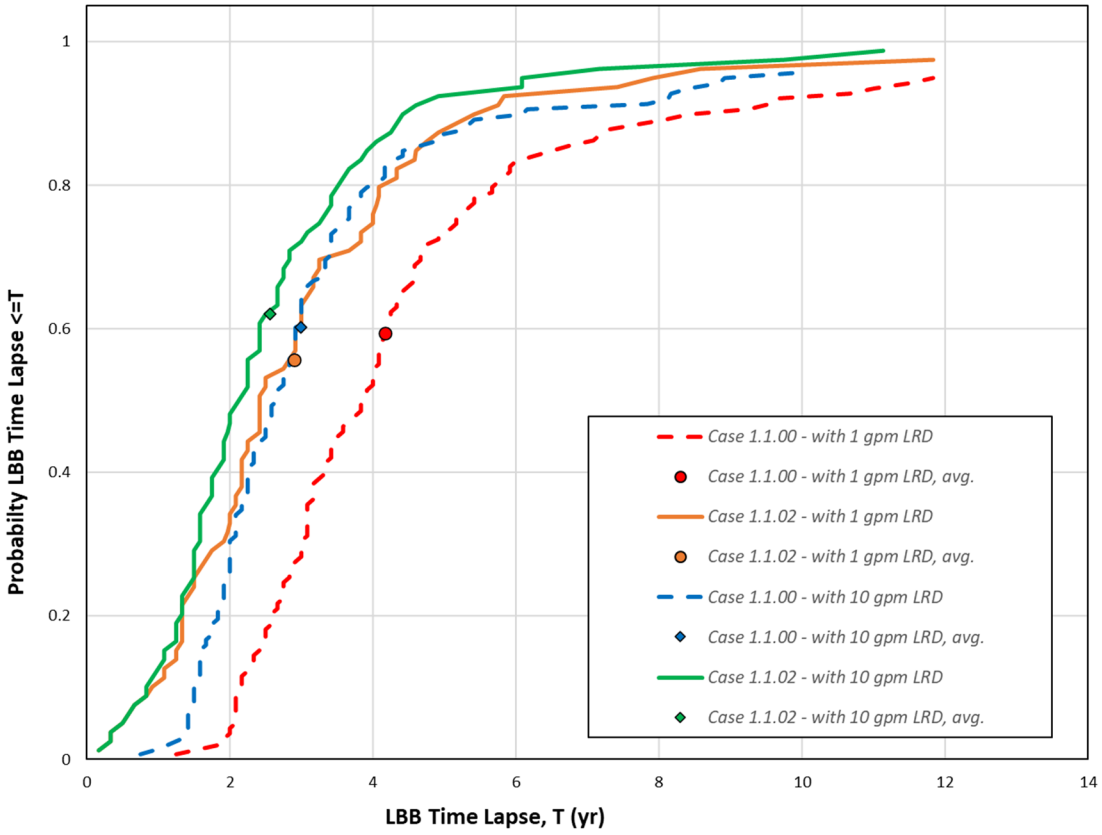


**Figure 3-37 Comparison of Case 1.1.2 LBB time lapse distributions with Case 1.1.0**

LBB Ratio

The mean LBB ratios and standard errors with 1 and 10 gpm leak rate detection capabilities were respectively as follows:

- 6.33 ± 0.25 (minimum observed: 1.37)
- 4.10 ± 0.083 (minimum observed: 1.37)

Figure 3-38 shows the LBB ratio CDF plots. It illustrates that the WRS profile also has a significant impact on the mean LBB ratio. When the WRS profile is more severe, the LBB ratio is lower with both 1 and 10 gpm leak rate detection capabilities. The CDF is also wider, indicating a greater range of possible values for the given inputs. The minimum LBB ratio calculated using both the 1 and 10 gpm leak rate detection capabilities was 1.37. This case was the only one in the study that that did not meet the deterministic acceptance criterion of 2.0 from SRP Section 3.6.3. The results demonstrate that the WRS profile has a significant impact in an LBB analysis.

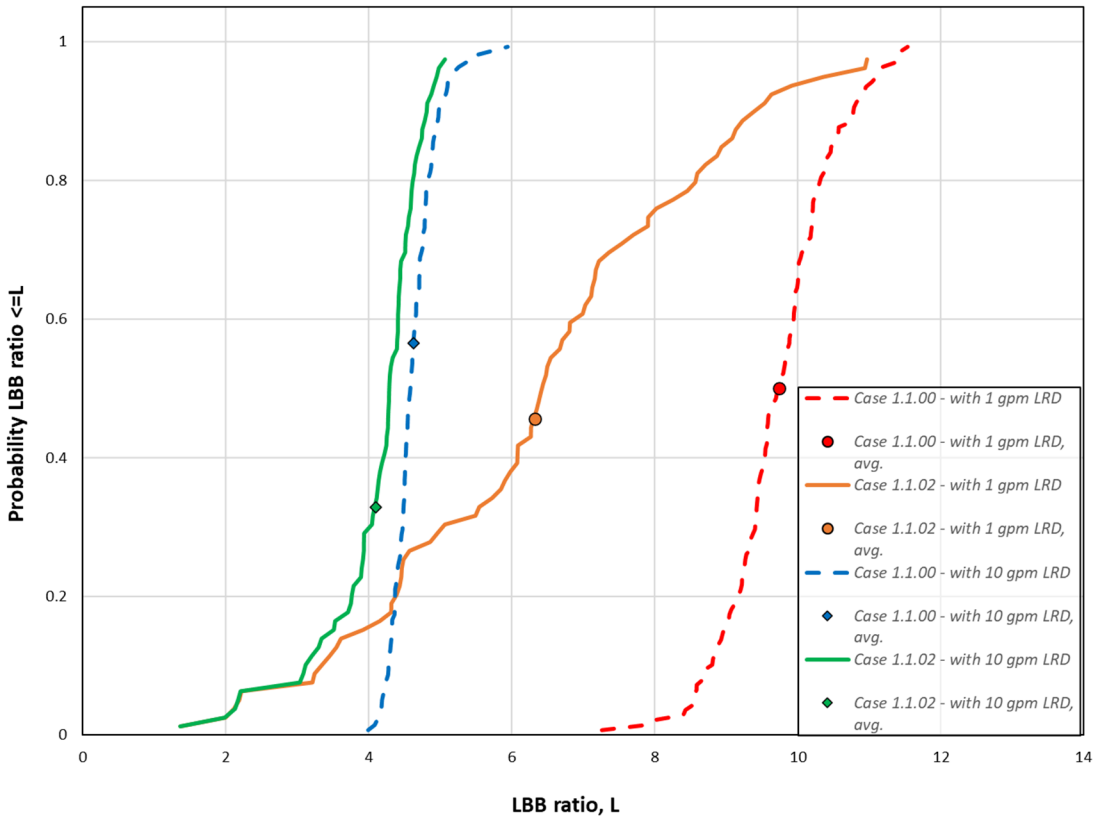


**Figure 3-38 Comparison of Case 1.1.2 LBB ratio distributions with Case 1.1.0**

Standard Indicators

Figure 3-39 shows the results of the standard indicators. The probability of first crack in Case 1.1.2 is much higher as compared to Case 1.1.0; however, it did not lead to earlier probabilities of first leak or rupture. In fact, the probabilities over time are lower using the more severe WRS profile. Both the probabilities of first leak and rupture at 80 EFPY are essentially equivalent in Cases 1.1.0 and 1.1.2. The reason for the lower probabilities of first leak and rupture using the more severe WRS profile is that the WRS values in the middle of the weld must be lower (i.e., more compressive) to maintain stress equilibrium with the increased WRS at the inside diameter. Figure 3-35 shows that, for the more severe WRS profile, at about one-fifth of the thickness, the WRS is almost 300 MPa less in Case 1.1.2. The effect is significantly reduced crack growth. The probabilities of first leak and rupture for both Cases 1.1.0 and 1.1.2 begin to merge close to 80 EFPY because, once a crack under the more severe WRS progresses through the middle of the weld, the stress becomes higher leading to faster crack growth. However, with the more compressive WRS zone used for Case 1.1.2, it is possible for the circumferential crack to grow longer around the inside diameter of the weld. This kind of crack growth could lead to a higher likelihood of failure during an upset load, which is analyzed in Section 3.2.2.1.3.

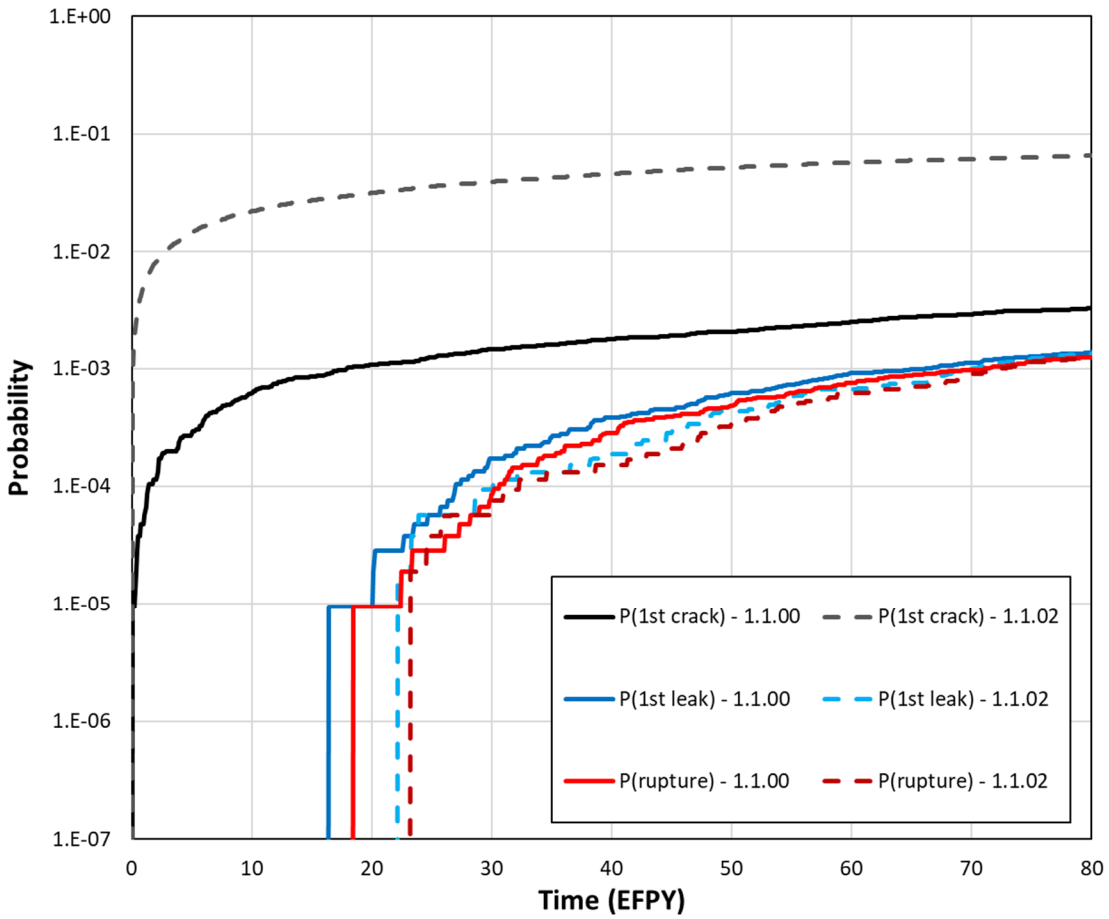


**Figure 3-39 Comparison of Case 1.1.2 time-dependent probabilities of first crack, first leak, and rupture with Case 1.1.0**

3.2.2.1.3 Supplemental Analyses

While the probabilities of first leak and rupture are similar between Cases 1.1.0 and 1.1.2, the probability of leak rate jump over 80 EFPY of simulated plant operation was not zero and the CDFs for the LBB ratio and LBB time lapse were more extreme. Thus, it is important to study the possibility of an undesirable break-before-leak scenario. In this scenario, a realization could lead to surface crack rupture or rupture during a seismic event.

Figure 3-40 shows a plot of the normalized crack inner half-length and depth for all surface cracks along with the regions of bending stress required for surface crack failure. Each band represents a range of bending stresses that would lead to surface crack rupture. The results show that some cracks may have long lengths, but they are associated with very shallow depths and thus should not become unstable. Therefore, in Case 1.1.2 surface crack rupture is unlikely even with the large compressive WRS zone.

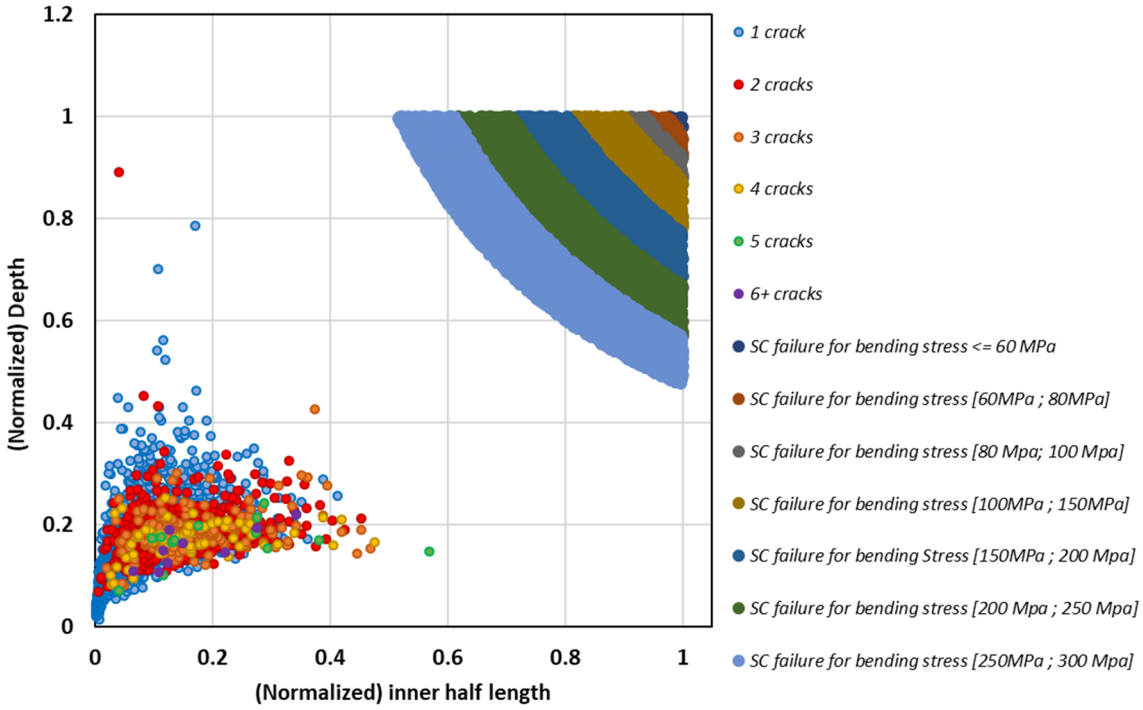


**Figure 3-40 Observed surface crack dimensions and comparison with surface crack failure regions**

### *3.2.2.2 Crack Initiation Model Uncertainty*

3.2.2.2.1 Case Description

The objective of Cases 1.1.3 and 1.1.4 was to assess crack initiation model uncertainty, with Case 1.1.3 using Direct Model 2 and Case 1.1.4 using the Weibull model. Both cases are like Case 1.1.0 except for the PWSCC initiation model used in the analysis. As in Case 1.1.0, seismic effects were also excluded in Cases 1.1.3 and 1.1.4. Direct Model 2 incorporates the level of cold work and other material properties as compared to Direct Model 1 while still using the operating temperature and surface stress as inputs. The Weibull model samples crack initiation from a lognormal distribution, and the model is not dependent on temperature and surface stress. As in Case 1.1.0, the initiation model parameters were based on the recommendations in [26].

The NRC team did not analyze Case 1.1.3 because Direct Model 2 includes an upper stress threshold beyond which a crack always initiates. In addition, because the model is not linked to the spatial discretization of the weld (i.e., the number of subunits), the number of cracks may be dependent on the number of subunits. Considering these limitations, the availability of calibrated inputs for use in Direct Model 1 and the Weibull model, and the results from the study presented in Appendix C to confirm the appropriateness of the Direct Model 1 parameters, the use of Direct Model 2 is not recommended. Section B4 describes the specific inputs and other simulation details used to analyze this case.

#### 3.2.2.2.2 Results and Analysis

Rupture with Leak Rate Detection

There were no ruptures with a 1 gpm leak rate detection capability for Case 1.1.4.

Leak Rate Jump

There were no leak rate jump events for Case 1.1.4.

LBB Time Lapse

The mean LBB time lapses and standard errors with 1 and 10 gpm leak rate detection capabilities for Case 1.1.4 were respectively as follows:

- 53.8 ± 1.5 months (minimum observed: 15 months)
- 37.8 ± 1.2 months (minimum observed: 10 months)

Note that, as with Case 1.1.0, all results beyond 12 EFPY were excluded as they strongly influence the mean. Figure 3-41 shows the LBB time lapse CDF plots using the Weibull model. As compared to Case 1.1.0, use of the Weibull model led to slightly longer LBB time lapses with a 1 gpm leak rate detection capability. The difference is just outside the standard error; it is small and can mostly be ignored.

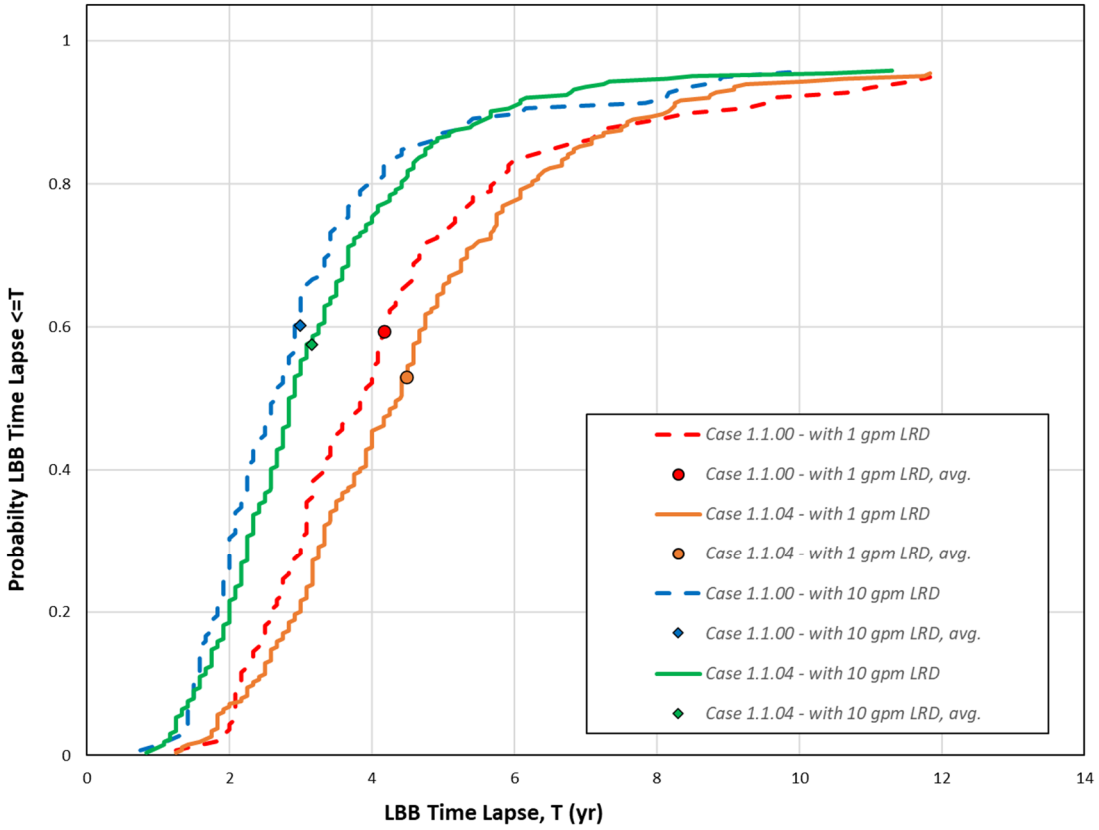


**Figure 3-41 Comparison of Case 1.1.4 LBB time lapse distributions with Case 1.1.0**

LBB Ratio

The mean LBB ratios and standard errors with 1 and 10 gpm leak rate detection capabilities for Case 1.1.4 were respectively as follows:

- 9.82 ± 0.051 (minimum observed: 4.96)
- 4.6 ± 0.015 (minimum observed: 3.89)

Figure 3-42 shows the LBB ratio CDF plots. It illustrates that the LBB ratios for Cases 1.1.0 and 1.1.4 are statistically equivalent. This is an expected result because neither the leakage nor the rupture crack sizes depend on the crack initiation model.

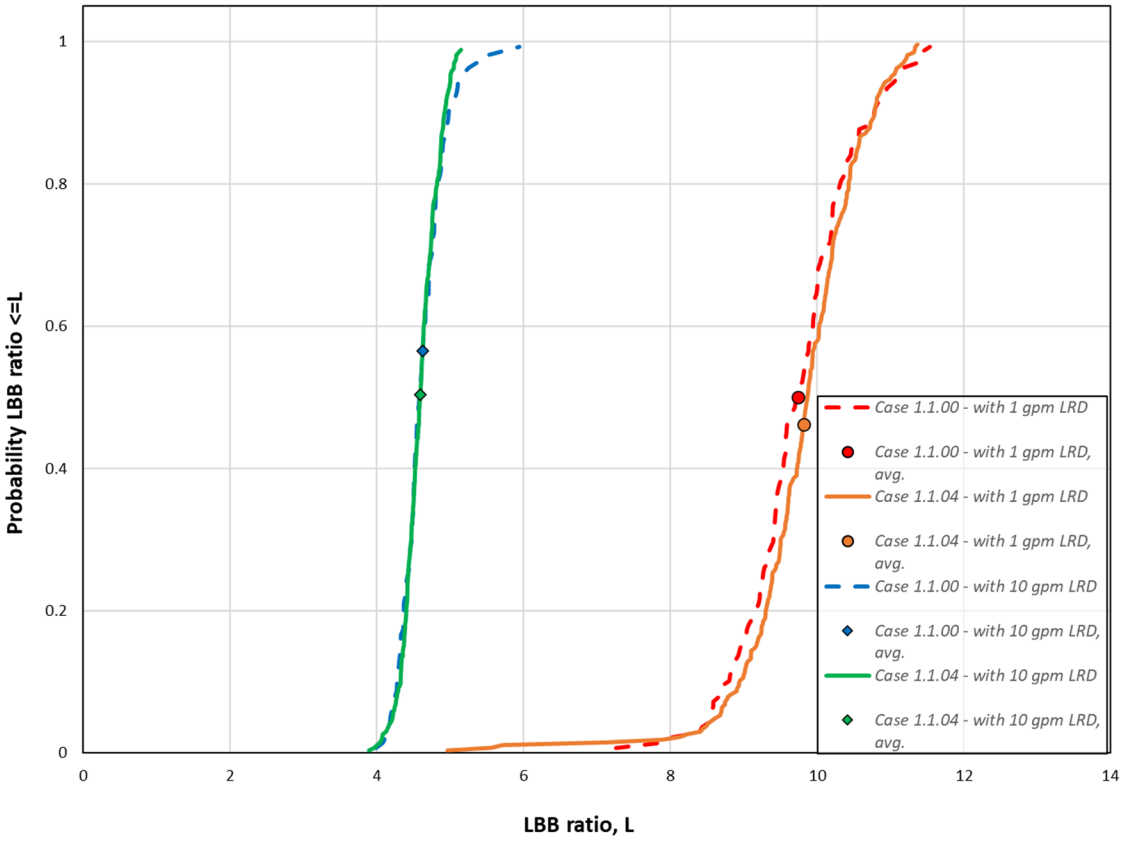


**Figure 3-42 Comparison of Case 1.1.4 LBB ratio distributions with Case 1.1.0**

Standard Indicators

Figure 3-43 shows the results from the standard indicators. Use of the Weibull model in Case 1.1.4 led to higher probabilities of first crack and as compared to use of Direct Model 1 in Case 1.1.0. The higher occurrence of cracks subsequently led to higher probabilities of first leak and rupture early in the simulation. Later, these probabilities were equivalent.

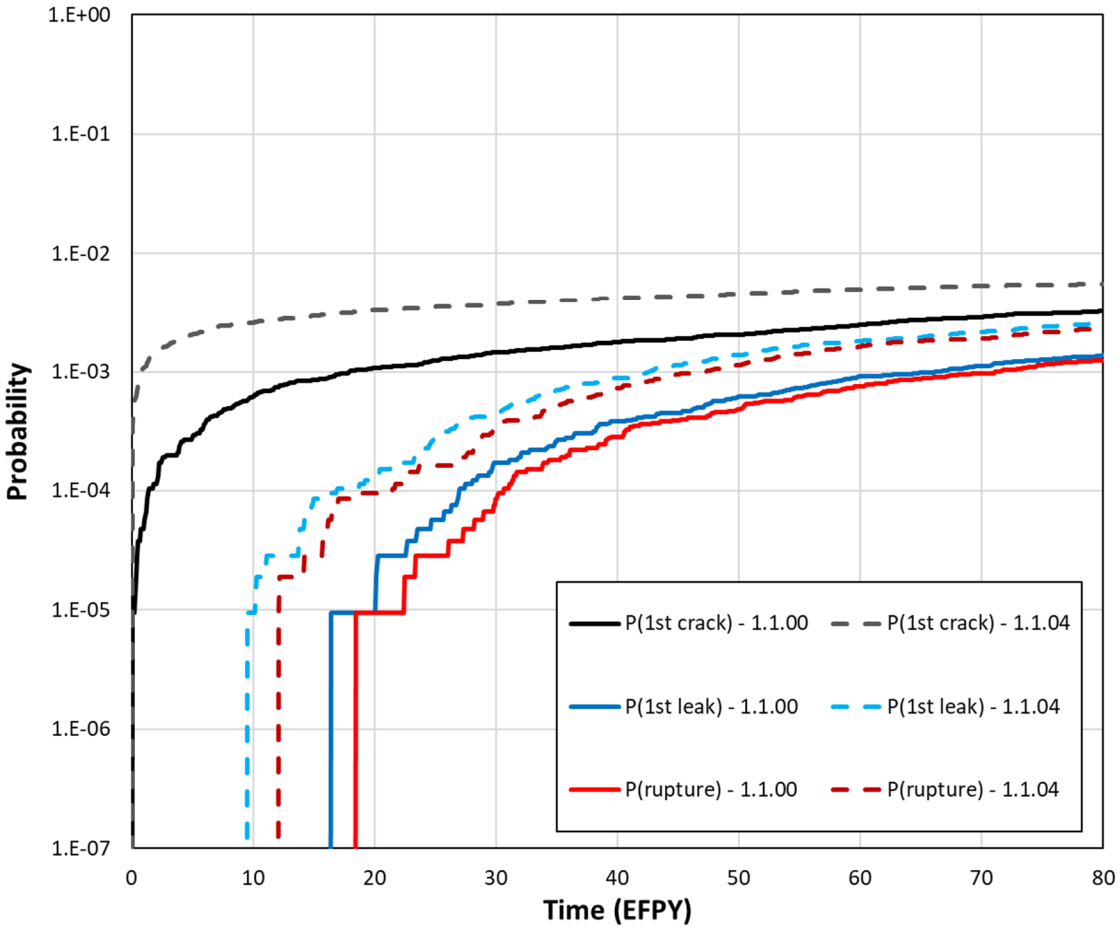


**Figure 3-43 Comparison of Case 1.1.4 time-dependent probabilities of first crack, first leak, and rupture with Case 1.1.0**

### *3.2.2.3 Safe Shutdown Earthquake*

3.2.2.3.1 Case Description

The objective of Case 1.1.5 was to assess the sensitivity of the likelihood of failure due to an SSE event. It is like Case 1.1.1 with the addition of SSE stresses and frequency of occurrence. Thus, the initial flaw density option with a single circumferential crack was used for the analysis. In consultation with seismology experts from the NRC Office of Nuclear Regulatory Research staff, two current seismic response profiles were considered. One profile was for a four-loop PWR on a rock substrate and the other was for a four-loop PWR on a soil substrate. Design-basis SSE stresses and peak ground accelerations were used in conjunction with the current seismic response profiles to estimate the SSE stresses at an annual event frequency near $1 \times 10^{-6}$. Such a frequency of occurrence is traditionally considered the lowest that would be included in a risk analysis. It leads to an upper bound in the peak ground acceleration and associated seismic stresses. The seismic response of the rock site was ultimately selected as the bounding case because its peak ground acceleration was almost twice as large for the annual frequency considered (0.89 g for the rock site vs. 0.5 g for soil site). Figure 3-44 shows

the axial and bending seismic stresses for the rock and soil sites as a function of the annual frequency of SSE occurrence. The figure demonstrates that considering the rock site stresses at a 1 x $10^{-6}$ frequency of occurrence bounds the seismic impact for the scope of this study. Therefore, the inputs for this case were developed from the rock site data. Section B5 describes the specific inputs and other simulation details used to analyze this case.

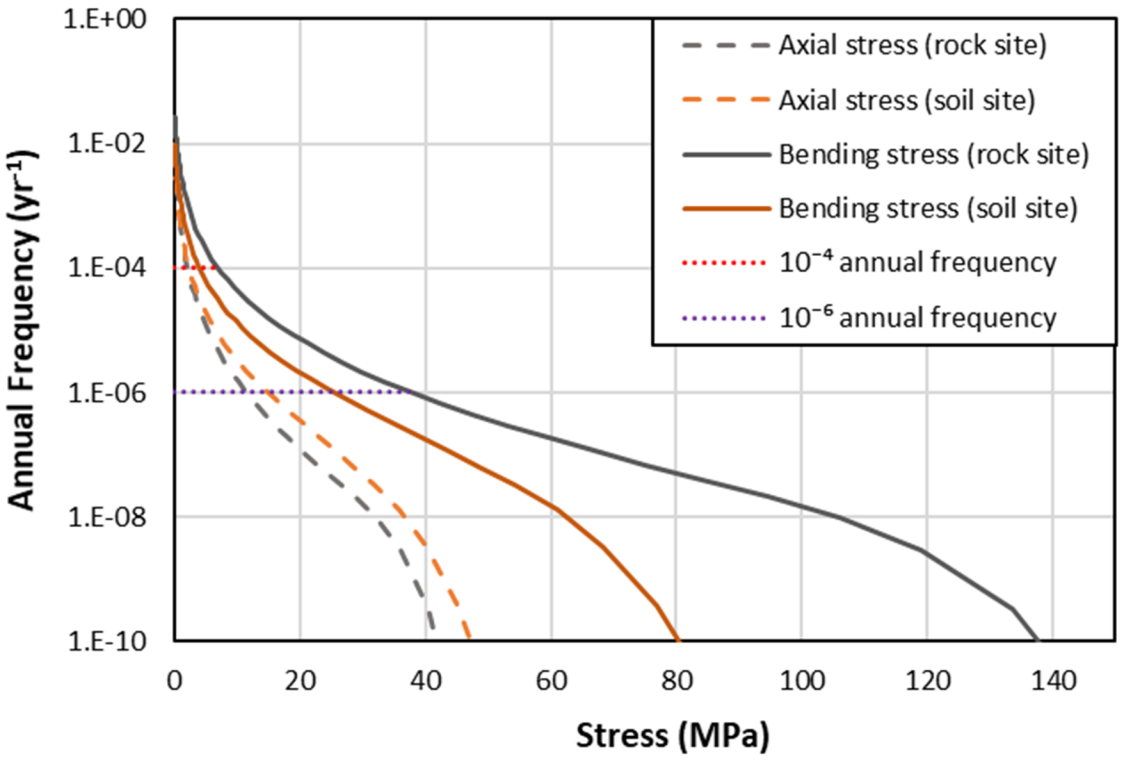


**Figure 3-44 Seismic stresses as a function of the annual frequency for selected rock and soil PWR sites**

3.2.2.3.2 Results and Analysis

Rupture with Leak Rate Detection

There were no ruptures with a 1 gpm leak rate detection capability for this case.

Leak Rate Jump

There were no leak rate jump events for this case.

LBB Time Lapse

The mean LBB time lapses and standard errors with 1 and 10 gpm leak rate detection capabilities were respectively as follows:

- 54.2 ± 0.4 months (minimum observed: 10 months)
- 37.4 ± 0.3 months (minimum observed: 6 months)

Note that, as with Case 1.1.0, all results beyond 12 EFPY were excluded as they strongly influence the mean.

Figure 3-45 shows that the LBB time lapses for Case 1.1.5 are slightly shorter as compared to Case 1.1.1. This is an expected result as the SSE stresses are added to the normal operating stresses, and the greater stresses will thus cause ruptures to occur earlier. However, as discussed in Section 3.2.2.3.3, the difference is small.

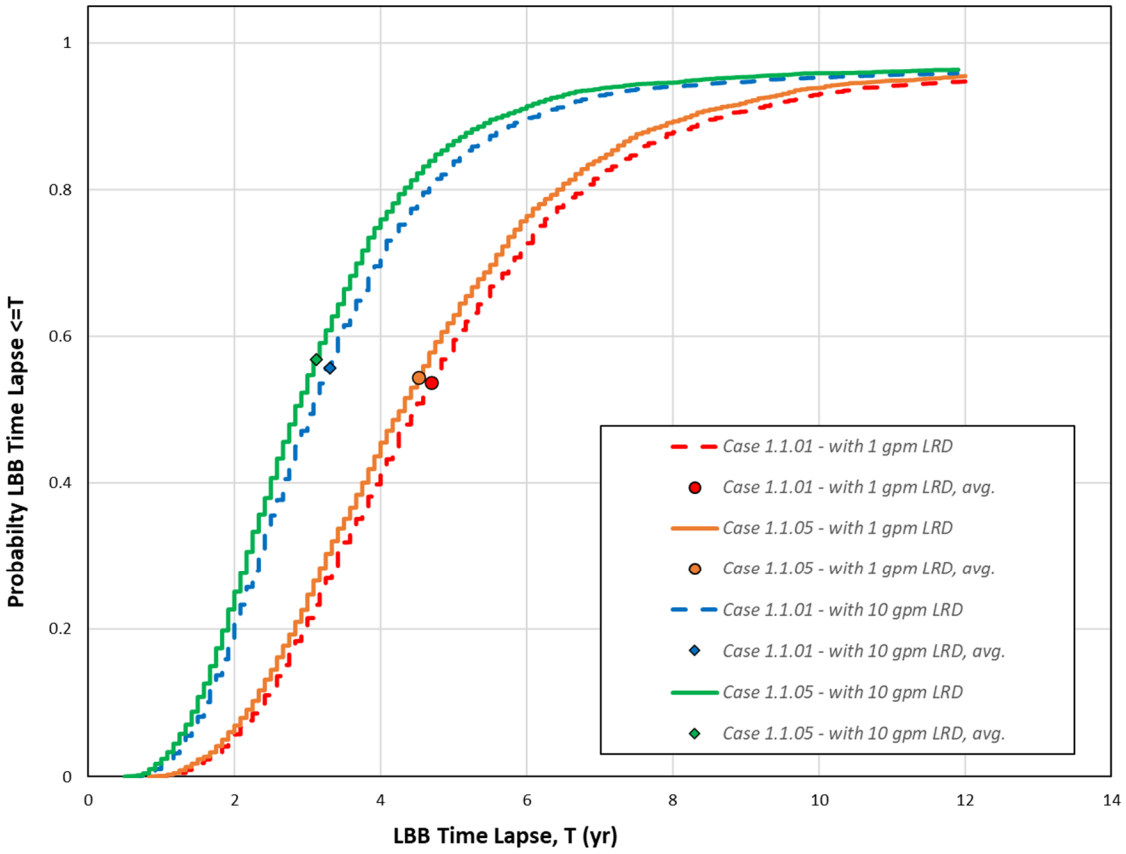


**Figure 3-45 Comparison of Case 1.1.5 LBB time lapse distributions with Case 1.1.1**

LBB Ratio

The mean LBB ratios and standard errors with 1 and 10 gpm leak rate detection capabilities were respectively as follows:

- 9.88 ± 0.012 (minimum observed: 7.13)
- 4.65 ± 0.005 (minimum observed: 3.45)

Figure 3-46 shows the LBB ratio CDF plots. It illustrates that the LBB ratios for Cases 1.1.1 and 1.1.5 are statistically equivalent, thereby demonstrating that SSE events have a minimal influence.

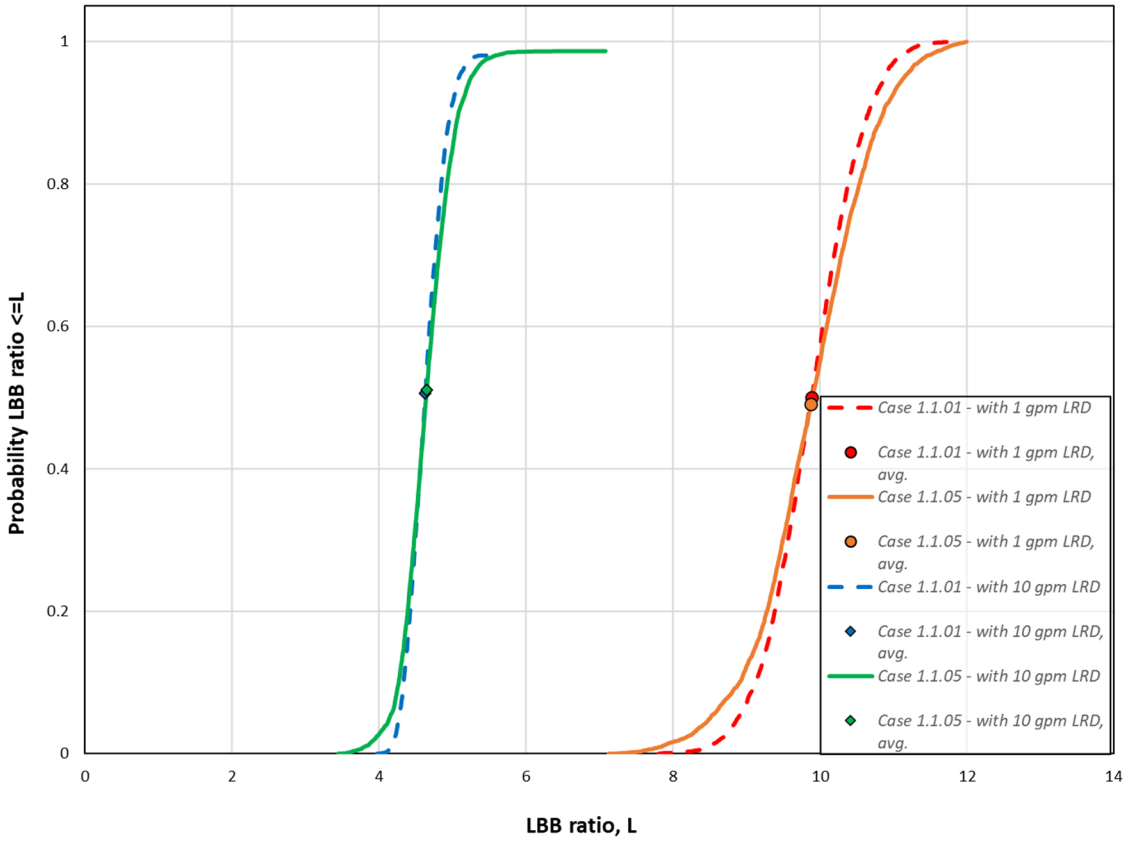


**Figure 3-46 Comparison of Case 1.1.5 LBB ratio distributions with Case 1.1.1**

Probability of Rupture

The probability of rupture at 80 EFPY of simulated plant operation conditional on having an initial crack is the same in Cases 1.1.1 and 1.1.5 due to the logic of the code. When a crack is determined to rupture because of the SSE stresses, the time of failure is recorded, but the realization continues until rupture is caused by the normal operating stresses. The probability of rupture reported for Case 1.1.5 is thus based on the normal operating stresses, and the impact of the SSE stresses can be seen through their effect on the LBB time lapse and LBB ratio QoIs.

3.2.2.3.3 Supplemental Analyses

Since identical sample sizes and random seeds were used in the analyses for Cases 1.1.1 and 1.1.5, and all other parameters except for the SSE events were also the same, it was possible to compare the differences in rupture times for each realization between the two cases. A CDF was constructed of the differences in rupture time to estimate the degree to which the stresses corresponding with an SSE event with an annual frequency of 1 x $10^{-6}$ affect the time of rupture. The result is shown in Figure 3-47. About 20 percent of the realizations see only a 1-month difference, 60 percent see a difference of 2 months or less, and 80 percent see a difference of 3 months or less. In conclusion, the impact of an SSE event is very limited and would only shorten the life of the component by a few months, if the event were to occur during that timeframe. The likelihood of having a seismic event within a 3- or 4-month timeframe is roughly a third of the 1 x $10^{-6}$ annual frequency of occurrence that was considered. In addition, considering that the LBB time lapse is longer than 3 months, SSE events do not lead to undesirable break-before-leak scenarios.

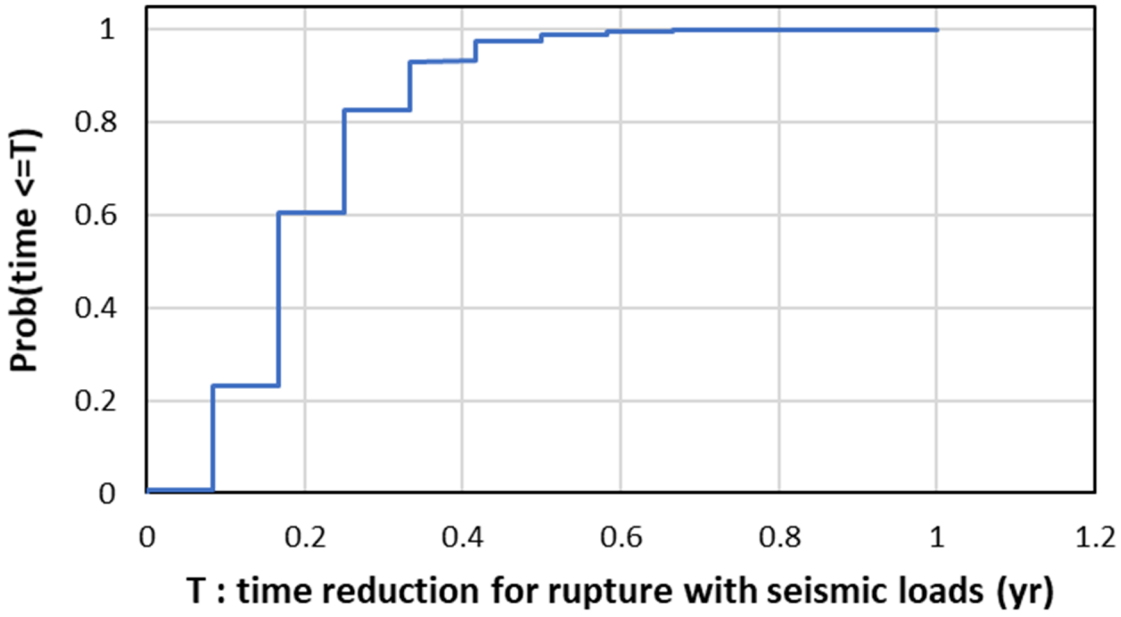


**Figure 3-47 CDF of reduction in time-to-rupture when seismic loads are included**

### *3.2.2.4 Axial Cracks*

3.2.2.4.1 Case Description

The objective of Case 1.1.6 was to assess the sensitivity of the likelihood of failure due to the inclusion of axial cracks in the analysis. It is like Case 1.1.0 with the addition of axial crack initiation and growth caused by PWSCC. Section B6 describes the specific inputs and other simulation details used to analyze this case.

#### 3.2.2.4.2 Results and Analysis

Rupture with Leak Rate Detection

There were no ruptures with a 1 gpm leak rate detection capability for this case.

Leak Rate Jump

There were no leak rate jump events for this case.

LBB Time Lapse

The mean LBB time lapses and standard errors with 1 and 10 gpm leak rate detection capabilities were respectively as follows:

- 46.4 ± 2.2 months (minimum observed: 16 months)
- 33.1 ± 1.7 months (minimum observed: 10 months)

Note that, as with Case 1.1.0, all results beyond 12 EFPY were excluded as they strongly influence the mean.

Figure 3-48 shows that the mean LBB time lapse when axial cracks are included is only few months less as compared to Case 1.1.0 where axial cracks were not included. However, the small differences are due to the tail of the distribution and reflect more on the change in random numbers than on the inclusion of axial cracks. More importantly, the CDFs overlay, which indicates similar results. This result is expected considering that few realizations had both axial and circumferential cracks as shown in Section 3.2.2.4.3, and the leak rates from axial cracks are too small (i.e., usually less than 0.1 gpm) to impact the estimates.

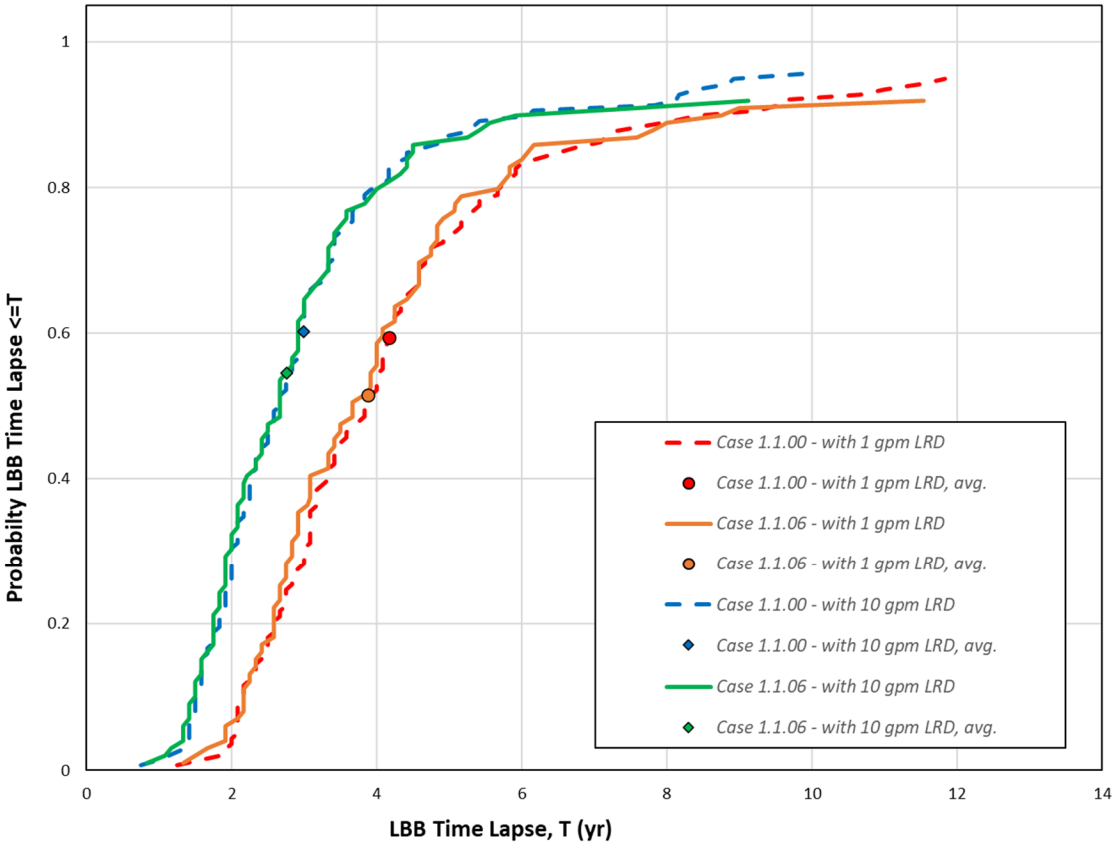


**Figure 3-48 Comparison of Case 1.1.6 LBB time lapse distributions with Case 1.1.0**

LBB Ratio

The mean LBB ratios and standard errors with 1 and 10 gpm leak rate detection capabilities were respectively as follows:

- 9.68 ± 0.09 (minimum observed: 6.55)
- 4.64 ± 0.06 (minimum observed: 3.04)

Figure 3-49 shows the LBB ratio CDF plots. It illustrates that the LBB ratios in Cases 1.1.0 and 1.1.6 are essentially the same. The mean LBB ratio with a 1 gpm leak rate detection capability is slightly lower with the inclusion of axial cracks, but the CDFs are still similar.

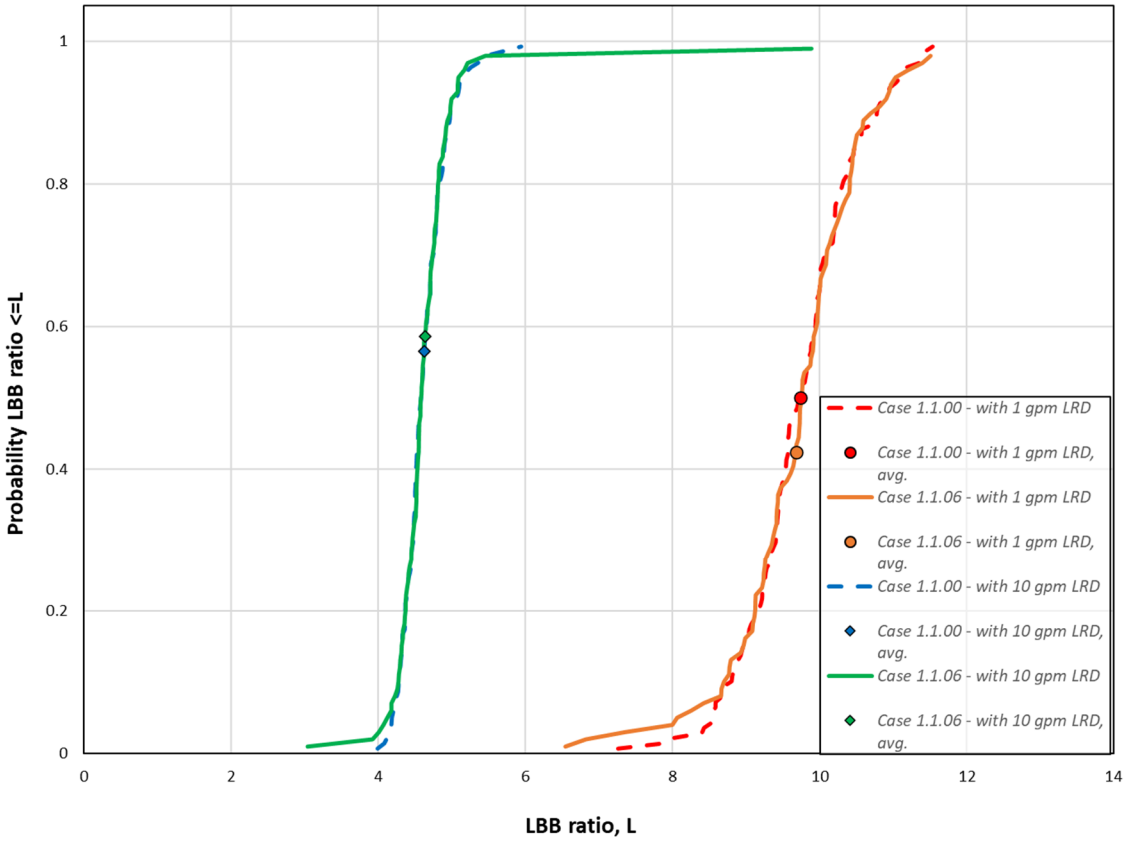


**Figure 3-49 Comparison of Case 1.1.6 LBB ratio distributions with Case 1.1.0**

Standard Indicators

Figure 3-50 shows the results from the standard indicators. It shows that the probability of first crack is higher in Case 1.1.6 where axial cracks are included in the analysis. The probability of first leak is also higher; however, the probability of rupture remains the same. This outcome is because axial cracks in the dissimilar metal weld are limited in length by the width of the weld and only the operating pressure drives crack growth. Therefore, axial cracks increase the overall likelihood of cracks and leaks, but they do not impact rupture.

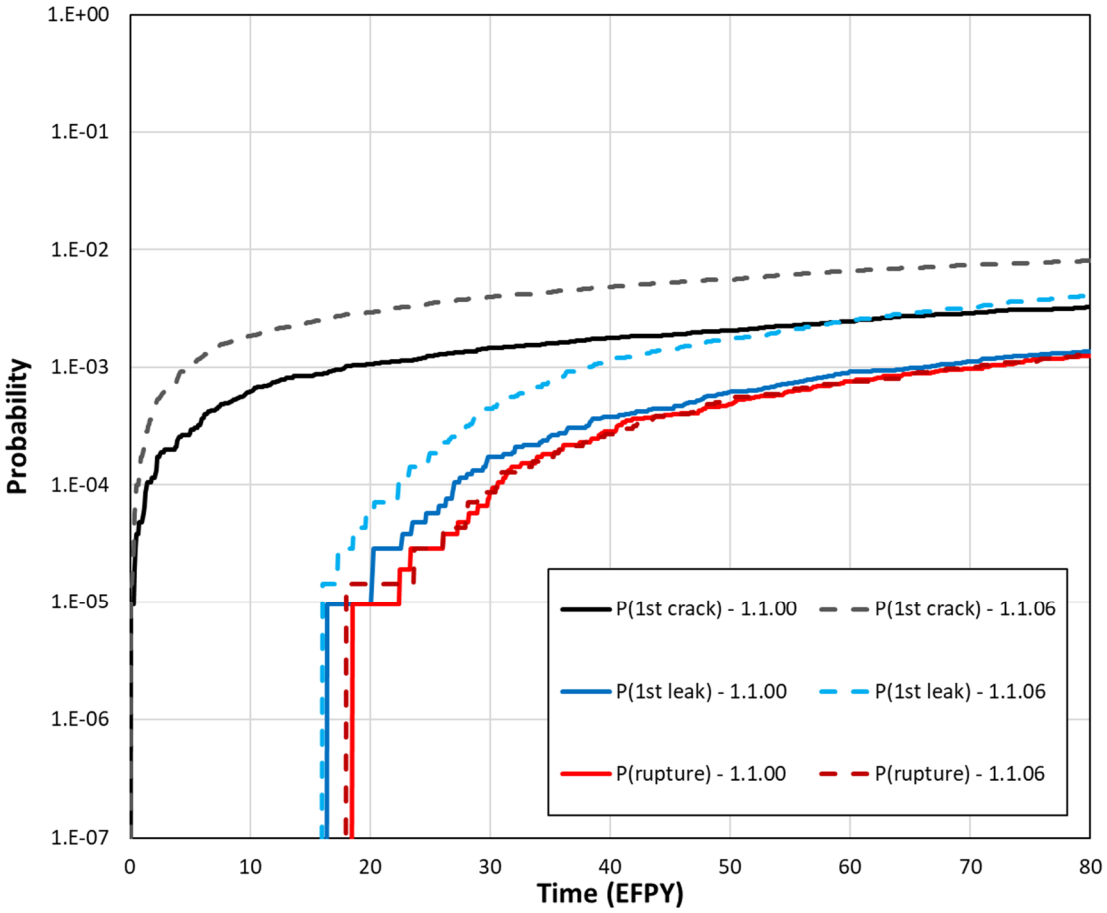


**Figure 3-50 Comparison of Case 1.1.6 time-dependent probabilities of first crack, first leak, and rupture with Case 1.1.0**

3.2.2.4.3 Supplemental Analyses

In the 70,000 realizations executed for Case 1.1.6, only 17 had both axial and circumferential cracks, 328 realizations had only axial cracks, and 220 realizations only had circumferential cracks. The probability of having both axial and circumferential cracks is thus around 2.5 x $10^{-4}$ at 80 EFPY of plant operation. Five of the 17 realizations with both crack orientations had no leakage. Of the remaining 12 realizations, only 4 had circumferential crack leaks, only 5 had axial crack leaks, and only 3 had leaks from both crack orientations. Thus, the likelihood of having an axial crack that influences the total leak rate and potential rupture is low (i.e., only 8 cases out of 70,000, which is around the 1 x $10^{-4}$ probability level at 80 EFPY of plant operation). Moreover, the contribution of the axial crack leak rates to the total leak rate is small enough such that it does not impact leak rate detection. Figure 3-51 displays the CDF for axial leak rate at 80 EFPY based on the 186 realizations with axial TWCs. The leak rates are between 0.005 and 0.02 gpm with a maximum of 0.017 gpm. In conclusion, axial cracks have a negligible impact on leak rate detection and rupture.

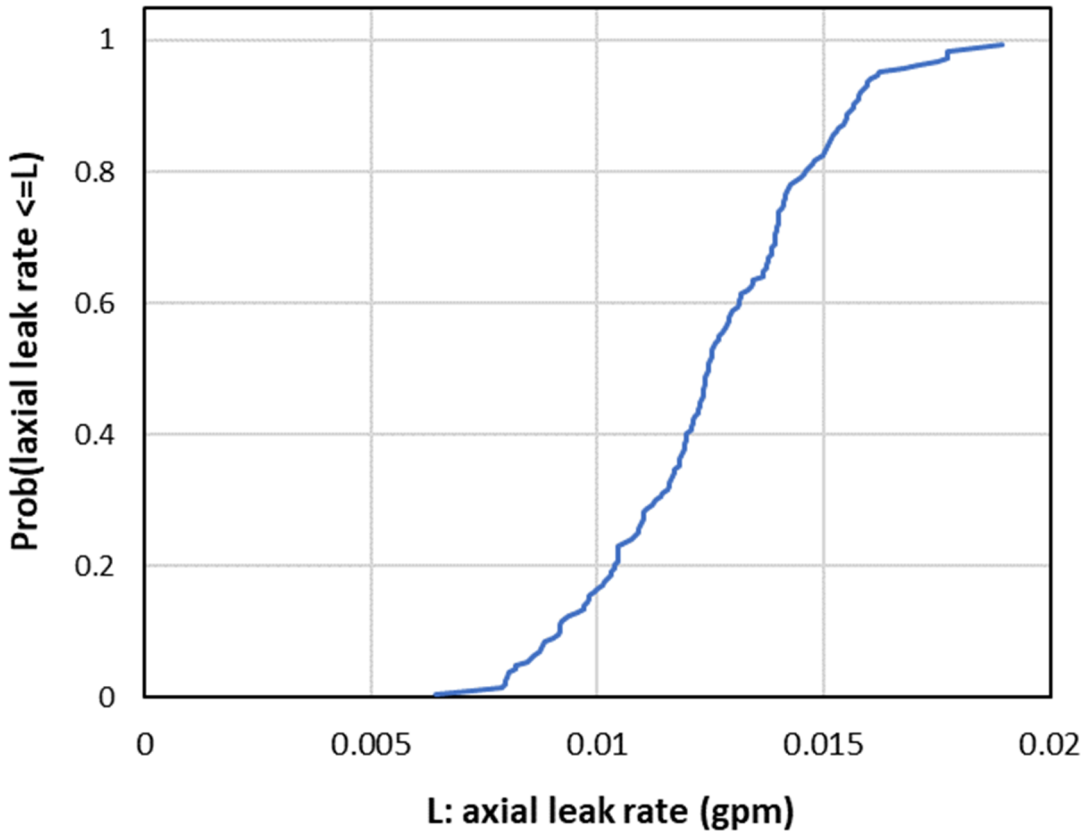


**Figure 3-51 CDF of axial crack leak rate for Case 1.1.6**

### *3.2.2.5 Normal Operating Loads*

3.2.2.5.1 Case Description

The objective of Case 1.1.7 was to assess the sensitivity of the likelihood of failure due to the normal operating stresses. It is like Case 1.1.0 only with higher normal operating stresses. The higher stresses used to analyze this case were developed from distributions fit to axial membrane and bending stress data developed from licensee LBB analyses. Figure 3-52 and Figure 3-53 show the resulting distributions, respectively. In these figures, each data point represents the applied stresses. The values are lower than the nominal stresses selected for this study.

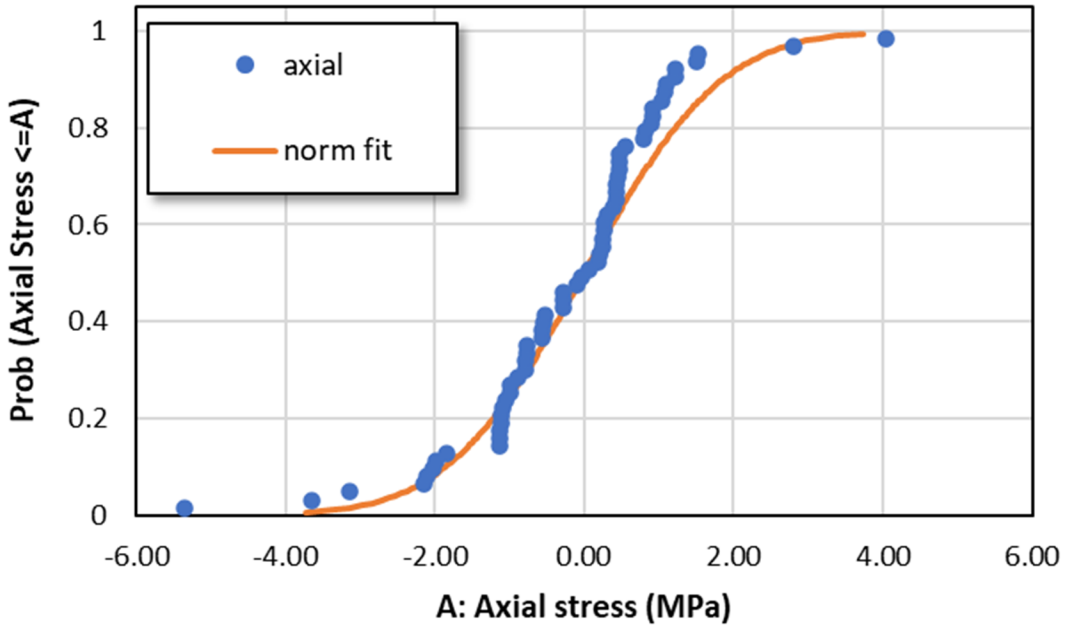


**Figure 3-52 Distribution of axial stresses**

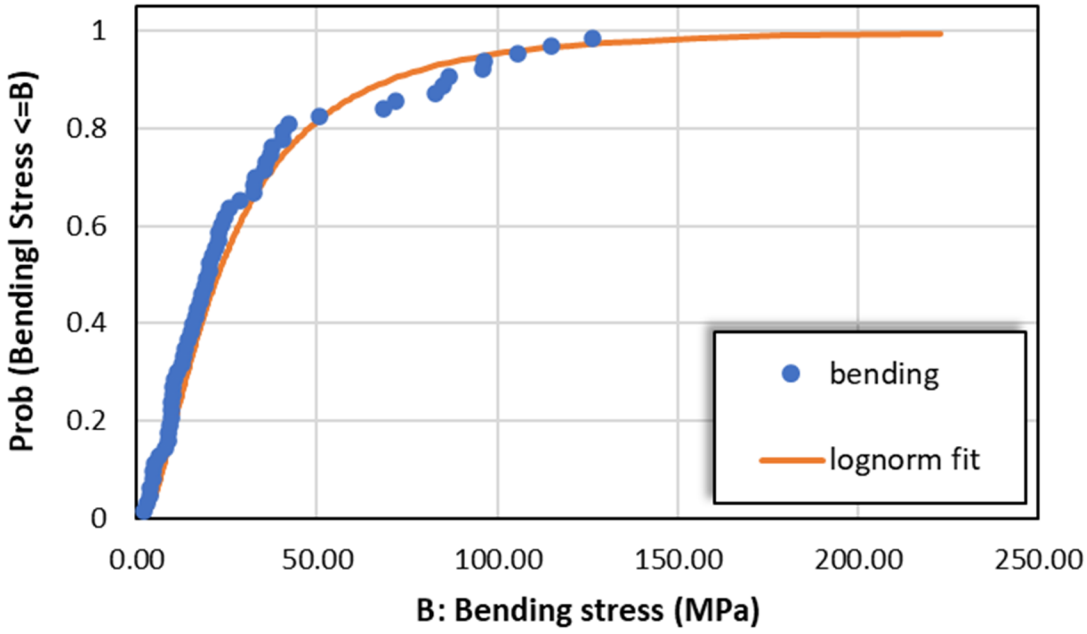


**Figure 3-53 Distribution of bending stresses**

A normal distribution was fit to the axial stress data, while a lognormal distribution was fit to the bending stress data. The fitted distributions were then used to estimate theoretical quantile values. The 95$^{th}$ percentile of the fitted distribution was lower than the stresses used in Case 1.1.0 and would thus lead to a low probability of crack initiation (e.g., around $8 \times 10^{-4}$).

Thus, the 99th percentiles were considered, which correspond to an axial stress of 3.37 MPa and a bending stress of 178 MPa. These stresses are higher than the stresses used in the Case 1.1.0 analysis (i.e., axial stress of -2.39 MPa and bending stress of 147 MPa). The data were also reduced to consider only nonproprietary data and data specific to RVON welds. In both cases, the 99th percentile of the bending stress was lower than 178 MPa; therefore, the stresses based on all the data were used in the analysis. The maximum operating pressure was also slightly higher than the 15.9 MPa value used to analyze Case 1.1.0, so a value of 16 MPa was used. Section B7 describes the specific inputs and other simulation details used to analyze this case.

3.2.2.5.2 Results and Analysis

Rupture with Leak Rate Detection

There were no ruptures with a 1 gpm leak rate detection capability for this case.

Leak Rate Jump

Two realizations out of 100,000 had a leak rate jump leading to a probability of $1.9 \times 10^{-5}$ over 80 EFPY of simulated plant operation. The results are plotted in Figure 3-54. With a 1 gpm leak rate detection capability, there would be no leak rate jump events.

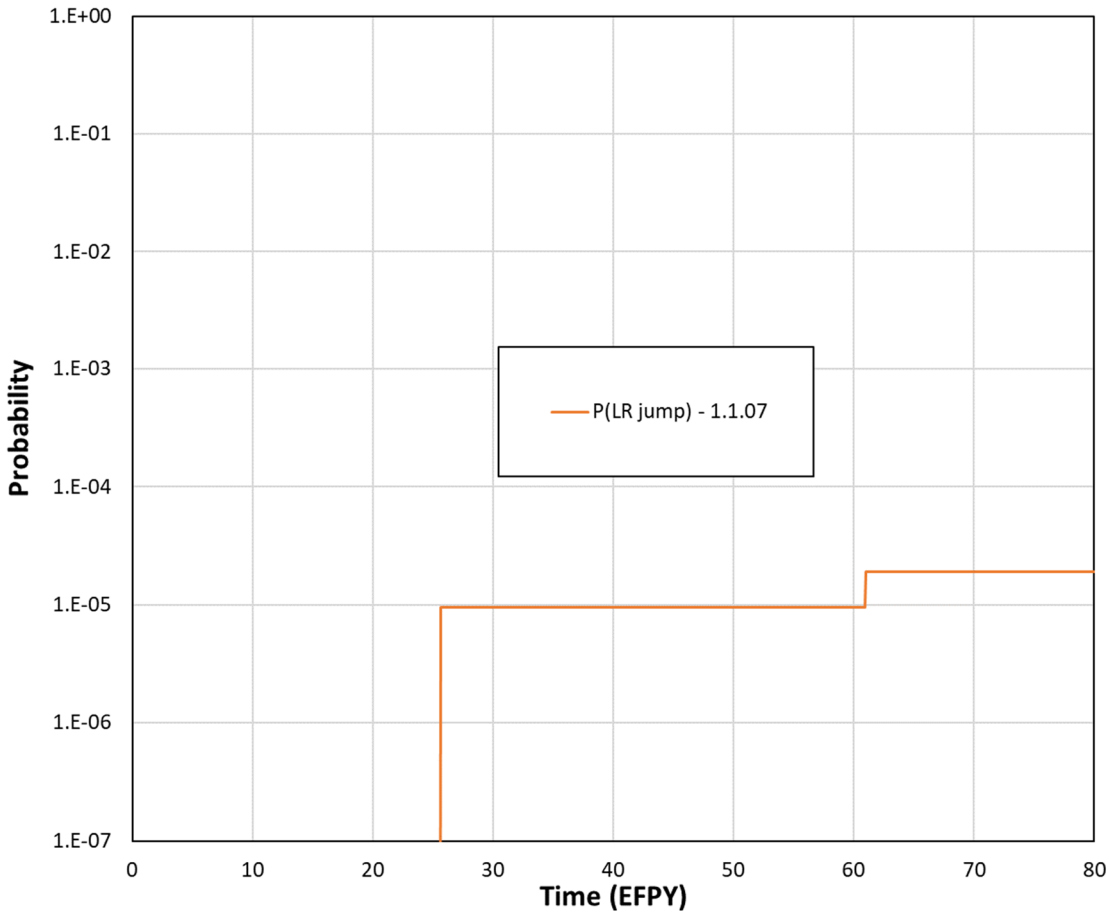


**Figure 3-54 Case 1.1.7 probability of leak rate jump**

In both cases, the leak rate jumps occurred in realizations where two TWCs coalesced. In the xLPR code, the coalescence of two TWCs occurs when their distance is lower than a threshold value, which was sampled uniformly between 0 and 0.5 m. If coalescence occurs, the extremities of the two coalescing cracks are used to determine the size of the resulting crack. In one of the cases, the distance between the coalesced cracks was 0.44 m and the coalescence distance rule threshold was sampled using a very conservative value of 0.49 m. The result is illustrated in Figure 3-55, which indicates a sudden jump in the leak rate. In the other case, which is illustrated in Figure 3-56, a similar event occurred. Here, the distance between the coalesced cracks was 0.17 m, and the coalescence distance rule threshold was sampled at 0.22 m.

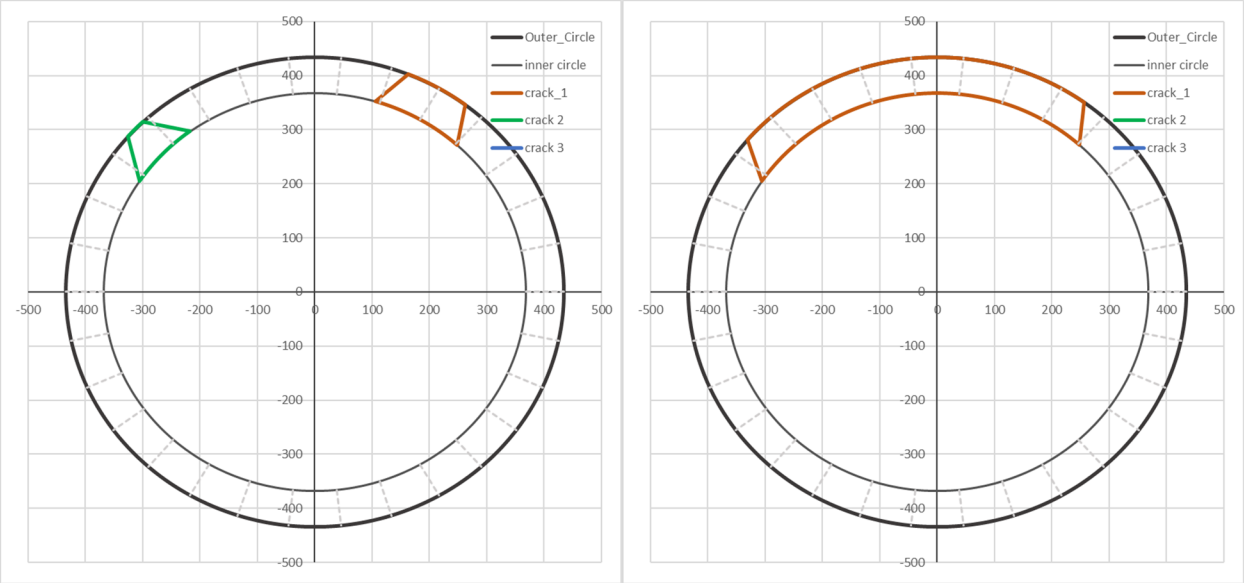


**Figure 3-55 First case of circumferential crack coalescence leading to leak rate jump for Case 1.1.7 just before (left) and after (right) coalescence**

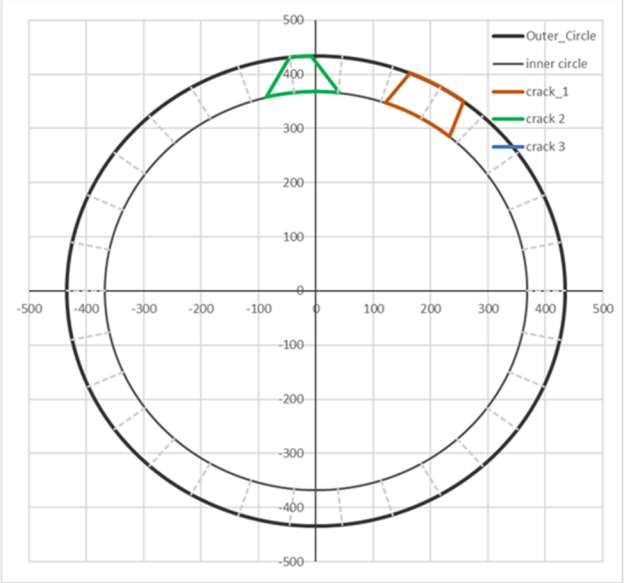


**Figure 3-56 Second case of circumferential crack coalescence leading to leak rate jump for Case 1.1.7 just before coalescence**

Considering these results, the coalescence distance rule threshold distribution used was found to be unrealistic based on engineering judgement. Realistically, coalescence is expected to be less abrupt and, therefore, would not lead to such large leak rate jumps. As such, these two results are not considered to be plausible, especially considering that the stresses used in the analysis were also strongly conservative.

LBB Time Lapse

The mean LBB time lapses and standard errors with 1 and 10 gpm leak rate detection capabilities were respectively as follows:

- 46.6 ± 1.0 months (minimum observed: 5 months)
- 34.0 ± 0.8 months (minimum observed: 5 months)

Note that, as with Case 1.1.0, all results beyond 12 EFPY were excluded as they strongly influence the mean.

Figure 3-57 shows the LBB time lapse CDF plots. Overall, the LBB time lapses in Case 1.1.7 were slightly shorter than in Case 1.1.0. This result was expected, because increased normal operating stresses would lead to faster crack growth and more realizations with leaks and ruptures. The reduced time is small enough to be considered negligible.

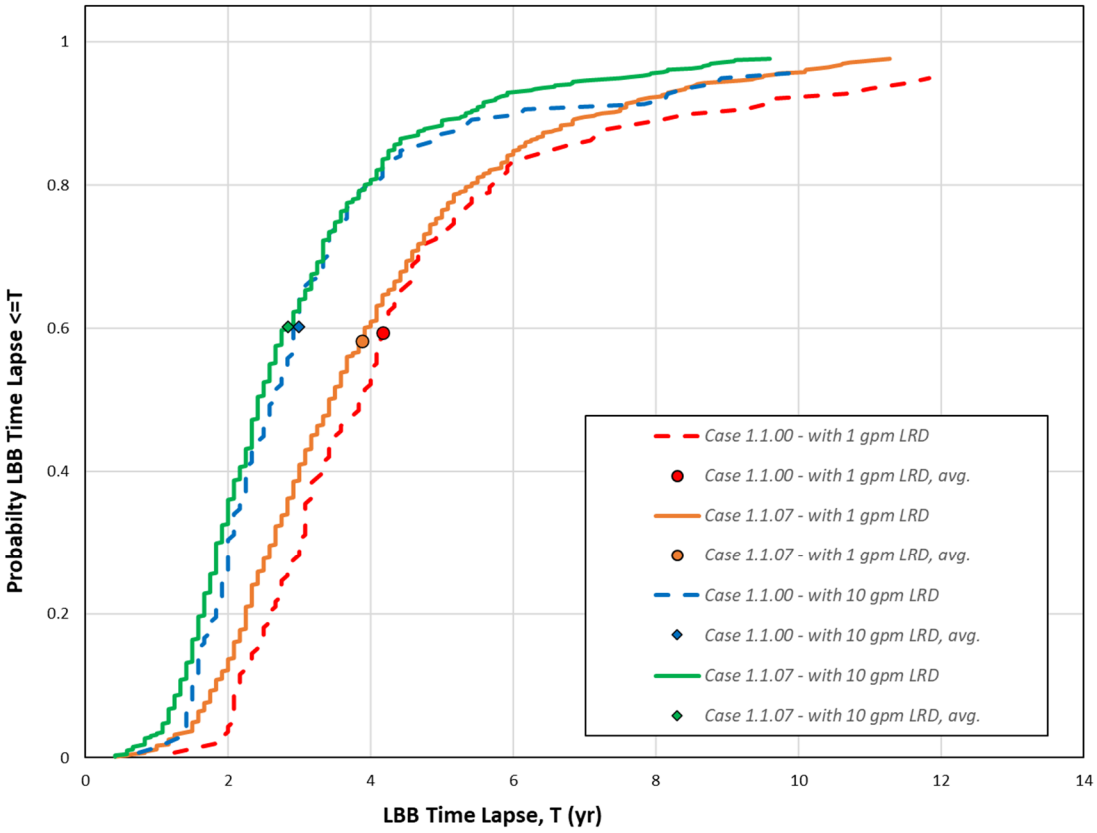


**Figure 3-57 Comparison of Case 1.1.7 LBB time lapse distributions with Case 1.1.0**

LBB Ratio

The mean LBB ratios and standard errors with 1 and 10 gpm leak rate detection capabilities were respectively as follows:

- 9.52 ± 0.04 (minimum observed: 2.74)
- 4.7 ± 0.017 (minimum observed: 2.71)

Figure 3-58 shows the LBB ratio CDF plots. It illustrates that the normal operating stresses do not have an impact on this QoI. The small variations may be explained by more realizations having ruptures in Case 1.1.7.

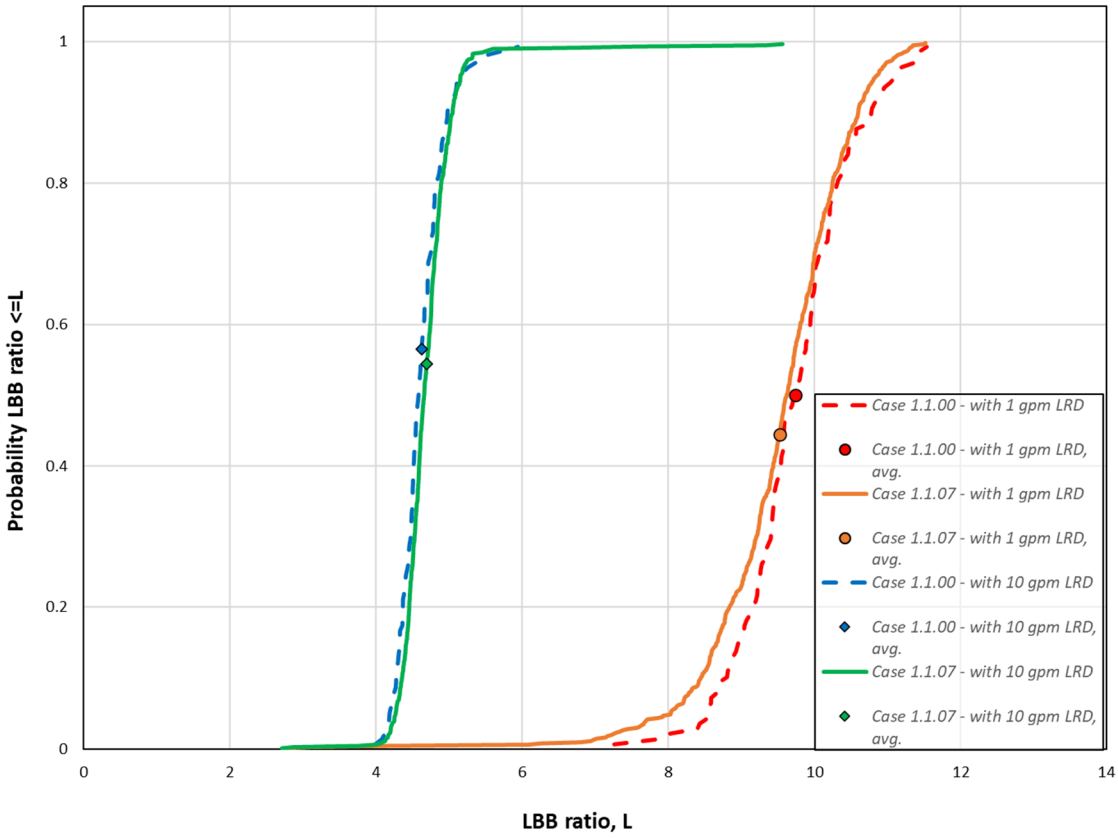


**Figure 3-58 Comparison of Case 1.1.7 LBB ratio distributions with Case 1.1.0**

Standard Indicators

Figure 3-59 shows the results from the standard indicators. It shows that the probabilities of first crack, first leak, and rupture all increase in Case 1.1.7 as compared to Case 1.1.0. The probabilities of first leak and rupture are also closer, which indicates a slightly shorter time between detectable leakage and rupture that is consistent with the LBB time lapse results.

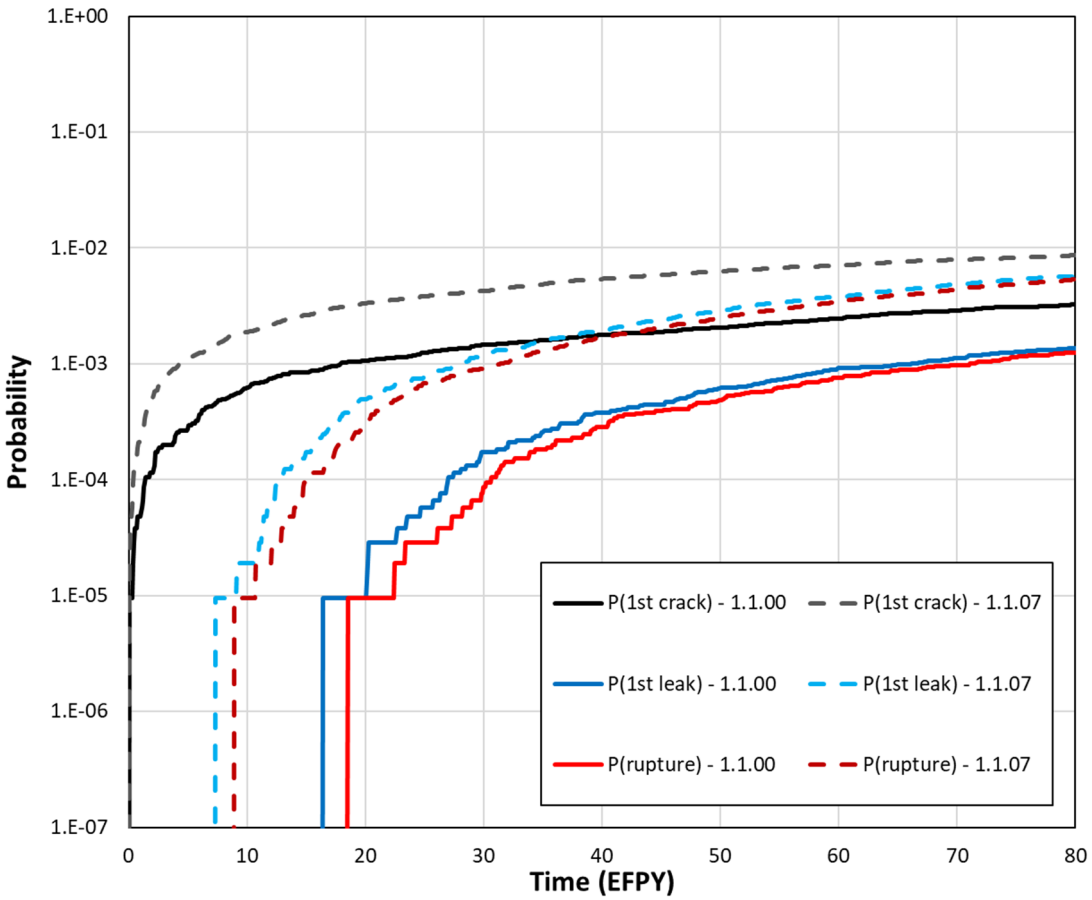


**Figure 3-59 Comparison of Case 1.1.7 time-dependent probabilities of first crack, first leak, and rupture with Case 1.1.0**

### *3.2.2.6 Detectable Leak Rate*

#### 3.2.2.6.1 Case Description

The objective of Case 1.1.8 was to assess the impacts of the leak rate detection capability on the likelihood of failure. It is like Case 1.1.0 only with a different detectable leak rate. A 10 gpm leak rate detection capability was used in the analysis of Case 1.1.0 for alignment with most of the deterministic licensee LBB analyses, which applied a factor of 10 to the plants' 1 gpm leak rate detection capabilities consistent with the guidance in SRP Section 3.6.3. Since Case 1.1.0 showed no occurrences of rupture with a 10 gpm leak rate detection capability, instead of performing another simulation, the results from Case 1.1.0 were analyzed to estimate the leak rates just prior to ruptures.

#### 3.2.2.6.2 Results and Analysis

Only the probability of rupture with leak rate detection was analyzed because all the other QoIs are either not affected by a change in the detectable leak rate or were already analyzed with both 1 and 10 gpm leak rate detection capabilities to gauge sensitivities to the detectable leak

rate. For each realization leading to rupture, the value of the leak rate 1 month prior to rupture was extracted and used to create a distribution of leak rates. The 1-month time was selected because it is equivalent to the simulation timestep and thus represents the highest level of accuracy in the results. Figure 3-60 shows the resulting distributions for all three of the Case 1.1.0 simulations. The minimum value observed is around 130 gpm. Any detection limit below this value would lead to the same results. Thus, any detectable leak rate in the range of 0.1 to 50 gpm would lead to the same results. No undesirable break-before-leak scenarios would occur under these conditions.

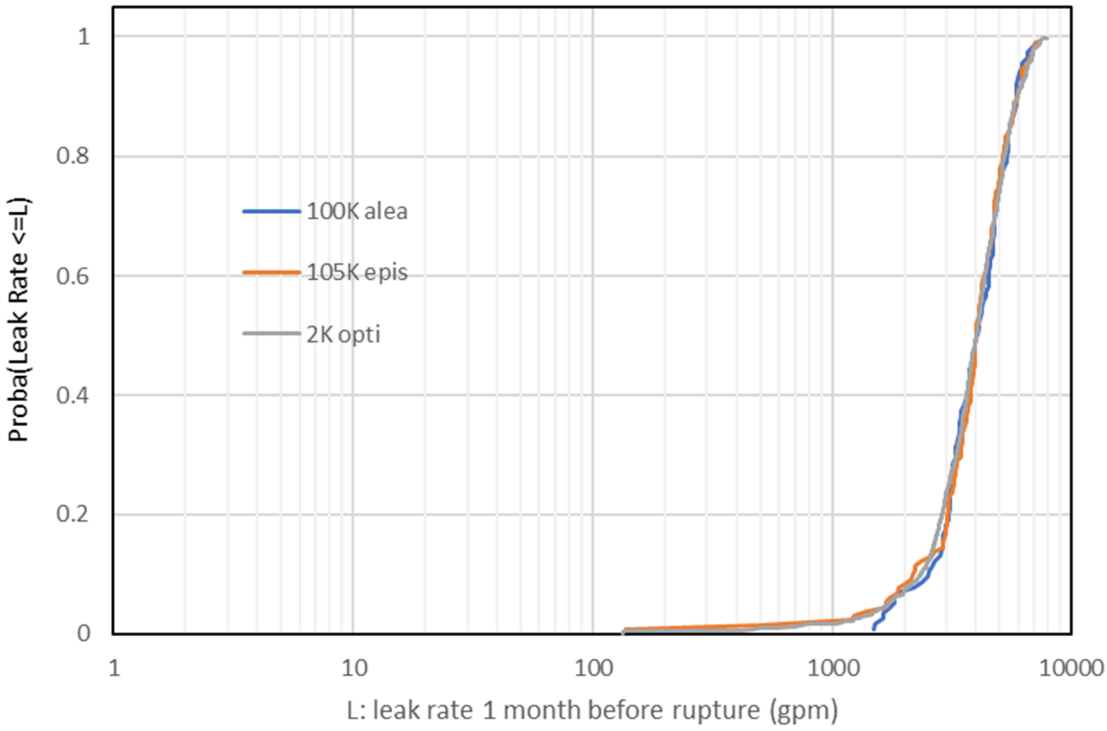


**Figure 3-60 Distribution of leak rate one month before rupture for Case 1.1.0**

### *3.2.2.7 Mechanical Stress Improvement*

3.2.2.7.1 Case Description

The objective of Case 1.1.9 was to assess the impacts of MSIP on the likelihood of failure. It is like Case 1.1.0 with the addition of MSIP for PWSCC mitigation. MSIP was selected because it is the most common mechanical mitigation technique used on RVON welds. It is modeled by changing the axial WRS profile at a specified time in the simulation. An analysis of MSIP applications using data from [33], [34], [35], [36], [37], and [38] determined that the average time of application was after 27 years of service with a comparable median value. A slightly more conservative time of MSIP application of 30 years was used to analyze this case considering that MSIP leads to a reduced likelihood of crack initiation and slower crack growth. Section B8 describes the specific inputs and other simulation details used to analyze this case.

#### 3.2.2.7.2 Results and Analysis

Rupture with Leak Rate Detection

There were no ruptures with a 1 gpm leak rate detection capability for this case.

Leak Rate Jump

There were no leak rate jump events for this case.

LBB Time Lapse

The mean LBB time lapses and standard errors with 1 and 10 gpm leak rate detection capabilities were respectively as follows:

- 41.6 ± 2.3 months (minimum observed: 15 months)
- 28.9 ± 2.0 months (minimum observed: 9 months)

Note that, as with Case 1.1.0, all results beyond 12 EFPY were excluded as they strongly influence the mean.

Figure 3-61 shows a comparison of the LBB time lapse CDFs between Cases 1.1.9 and 1.1.0. It shows that the LBB time lapses with both 1 and 10 gpm leak rate detection capabilities are less with the MSIP. This result is expected because the results are conditional on having both leaks and ruptures, which occur before the MSIP is applied. The results thus bias the CDF toward the lower values as compared to Case 1.1.0.

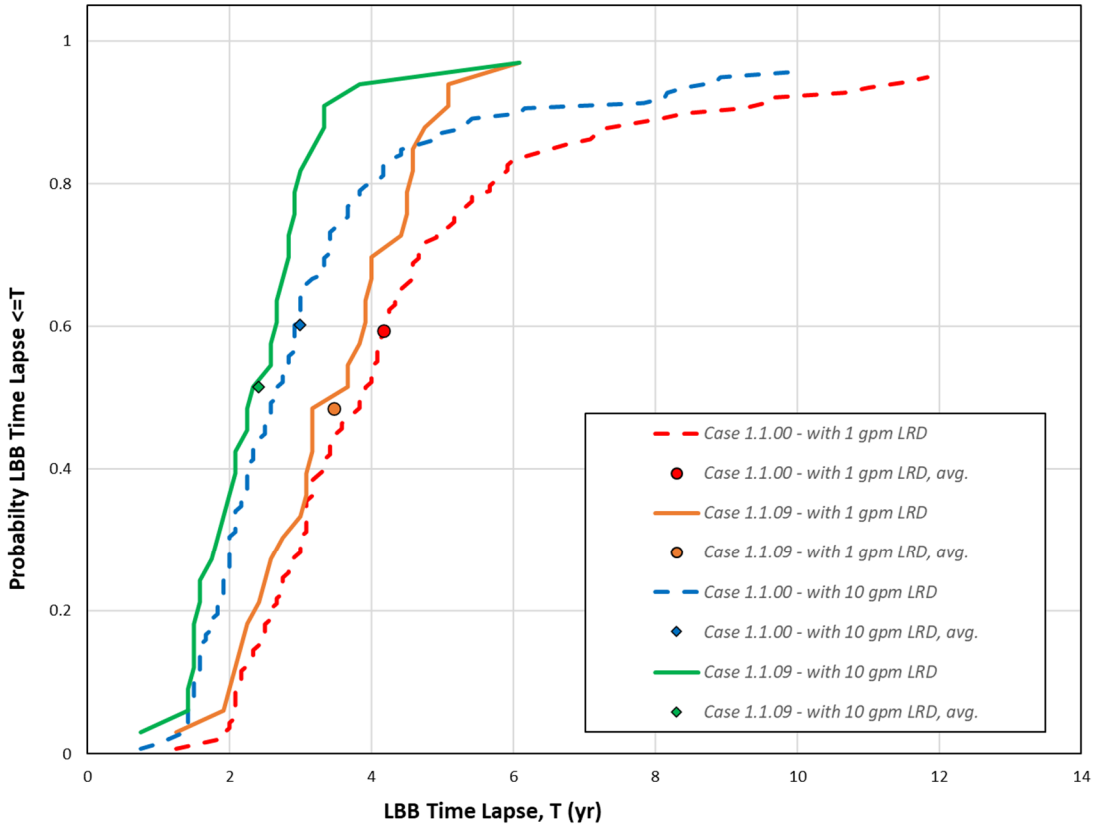


**Figure 3-61 Comparison of Case 1.1.9 LBB time lapse distributions with Case 1.1.0**

LBB Ratio

The mean LBB ratios and standard errors with 1 and 10 gpm leak rate detection capabilities were respectively as follows:

- 10.29 ± 0.15 (minimum observed: 8.70)
- 4.81 ± 0.13 (minimum observed: 4.25)

Figure 3-62 shows the LBB ratio CDF plots. It illustrates that the LBB ratio is higher when MSIP is applied. The difference is more pronounced with a 1 gpm leak rate detection capability. The difference is likely due to the small sample size (i.e., only 30 realizations had a rupture before MSIP was applied).

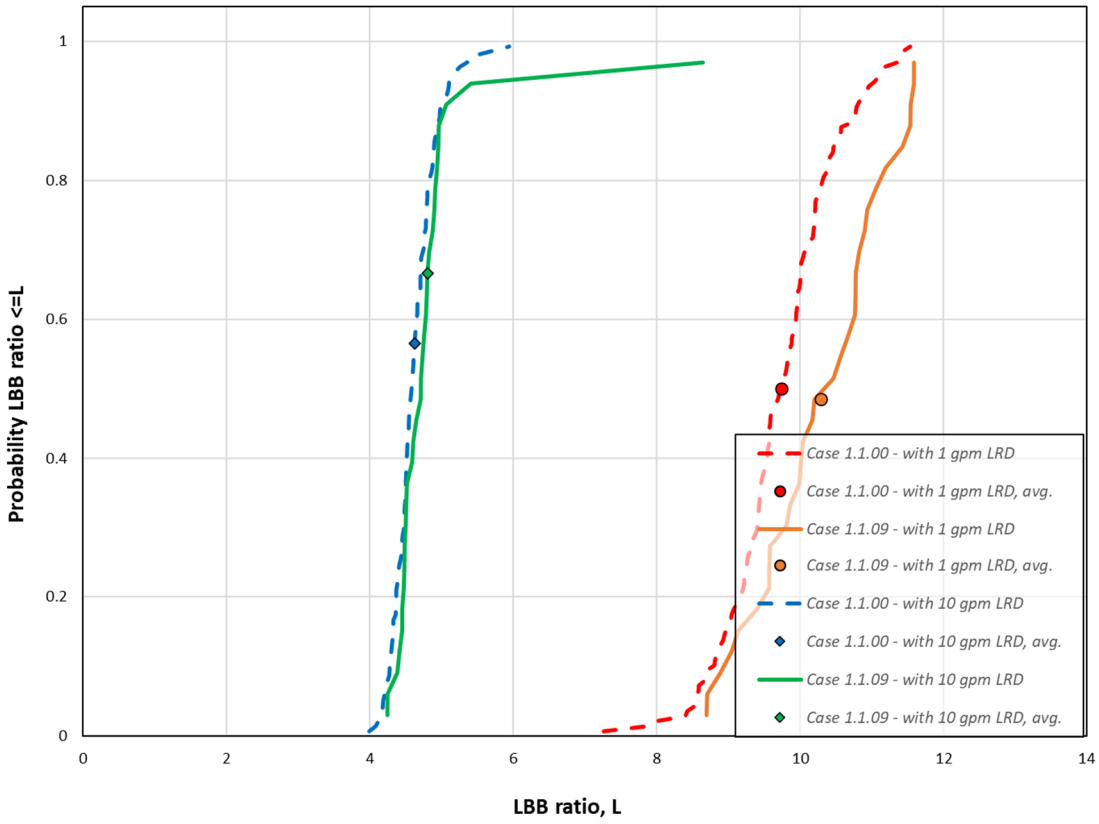


**Figure 3-62 Comparison of Case 1.1.9 LBB ratio distributions with Case 1.1.0**

Standard Indicators

Figure 3-63 shows the results from the standard indicators. It clearly shows the impact that MSIP has on the probabilities of first crack, first leak, and rupture. When MSIP is applied at 30 years, all these probabilities begin to level-off and then remain constant. The probabilities are thus significantly lower at 80 EFPY than in Case 1.1.0.

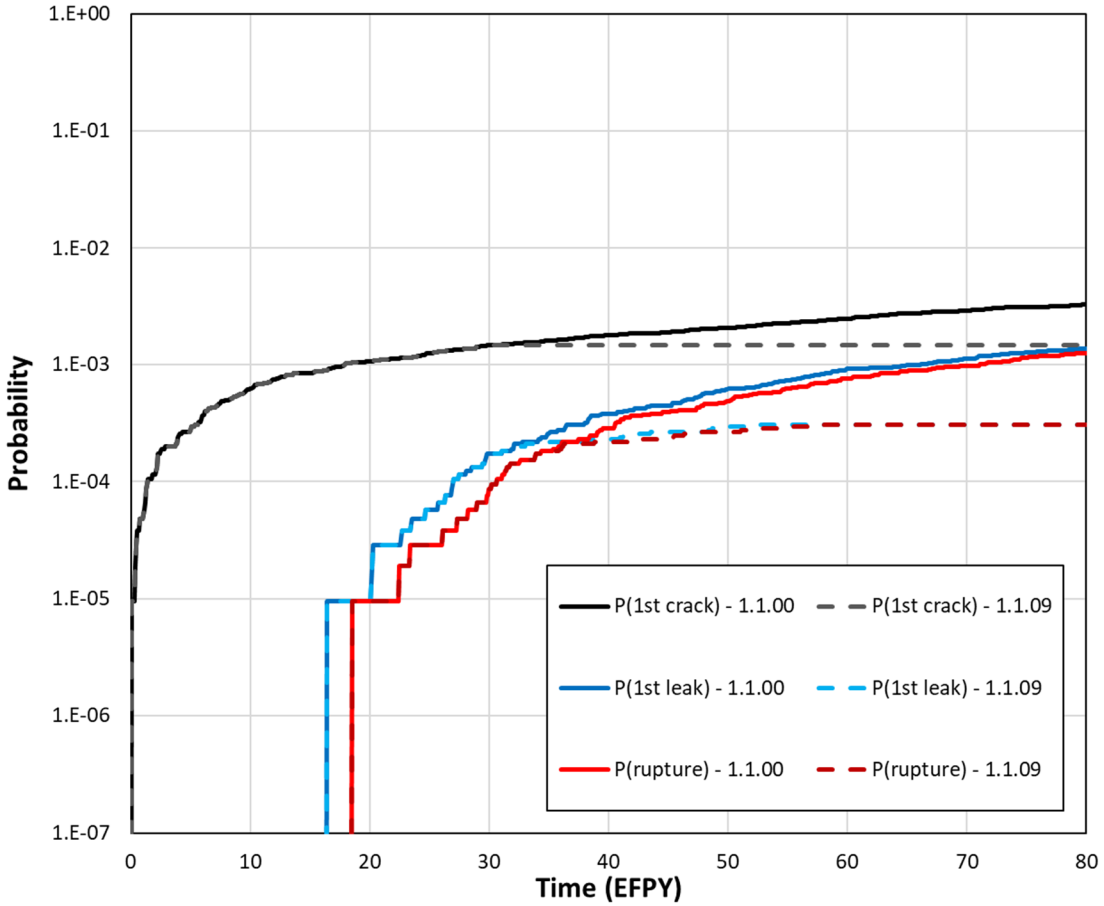


**Figure 3-63 Comparison of Case 1.1.9 time-dependent probabilities of first crack, first leak, and rupture with Case 1.1.0**

### *3.2.2.8 Inservice Inspection*

3.2.2.8.1 Case Description

The objective of Cases 1.1.10 and 1.1.11 was to assess the impacts of the ISI model parameters and inspection frequencies on the likelihood of failure. These cases are like Case 1.1.1 with the addition of ISI. As in Case 1.1.1, seismic effects were also excluded in Cases 1.1.10 and 1.1.11, and the hydrogen in the reactor coolant system was set to an unmitigated concentration of 37 cc/kg. Case 1.1.10 used the probability of detection (POD) model parameters developed from the EPRI Performance Demonstration Initiative (PDI) program data as detailed in [25]. Case 1.1.11 used a set of POD model parameters developed for the NRC by Pacific Northwest National Laboratories (PNNL) as documented in PNNL-28090, "Analysis of Empirical Probability of Detection Data for Dissimilar Metal Welds," issued July 2019 [39]. Figure 3-64 shows a comparison of the mean POD curves with 95$^{th}$ percentile confidence intervals. It demonstrates that the POD curve based on the PNNL-recommended model is higher beyond 20 percent of the weld thickness. The PNNL report also recommends a minimum detectable crack depth of 1 percent of the weld thickness; however, this value was

considered too optimistic for the analysis, and a value of 10 percent was used instead. Results based on inspections performed every 5 and 10 years were considered in both cases to assess the impact of the length of time between inspections. The specific inputs and other simulation details used to analyze these cases are in Sections B9 and B10.

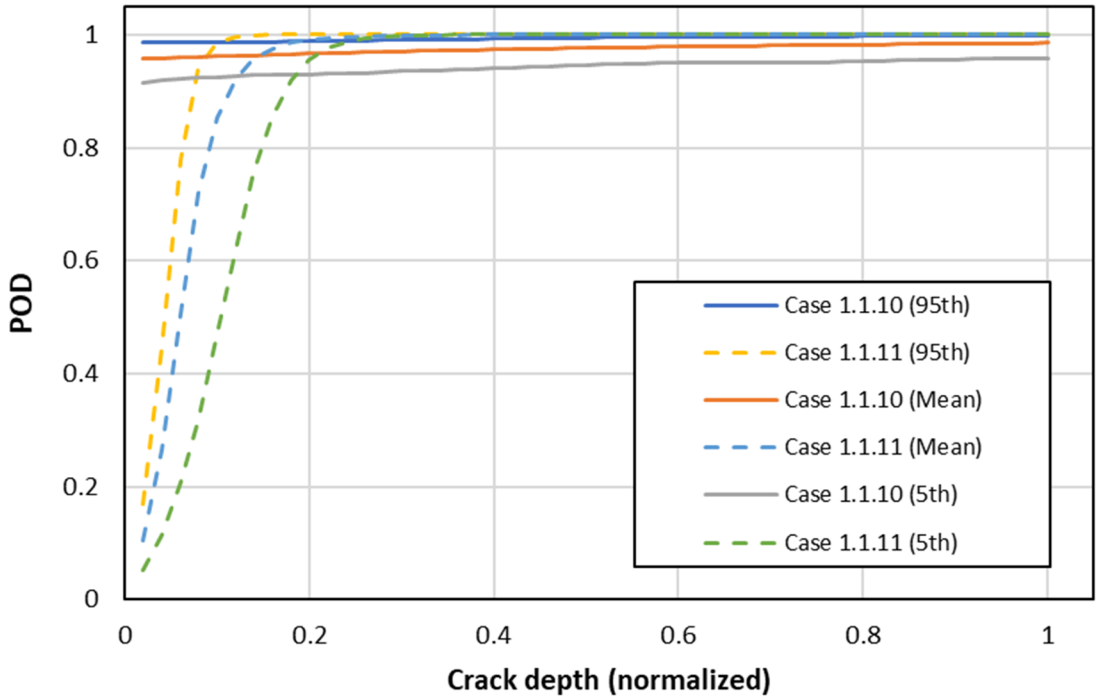


**Figure 3-64 Comparison of POD curves using different model parameters**

3.2.2.8.2 Results and Analysis

Rupture with Leak Rate Detection

There were no ruptures with a 1 gpm leak rate detection capability for these cases.

Leak Rate Jump

There were no leak rate jump events for these cases.

LBB Time Lapse

ISI has no impact on the LBB time lapse distributions based on the way that it is implemented in the xLPR code, because inspections are used to weight the realizations in the code's post-processing calculations. Thus, inspections have no effect on results that are conditional on rupture. Therefore, the mean LBB time lapses are the same as in Case 1.1.1.

LBB Ratio

ISI has no impact on the LBB ratio distributions based on the way that it is implemented in the xLPR code, because inspections do not affect the leakage or critical crack sizes. Therefore, the mean LBB ratios are the same as in Case 1.1.1.

Standard Indicators

Results from the standard indicators are shown in the next set of figures. Figure 3-65 shows the Case 1.1.10 results based on a 10-year inspection interval, conditional on having a crack at the beginning of every realization. Both the curves representing the probabilities of first leak and rupture are flatter at 10 EFPY as compared to Case 1.1.1, and then they remain essentially constant after 20 EFPY. At 80 EFPY, the probabilities of first leak and rupture are two orders of magnitude lower than in Case 1.1.1.

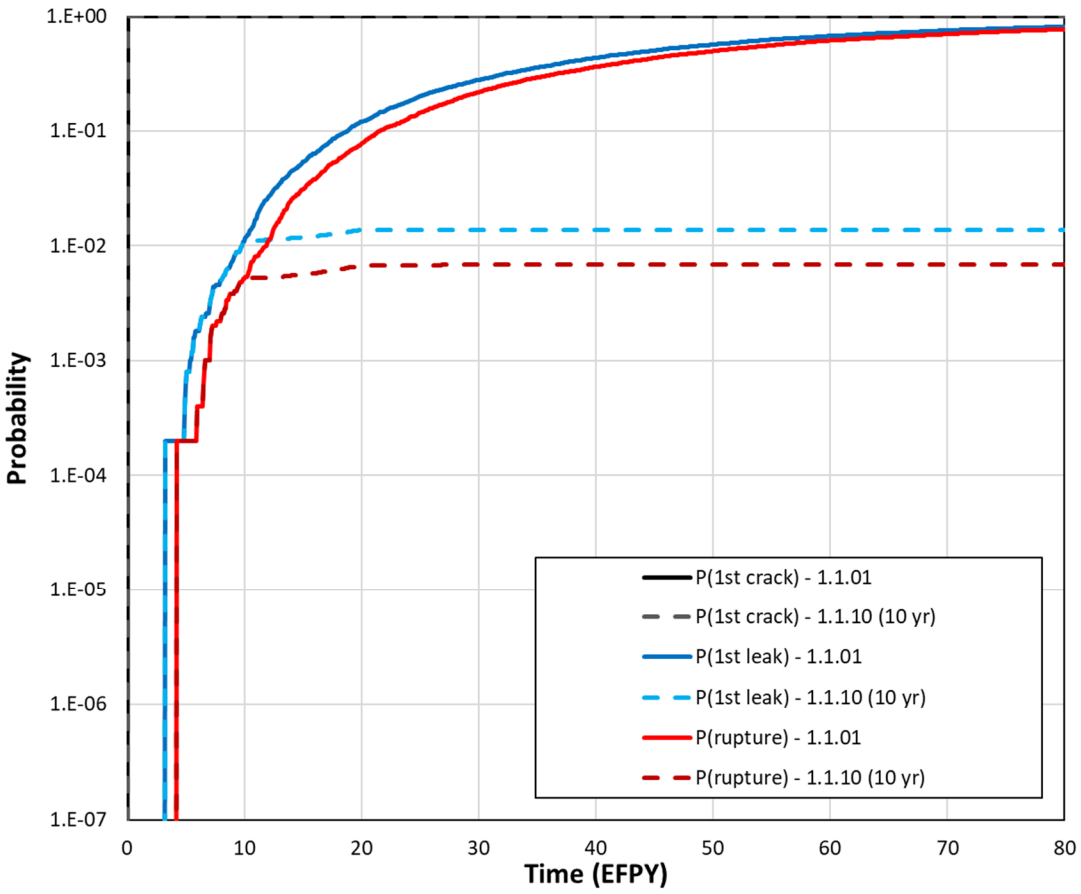


**Figure 3-65 Comparison of Case 1.1.10 time-dependent probabilities of first crack, first leak, and rupture with Case 1.1.1 with ISI every 10 years and EPRI-developed POD model parameters**

Figure 3-66 shows the Case 1.1.10 results based on a 5-year inspection interval, conditional on having a crack at the beginning of every realization. The Case 1.1.10 analysis used POD model parameters developed from the EPRI PDI program. Both the curves representing the

probabilities of first leak and rupture flatten as compared to Case 1.1.1 when the first and second inspections occur at 5 and 10 years, respectively. Then they remain essentially constant over the remainder of the simulated period of plant operation. Since the first inspection occurs earlier in this simulation, the probabilities of leak are about 3 orders of magnitude lower than in Case 1.1.1. These results show a reduction of 3.5 orders of magnitude in the probabilities of rupture.

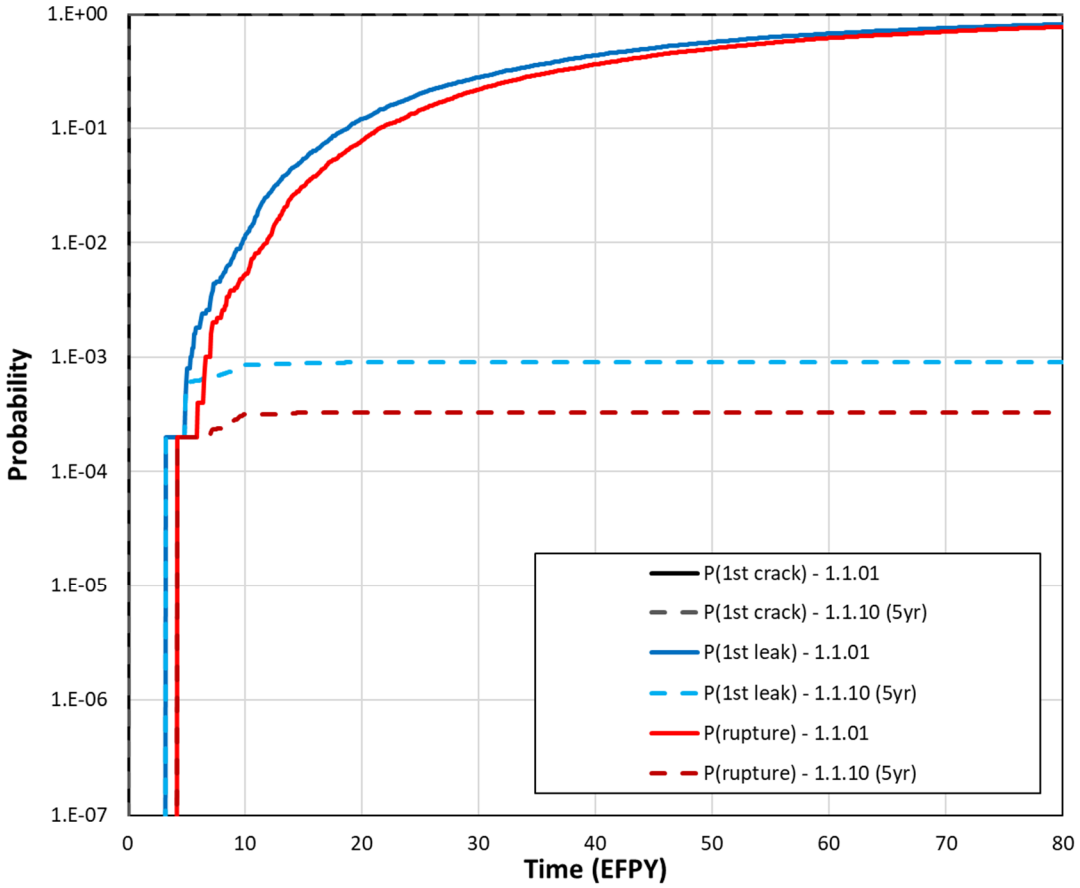


**Figure 3-66 Comparison of Case 1.1.10 time-dependent probabilities of first crack, first leak, and rupture with Case 1.1.1 with ISI every 5 years and EPRI-developed POD model parameters**

Figure 3-67 shows the Case 1.1.11 results based on a 10-year inspection interval, conditional on having a crack at the beginning of every realization. The Case 1.1.11 analysis used POD model parameters developed by PNNL. The trends are similar to those for Case 1.1.10 as shown in Figure 3-65 for both the probabilities of first leak and rupture. However, the probabilities in Case 1.1.11 are about 30 percent lower using the PNNL-recommended POD model parameters.

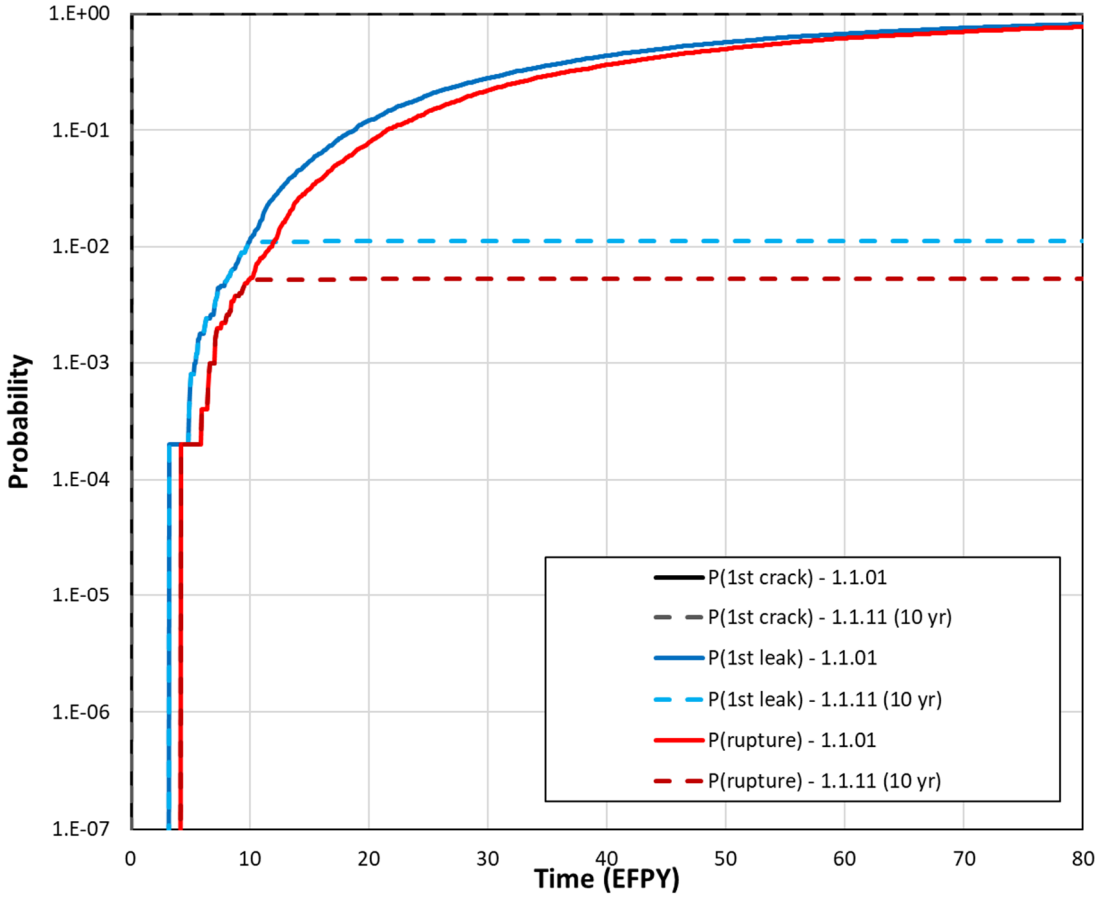


**Figure 3-67 Comparison of Case 1.1.11 time-dependent probabilities of first crack, first leak, and rupture with Case 1.1.1 with ISI every 10 years and PNNL-developed POD model parameters**

Figure 3-68 shows the Case 1.1.11 results based on a 5-year inspection interval, conditional on having a crack at the beginning of every realization. The trends are again similar to those for Case 1.1.10 as shown in Figure 3-66 for both the probabilities of first leak and rupture. However, the probabilities in Case 1.1.11 are about 40 percent lower using the PNNL-recommended POD model parameters.

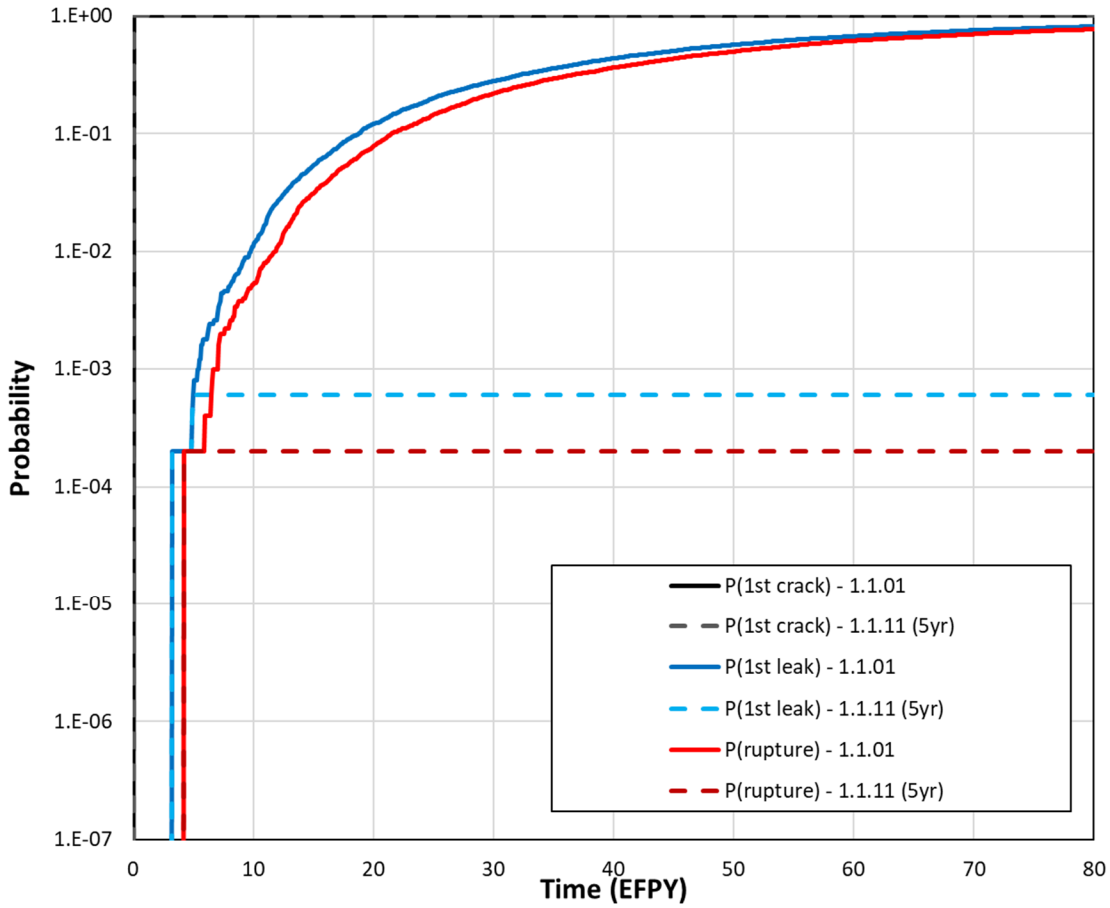


**Figure 3-68 Comparison of Case 1.1.11 time-dependent probabilities of first crack, first leak, and rupture with Case 1.1.1 with ISI every 5 years and PNNL-developed POD model parameters**

### *3.2.2.9 Hydrogen Concentration*

3.2.2.9.1 Case Description

The objective of Case 1.1.14 was to assess the impacts of the hydrogen concentration on the likelihood of failure. It is like Case 1.1.1 but with a different hydrogen concentration. The hydrogen concentration in the reactor coolant system only affects the crack growth rate. The hydrogen concentration in Case 1.1.1 was set to 37 cc/kg, whereas, in Case 1.1.14 it was set to 25 cc/kg to bound the operating experience of PWRs as reported in [29]. This is a conservative choice as it leads to faster crack growth. Section B11 describes the specific inputs and other simulation details used to analyze this case.

3.2.2.9.2 Results and Analysis

Rupture with Leak Rate Detection

There were no ruptures with a 1 gpm leak rate detection capability for this case.

Leak Rate Jump

There were no leak rate jump events for this case.

LBB time lapse

The mean LBB time lapses and standard errors with 1 and 10 gpm leak rate detection capabilities were respectively as follows:

- 39.0 ± 0.25 months (minimum observed: 10 months)
- 26.8 ± 0.2 months (minimum observed: 7 months)

Note that, as with Case 1.1.0, all results beyond 12 EFPY were excluded as they strongly influence the mean.

Figure 3-69 shows the LBB time lapse results. Since these results are based on faster crack growth rates, it follows that the time between detectable leaks and ruptures is less than in Case 1.1.1.

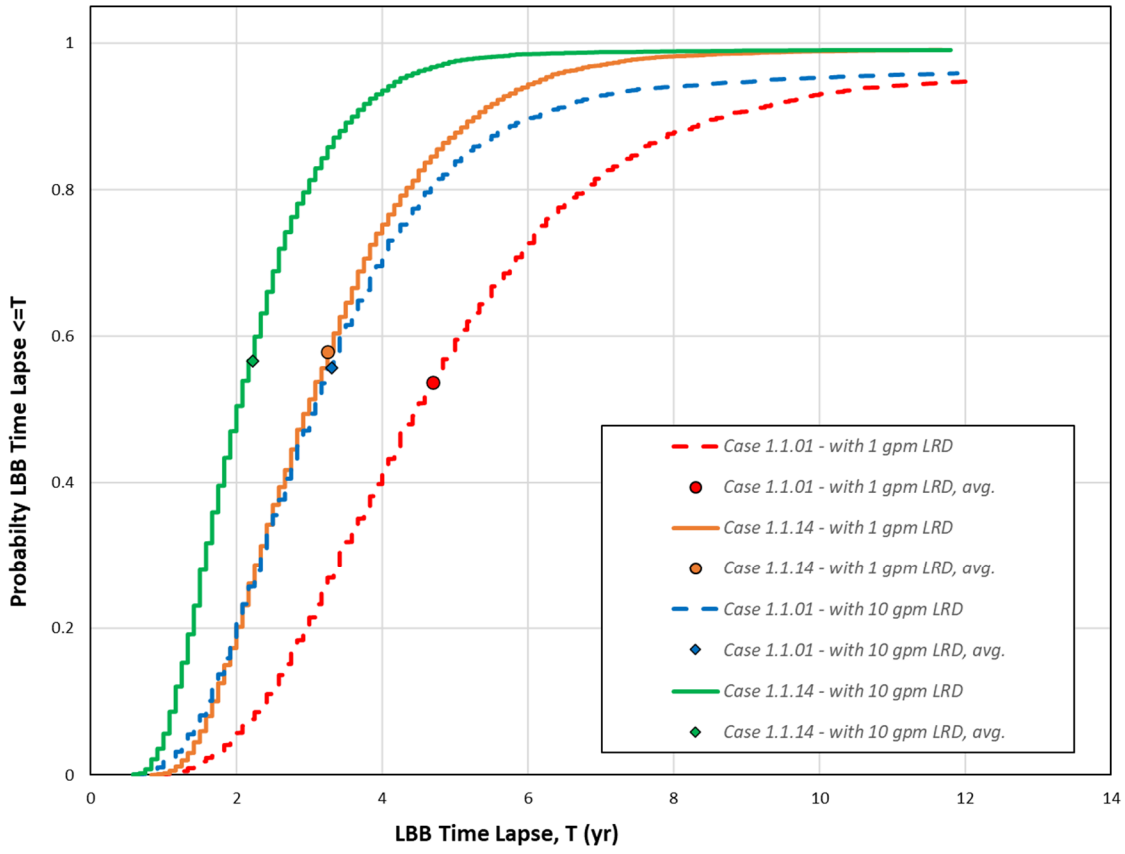


**Figure 3-69 Comparison of Case 1.1.14 LBB time lapse distributions with Case 1.1.1**

LBB Ratio

The mean LBB ratios and standard errors with 1 and 10 gpm leak rate detection capabilities were respectively as follows:

- 9.85 ± 0.01 (minimum observed: 7.50)
- 4.63 ± 0.003 (minimum observed: 3.99)

Figure 3-70 shows the LBB ratio CDF plots. It illustrates that the hydrogen concentration has almost no influence on the LBB ratio. This result is expected because the hydrogen concentration only affects the crack growth rate, and neither the leakage nor rupture crack sizes are impacted by the crack growth rate.

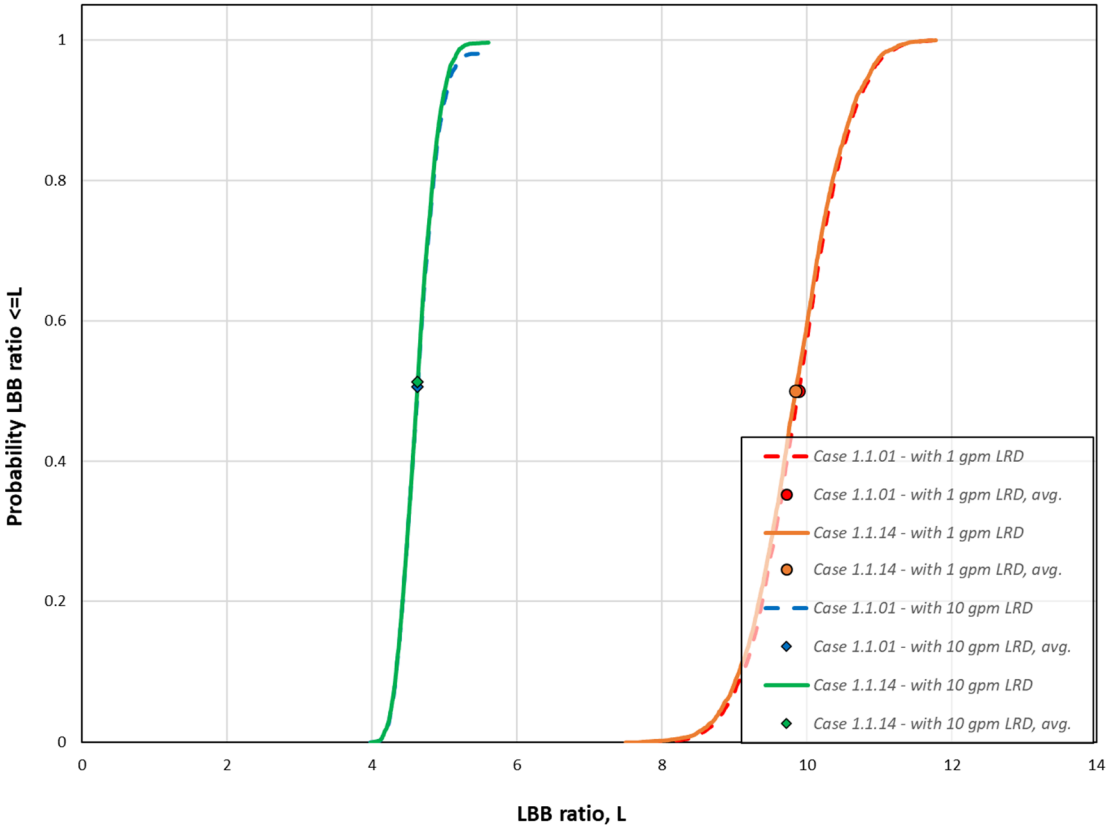


**Figure 3-70 Comparison of Case 1.1.14 LBB ratio distributions with Case 1.1.1**

Standard Indicators

Figure 3-71 shows the results from the standard indicators. It shows that the decreased hydrogen concentration in Case 1.1.14 impacts the probabilities of first leak and rupture. As expected, the faster crack growth rates lead to more leaks and ruptures; however, the impact is small.

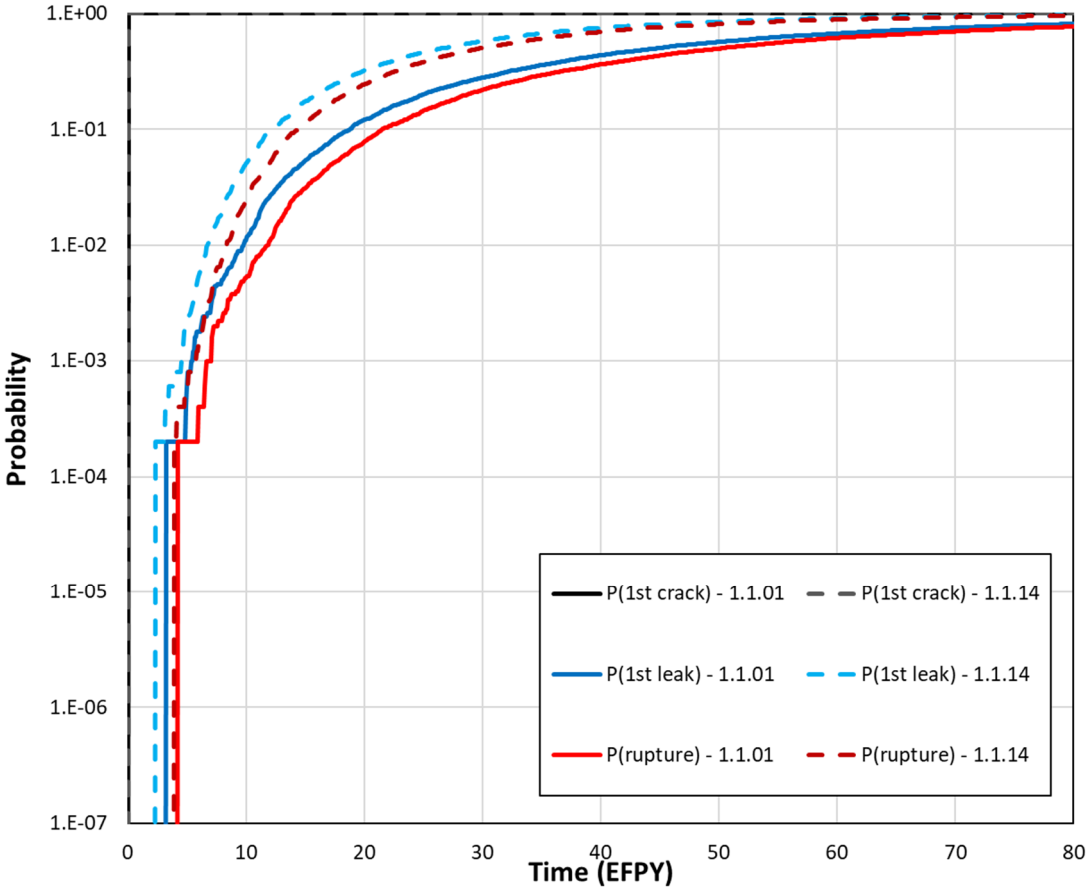


**Figure 3-71 Comparison of Case 1.1.14 time-dependent probabilities of first crack, first leak, and rupture with Case 1.1.1**

### *3.2.2.10 Combined Effects of PWSCC and Fatigue*

3.2.2.10.1 Case Description

The objective of Case 1.1.15 was to assess the impacts of the combined effects of PWSCC and fatigue. Most of the fatigue inputs used to analyze this case came from Case 1, Scenario 10 as detailed in [25]. Otherwise, the inputs for Case 1.1.15 are the same as in Case 1.1.0. The following transients were considered in the analysis:

- plant heat-up (10 cycles every 3 years)
- plant cool-down (10 cycles every 3 years)
- plant loading (305 cycles every year)
- plant unloading (305 cycles every year)
- step load increase (100 cycles every 3 years)
- step load decrease (100 cycles every 3 years)

- large step load decrease (10 cycles every 3 years)
- loss of load (4 cycles every 3 years)
- partial loss of flow (4 cycles every 3 years)
- reactor trip (20 cycles every 3 years)

Section B12 describes the specific inputs and other simulation details used to analyze this case.

3.2.2.10.2 Results and Analysis

Rupture with Leak Rate Detection

There were no ruptures with a 1 gpm leak rate detection capability for this case.

Leak Rate Jump

There were no leak rate jump events for this case.

LBB Time Lapse

The mean LBB time lapses and standard errors with 1 and 10 gpm leak rate detection capabilities were respectively as follows:

- 14 ± 0.8 months (minimum observed: 7 months)
- 10.3 ± 0.7 months (minimum observed: 5 months)

Note that, as with Case 1.1.0, all results beyond 12 EFPY were excluded as they strongly influence the mean.

The next set of figures show the LBB time lapse results. The distributions for Case 1.1.15 are significantly higher as compared to the distributions for Case 1.1.0 as shown in Figure 3-72. As shown in Figure 3-73, they are also higher as compared to Case 1.1.6, which considers both axial and circumferential cracks with PWSCC growth only. The differences in the results are due to the stress intensity factors produced by the transients, which become high when the cracks penetrate through-wall and lead to accelerated crack growth. However, the shapes of the CDFs resemble a lognormal distribution, which indicate that the likelihood of an LBB time lapse of 1 or 2 months is still quite small.

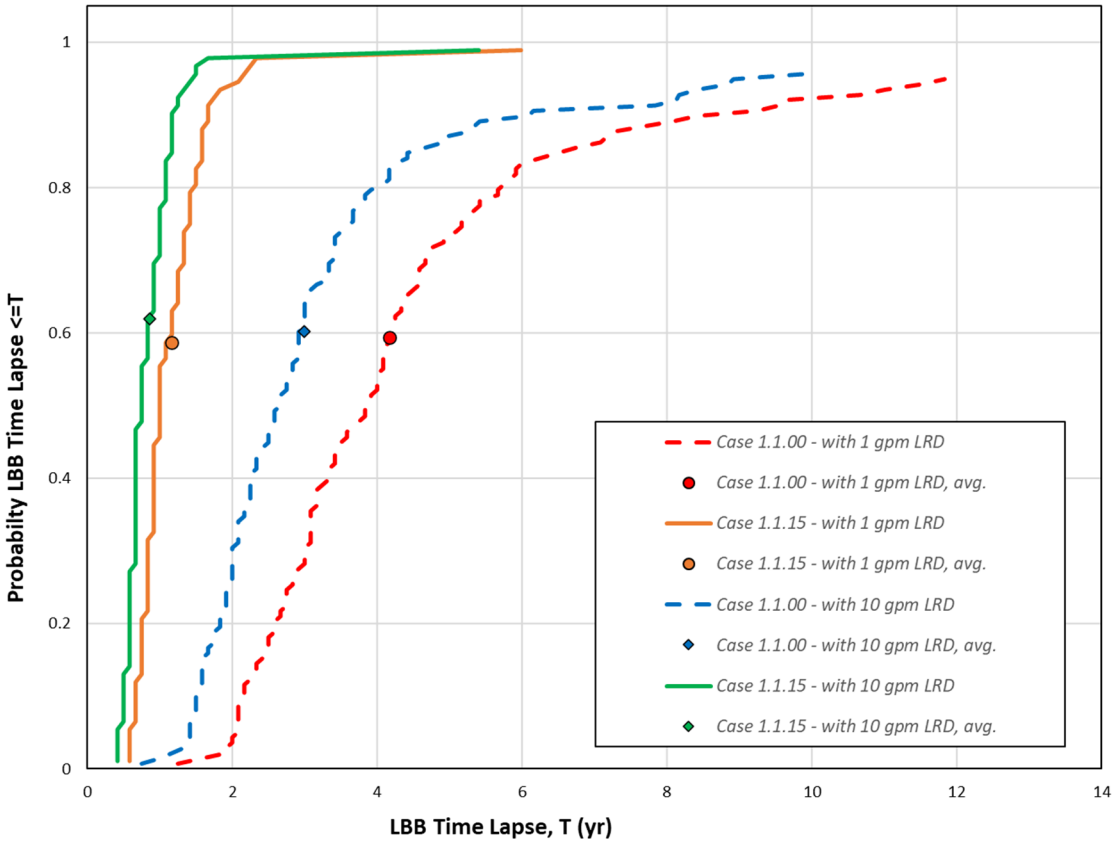


**Figure 3-72 Comparison of Case 1.1.15 LBB time lapse distributions with Case 1.1.0**

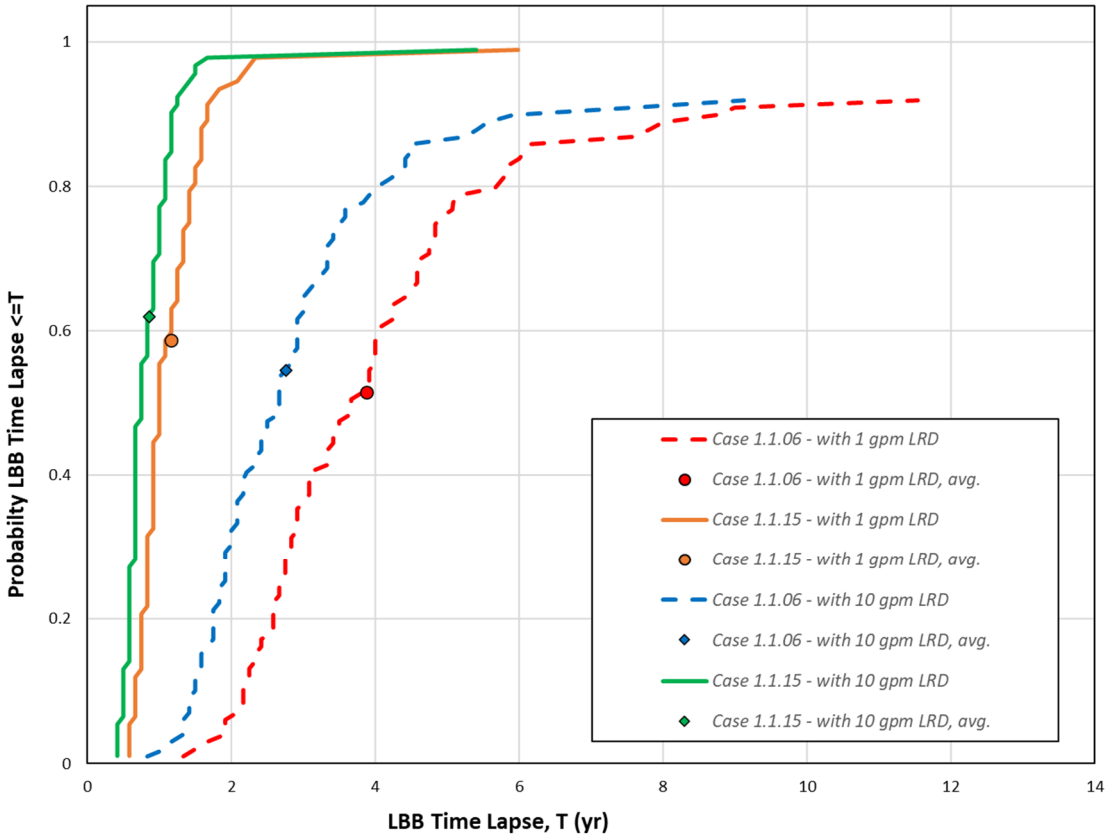


**Figure 3-73 Comparison of Case 1.1.15 LBB time lapse distributions with Case 1.1.6**

LBB Ratio

The mean LBB ratios and standard errors with 1 and 10 gpm leak rate detection capabilities were respectively as follows:

- 9.73 ± 0.09 (minimum observed: 6.17)
- 4.53 ± 0.03 (minimum observed: 3.71)

Figure 3-74 shows the LBB ratio CDF plots. It illustrates that both the mean and CDF are comparable to Case 1.1.0; therefore, the inclusion of axial cracks and fatigue do not affect the LBB ratio.

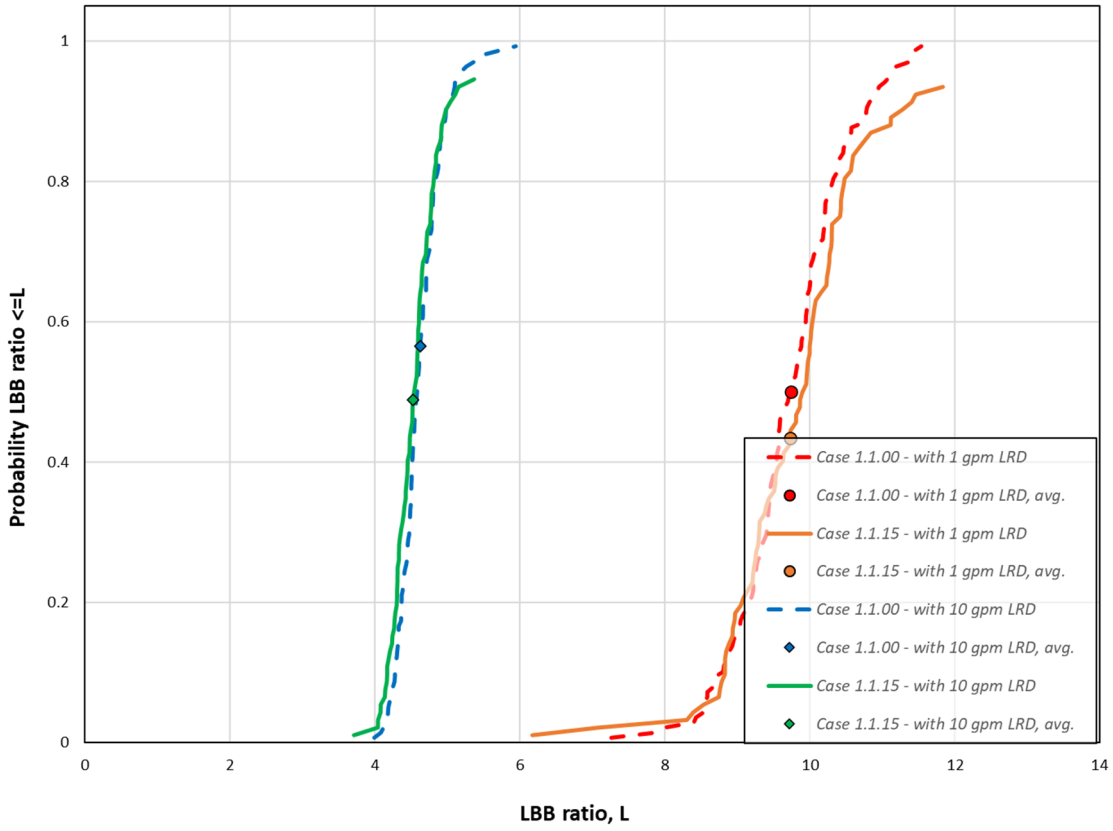


**Figure 3-74 Comparison of Case 1.1.15 LBB ratio distributions with Case 1.1.0**

Standard Indicators

The next set of figures shows the results from the standard indicators. As shown in Figure 3-75, the probabilities of first crack and first leak are higher as compared to Case 1.1.0, while the probabilities of rupture are equivalent. This result is expected and consistent with the impact of axial cracks, which are more likely to occur than circumferential cracks. This result also shows the negligible impact of fatigue on the probability of rupture. Figure 3-76 shows how the results compare with Case 1.1.6. The probabilities of first crack are essentially the same, and there is close agreement between the probabilities of first leak and rupture. The slightly earlier increase is consistent with the role of fatigue in accelerating crack growth once the crack has or is close to penetrating through-wall.

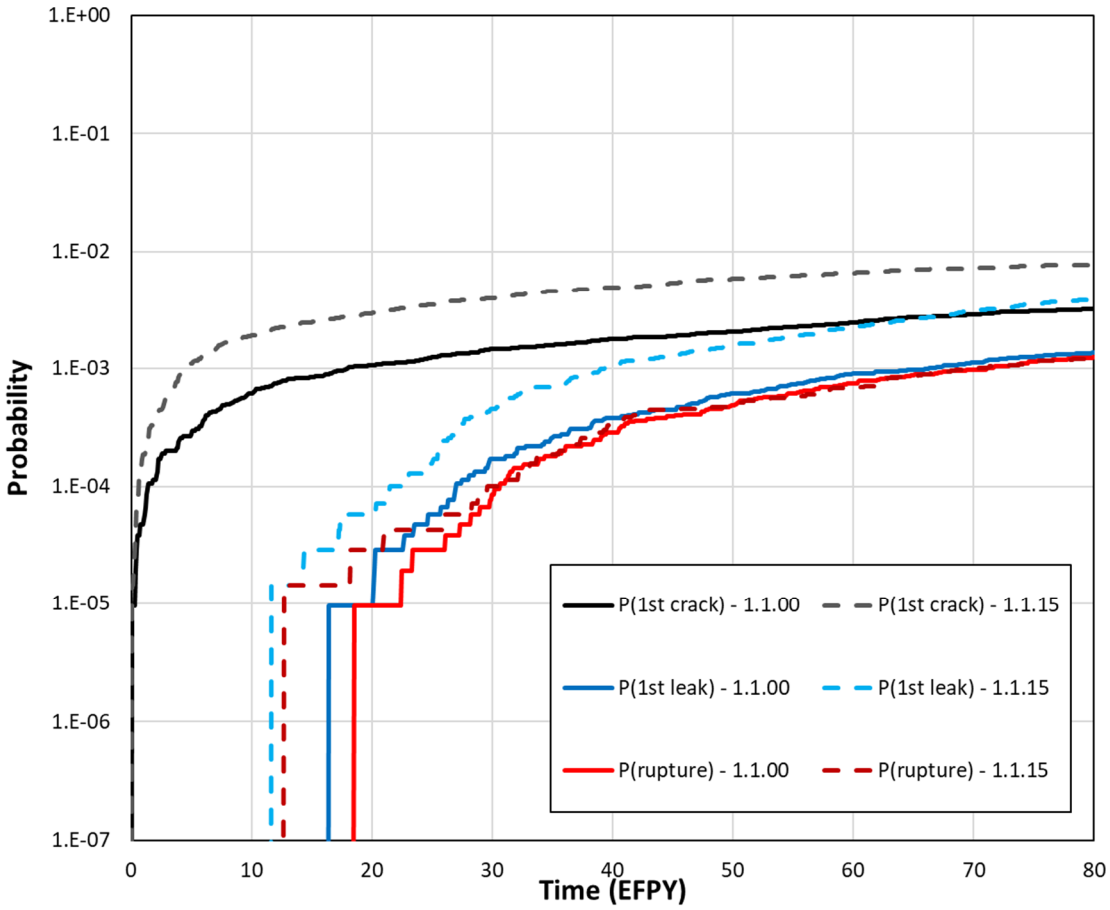


**Figure 3-75 Comparison of Case 1.1.15 time-dependent probabilities of first crack, first leak, and rupture with Case 1.1.0**

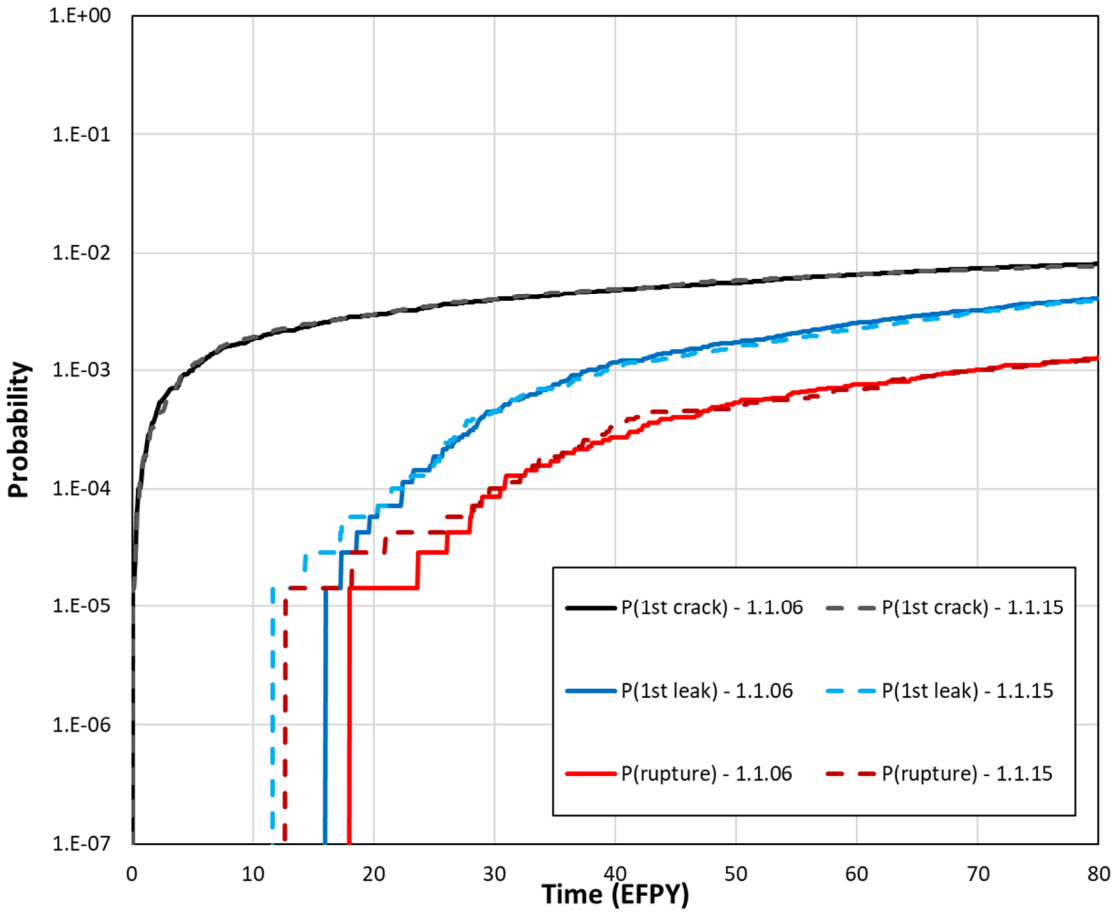


**Figure 3-76 Comparison of Case 1.1.15 time-dependent probabilities of first crack, first leak, and rupture with Case 1.1.6**

3.2.2.10.3 Supplemental Analyses

Axial cracks can grow in the base metal due to fatigue and thus could be longer than the weld width. A supplemental analysis was performed to understand the effect of these larger cracks on the leak rates. Due to the small width relative to the weld thickness, all the leaking axial cracks were at least the width of the weld. Figure 3-77 displays the leak rates as a function of the crack inner half-length normalized by the weld width. The same representation shows more variability when the average of the inner and outer half-lengths is considered. The maximum leak rate observed was lower than 0.1 gpm, which is lower than the 1 gpm leak rate detection threshold considered in this study. Thus, the leak rate from an axial crack would not be large enough to aid in the detection of a circumferential crack that occurs in the same realization. The crack lengths varied between weld width and more than twice the weld width.

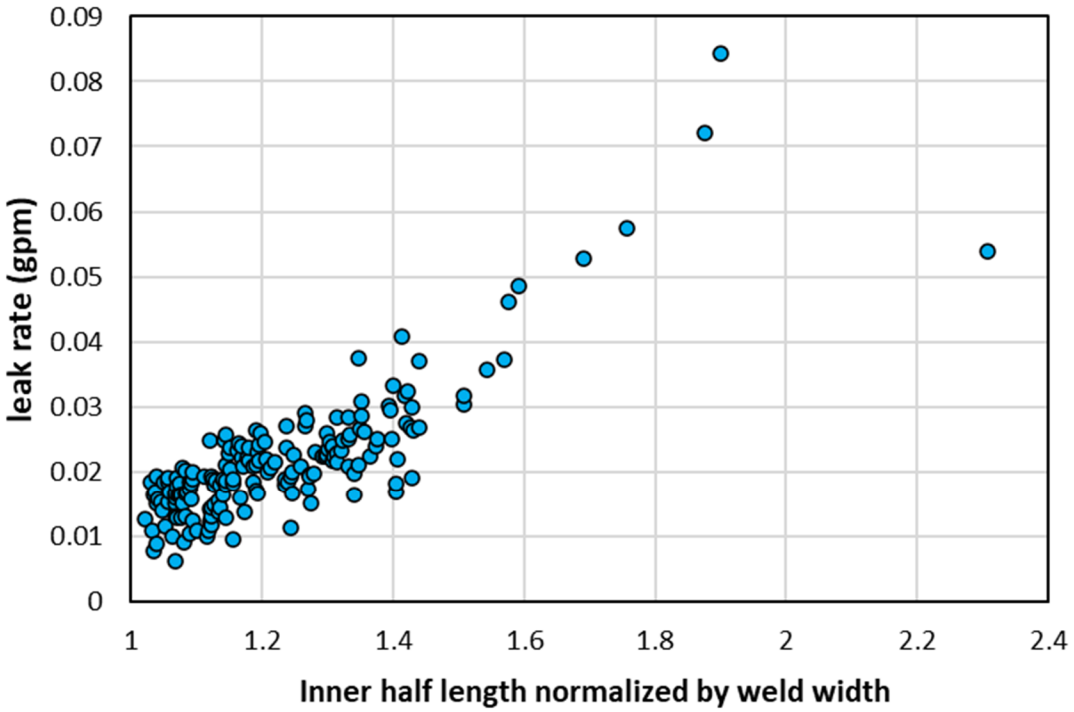


**Figure 3-77 Leak rate as a function of crack inner half-length for leaking axial cracks in Case 1.1.15**

Figure 3-78 shows two extrapolations: (1) using a second-order polynomial fit, and (2) using a power law constant on the longest six cracks. The outlier point shown on the figure was conservatively ignored in both fittings as it would have lowered the leak rate prediction. Based on these extrapolations, even if a weld width three times longer than the reference weld width was considered, the leak rate would be between 0.3 and 0.45 gpm, which is well below the range considered for leak rate detection in this study. These results indicate that axial cracks play a limited role in LBB because of the low likelihood of occurrence of both axial and circumferential cracks and because of their low leak rates.

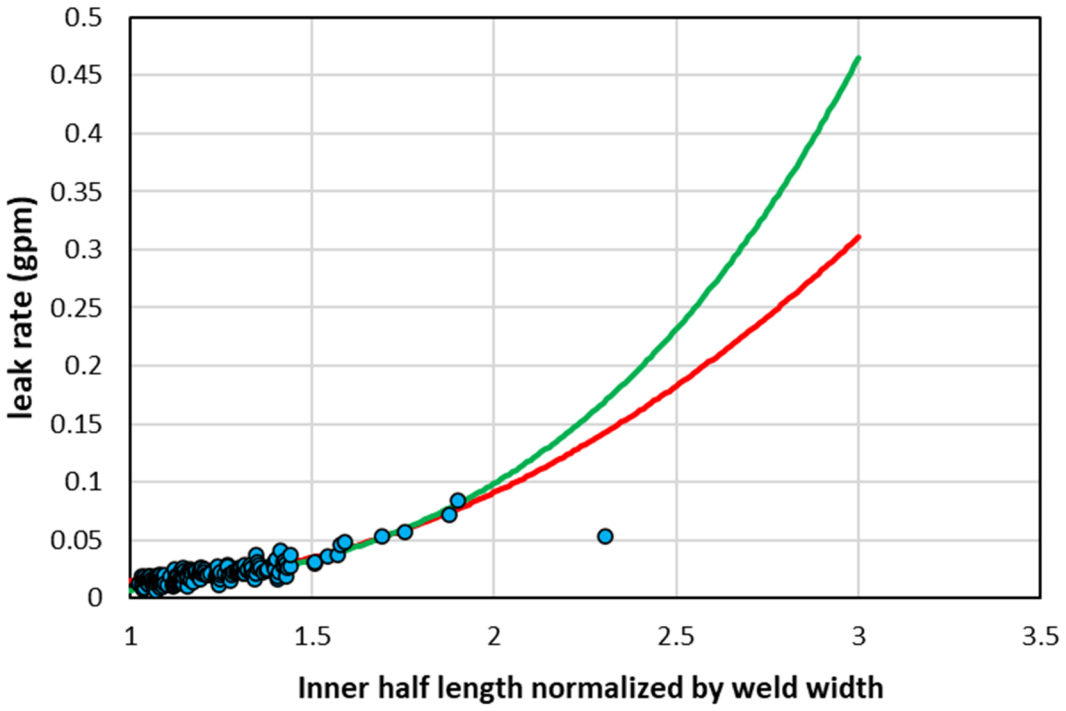


**Figure 3-78 Extrapolation of potential leak rate for axial cracks**

### *3.2.2.11 Fatigue Crack Initiation*

3.2.2.11.1 Case Description

The objective of Case 1.1.16 was to assess the likelihood of fatigue crack initiation. It is like Case 1.1.15 but considers only the effect of circumferential fatigue crack initiation. Section B13 describes the specific inputs and other simulation details used to analyze this case.

3.2.2.11.2 Results and Analysis

The transient cycles considered in the analysis were not sufficient to generate a single fatigue crack initiation in the 70,000 realizations performed for this case; therefore, none of the QoIs were relevant. These results demonstrate that PWSCC is the dominant crack initiation mechanism.

### *3.2.2.12 Large Initial Flaw with Fatigue Crack Growth*

3.2.2.12.1 Case Description

The objective of Case 1.1.17 was to assess the sensitivity of the likelihood of failure due to fatigue crack growth only from a large initial crack size. It is like Case 1.1.15 but uses the initial flaw density option instead of the fatigue crack initiation model. To analyze this case, the initial crack depth was set to a constant value of 3.16 mm. This value corresponds with the 99.9$^{th}$ percentile of the lognormal distribution used in Case 1.1.15, which had a mean of 3 mm

and a standard deviation of 0.05 mm. The crack full-length was set to a constant value of 38 mm. This value corresponds with the 99.9$^{th}$ percentile of the lognormal distribution used in Case 1.1.15, which had a mean of 8.61 mm and standard deviation of 4.85 mm. Section B14 describes the specific inputs and other simulation details used to analyze this case.

#### 3.2.2.12.2 Results and Analysis

There were no leaks or ruptures for this case because of extremely slow crack growth when only fatigue is considered; therefore, none of the QoIs were relevant.

#### 3.2.2.12.3 Supplemental Analyses

Since the QoIs selected for this study do not indicate how close a crack is to penetrating through-wall, a supplemental analysis was conducted to study the distribution of crack depth over time. Figure 3-79 displays 200 of the 5,000 time-dependent crack depths over the weld thickness as well as statistics (i.e., mean, median, and the 5$^{th}$ and 95$^{th}$ percentiles) estimated using the whole set of 5,000 realizations from Case 1.1.17. The maximum amount of crack growth in all 5,000 realizations is about 8 percent of the thickness, which represents about 5 mm. This value is low enough to conclude that fatigue crack growth does not affect the results.

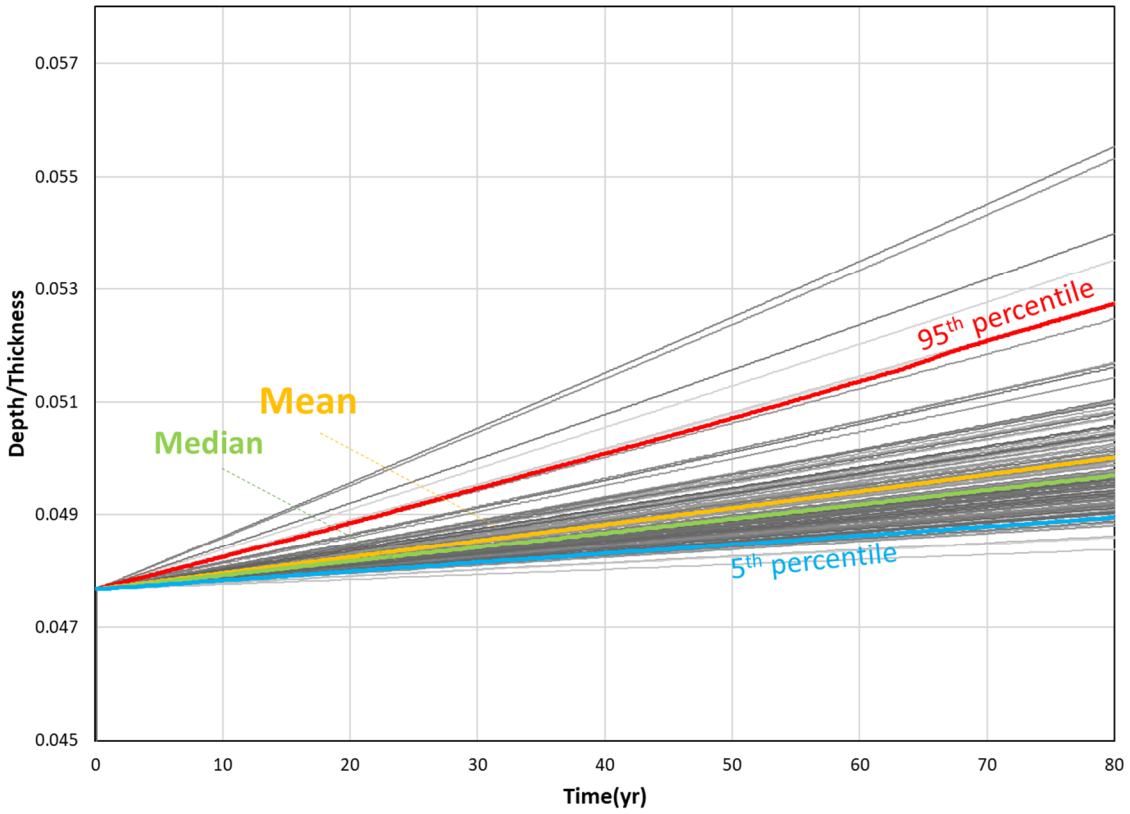


**Figure 3-79 Distribution of crack depth over weld thickness for Case 1.1.17**

### *3.2.2.13 Weld Geometry*

3.2.2.13.1 Case Description

The objective of Case 1.1.19 was to assess the sensitivity of the likelihood of failure due to the weld width and thickness. It is like Case 1.1.1, which uses the initial flaw density option, but with a different piping geometry.

The same data sources used to develop the distributions of normal operating stresses for Case 1.1.7 were used to construct distributions for the pipe outside diameter and weld thickness for Case 1.1.19. All but two of the data are clustered in the same area as shown in Figure 3-80 and Figure 3-81 for the outside diameter and weld thickness, respectively. The deterministic values for the outside diameter (0.869 m) and weld thickness (0.0663 m) are near the 80$^{th}$ percentile of these distributions.

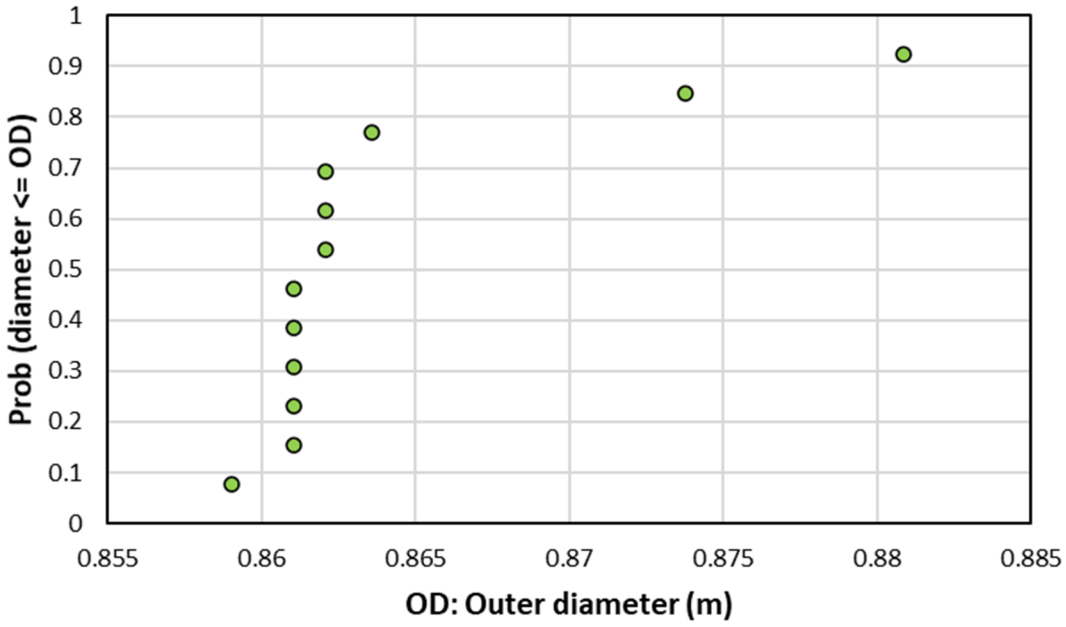


**Figure 3-80 Distribution of RVON weld outside diameters**

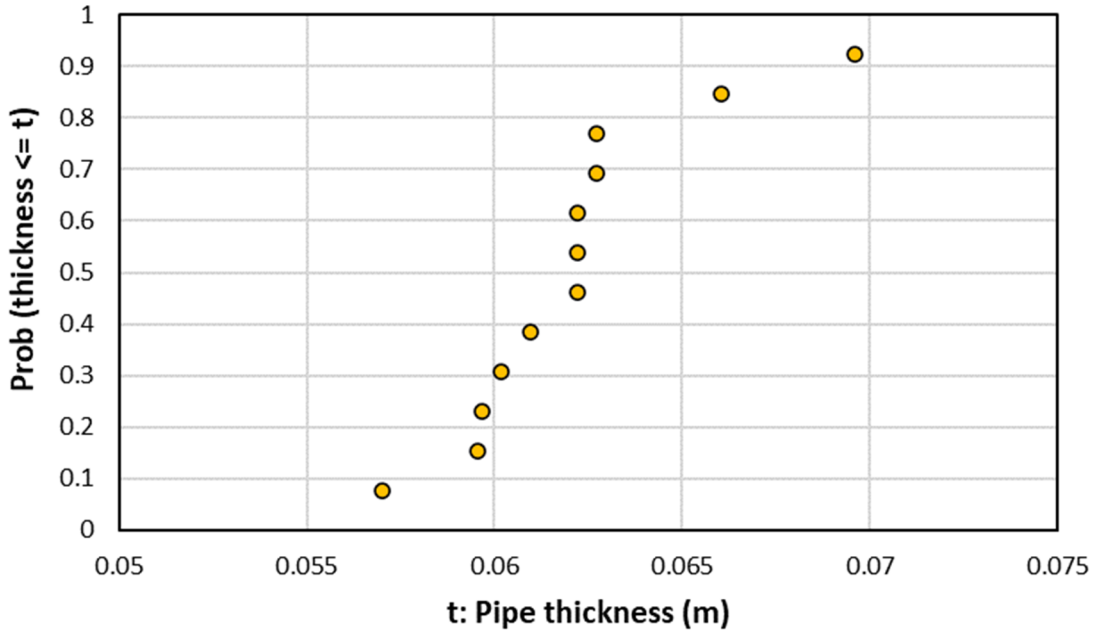


**Figure 3-81 Distribution of RVON weld thicknesses**

It is worthwhile to note that there is a correlation between the outside diameter and the weld thickness as shown in Figure 3-82. However, the xLPR code does not currently support correlation of these inputs.

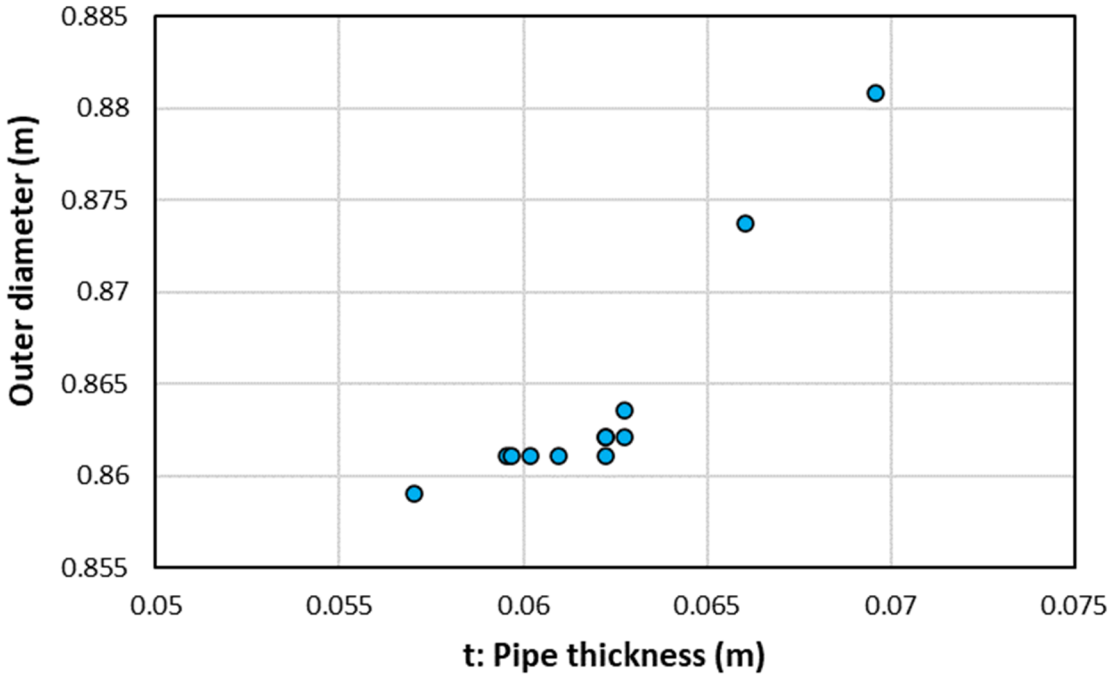


**Figure 3-82 RVON weld outside diameter as a function of pipe thickness**

A triangular distribution was used to fit the thickness data and a Weibull distribution was used to fit the outside diameter data using a least squares technique. The distribution fits are shown in Figure 3-83 and Figure 3-84, respectively. The Weibull distribution was truncated at the 95$^{th}$ percentile.

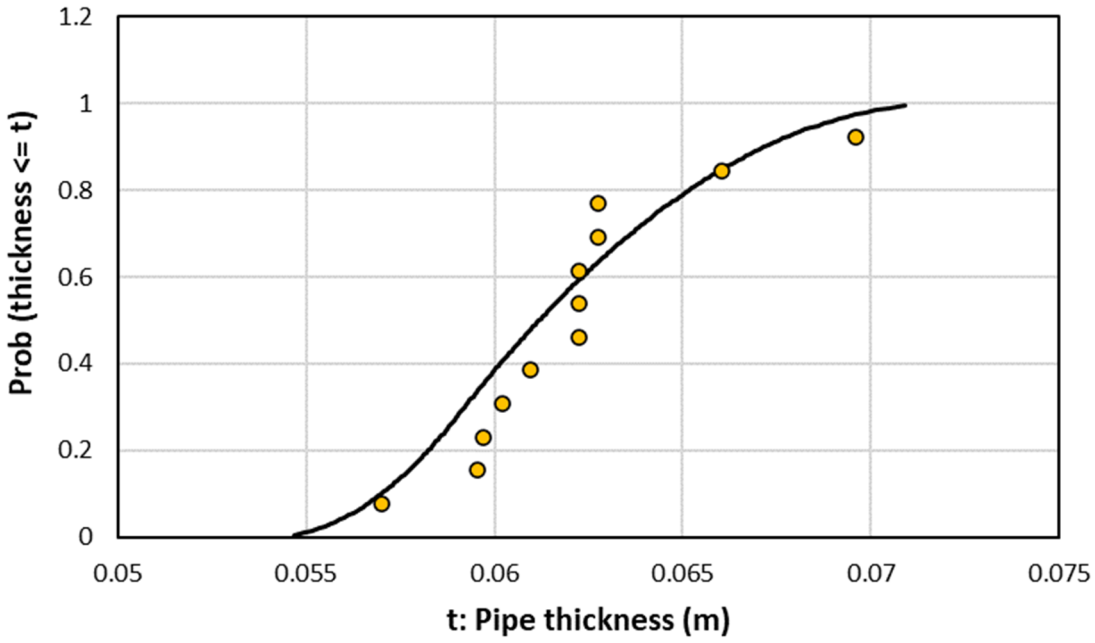


**Figure 3-83 Triangular distribution fitting to RVON weld thickness**

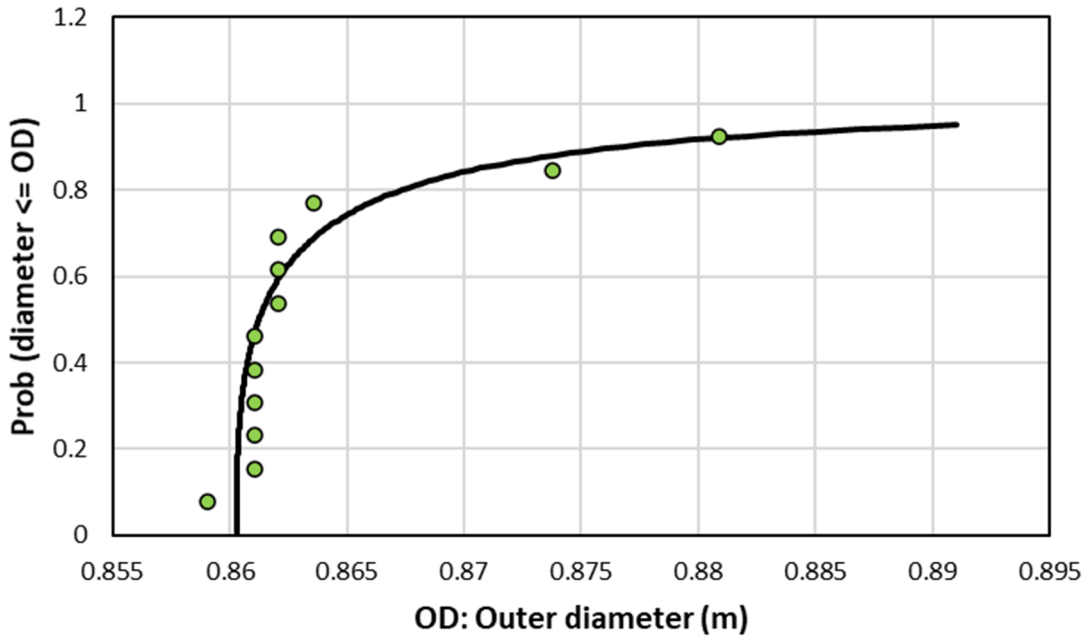


**Figure 3-84 Weibull distribution fitting to RVON weld outside diameter**

This case was initially defined to include axial cracks as a change in the weld width could affect the leak rate from an axial crack. However, as demonstrated in Section 3.2.2.10.3, an increase in the weld width by a factor of three does not impact the results. As such, axial cracks were not modeled in Case 1.1.19. A second simulation was, however, performed using constant values for the largest outside diameter and smallest weld thickness (referred to as Case 1.1.19a). Section B15 describes the specific inputs and other simulation details used to analyze this case.

#### 3.2.2.13.2 Results and Analysis

Rupture with Leak Rate Detection

There were no ruptures with a 1 gpm leak rate detection capability for this case.

Leak Rate Jump

There were no leak rate jump events for this case.

LBB Time Lapse

The mean LBB time lapses and standard errors with 1 and 10 gpm leak rate detection capabilities for Case 1.1.19 were respectively as follows:

- 57 ± 0.40 months (minimum observed: 10 months)
- 39.9 ± 0.31 months (minimum observed: 6 months)

Note that, as with Case 1.1.0, all results beyond 12 EFPY were excluded as they strongly influence the mean.

Figure 3-85 shows the LBB time lapse CDF plots for Case 1.1.19. A comparison with the Case 1.1.1 results indicates that use of the outside diameter and weld thickness distributions do not affect the results.

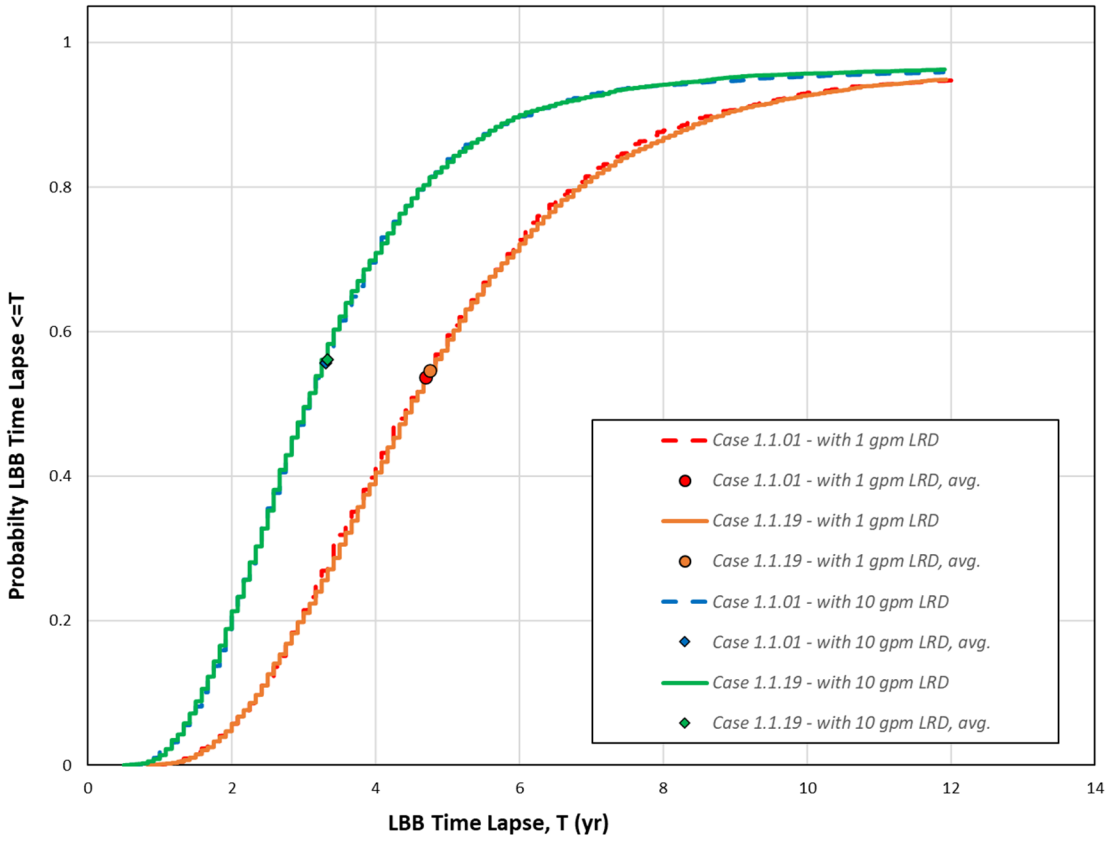


**Figure 3-85 Comparison of Case 1.1.19 LBB time lapse distributions with Case 1.1.0**

The mean LBB time lapses and standard errors with 1 and 10 gpm leak rate detection capabilities for Case 1.1.19a were respectively as follows:

- 58.42 ± 0.39 months (minimum observed: 10 months)
- 40.12 ± 0.30 months (minimum observed: 6 months)

The CDF plots in Figure 3-86 show that even the conservative geometry used in the analysis of Case 1.1.19a has a negligible effect. The results are slightly higher than in Case 1.1.19; however, the difference is small and the number of realizations with ruptures in Case 1.1.19a is higher.

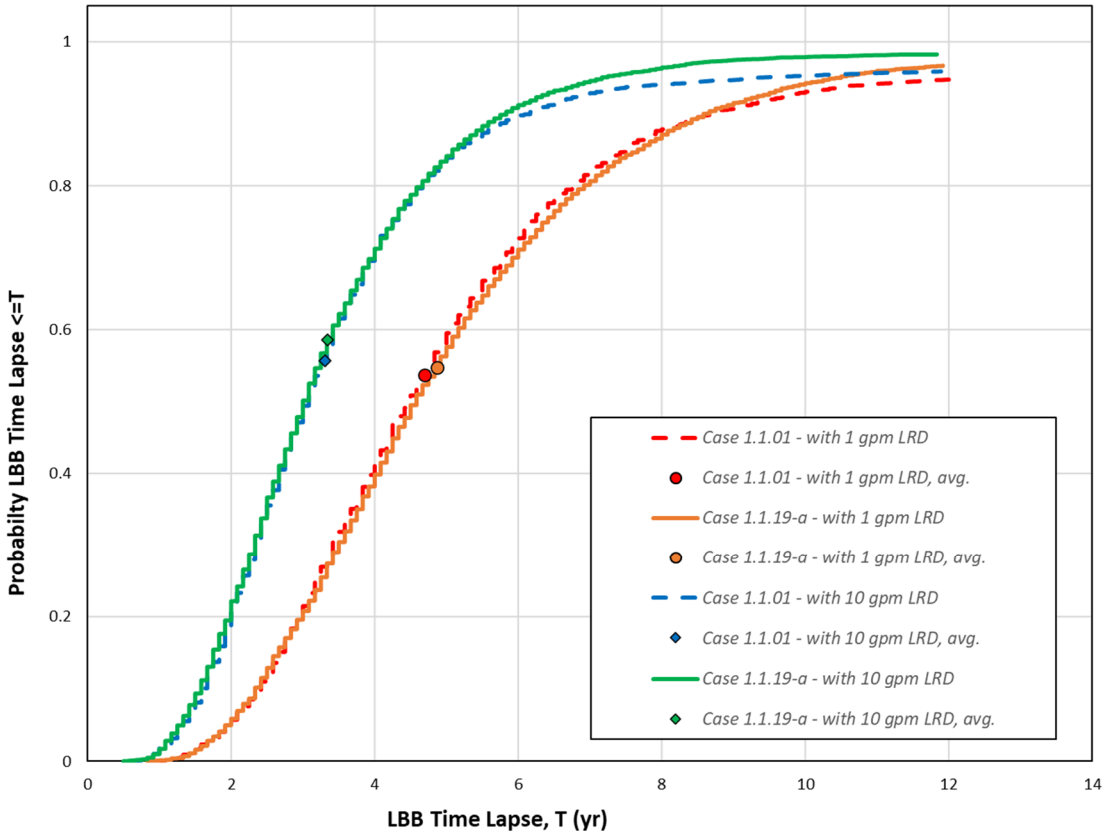


**Figure 3-86 Comparison of Case 1.1.19a LBB time lapse distributions with Case 1.1.0**

LBB Ratio

The mean LBB ratios and standard errors with 1 and 10 gpm leak rate detection capabilities for Case 1.1.19 were respectively as follows:

- 10.17 ± 0.01 (minimum observed: 7.64)
- 4.67 ± 0.004 (minimum observed: 3.95)

Figure 3-87 shows the LBB ratio CDF plots for Case 1.1.19. The results are comparable with Case 1.1.1, which indicates that the geometry does not strongly affect the LBB ratio.

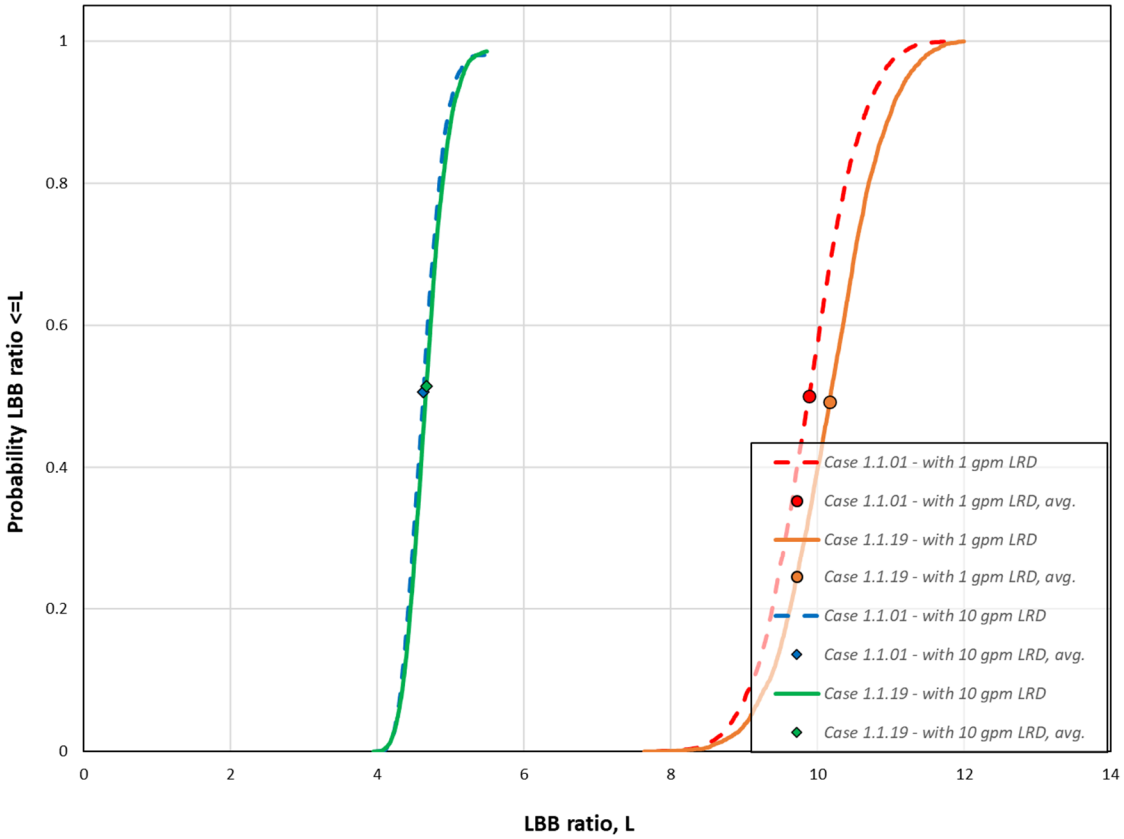


**Figure 3-87 Comparison of Case 1.1.19 LBB ratio distributions with Case 1.1.0**

The mean LBB ratios and standard errors with 1 and 10 gpm leak rate detection capabilities for Case 1.1.19a were respectively as follows:

- 10.76 ± 0.0087 (minimum observed: 8.87)
- 4.84 ± 0.004 (minimum observed: 4.05)

Figure 3-88 shows the LBB ratio CDF plots for Case 1.1.19a. Like in Case 1.1.19, there was no significant effect from the change in geometry parameters.

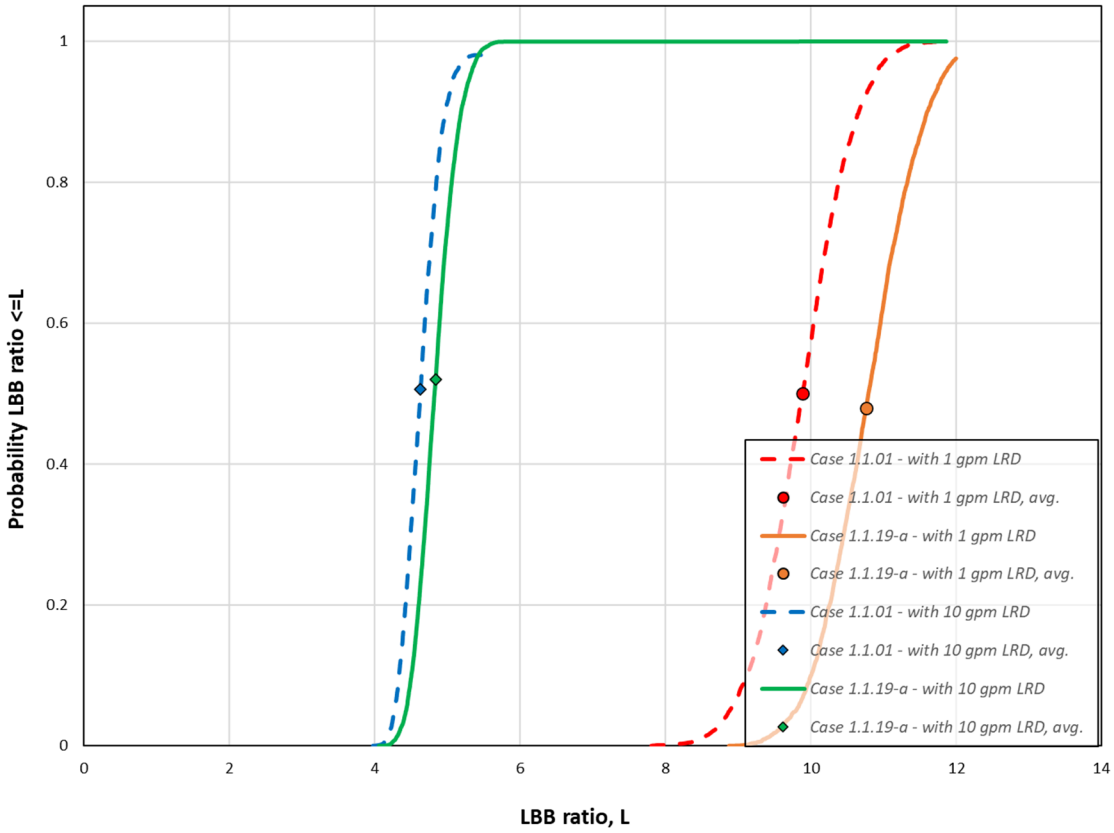


**Figure 3-88 Comparison of Case 1.1.19a LBB ratio distributions with Case 1.1.0**

Standard Indicators

Figure 3-89 and Figure 3-90 show the results from the standard indicators for Cases 1.1.19 and 1.1.19a, respectively. The probabilities tend to increase as compared to Case 1.1.1, which is expected. However, the increases as well as the other QoIs confirm that the influence of the weld geometry is reasonably small.

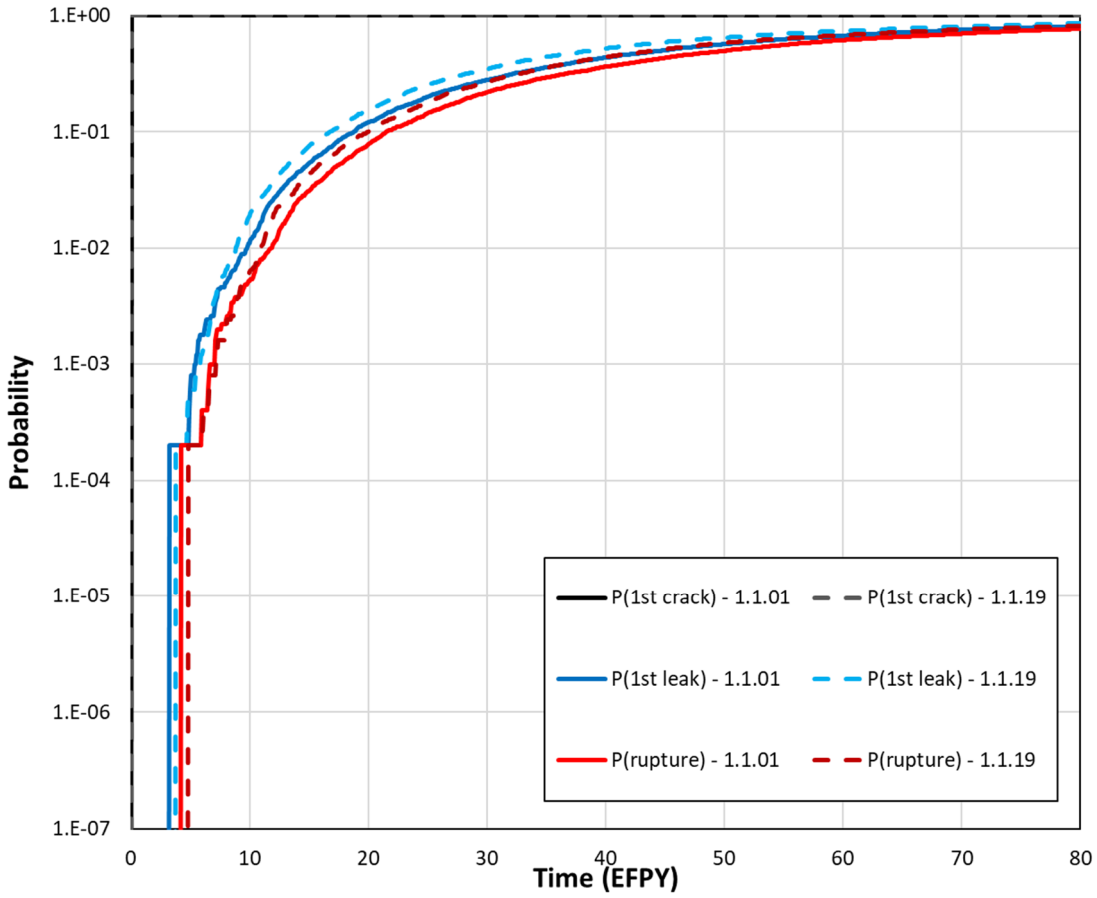


**Figure 3-89 Comparison of Case 1.1.19 time-dependent probabilities of first crack, first leak, and rupture with Case 1.1.1**

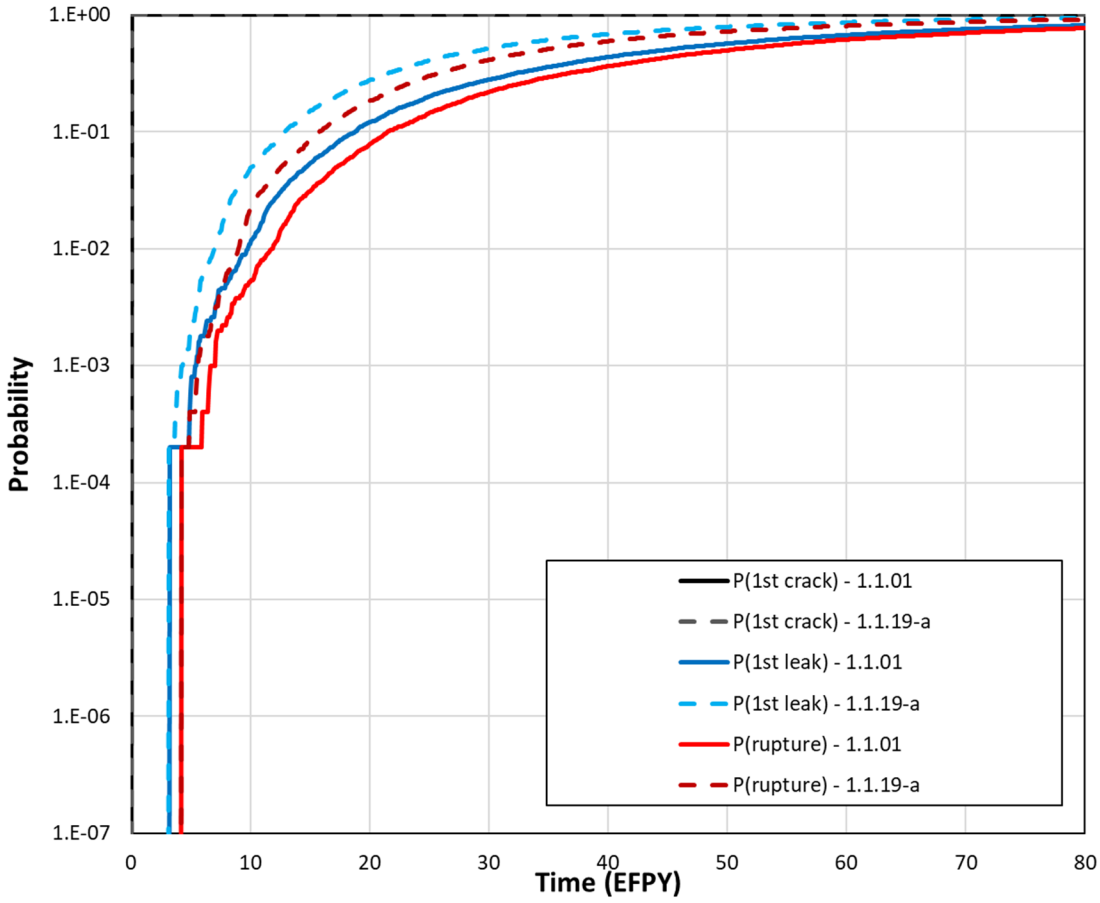


**Figure 3-90 Comparison of Case 1.1.19a time-dependent probabilities of first crack, first leak, and rupture with Case 1.1.1**

### *3.2.2.14 Operating Temperature*

3.2.2.14.1 Case Description

The objective of Case 1.1.20 was to assess the sensitivity of the likelihood of failure due to the operating temperature. It is like Case 1.1.0 but with a different normal operating temperature. In the xLPR code, the operating temperature represents the average value over the entire simulation time or up to three fixed portions thereof. This parameter is closely controlled in PWRs and thus a constant, representative value was used to analyze Case 1.1.0. However, this value did not bound the range of operating temperatures in all the Westinghouse four-loop PWR primary loop piping systems that were considered in this study. Additionally, it was deemed appropriate to study the effects of this parameter explicitly because it influences both the crack initiation and growth models and has been shown in prior sensitivity analyses to be one of the most influential parameters [28]. An upper-bound value of 330 °C was selected based on an analysis of plant operating temperate data. Section B16 describes the specific inputs and other simulation details used to analyze this case.

#### 3.2.2.14.2 Results and Analysis

Rupture with Leak Rate Detection

There were no ruptures with a 1 gpm leak rate detection capability for this case.

Leak Rate Jump

There were no leak rate jump events for this case.

LBB Time Lapse

The mean LBB time lapses and standard errors with 1 and 10 gpm leak rate detection capabilities were respectively as follows:

- 34 ± 1 months (minimum observed: 9 months)
- 23.6 ± 0.78 months (minimum observed: 6 months)

Note that, as with Case 1.1.0, all results beyond 12 EFPY were excluded as they strongly influence the mean.

As shown in Figure 3-91, the LBB time lapse is reduced by the higher operating temperature as compared to Case 1.1.0. This result is expected considering the role of temperature in both the crack initiation and growth models.

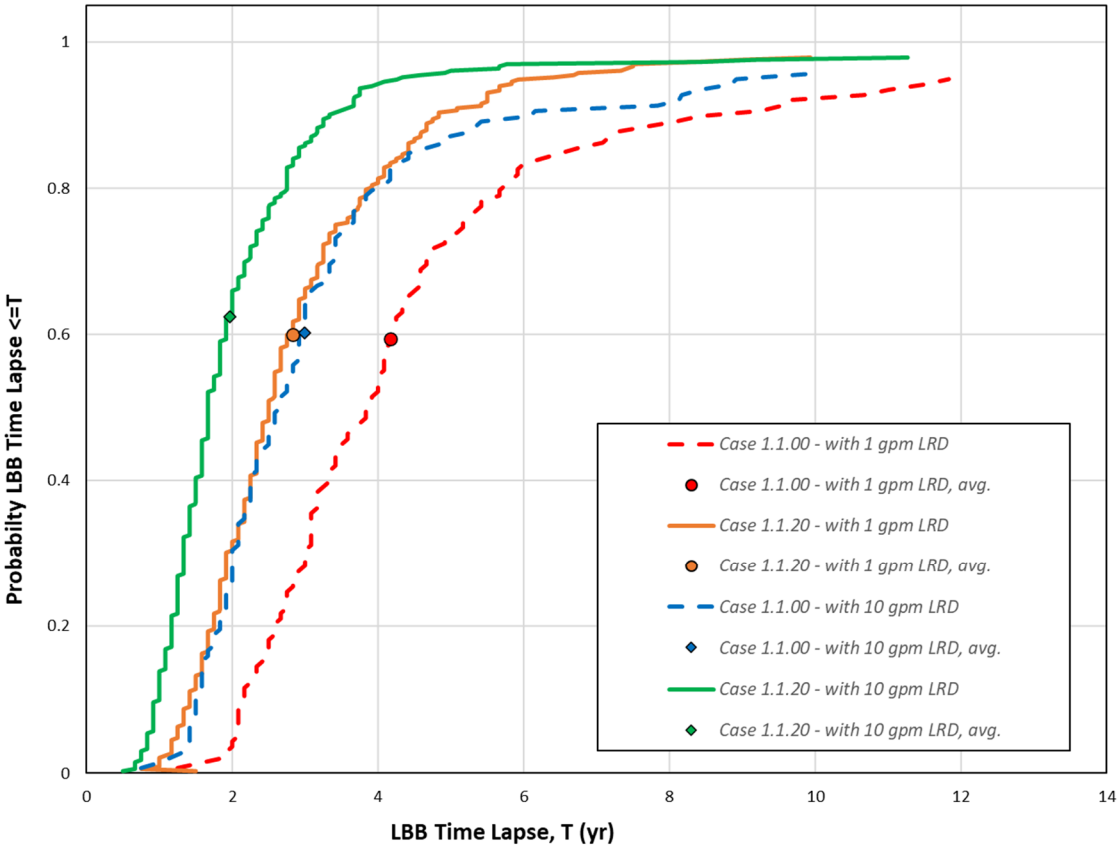


**Figure 3-91 Comparison of Case 1.1.20 LBB time lapse distributions with Case 1.1.0**

LBB Ratio

The mean LBB ratios and standard errors with 1 and 10 gpm leak rate detection capabilities were respectively as follows:

- 9.37 ± 0.04 (minimum observed: 6.37)
- 4.42 ± 0.01 (minimum observed: 3.79)

Figure 3-92 shows the LBB ratio CDF plots. It illustrates that a change in operating temperature does not affect the LBB ratio. The CDFs and mean values are thus like the ones for Case 1.1.0.

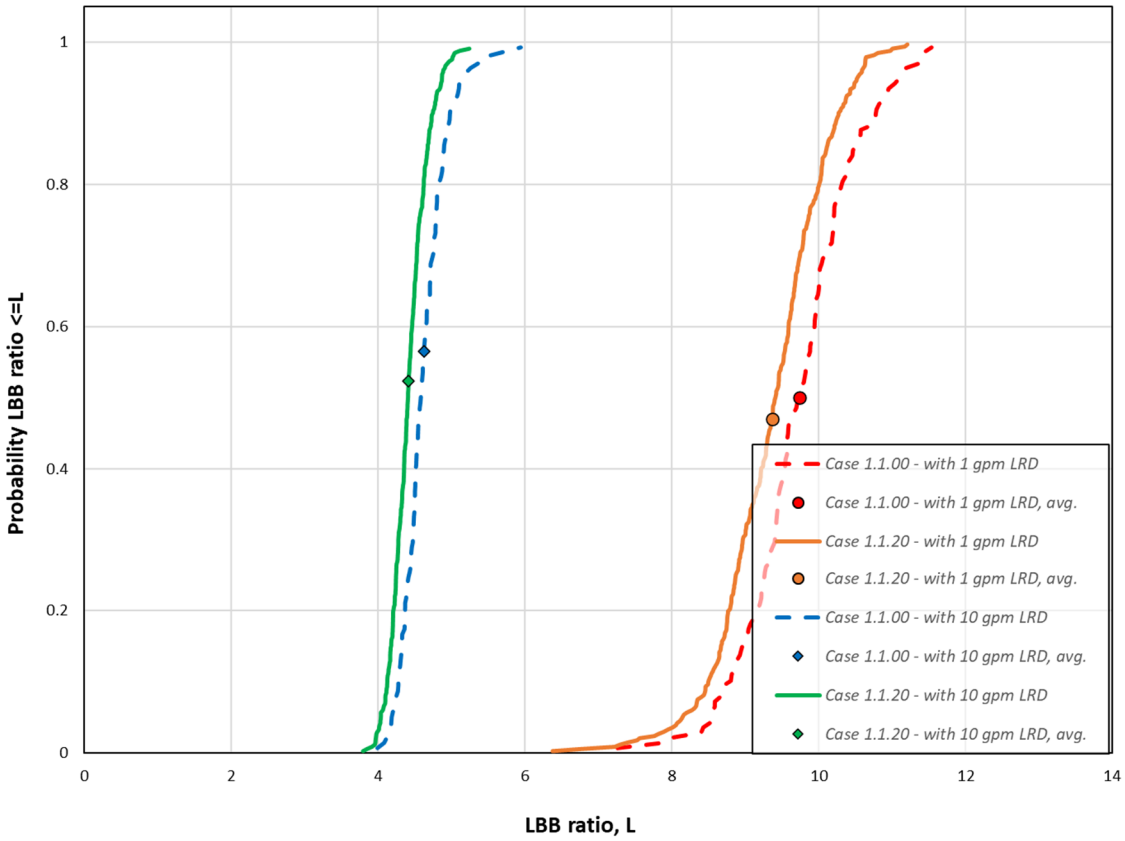


**Figure 3-92 Comparison of Case 1.1.20 LBB ratio distributions with Case 1.1.0**

Standard Indicators

Figure 3-93 shows the results from the standard indicators. It shows that the probabilities of first crack, first leak, and rupture are all higher in Case 1.1.20 as compared to Case 1.1.0. Again, these results are expected because of the role that the operating temperature plays in the crack initiation and growth models.

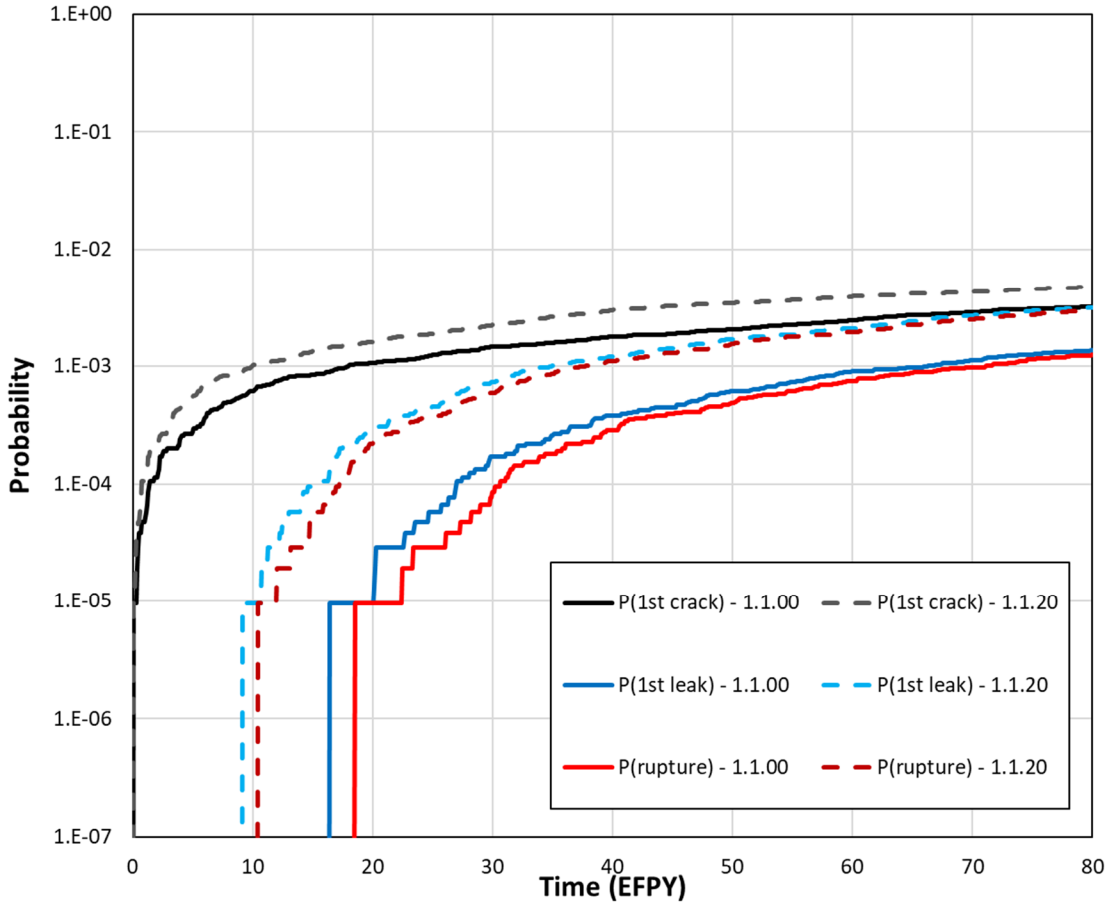


**Figure 3-93 Comparison of Case 1.1.20 time-dependent probabilities of first crack, first leak, and rupture with Case 1.1.0**

### *3.2.2.15 Initial PWSCC Flaw Size*

3.2.2.15.1 Case Description

The objective of Case 1.1.21 was to assess the sensitivity of the likelihood of failure due to the initial flaw dimensions. It is like Case 1.1.1 but with different initial flaw sizes. The initial PWSCC crack size distributions used to analyze Cases 1.1.0 and 1.1.1 were based on engineering judgment, so more conservative values were selected from these distributions for the analysis of Case 1.1.21. The full crack length was set to a constant value of 5.7 centimeters (cm). This value corresponds to the 99.9$^{th}$ percentile of the lognormal distribution used for the PWSCC-initiated crack length in Cases 1.1.0 and 1.1.1. This distribution had a mean of log $\mu =$ -5.35 and a standard deviation of log $\sigma = 0.8$. The crack depth distribution was kept the same, however. This approach was taken because fixing the length to a high quantile while varying the depth was expected to generate larger crack aspect ratios. Such aspect ratios could result in a greater likelihood of long, shallow cracks and undesirable break-before-leak scenarios. As shown in Figure 3-94, the simulated crack aspect ratios, whose variation depends only on the crack depth distribution, should follow a lognormal distribution ranging from 10 to 33 between

the 5th and 95th percentiles. Section B17 describes the specific inputs and other simulation details used to analyze this case.

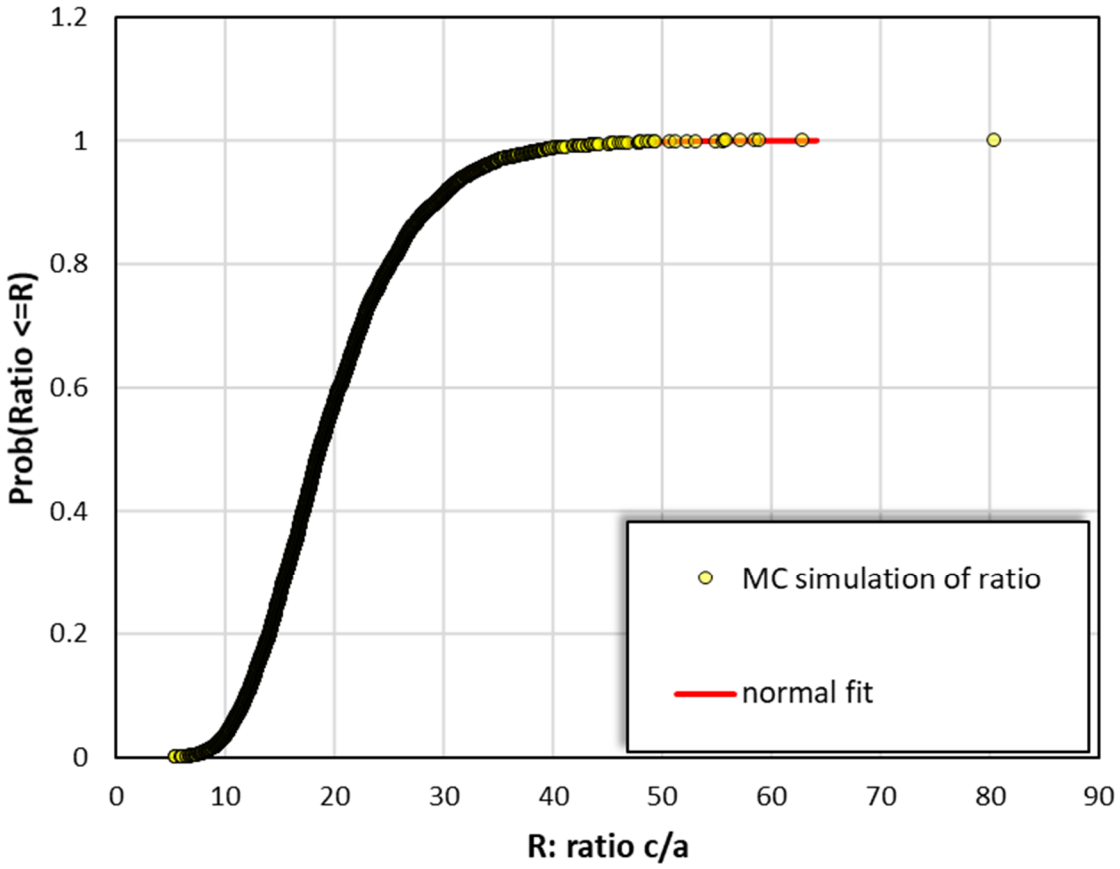


**Figure 3-94 Distribution of the ratio of crack half-length to crack depth**

3.2.2.15.2 Results and Analysis

Rupture with Leak Rate Detection

There were no ruptures with a 1 gpm leak rate detection capability for this case.

Leak Rate Jump

There were no leak rate jump events for this case.

LBB Time Lapse

The mean LBB time lapses and standard errors with 1 and 10 gpm leak rate detection capabilities were respectively as follows:

- 58.1 ± 0.4 months (minimum observed: 10 months)
- 42.3 ± 0.32 (minimum observed: 7 months)

Note that, as with Case 1.1.0, all results beyond 12 EFPY were excluded as they strongly influence the mean.

Figure 3-95 shows that the LBB time lapse distributions are like Case 1.1.1. Thus, there is no discernable impact of the initial crack sizes.

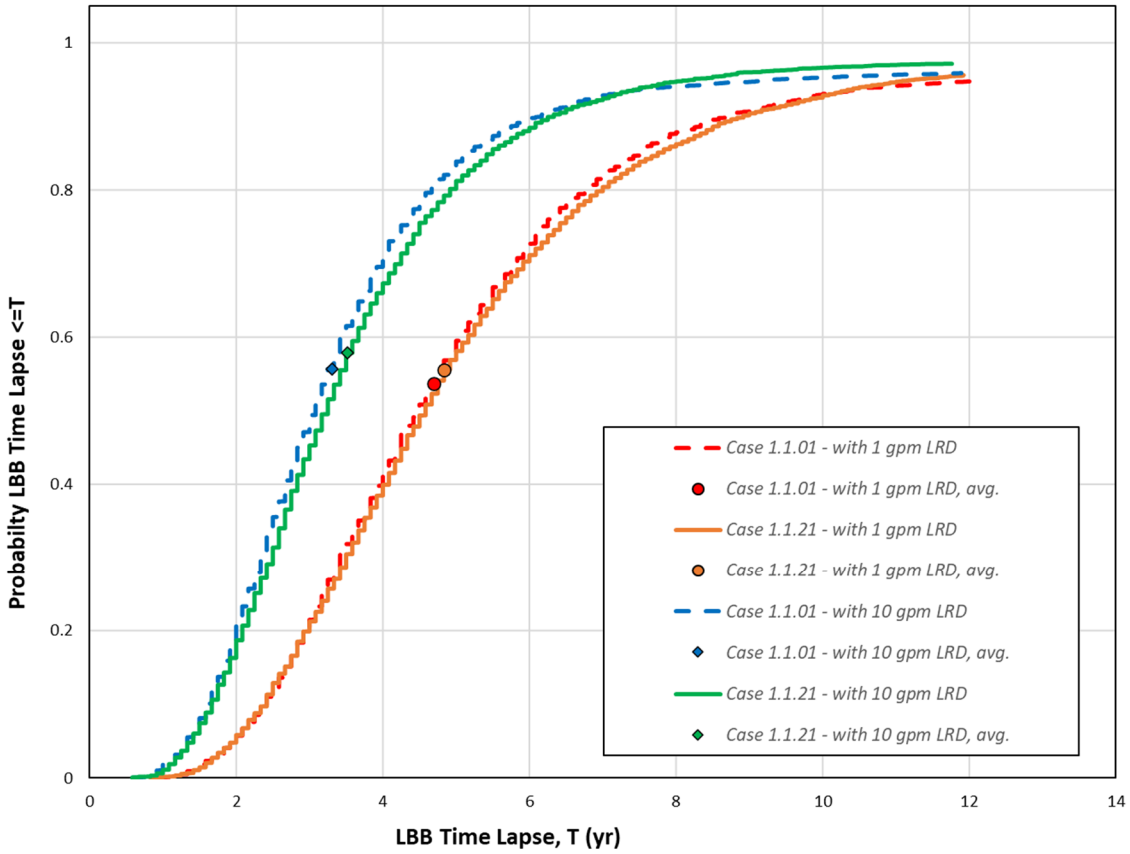


**Figure 3-95 Comparison of Case 1.1.21 LBB time lapse distributions with Case 1.1.1**

LBB Ratio

The mean LBB ratios and standard errors with 1 and 10 gpm leak rate detection capabilities were respectively as follows:

- 9.45 ± 0.01 (minimum observed: 6.75)
- 4.64 ± 0.004 (minimum observed: 3.94)

Figure 3-96 shows the LBB ratio CDF plots. It illustrates that the CDF based on a 10 gpm leak rate detection capability overlays the corresponding CDF from Case 1.1.1, and there is a slight shift in the CDF based on a 1 gpm leak rate detection capability. This shift is expected, because many of the cracks had a leak rate greater than 1 gpm. Using a larger initial crack length may generate slightly larger TWCs at the time of first leak and thus lead to a lower LBB ratio. The time to rupture does not seem to be impacted though.

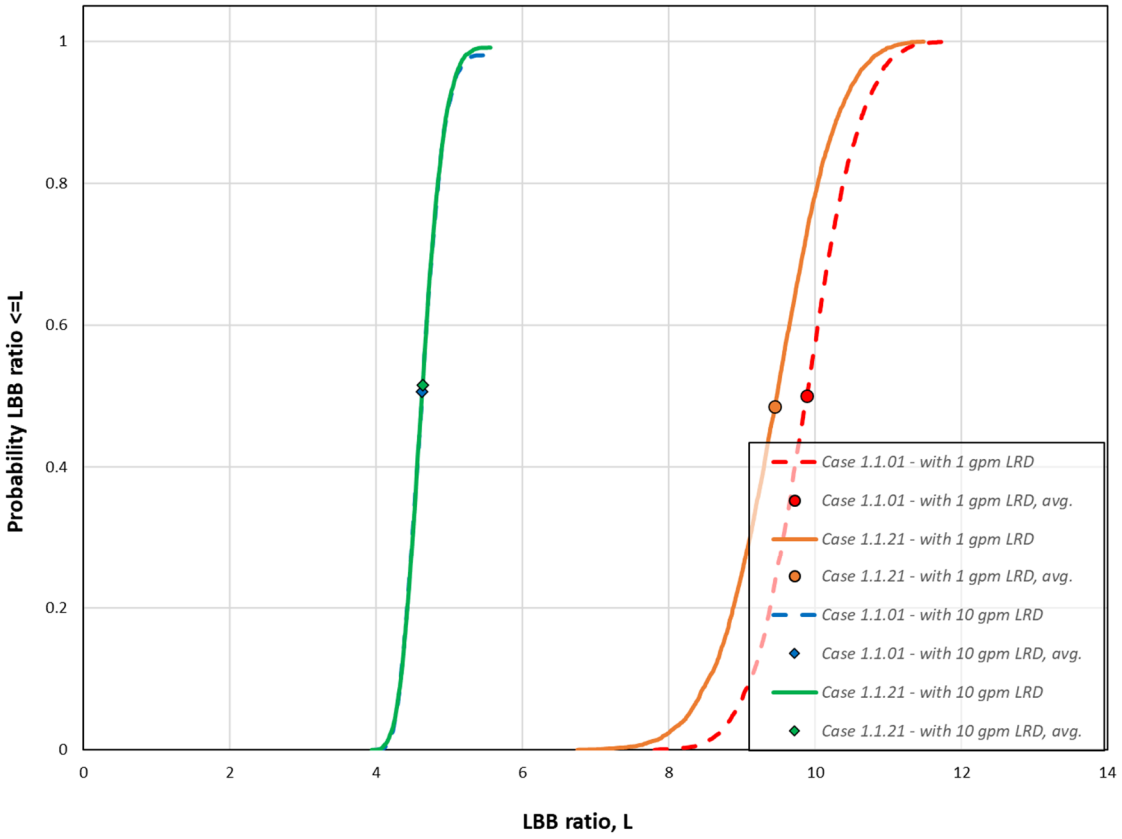


**Figure 3-96 Comparison of Case 1.1.21 LBB ratio distributions with Case 1.1.1**

Standard Indicators

Figure 3-97 shows the results from the standard indicators. There is a slight increase in the probabilities of first leak and rupture in Case 1.1.21 as compared to Case 1.1.1. The earlier times of first leak are consistent with starting from larger crack sizes; however, the distance between the probabilities of first leak and rupture is preserved. This result confirms that, once a crack leaks, its behavior is like that shown in Case 1.1.1. A similar observation can be made on the LBB time lapse results.

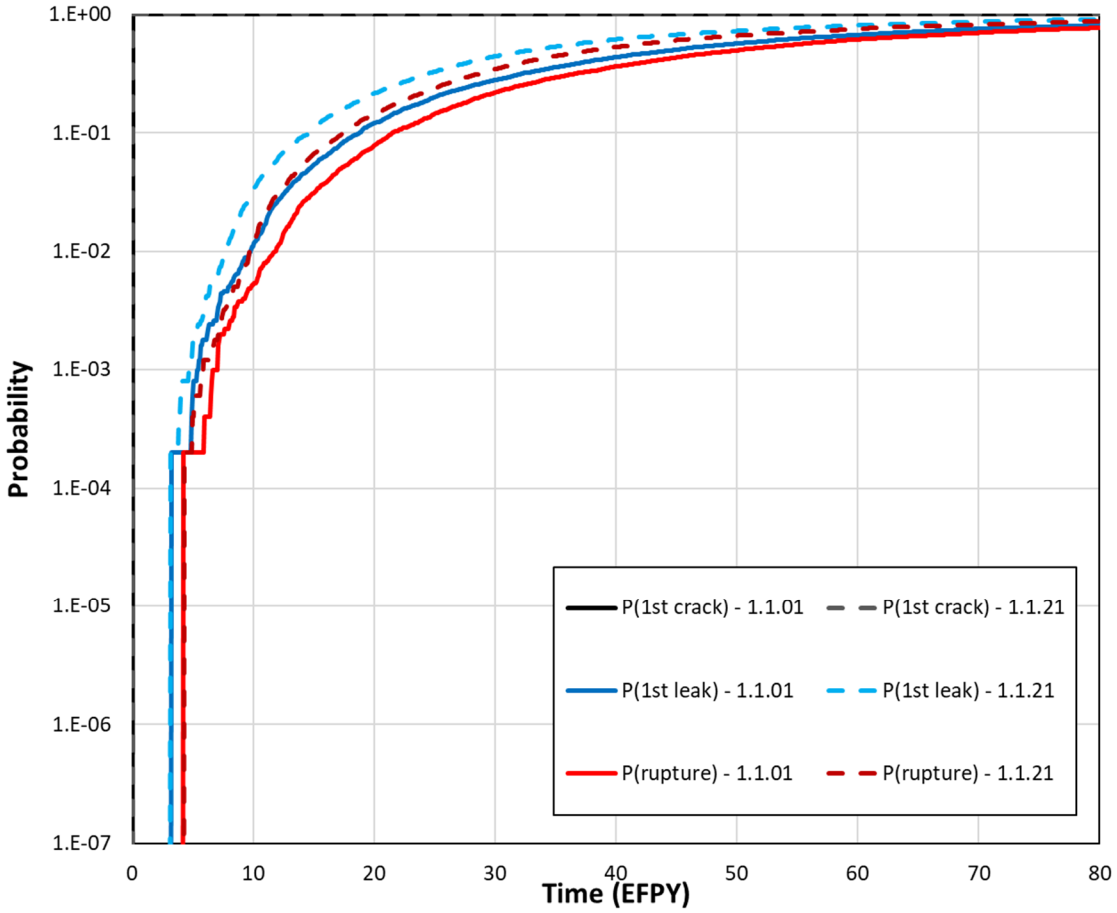


**Figure 3-97 Comparison of Case 1.1.21 time-dependent probabilities of first crack, first leak, and rupture with Case 1.1.1**

### *3.2.2.16 Time Step*

3.2.2.16.1 Case Description

The objective of Case 1.1.22 was to assess the sensitivity of the likelihood of failure due to the time step used in the simulation. It is like Case 1.1.1 except that the time step was varied. Time steps of 0.5, 1, 2, 6, and 12 months were used in separate simulations. This study used the initial flaw density option because the time step setting has no impact on the crack initiation calculations. Section B18 describes the specific inputs and other simulation details used to analyze this case.

3.2.2.16.2 Results and Analysis

Rupture with Leak Rate Detection

There were no ruptures with a 1 gpm leak rate detection capability for this case.

Leak Rate Jump

There were no leak rate jump events for this case.

LBB Time Lapse

Figure 3-98 and Figure 3-99 show a comparison of the LBB time lapse distributions generated with different time steps for 1 and 10 gpm leak rate detection capabilities, respectively. The 2-, 6-, and 12-month time step results have an uneven contour, which suggests a loss in accuracy. The 0.5- and 1-month time step results are much smoother in comparison, and their curves nearly overlay.

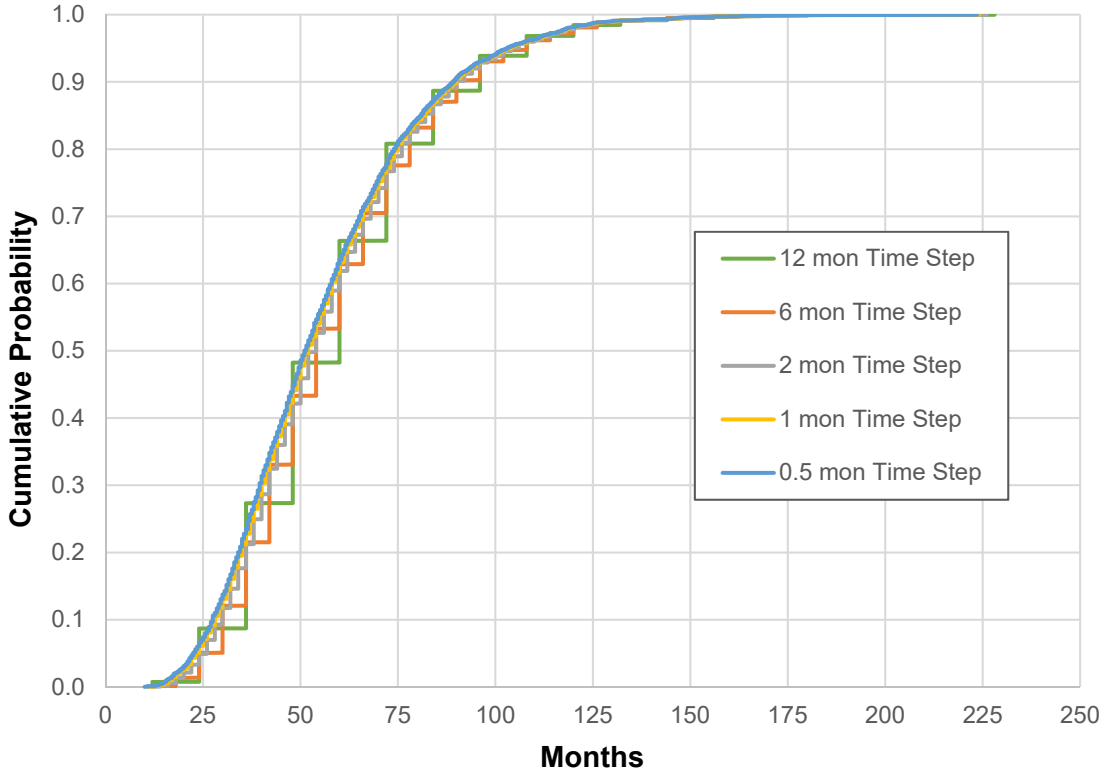


**Figure 3-98 Comparison of Case 1.1.22 LBB time lapse distributions with a 1 gpm leak rate detection capability generated with different time steps**

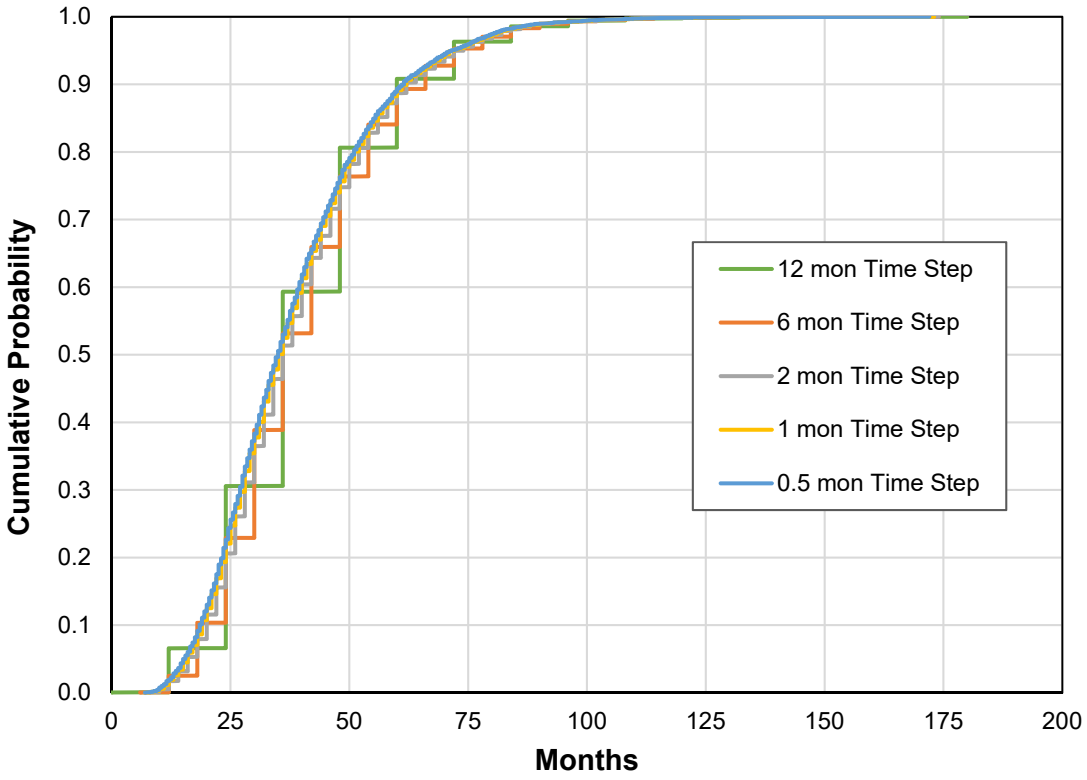


**Figure 3-99 Comparison of Case 1.1.22 LBB time lapse distributions with a 10 gpm leak rate detection capability generated with different time steps**

LBB Ratio

Figure 3-100 and Figure 3-101 show a comparison of the LBB ratio distributions generated with different time steps for 1 and 10 gpm leak rate detection capabilities, respectively. In the lower tails, which are the regions of interest, the 0.5-, 1-, and 2-month time step results are all consistent.

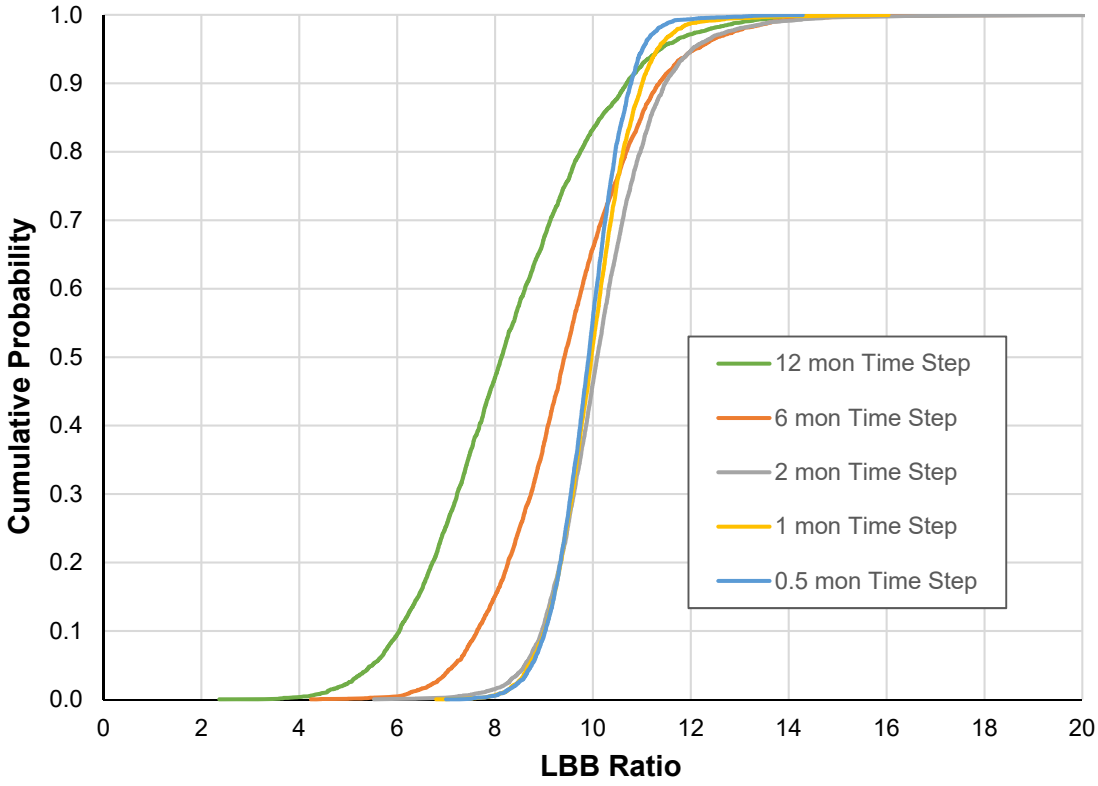


**Figure 3-100 Comparison of Case 1.1.22 LBB ratio distributions with a 1 gpm leak rate detection capability generated with different time steps**

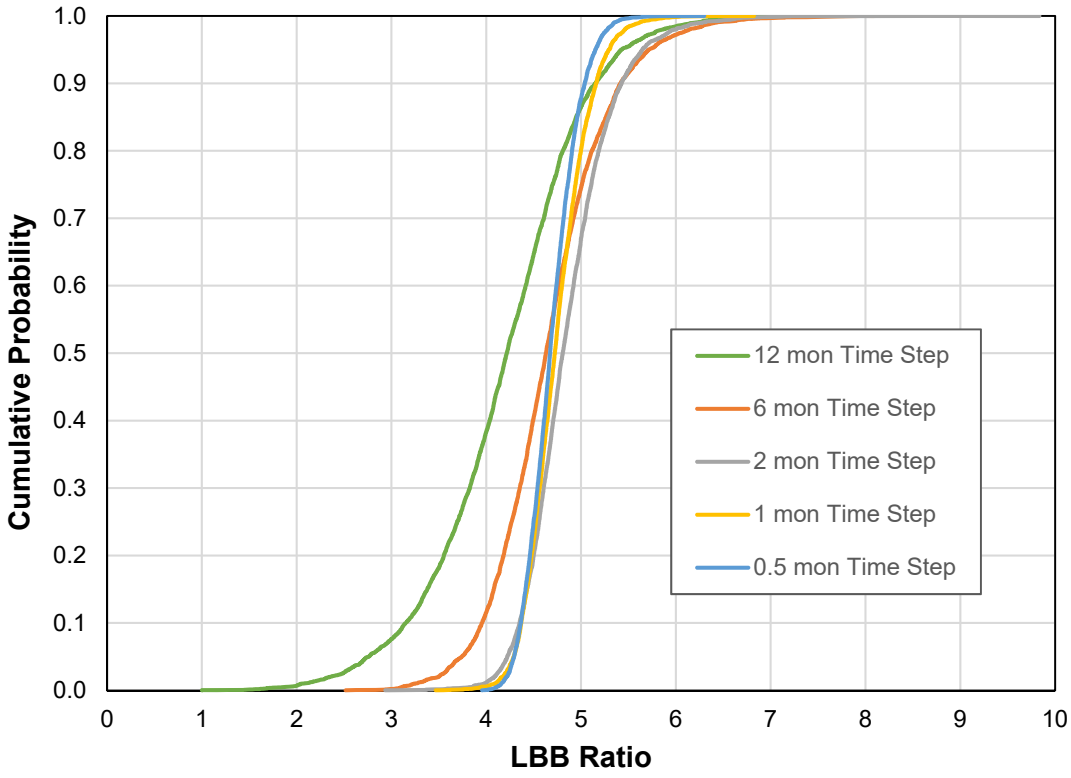


**Figure 3-101 Comparison of Case 1.1.22 LBB ratio distributions with a 10 gpm leak rate detection capability generated with different time steps**

Standard Indicators

Figure 3-102 and Figure 3-103 show a comparison of the probabilities of first leak and rupture generated with different time steps. The results all converge before 10 EFPY and then provide nearly identical predictions out to 80 EFPY.

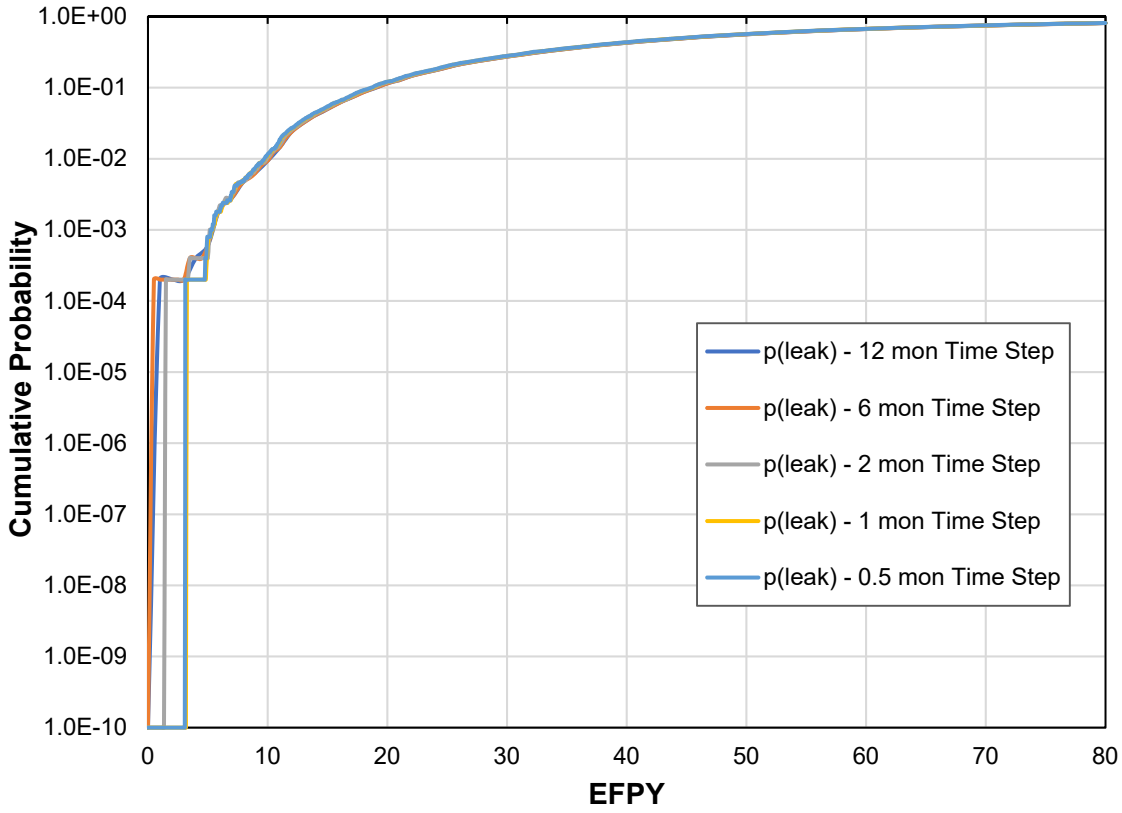


**Figure 3-102 Comparison of Case 1.1.22 time-dependent probabilities of first leak generated with different time steps**

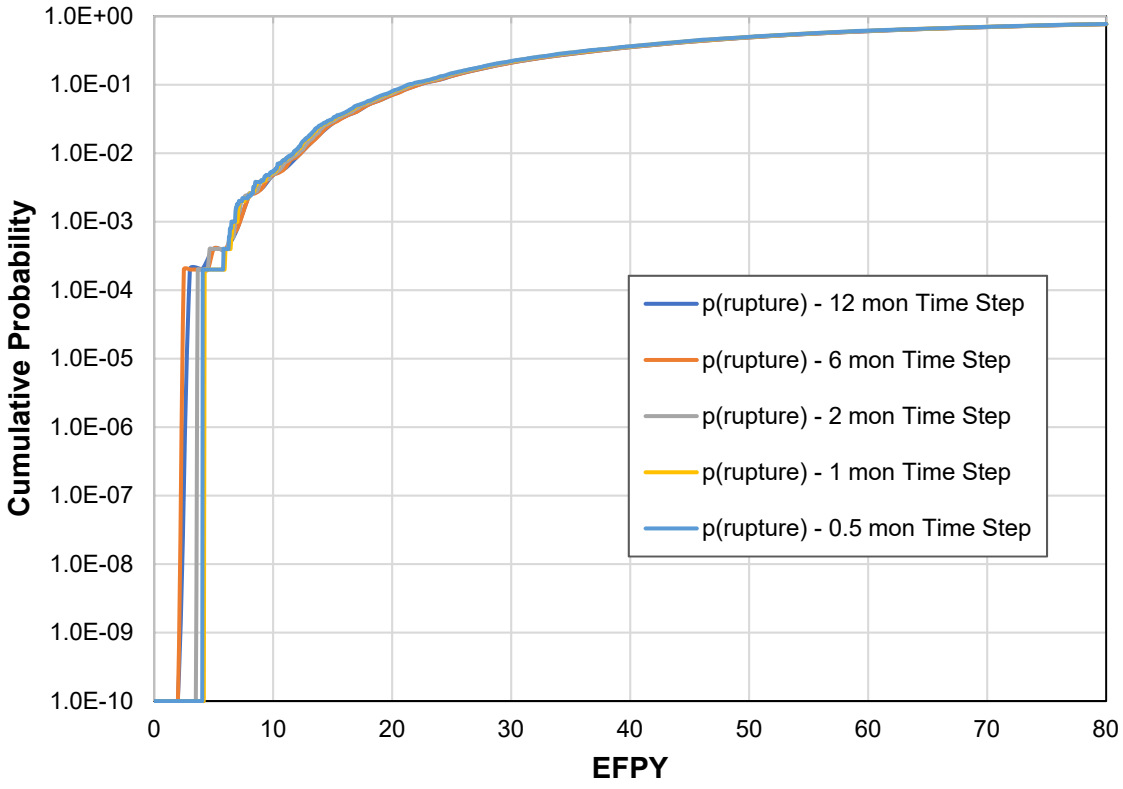


**Figure 3-103 Comparison of Case 1.1.22 time-dependent probabilities of rupture generated with different time steps**

Supplemental Analyses

Figure 3-104 shows a comparison of the crack inner half-length over time for Realization 4481, which had the quickest growing crack to rupture in the 0.5- and 1-month time step simulations. It shows that the 1-month time step simulation results are comparable with the more accurate, 0.5-month time step results, but there is a loss of accuracy with the 2-, 6-, and 12-month time step results. In conclusion, the default, 1-month time step provided the appropriate level of accuracy for the QoIs in this study.

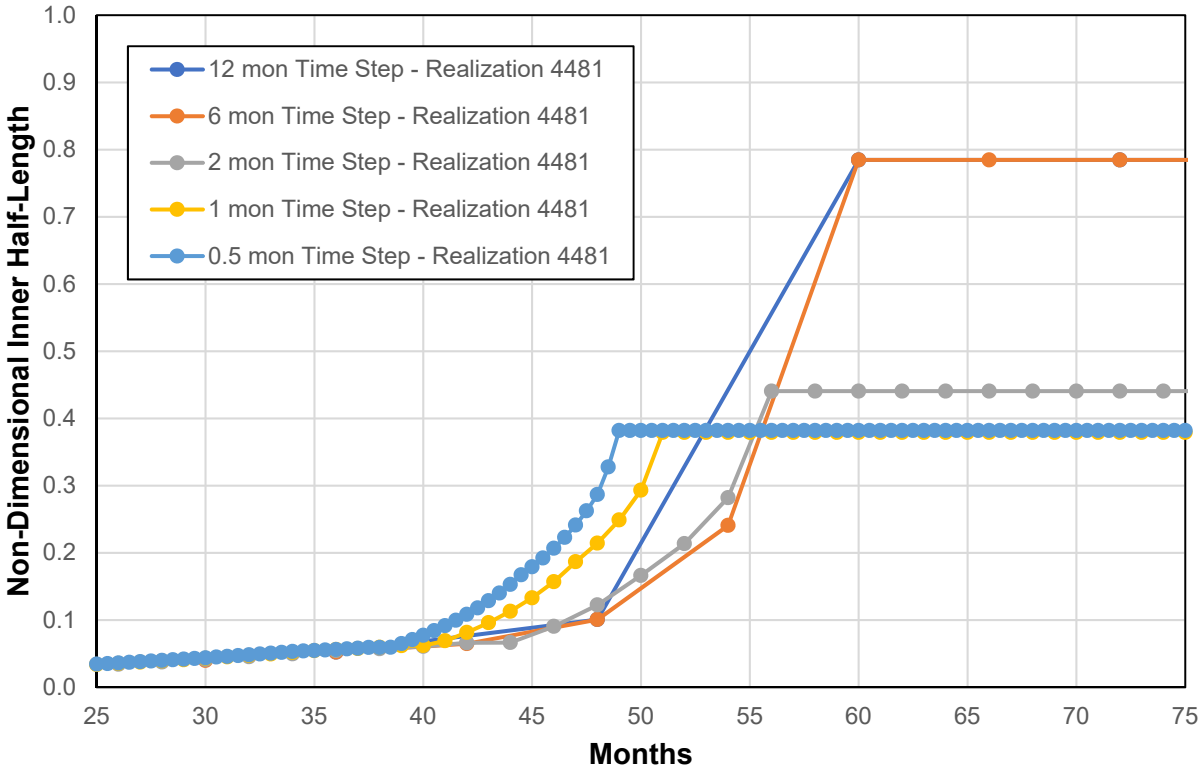


**Figure 3-104 Comparison of Case 1.1.22 quickest growing cracks to rupture**

### *3.2.2.17 Separation of Aleatory and Epistemic Uncertainties*

3.2.2.17.1 Case Description

The objective of Case 1.1.23 was to assess the impacts of separating aleatory and epistemic uncertainties. It is like Case 1.1.1 with the uncertainty types set to the selections as detailed in [25] instead of being strictly epistemic.

As described in Section 2.3, a single uncertainty type was used for all the previous cases in this study because it provides adequately converged results for the mean values of the QoIs with reasonable sample sizes. It was confirmed that the choice of sampling loop does not affect the results as shown in Section 3.2.1.1.2. However, separation of the aleatory uncertainties (which represent the inherent risk that is irreducible) and the epistemic uncertainties (which represent the lack of knowledge, and therefore, uncertainty over that risk) may provide additional insights and confidence on the risk estimates.

Case 1.1.23 thus explores the separation of uncertainty types to assess the value of the additional information generated. This case was aligned with Case 1.1.1 instead of Case 1.1.0 because the results for the latter are driven by the low likelihood of crack initiation (in the range of $1 \times 10^{-3}$), which would require a large sample size for both the aleatory and epistemic loops for stable results. Furthermore, when crack initiation is modeled, it controls all the results and masks any other potential effects. For Case 1.1.1, a 5,000-realization, all-epistemic uncertainty

simulation was performed. For Case 1.1.23, sample sizes of 200 were used for the epistemic (outer) loop and 100 for the aleatory (inner) loop, which led to a total sample size of 20,000. Section B19 describes the specific inputs and other simulation details used to analyze this case.

#### 3.2.2.17.2 Results and Analysis

A comparison of conditional results, such as the LBB time lapse and LBB ratio, would not be informative in this case. The results would be similar because of the same input distributions being used in the simulations. Also, there were no occurrences of leak rate jump or rupture with leak rate detection, so it was not possible to compare results for these QoIs. As such, the comparison focused on the probabilities of first leak and rupture.

Figure 3-105 shows similar results between Cases 1.1.23 and 1.1.1. With a sufficiently large sample size and considering that the uncertainties in both cases are represented by the same input distributions, the mean probability over two loops should converge to the probability over a single loop. This result also indicates that the sample sizes selected for Case 1.1.23 were large enough.

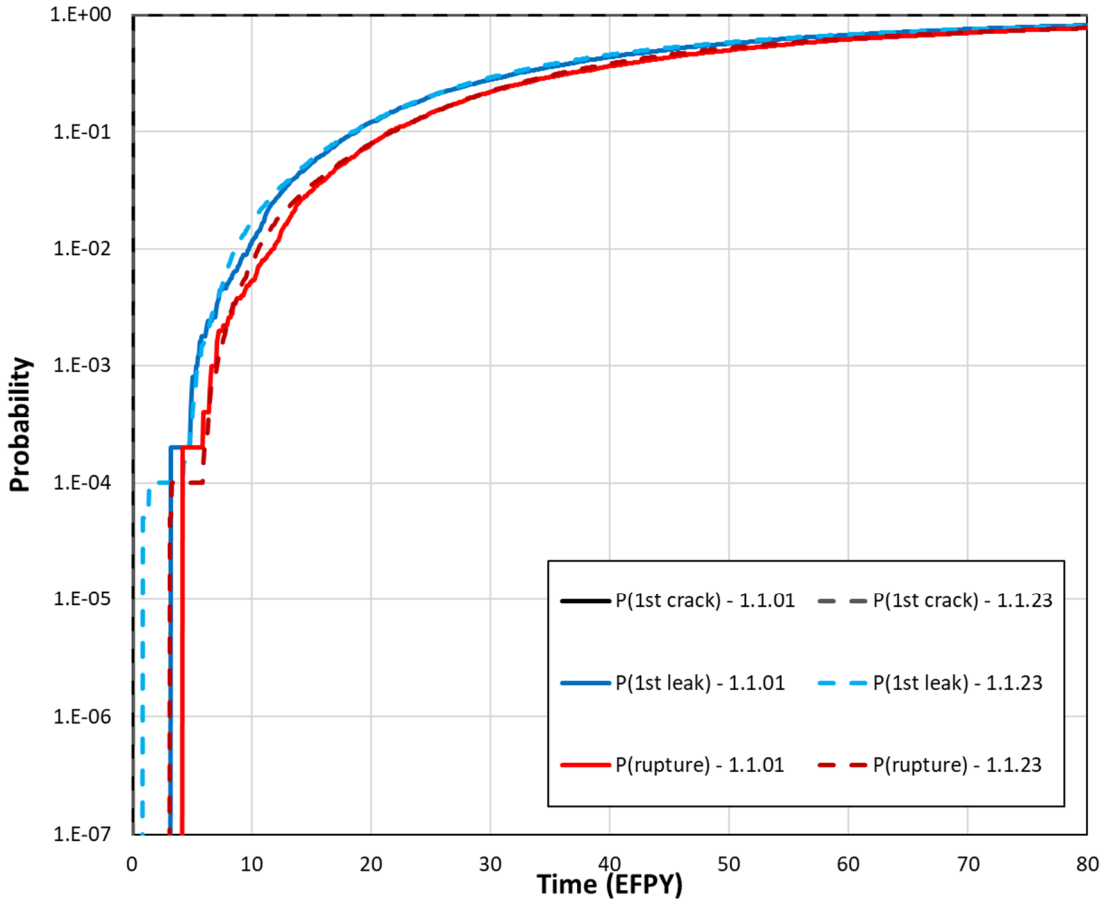


**Figure 3-105 Comparison of Case 1.1.23 time-dependent probabilities of first crack, first leak, and rupture with Case 1.1.1**

The main difference arising from the separation of epistemic and aleatory uncertainties is that these “mean” probabilities are estimated as the average of the probability over aleatory uncertainty. For each of the 200 epistemic realizations, a probability can be constructed to represent the mean over 100 aleatory values. All the epistemic realizations give a collection of probability curves on which statistics such as the mean, but also quantiles, can be estimated. These curves are shown in Figure 3-106 for the probability of first leak and Figure 3-107 for the probability of rupture. In these figures, each gray curve represents an epistemic trial (i.e., one iteration of the outer loop). The spread in each single curve represents the impact of aleatory uncertainty for the corresponding epistemic realization. The variation between the gray curves represents the impact of epistemic uncertainty, which is summarized with the colored statistics.

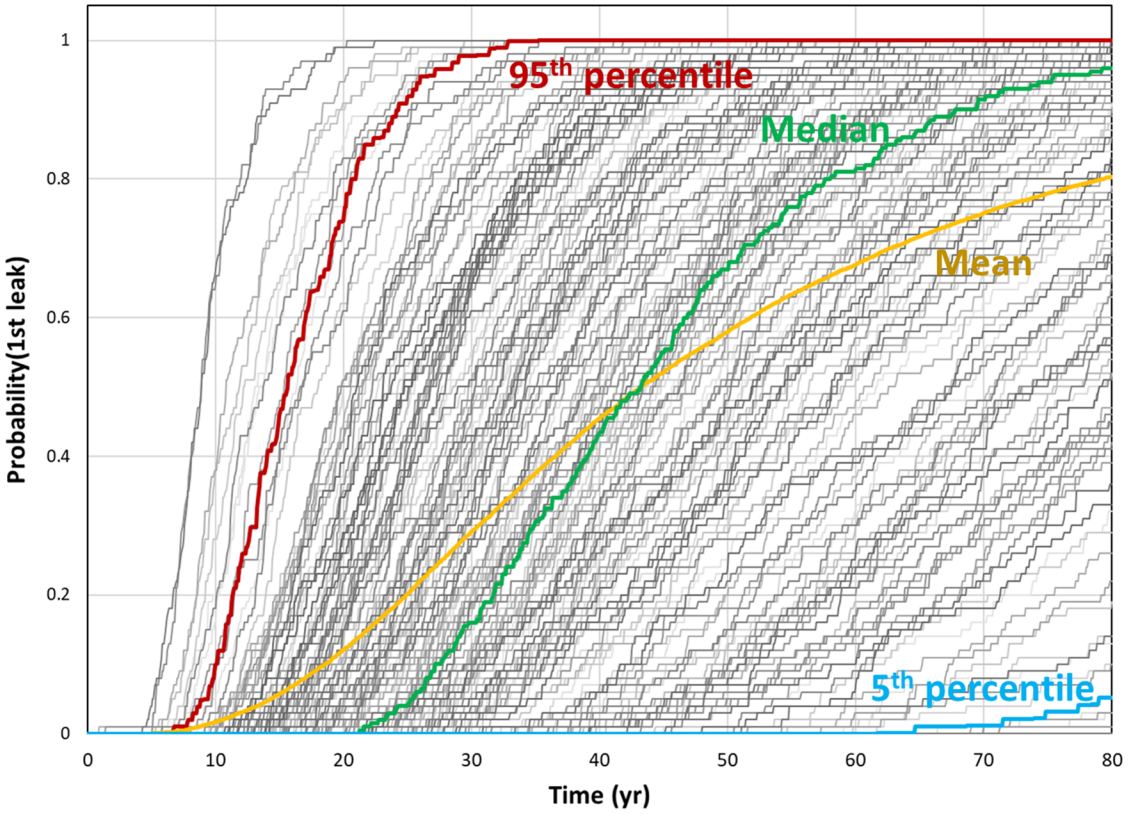


**Figure 3-106 Epistemic probabilities of first leak and statistics over the probabilities from Case 1.1.23 using 200 epistemic by 100 aleatory samples**

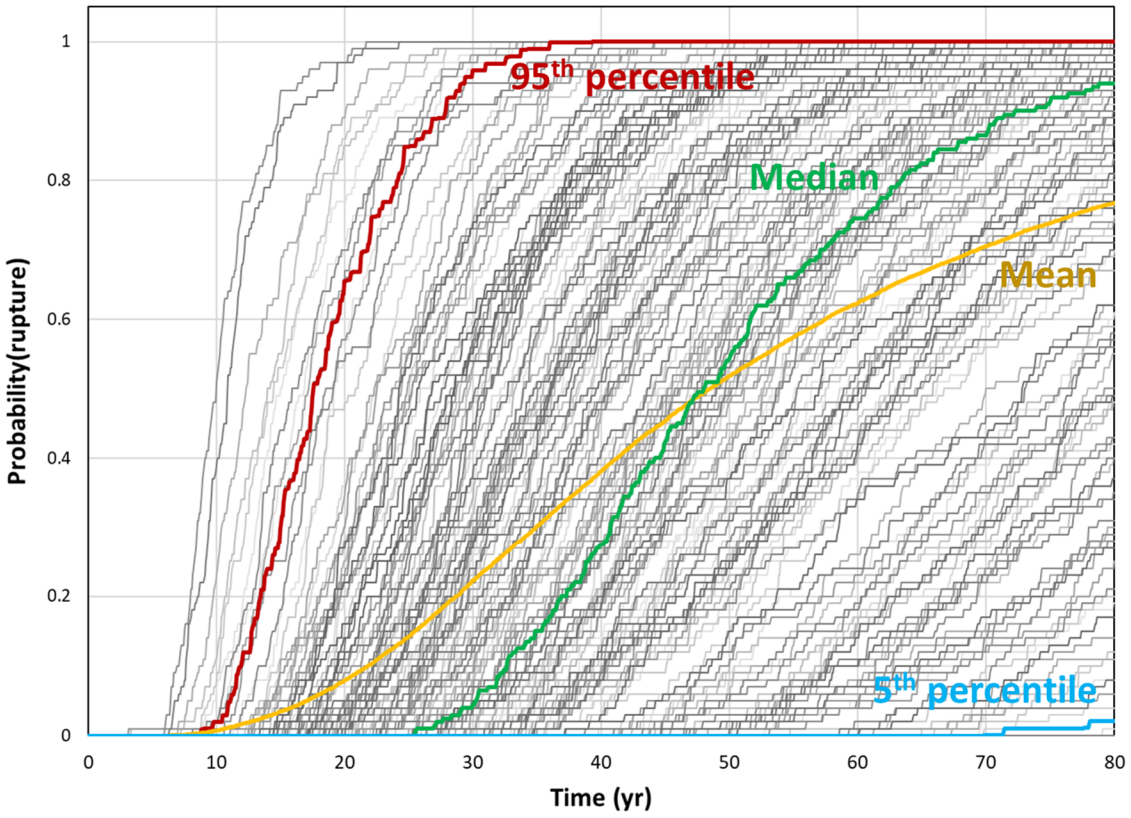


**Figure 3-107 Epistemic probabilities of rupture and statistics over the probabilities from Case 1.1.23 using 200 epistemic by 100 aleatory samples**

These results are specific to the selection of the aleatory and epistemic uncertainties. A change in the categorization would not change the mean curve, but it would affect both the gray curves and the quantiles. Any change would vary between the two extremes of setting all the uncertain inputs to aleatory and setting them to epistemic. Setting all the uncertainties to epistemic would change all the gray curves to straight, vertical lines (i.e., aleatory uncertainties would have no impact, so their probabilities would be either 0 or 1). In the other extreme, setting all the uncertainties to aleatory* would superimpose all the gray curves on top of each other (i.e., the variation would only reflect the change in the aleatory random numbers from one epistemic realization to another). As described in Section 2.3, such a choice would not affect the results for the quantities of interest selected for this study. Therefore, the separation of aleatory and epistemic uncertainties is considered to enhance understanding of the problem, but it does not affect any of the conclusions drawn, nor does it increase confidence in the mean results.

* Supposing that the same random seed is used for the aleatory sampling for each distinct epistemic run

## 3.3 Reactor Vessel Inlet Nozzle Weld

The RVIN weld analyses consisted of one base case and one sensitivity study. The analysis results are presented in Sections 3.3.1 and 3.3.2, respectively.

### 3.3.1 Base Case Considering PWSCC Initiation with Direct Model 1

#### *3.3.1.1 Case Description*

The objective of Case 1.2.0 was to assess the base likelihood of failure caused by PWSCC initiation and growth with no ISI, mitigation, or seismic effects. It served as the reference case for the RVIN weld analysis.

Most of the inputs used to analyze this case came from Case 1.1.0. Accordingly, Direct Model 1 was used for circumferential crack initiation with the parameters recommended in the technical report on PWSCC initiation model parameter development, confirmatory analyses, and validation [26]. Based on similarities between the RVON and RVIN weld geometries, this case also used the RVON weld no-repair WRS profile as documented in [27] and shown in Figure 3-1. The geometry and loads were developed from the information in Appendix D of [25], which resulted in different stresses. As with Case 1.1.0, the normal operating stresses used in the analysis were representative of design-basis values, which added a degree of conservatism. In addition, since the RVIN weld is on the cold leg, the operating temperature was reduced to 288 °C. The effects of ISI and seismic events were excluded as they were considered as part of the RVON sensitivity studies. The hydrogen concentration in the reactor coolant system was set to 37 cc/kg, which is the median, unmitigated concentration reported in [29].

Two simulations were performed for Case 1.2.0 as follows:

- The first simulation placed all uncertain inputs on the epistemic (outer) loop with the aleatory (inner) sample size set to 1. Each sample size was limited to 15,000 as this approach stores more information in memory. As a result, a total of 7 runs were performed to generate an aggregate sample of size 105,000.
- The second simulation used an optimized Direct Model 1 as described in [24]. One simulation with 3,000 realizations was performed with all uncertain inputs placed on the aleatory (inner) loop. The epistemic (outer) loop sample size was set to 1.

Section B20 describes the specific inputs and other simulation details used to analyze this case.

#### *3.3.1.2 Results and Analysis*

No cracks occurred in the 105,000-realization composite simulation. Thus, the annual frequency of such events would be lower than $1 \times 10^{-6}$, and it follows that there were no leak rate jump, LBB ratio, LBB time lapse, leak, or rupture data to consider. The 3,000-realization simulation using the optimized Direct Model 1 indicates that the probability of first crack is around $1 \times 10^{-6}$ as shown in Figure 3-108. These results explain why there were no crack occurrences in the 105,000-realization simulation, because on average only one in

10 simulations with such a sample size would have a realization with a crack. Given other similarities to Case 1.1.0 for the RVON weld, the results for Case 1.2.0 can be attributed to the lower operating temperature of the RVIN weld, which has an impact on the crack initiation model.

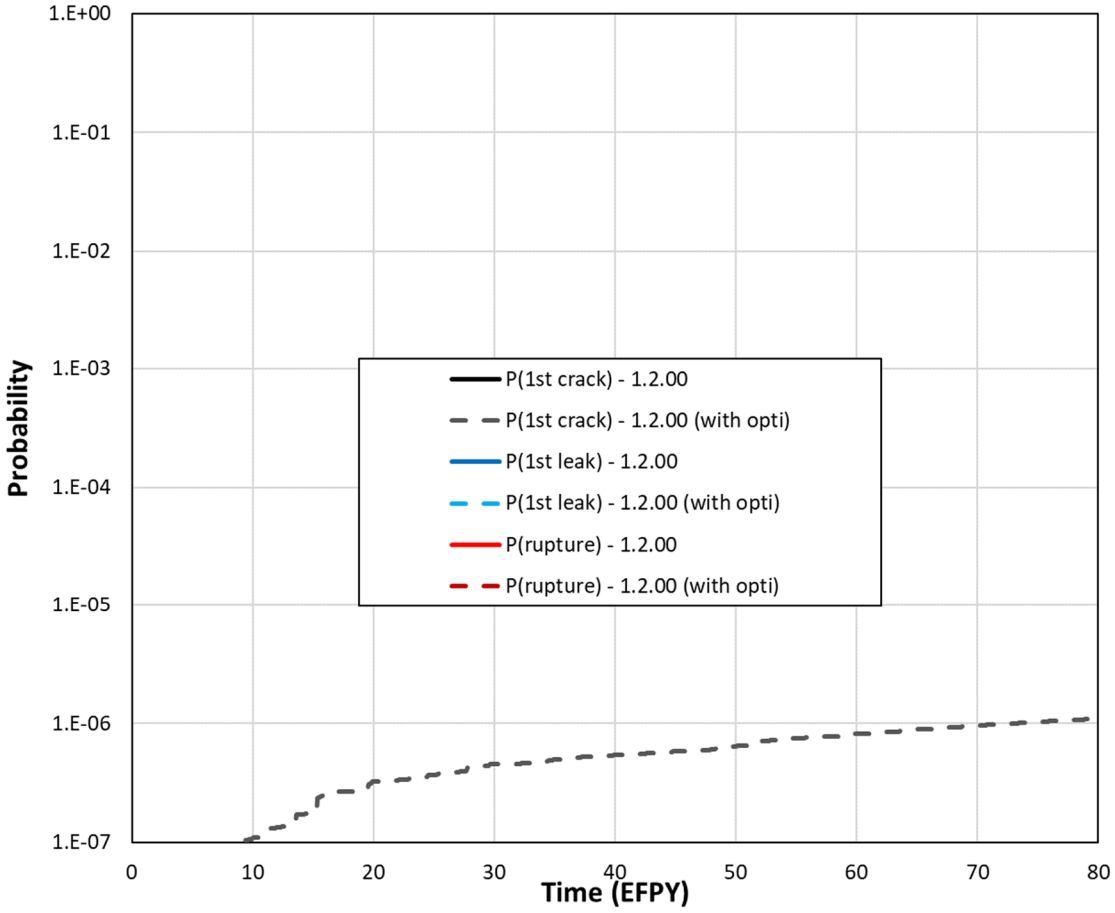


**Figure 3-108 Case 1.2.1 time-dependent probabilities of first crack, first leak, and rupture**

#### *3.3.1.3 Summary*

Based on the analysis of the Cases 1.2.0 results, the probability of failure of the RVIN weld is extremely low.

### 3.3.2 Sensitivity Study Case Considering Impacts of Fatigue

#### *3.3.2.1 Case Description*

The objective of Case 1.2.1 was to assess the impacts of the combined effects of PWSCC and fatigue. It was like Case 1.2.0 but with the addition of transients. This sensitivity study case was included because fatigue or the combination of fatigue and PWSCC could potentially play a more important role in the RVIN weld due to the lower operating temperature. Section B21 describes the specific inputs and other simulation details used to analyze this case.

#### *3.3.2.2 Results and Analysis*

There were no leak or rupture events for this case. Thus, the annual frequencies of such events would be lower than $1 \times 10^{-6}$, and it follows that there were no leak rate jump, LBB ratio, or LBB time lapse data to consider.

# 4 PIPING SYSTEM FAILURE PROBABILITY

The xLPR code can only analyze one weld in a simulation. However, in a typical Westinghouse four-loop PWR there are four RVON welds and four RVIN welds. Thus, a system-level analysis is necessary to combine the individual weld results and estimate a total probability of failure.

## 4.1 Historical Approaches

In Section 4.2 of NUREG/CR-2189, Volume 5 [3], two methods are presented for combining the failure probabilities of multiple welds to estimate a single, system-level failure probability. The first method considers all welds to be independent. This method provides an upper bound on the probability of failure. The second method considers only a single weld associated with the worst-case conditions as the weld that will fail first. This method provides a lower bound on the probability of failure and considers the properties and conditions to be perfectly correlated among all the welds. In practice, the true probability should lie between these two bounds; however, depending on the analysis considered, one of the bounds may be more representative of the true value than the other.

Historically, both methods have been used. In NUREG/CR-2189, Volume 5, the first method was selected for conservatism. Other analyses have successfully used the second method, such as documented in Westinghouse Electric Co. reports WCAP-14572, Revision 1-NP-A, "Westinghouse Owners Group Application of Risk-Informed Methods to Piping Inservice Inspection Topical Report," issued February 1999 [40], and WCAP-16168-NP-A, "Risk-Informed Extension of the Reactor Vessel In-Service Inspection Interval," Revision 3, issued October 2011 [41]. In the Westinghouse Electric Co. applications, fatigue was the primary degradation mechanism, and transients are typically expected to similarly affect each component in the system. Furthermore, the analyses were able to identify a worst-case weld and estimate its probability of failure.

## 4.2 Rationale in Methodology Selection

In selecting the most appropriate methodology, it is important to consider the degradation mechanisms being modeled. PWSCC is unlike fatigue because it can affect components differently. Some parameters affecting PWSCC can be common in all the welds, or at least strongly correlated. Other parameters, however, will be specific to an individual weld. In the present study, common parameters such as the operating temperature and pressure were considered constant, so by default they apply to each weld. The parameters varying from weld to weld were treated as distributions and sampled differently for each realization. Thus, the modeling assumptions support the conclusion that the true probabilities for a system-level analysis should be closer to the first method where all welds are considered independently. Further, since all the influential uncertain parameters are expected to vary from weld to weld, the results from this method are expected to be the closer to the true values.

Since the RVON weld in this study represented a generic weld and not a worst-case weld, it would be natural to assume that when the number of welds in the system is increased, the probability of having a failure-prone weld would increase by the same factor. Furthermore, the worst of 20 generic welds would be expected to be more failure-prone than the worst of 4 generic welds from the same distribution. Thus, an analysis based on the parameters of a generic weld does not appropriately represent the worst-case in a population of welds.

When specific welds were analyzed to validate the xLPR code (e.g., PWSCC found in welds in Virgil C. Summer Nuclear Generating Station, Unit 1; Ringhals Nuclear Power Plant, Unit 4; North Anna Power Station, Unit 1; and Tsuruga Nuclear Power Plant, Unit 2), they represented the worst-cases and were not reflective of the other welds in these plants, which can be considered generically. In such cases, the worst-case weld would likely dominate the probability of failure. The worst-case situations were modeled by adapting the analysis parameters to represent the specific welds. For instance, a different WRS profile was used as opposed to the WRS profile used to represent other welds in the plant. It would be overly conservative to consider all welds to have the same worst-case conditions, and thus the worst-case method would provide a reasonable estimate of the overall likelihood of failure. Considering the worst-case weld and three generic welds and then treating them as independent would lead to a value close to the worst-weld estimate; however, it could not be considered as the lower bound because it includes all the welds.

In theory, it should be possible to create a distribution of properties to represent the worst among $N$ welds, as it was done for specific plants. However, this approach would quickly become cumbersome and could lead to overly conservative assumptions if all the information is not readily available (e.g., always taking a conservatively biased 75$^{th}$ percentile of the distribution for each uncertain input). Such an approach would generate far worse and far less likely results as the number of inputs increases. In conclusion, it was determined that the most appropriate method for the present study was to consider all the welds independently. This approach is more realistic and more defensible than the lower-bound method. The remainder of this section illustrates application of this method to combine results for multiple welds and arrive at a system-level risk estimate.

## 4.3 Combining Probabilities

### 4.3.1 Similar Welds

In theory, the independence can be expressed by considering $N$ similar welds. Each weld has a probability of failing, $p$, and a probability of not failing, $q = 1 - p$. The probability to have $x$ welds fail, with $0 \leq x \leq N$, is thus:

$$P(fail = x) = C_x^N p^x . q^{N-x}$$

Here, $C_x^N$ represents the statistical combination of $x$ elements from a pool of $N$ elements.

As an example, consider that failure is defined by the occurrence of a circumferential crack. Such a failure definition would be overly conservative for GDC 4 decisionmaking purposes;

however, it was chosen for illustration purposes here because it was the only QoI that could be estimated for the RVIN weld.

If there are 4 RVON welds, each with a probability of failure of $p = 3 \times 10^{-3}$ ($q = 1 - p = 9.97 \times 10^{-1}$), then:

- $P(fail = 4\ welds) = C_4^4 p^4 q^0 \cong 1 \times 8.11 \times 10^{-11} \times 1 \cong 8.11 \times 10^{-11}$
- $P(fail = 3\ welds) = C_3^4 p^3 q^1 \cong 4 \times 2.07 \times 10^{-8} \times 0.997 \cong 1.08 \times 10^{-7}$
- $P(fail = 2\ welds) = C_2^4 p^2 q^2 \cong 6 \times 9 \times 10^{-6} \times 0.994 \cong 5.37 \times 10^{-5}$
- $P(fail = 1\ weld) = C_1^4 p^1 q^3 \cong 4 \times 3 \times 10^{-3} \times 0.991 \cong 1.2 \times 10^{-2}$
- $P(fail = 0\ welds) = C_0^4 p^0 q^4 \cong 1 \times 1 \times 0.988 \cong 9.88 \times 10^{-1}$

The sum of all these probabilities is 1.0.

From this illustration, the probability of one failure is 1.2 in 100, which is approximately 4 times the probability of failure of a single weld. This result is expected because the welds are considered independently. The probability of 2 failures is between 5 and 6 over 100,000. The ratio between these two probabilities is 221, which indicates that, if there is a failure (i.e., a failure conditional on a 1.2 in 100 chance already), then roughly 4 times out of 1,000 there would be 2 failures instead of 1. In all the other cases (i.e., 996 out of 1,000 failures), there would be only one failure, which would be equivalent to the single-weld scenario. In this illustration, because of the number of welds considered and the low probability of the adverse event, the probability of failure of $N$ identical welds, each with an individual probability of failure $p$, can be approximated as $P(fail = 1\ weld) \cong N \times p$.

In addition, the time of crack initiation between the two welds is likely to be large enough such that leakage would be detected in one weld before a crack occurs in the second weld. Figure 4-1 illustrates this behavior.

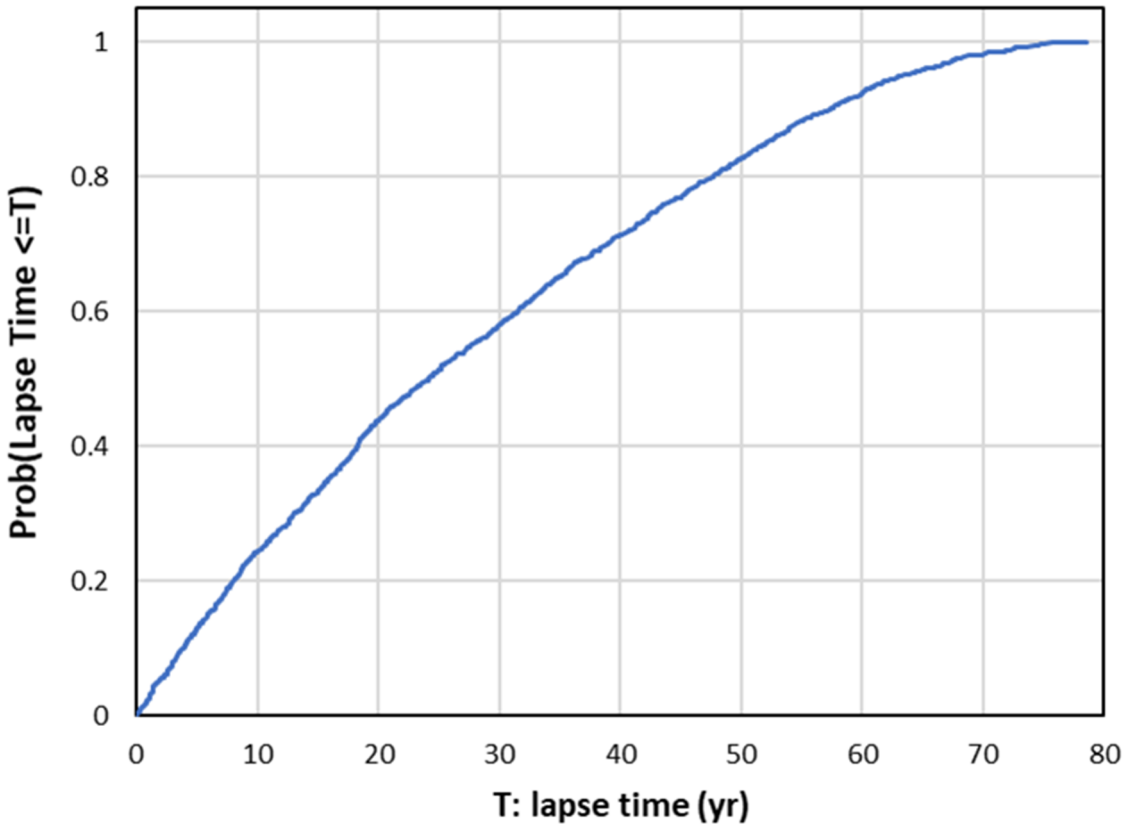


**Figure 4-1 CDF of time lapse between events for two welds of the same sort treated independently**

Thus, by treating all the welds independently, most of the failure realizations would only have one weld failure. In the other realizations, it is likely that the differences in the times to failure would be such that one weld would be dominant (i.e., leak or rupture well before the other weld sees any substantial crack growth). This behavior is consistent with the operating experience of PWRs. It also considers that the risk is greater if there are more degraded components in the system.

### 4.3.2 Different Welds

The previous equation can also be extended to different types of welds each with their own specific $p$ and $q$ values. Let $\{W_1, W_2, \dots, W_k\}$ be the $k$ weld types considered with the respective number per type being $\{N_1, N_2, \dots, N_k\}$, and let the probabilities of having the event occurring at time $\tau$ be $\{p_1, p_2, \dots, p_k\}$. Then, the probability of having $x_1$ welds of type $W_1$, $x_2$ welds of type $W_2$, and so on up to $x_n$ welds of type $W_n$, would be:

$$P(events = \{x_1, x_2, \dots, x_n\}) = \prod_{i=1}^{k} C_{x_i}^{N_i} p_i^{x_i} . (1 - p_i)^{N_i - x_i}$$

This equation is the generic form of Equation 4.1 in NUREG/CR-2189, Volume 5. It was used in that report to consider a system of 14 joints per loop over 4 reactor coolant system piping loops.

It may, however, be unnecessary to include some of the welds if their probabilities of failure are negligible compared to the other welds. As an example, consider the same 4 RVON welds each with an assumed probability of failure of 3 x $10^{-3}$ coupled with 4 RVIN welds each with an assumed probability of failure of $1 \times 10^{-6}$ over 80 EFPY of plant operation. The possible combinations are summarized in Table 4-1. The first row of the table lists the probabilities associated with multiple RVIN welds when no RVON welds are considered.

**Table 4-1 Illustration of probabilities estimated for a combination of welds failing based on two different weld types with four welds per type**

| | | Number of Failed RVIN Welds | | | | | No RVIN Welds |
|---|---|---|---|---|---|---|---|
| | | 0 | 1 | 2 | 3 | 4 | |
| Number of Failed RVON Welds | 0 | 9.88E-01 | 3.95E-06 | 5.93E-12 | 3.95E-18 | 9.88E-25 | 9.88E-01 |
| | 1 | 1.19E-02 | 4.76E-08 | 7.14E-14 | 4.76E-20 | 1.19E-26 | 1.19E-02 |
| | 2 | 5.37E-05 | 2.15E-10 | 3.22E-16 | 2.15E-22 | 5.37E-29 | 5.37E-05 |
| | 3 | 1.08E-07 | 4.31E-13 | 6.46E-19 | 4.31E-25 | 1.08E-31 | 1.08E-07 |
| | 4 | 8.10E-11 | 3.24E-16 | 4.86E-22 | 3.24E-28 | 8.10E-35 | 8.10E-11 |
| No RVON Welds | | 1.00E-00 | 4.00E-6 | 6.00E-12 | 4.00E-18 | 1.00E-24 | |

In this example, including the RVIN welds does not change the results. Specifically, the figures in the first column (0 RVIN welds) are the same as the figures in the last column (with no RVIN welds). The likelihood of having 1 out of 4 RVIN welds crack (with no RVON weld having a crack) is the only case worth considering with a probability of $4 \times 10^{-6}$, but it is 3,000 times less likely than having an RVON weld with a crack. The likelihood of having leakage from the RVIN weld is even lower, which further makes this case inconsequential. However, there are significant differences in the inverse case of no RVON welds present in the system, as represented by the last row in Table 4-1, and no RVON weld failures, as represented by the first row of Table 4-1.

In such situations, the calculations can be simplified to not include the RVIN welds in the final statistics. They may, however, be included for completeness and to avoid ambiguity. In the present study, this summary table is adequate. In future analyses, the following approach is recommended: ignore the data in the final statistics if the failure probability of a given weld type multiplied by the number of welds of the type in the system is less than an order of magnitude below the probability of the same event for the worst-case weld type. Otherwise, it is best to consider the data.

### 4.3.3 Considerations for Events Affecting the Entire Plant

Caution is necessary in the case of events affecting the entire plant, such as an earthquake. The likelihood of a seismic event should not be added independently to each weld because it would artificially increase the probability of having such an event. In such situations, the results should be aggregated prior to the correction applied for a seismic event. Once the probability for the set of welds under consideration is known, conditional on having a seismic event, then the probability of having such an event can be applied.

### 4.3.4 Welds with Different Consequences

In Section 4.3.3, the failure events were all considered to have similar consequences. This is an acceptable approach when the same weld type is considered; however, it may not be appropriate for different weld types. For instance, some welds may have larger probabilities of occurrence of leakage and rupture, and they would drive the probability if included. However, if these welds do not have an adverse consequence as large as the other welds, then they may create a larger risk that is misleading.

As an example, consider the addition of 4 hypothetical small diameter welds into the piping system. Each of these welds is assumed to have a $1 \times 10^{-2}$ probability of failure over 80 EFPY of plant operation. They are considered along with the 4 RVON welds each with the previously assumed probability of failure of 3 x $10^{-3}$. The impact would be to greatly reduce the role of the RVON weld in terms of the probability as shown in Table 4-2. This illustration uses fictitious numbers to demonstrate the concepts involved in accounting for the different consequences associated with different types of welds.

**Table 4-2 Illustration of probabilities estimated for a combination of welds failing based on four RVON welds and hypothetical high failure probability small diameter welds**

| | | Number of Failed RVON Welds | | | | | No RVON Welds |
|---|---|---|---|---|---|---|---|
| | | 0 | 1 | 2 | 3 | 4 | |
| Number of Failed Hypothetical Welds | 0 | 8.04E-01 | 1.06E-02 | 5.29E-05 | 1.17E-07 | 9.66E-11 | 8.15E-01 |
| | 1 | 1.69E-01 | 2.24E-03 | 1.11E-05 | 2.46E-08 | 2.03E-11 | 1.71E-01 |
| | 2 | 1.34E-02 | 1.77E-04 | 8.79E-07 | 1.94E-09 | 1.61E-12 | 1.35E-02 |
| | 3 | 4.69E-04 | 6.21E-06 | 3.08E-08 | 6.81E-11 | 5.63E-14 | 4.75E-04 |
| | 4 | 6.17E-06 | 8.17E-08 | 4.06E-10 | 8.95E-13 | 7.41E-16 | 6.25E-06 |
| No Hypothetical Welds | | 9.88E-01 | 1.19E-02 | 5.37E-05 | 1.08E-07 | 8.10E-11 | |

The probability of failure between the hypothetical small diameter weld and the RVON weld is about $1 - 8.04 \times 10^{-1} = 0.196$ (i.e., nearly 20 percent). However, this estimate would not be correct if a crack in the hypothetical small diameter weld is of no consequences. There is a

20 percent chance of having an RVON weld or another weld fail, but there is still a 1.2 percent chance that one of the RVON welds would fail.

If consequences are considered, the correct approach is to calculate the risk based on the set of consequences in a tabular format, such as shown in Table 4-1 and Table 4-2. Once the probabilities are known, the consequences can be estimated conditionally (using independency for each weld and conditional results) and associated with each case.

As an example, suppose that each RVON weld with a crack has a consequence of 1.0, meaning that 2 RVON welds would have a consequence of 2.0, and each hypothetical small diameter weld has a consequence of $1.0 \times 10^{-3}$. Table 4-3 displays the associated risks based on the failure probabilities from Table 4-2 multiplied by the assumed consequences of failure. This illustration shows that the risk of considering only the RVON welds (labelled as "Prob(RVON).N(RVON)") and the risk of considering the hypothetical small diameter welds are about the same. This result is expected due to the small impact assigned to the hypothetical small diameter welds.

**Table 4-3 Illustration of risk matrix(probabilities multiplied by consequences)**

| | | Number of Failed RVON Welds | | | | |
|---|---|---|---|---|---|---|
| | | 0 | 1 | 2 | 3 | 4 |
| Number of Failed Hypothetical Welds | 0 | 0.00E+00 | 1.06E-02 | 1.06E-04 | 3.50E-07 | 3.86E-10 |
| | 1 | 1.69E-04 | 2.24E-03 | 2.23E-05 | 7.37E-08 | 8.14E-11 |
| | 2 | 2.67E-05 | 1.77E-04 | 1.76E-06 | 5.82E-09 | 6.42E-12 |
| | 3 | 1.41E-06 | 6.23E-06 | 6.18E-08 | 2.04E-10 | 2.25E-13 |
| | 4 | 2.47E-08 | 8.20E-08 | 8.13E-10 | 2.69E-12 | 2.97E-15 |
| Sum | | 1.97E-04 | 1.31E-02 | 1.30E-04 | 4.30E-07 | 4.74E-10 |
| Prob RVON.N(RVON) | | 0 | 1.31E-02 | 1.30E-04 | 4.30E-07 | 4.74E-10 |

## 4.4 Piping System Failure Frequency Results

In this study, the probability of rupture with leak rate detection serves as the QoI used to assess whether a representative Westinghouse four-loop PWR primary coolant loop piping system demonstrates an extremely low probability of rupture consistent with the requirements of GDC 4 when considering the effects of PWSCC. Over 80 EFPY of simulated plant operation, this probability was estimated to be zero for an individual RVON weld as shown in Section 3.2.1. It is thus unnecessary to analyze this QoI at the system-level.

To provide additional insights at the system-level, annual results for the probabilities of first crack and first leak without ISI were analyzed. Only the RVON welds were considered because the RVIN contributions were shown to be negligible. Figure 4-2 shows the probability of first crack, and Figure 4-3 shows the probability of first leak without ISI. In these figures, P(x weld)

represents the probability of having exactly *x* welds out of 4 with a crack or a leak occurring, respectively. When 4 RVON welds are considered in the piping system, the annual frequency of crack initiation in any weld over 80 EFPY is $1.6 \times 10^{-4}$. The likelihood of multiple welds cracking is low enough to be ignored when considering the annual frequencies. Furthermore, the expected time between two welds cracking is large enough such that the second event would be of no consequence. The annual frequency of leakage without ISI is $6.9 \times 10^{-5}$.

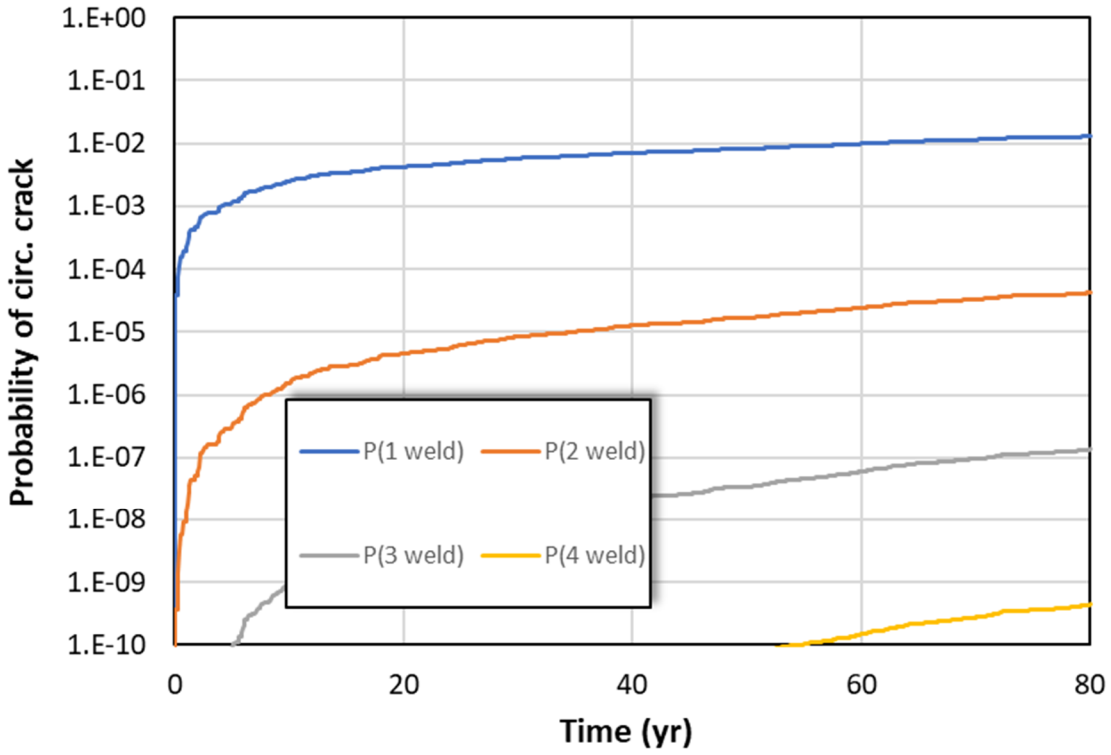


**Figure 4-2 Probabilities of multiple RVON welds having a crack over 80 EFPY**

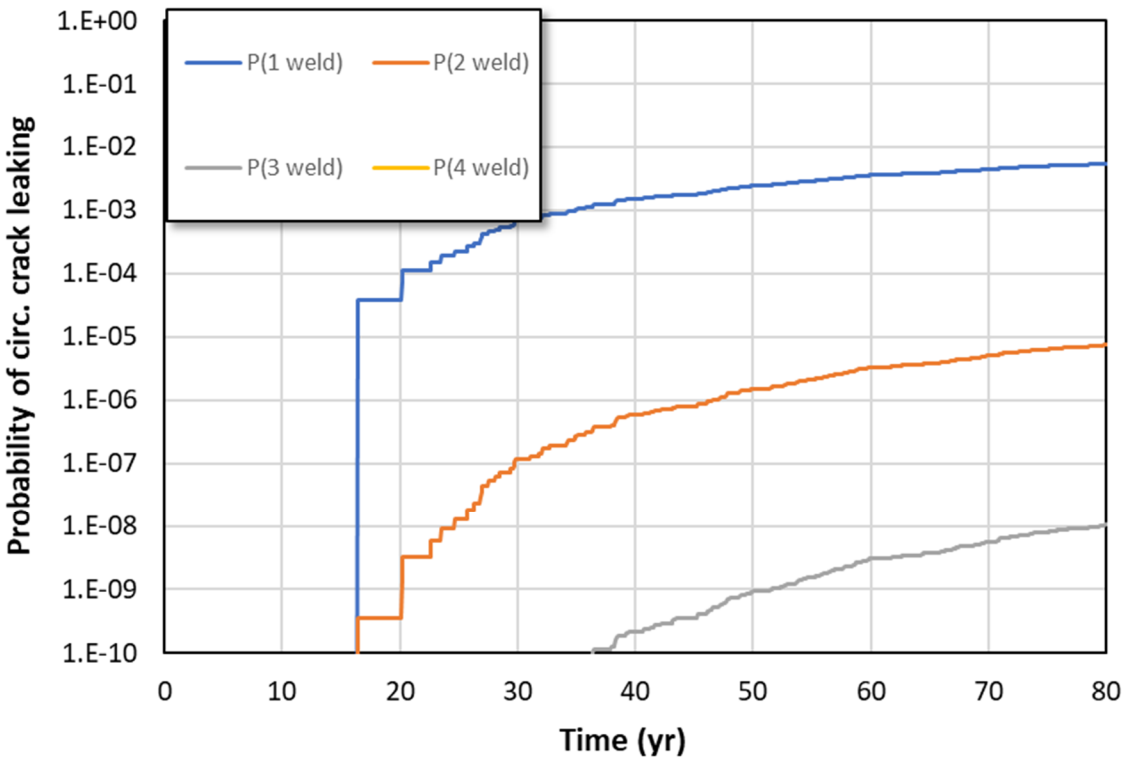


**Figure 4-3 Probabilities of multiple RVON welds having a leak over 80 EFPY without ISI**

# 5 SUMMARY AND CONCLUSIONS

This study was undertaken to satisfy two primary objectives:

1. Use the xLPR code to generate numerical failure frequency estimates with uncertainties for welds in a representative PWR piping system considering the effects of PWSCC and other key parameters, such as leak rate detection, ISI, mitigation, and seismic events.
2. Combine the estimates from multiple welds to generate an annual, piping system-level failure frequency to determine whether the requirements of GDC 4 are met.

A representative Westinghouse four-loop PWR primary coolant loop piping system was selected for the study because it is the predominant piping system for which the NRC staff has granted approvals for LBB. The system typically contains eight welds that are susceptible to PWSCC: four RVON welds and four RVIN welds. The simulated period was 80 EFPY to bound plant operation as would be authorized by an original 40-year operating license and two renewed operating licenses. Several probabilistic QoIs were defined and studied for each of these weld types to support the desired safety conclusions. These QoIs were the probability of rupture with leak rate detection, leak rate jump, LBB time lapse, and LBB ratio. The analyses for each weld type included base cases and sensitivity study cases to investigate the effects of specific analysis parameters and assumptions.

The probability of rupture with leak rate detection served as the QoI used to assess whether such piping systems demonstrate an extremely low probability of rupture consistent with the requirements of GDC 4. None of the RVON and RVIN weld cases had any ruptures with a 1 gpm leak rate detection capability. These results indicate that such an event would have an annual frequency lower than 1 x $10^{-6}$ per year and likely at least one order of magnitude lower.

The next QoI considered was the probability of leak rate jump as defined in [22]. This QoI was considered to provide additional insights into the behavior of the piping system. None of the RVIN weld cases showed a probability of leak rate jump. Only two RVON weld cases had a non-zero probability of leak rate jump. Case 1.1.2, which investigated the impacts of a more severe WRS profile, exhibited a probability of $9.5 \times 10^{-5}$ over 80 EFPY, which gives an annual frequency estimate of around $1.2 \times 10^{-6}$. Case 1.1.7, which investigated sensitivities due to the normal operating loads, exhibited a probability of $1.9 \times 10^{-5}$ over 80 EFPY, which gives an annual frequency estimate of around $2.4 \times 10^{-7}$. These probabilities can be compared to the recommended annual frequency acceptance criterion of $1 \times 10^{-6}$. However, further analyses showed that the results were due to instances where two TWCs coalesced as a result of sampling a large and unrealistic coalescence distance rule. For instance, in one case the cracks were 40 cm apart, but they still coalesced.

The next QoI considered was the probability of LBB time lapse, which is the time between a detectable leak and rupture for realizations when both leaks and ruptures occur. This QoI was also considered to provide additional insights into the behavior of the piping system. None of the RVIN weld cases showed LBB time lapses because no cracks were generated. For the

RVON weld cases, the mean LBB time lapse was typically around 30 months with a 10 gpm leak rate detection capability and between 50 and 60 months with a 1 gpm leak rate detection capability. However, there were a few exceptions as follows:

- In Case 1.1.2, which analyzed the sensitivity due to a more severe WRS profile, the mean LBB time lapse with a 1 gpm leak rate detection capability was 34 months, which was close to the 30-month LBB time lapse based on a 10 gpm leak rate detection capability. This outcome highlights that a more conservative WRS profile, especially at the inside diameter of the weld, will lead to larger surface cracks that will tend to have higher leak rates when they penetrate through-wall.
- In Case 1.1.9, which investigated the impact of MSIP, the mean LBB time lapse was relatively shorter at 28 and 41 months with 10 and 1 gpm leak rate detection capabilities, respectively. However, this outcome was expected because all the ruptures occurred before MSIP application, and this behavior was the result of sampled faster crack growth rates. The lower mean values are thus driven by the early cases of failure, which no longer occur after MSIP is applied.
- In Case 1.1.14, which investigated the sensitivity due to the hydrogen concentration, the mean LBB time lapse was also on the low side of the spectrum at 27 and 39 months with 10 and 1 gpm leak rate detection capabilities, respectively. This outcome is the result of the lower-bound hydrogen concentration that was used to analyze this case. The decreased hydrogen concentration led to faster crack growth rates.
- In Case 1.1.15, which investigated the impact of fatigue, the mean LBB time lapse was considerably lower at 10 and 14 months with 10 and 1 gpm leak rate detection capabilities, respectively. It was found that when the cracks are close to or already penetrating through-wall, the impact of the transients considered is more significant and accelerates crack growth.
- In Case 1.1.20, which investigated the sensitivity due to the normal operating temperature, the mean LBB time lapse was 23 and 33 months with 10 and 1 gpm leak rate detection capabilities, respectively. This outcome is the result of the role that temperature plays in the crack growth model. Specifically, the crack growth rate increases with increases in the normal operating temperature.

The last QoI considered was the probability of LBB ratio, which is the probabilistic analog to the SRP Section 3.6.3 deterministic acceptance criteria. It too was considered for informational purposes. None of the RVIN weld cases showed LBB ratios because no cracks were generated, which was primarily the result of the lower operating temperature of this weld. For the RVON weld cases, the mean LBB ratios were around 4 with a 10 gpm leak rate detection capability. With a 1 gpm leak rate detection capability, the mean LBB ratios increase to 9 or 10. The exception was in Case 1.1.2, where the mean LBB ratio was around 6. All these LBB ratios are well above the deterministic acceptance margin of 2.0 from SRP Section 3.6.3. The results highlight conservatisms present in the deterministic LBB approach, which may be reduced using probabilistic approaches.

The individual RVON and RVIN weld results with zero probabilities of rupture with a 1 gpm leak rate detection capability demonstrate that a typical primary loop piping system in a Westinghouse four-loop PWR continues to meet the requirements of GDC 4 when subject to the effects of PWSCC. An analysis was performed using the other QoIs to illustrate how the results from multiple welds can be aggregated for a system-level safety assessment. Only the results for the four RVON welds were considered in this aggregation because the RVIN weld results were small enough to have no impact. The approach used to aggregate the results considered each RVON weld independently, which is reasonably conservative. Since the individual RVON weld probabilities were small, their combination only increased the system-level estimate by roughly a factor of 4, which is the same as the number of RVON welds in the piping system. Thus, the system-level results do not affect the conclusions drawn on an individual weld basis and remain below the $1 \times 10^{-6}$ ruptures per year acceptance threshold set for this study consistent with the basis for the GDC 4 rulemaking.

This study represented the first comprehensive application of the xLPR code to support risk-informed regulatory decisionmaking. As such, it provided an excellent opportunity to build experience applying the xLPR code and interpreting the results to resolve a safety-significant questions. The analysts identified best practices during the process of defining the analysis cases, inputs, and outputs, and in running the analyses and analyzing the results. The breadth of the sensitivity studies and QoIs considered also led to many observations on the impacts of various factors that influence the behavior of dissimilar metal welds in PWR primary coolant loop piping systems. The following observations were made on the QoIs that were considered:

- Since the probabilities of rupture with leak rate detection and leak rate jump were zero in nearly all the cases, it can be useful to supplement these results with another QoI calculated from non-zero events. In particular, the LBB time lapse QoI showed more variation than the other QoIs and provided key insights into the time-dependent aspects of the problem. This QoI was found to be useful for ranking the different scenarios considered in the study.
- The LBB ratio could play a role in understanding the transition from static, deterministic LBB analyses to dynamic, probabilistic LBB analyses. Historically, the LBB ratio is influenced by material property changes, so this QoI could also be useful in performing sensitivity studies where the material properties (e.g., yield and ultimate strength) are varied.

In addition, based on all the cases that were analyzed in this study, the following key observations were made:

- The probability of a rupture occurring before a leak is detected (i.e., an undesirable break-before-leak scenario) is extremely low and should not be an issue for either the RVON or RVIN welds considering the inputs used in this study.
- The WRS profile and its uncertainty were again found to be one of the most influential inputs.

- Axial cracks only impacted the probability of first leak, but the predicted leak rates were so small that the cracks would only be detected through ISI. Furthermore, the likelihood of having both an axial crack and a circumferential crack was so low that it did not affect the results. Therefore, it would be appropriate to exclude axial cracks under similar analysis conditions.

The methods and results presented in this report may be used as the basis for performing additional probabilistic LBB analyses for nuclear power plant piping systems.

# 6 REFERENCES


[1] Westinghouse Electric Corporation, WCAP-9570, “Mechanistic Fracture Evaluation of Reactor Coolant Pipe Containing a Postulated Circumferential Through-Wall Crack,” Rev. 2, June 1981, ADAMS Accession No. ML19352B279.

[2] Westinghouse Electric Corporation, WCAP 9788, “Tensile and Toughness Properties of Primary Piping Weld Metal for Use in Mechanistic Fracture Evaluation,” June 1981, ADAMS Accession No. ML19352B277.

[3] NRC, NUREG/CR-2189, “Probability of Pipe Fracture in the Primary Coolant Loop of a PWR Plant, Vol. 5, Probabilistic Fracture Mechanics Analysis, Load Combination Program, Project I Final Report,” August 1981, ADAMS Accession No. ML15300A304.

[4] NRC, “Modification of General Design Criterion 4 Requirements for Protection Against Dynamic Effects of Postulated Pipe Ruptures,” *Federal Register*, pp. 27,006–27,009, July 1, 1985.

[5] NRC, “Modification of General Design Criterion 4 Requirements for Protection Against Dynamic Effects of Postulated Pipe Ruptures,” *Federal Register*, pp. 41,288–41,295, October 27, 1987.

[6] NRC, NUREG-1061, “Report of the U.S. Nuclear Regulatory Commission Piping Review Committee, Vol. 3, Evaluation of Potential Pipe Breaks,” November 1984, ADAMS Accession No. ML093170485.

[7] U.S. Code of Federal Regulations, “Domestic licensing of production and utilization facilities,” Part 50, Chapter I, Title 10, “Energy.”

[8] NRC, “Standard Review Plan; Public Comment Solicited,” *Federal Register*, pp. 32626–32633, August 28, 1987.

[9] NRC, Information Notice 2004-11, “Cracking in Pressurizer Safety and Relief Nozzles and in Surge Line Nozzle,” May 6, 2004, ADAMS Accession No. ML041260136.

[10] NRC, Regulatory Issue Summary 2008-25, “Regulatory Approach for Primary Water Stress Corrosion Cracking of Dissimilar Metal Butt Welds in Pressurized Water Reactor Primary Coolant System Piping,” October 22, 2008, ADAMS Accession No. ML081890403.

[11] NRC, Bulletin 2004-01, “Inspection of Alloy 82/182/600 Materials Used in the Fabrication of Pressurizer Penetrations and Steam Space Piping Connections at Pressurized-Water Reactors,” May 28, 2004, ADAMS Accession No. ML041480034.

[12] EPRI, Report 1009549, “Materials Reliability Program: Alloy 82/182 Pipe Butt Weld Safety Assessment for U.S. PWR Plant Designs (MRP-113),” Palo Alto, CA, 2006.

[13] EPRI, Report 1010087, “Materials Reliability Program: Primary System Piping Butt Weld Inspection and Evaluation Guidelines (MRP-139),” Palo Alto, CA, 2005.

[14] EPRI, Report 1015009, “MRP-139 Revision 1: Primary System Piping Butt Welds Inspection and Evaluation Guideline,” Palo Alto, CA, 2008.

[15] Nuclear Energy Institute, NEI 03-08, “Guideline for the Management of Materials Issues,” Washington, DC, 2003.

[16] J. Grobe, Director, Division of Component Integrity, Office of Nuclear Reactor Regulation, NRC, letter to A. Marion, Senior Director of Engineering, Nuclear Energy Institute, Nuclear Generation Division, March 2, 2006, ADAMS Accession No. ML060650193.

[17] J.E. Dyer, Director, Office of Nuclear Reactor Regulation, NRC, letter to Gary C. Park, Chairman, ASME Subcommittee on Nuclear Inservice Inspection, December 20, 2005, ADAMS Accession No. ML053480359.

[18] ASME, Case N-770-1, “Alternative Examination Requirements and Acceptance Standards for Class 1 PWR Piping and Vessel Nozzle Butt Welds Fabricated With UNS N06082 or UNS W86182 Weld Filler Material With or Without Application of Listed Mitigation Activities,” in Cases of ASME Boiler and Pressure Vessel Code, New York, NY, December 25, 2009.

[19] NRC, “American Society of Mechanical Engineers (ASME) Codes and New and Revised ASME Code Cases,” Federal Register, Vol. 76, No. 119, pp. 36232–36279, 2011.

[20] NRC, NUREG-0800, “Standard Review Plan for the Review of Safety Analysis Reports for Nuclear Power Plants: LWR Edition,” Section 3.6.3, Rev. 1, “Leak-Before-Break Evaluation Procedures,” March 2007, ADAMS Accession No. ML063600396.

[21] NRC, NUREG-2110, “xLPR Pilot Study Report,” May 2012, ADAMS Accession No. ML12145A470.

[22] R. Hardies, et al., “xLPR Version 2.0 Technical Basis Document—Acceptance Criteria,” October 28, 2016, ADAMS Accession No. ML16271A436.

[23] NRC and EPRI, “Addendum to Memorandum of Understanding between U.S. Nuclear Regulatory Commission and Electric Power Research, Inc. on Cooperative Nuclear Safety Research—xLPR Version 2 Code Documentation and Leak-Before-Break Applications,” May 10, 2017, ADAMS Accession No. ML17040A146.

[24] C. Sallaberry and R. Kurth, “Optimization of Deterministic Submodel to Reduce Large Sample Size Runs,” in Proceedings of the 30th European Safety and Reliability Conference and the 15th Probabilistic Safety Assessment and Management Conference, Venice, Italy, 2020.

[25] M. Homiack, “xLPR Group Report—Inputs Group, Version 1.0,” December 19, 2017, ADAMS Accession No. ML19337B876.

[26] K. Schmitt and G. Troyer, “xLPR Technical Report—Primary Water Stress-Corrosion Cracking Initiation Model Parameter Development, Confirmatory Analyses, and Validation, Version 2.0,” July 28, 2017, ADAMS Accession No. ML19337C202.

[27] F. Brust, “xLPR Models Subgroup Report—Welding Residual Stresses, Version 1.0,” October 5, 2016, ADAMS Accession No. ML16341B049.

[28] NRC, TLR-RES/DE/CIB-2021-11, "Sensitivity Studies and Analyses Involving the Extremely Low Probability of Rupture Code," May 2021, ADAMS Accession No. ML21133A485.

[29] EPRI, Report 1022852, “Materials Reliability Program: Probabilistic Assessment of Chemical Mitigation of Primary Water Stress Corrosion Cracking in Nickel-Base Alloys (MRP 307), Zinc Addition and Hydrogen Optimization to Mitigate Primary Water Stress Corrosion,” Palo Alto, CA, 2011.

[30] B. Efron and R. J. Tibshirani, An Introduction to the Bootstrap, CRC Press, Boca Raton, FL, 1994.

[31] NRC, NUREG/CR-4599, “Short Cracks in Piping and Piping Welds—Semiannual Report October 1992 – March 1993, Vol. 3, No. 2,” March 1994, ADAMS Accession No. ML20065B487.

[32] D. Rudland, et al., “Evaluation of the Inlay Process as a Mitigation Strategy for Primary Water Stress Corrosion Cracking in Pressurized Water Reactors,” April 2010, ADAMS Accession No. ML101260554.

[33] EPRI, Report 3002005509, “Materials Reliability Program: Inspection Data Survey Report (MRP-219, Revision 11),” Palo Alto, CA, 2015.

[34] J. Connolly, Site Vice President, STP Nuclear Operating Company, letter to U.S. NRC Document Control Desk, “South Texas Project, Units 1 & 2, Docket Nos. STN 50-498, STN 50-499, First Set of Responses to April 11, 2016 Requests for Additional Information, Regarding STP Risk-Informed GSI-191 Licensing Application, (TAC NOs MF2400 and MF2401),” May 11, 2016, ADAMS Accession No. ML16154A117.

[35] K. M. Wallis, Manager, Systems Engineering, STP Nuclear Operating Company, letter to U.S. NRC Document Control Desk, “South Texas Project, Unit 1, Docket No. STN 50-498, Inservice Inspection Summary Report – 1RE20,” July 20, 2017, ADAMS Accession No. ML17205A575.

[36] A. Blamey, Chief, Reactor Projects Branch 6, Division of Reactor Projects, U.S. NRC Region II, letter to J. W. Shea, Vice President, Nuclear Licensing, Tennessee Valley Authority, “Watts Bar Nuclear Plant – NRC Integrated Inspection Report 05000390, 05000391/2015004 and 07201048/2015002,” February 12, 2016, ADAMS Accession No. ML16043A214.

[37] P. Simmons, Site Vice President, Watts Bar Nuclear Plant, Tennessee Valley Authority, letter to U.S. NRC Document Control Desk, “American Society of Mechanical Engineers, Section XI, Second and Third 10-Year Inspection Interval, Inservice Inspection Owner’s Activity Report for Cycle 14 Operation,” July 31, 2017, ADAMS Accession No. ML17212A550.

[38] Tennessee Valley Authority, WBN-2 PSI, “Watts Bar Nuclear Plant Unit 2 Preservice Inspection Program Plan,” Rev. 11, June 30, 2016, ADAMS Accession No. ML16293A336.

[39] PNNL, PNNL-28090, “Analysis of Empirical Probability of Detection Data for Dissimilar Metal Welds,” July 2019, ADAMS Accession No. ML19204A260.

[40] Westinghouse Electric Co., WCAP-14572, Rev. 1-NP-A, “Westinghouse Owners Group Application of Risk-Informed Methods to Piping Inservice Inspection Topical Report,” February 1999, ADAMS Accession No. ML20207J335.

[41] Westinghouse Electric Co., WCAP-16168-NP-A, “Risk-Informed Extension of the Reactor Vessel In-Service Inspection Interval,” Rev. 3, October 2011, ADAMS Accession No. ML11306A084.

[42] EPRI, Report 3002007383, “Materials Reliability Program: Technical Basis for ASME Section XI Code Case N-838—Flaw Tolerance Evaluation of Cast Austenitic Stainless Steel (CASS) Piping Components (MRP-362 Rev. 1),” Palo Alto, CA, 2016.

# APPENDIX A
# SUMMARY OF RESULTS

The following table summarizes the results of the probabilistic LBB evaluation of representative Westinghouse four-loop PWR primary coolant loop piping welds using the xLPR code. The numerical results are presented as mean estimates for each case with the standard error to provide an indication of the level of uncertainty in the estimates. The results for the probability of rupture with a 1 gpm leak rate detection capability were zero for all cases and are thus not reported in the table.

| Case No. | xLPR Beta Version | Sample Size and Other Key Parameters | Mean Occurrence of Leak Rate Jump at 80 EFPY | Mean LBB Time Lapse | | Mean LBB Ratio [1] | | Probability of 1st Crack at 80 EFPY | Probability of 1st Leak at 80 EFPY | Probability of Rupture at 80 EFPY [2] |
|---|---|---|---|---|---|---|---|---|---|---|
| | | | | 1 gpm Leak Rate Detection Capability (Months) | 10 gpm Leak Rate Detection Capability (Months) | 1 gpm Leak Rate Detection Capability | 10 gpm Leak Rate Detection Capability | | | |
| 1.1.0 | xLPR-2.0a_003 | 105,000 [3] | 0 | 50 ± 2.2 | 35.4 ± 1.7 | 10.1 ± 0.03 | 4.62 ± 0.03 | 3.25E-03 ± 1.8E-04 | 1.37E-03 ± 1.2E-04 | 1.25E-03 ± 1.1E-04 |
| | xLPR-2.0a_002 | 100,000 [4] | 0 | 48.5 ± 1.7 | 33.7 ± 1.1 | 9.37 ± 0.09 | 4.59 ± 0.02 | 3.40E-03 ± 1.8E-04 | 1.34E-03 ± 1.2E-04 | 1.14E-03 ± 1.1E-04 |
| 1.1.1 | xLPR-2.0a_003 | 5,000 [5] | 0 | 56.3 ± 0.4 | 39.7 ± 0.3 | 9.88 ± 0.01 | 4.63 ± 0.04 | 1.00E+00 | 8.12E-01 ± 5.5E-03 | 7.68E-01 ± 6E-03 |
| 1.1.2 | xLPR-2.0a_003 | 105,000 [3] | 9.43E-05 | 34.8 ± 2.7 | 30.7 ± 2.5 | 6.33 ± 0.25 | 4.1 ± 0.08 | 6.55E-02 ± 7.6E-04 | 1.32E-03 ± 1.12E-04 | 1.23E-03 ± 1.1E-04 |
| 1.1.3 | Not analyzed due to inherent limitations of Direct Model 2 | | | | | | | | | |
| 1.1.4 | xLPR-2.0a_003 | 105,000 [3] | 0 | 53.8 ± 1.5 | 37.8 ± 1.2 | 9.82 ± 0.05 | 4.6 ± 0.015 | 5.50E-03 ± 2.3E-04 | 2.50E-03 ± 1.6E-04 | 2.30E-03 ± 1.5E-04 |
| 1.1.5 | xLPR-2.0a_003 | 5,000 [5] | 0 | 54.2 ± 0.4 | 37.4 ± 0.3 | 9.88 ± 0.01 | 4.65 ± 0.005 | 1.00E+00 | 8.12E-01 ± 5.5E-03 | 7.68E-01 ± 6.0E-03 |

| Case No. | xLPR Beta Version | Sample Size and Other Key Parameters | Mean Occurrence of Leak Rate Jump at 80 EFPY | Mean LBB Time Lapse | | Mean LBB Ratio [1] | | Probability of 1st Crack at 80 EFPY | Probability of 1st Leak at 80 EFPY | Probability of Rupture at 80 EFPY [2] |
|---|---|---|---|---|---|---|---|---|---|---|
| | | | | 1 gpm Leak Rate Detection Capability (Months) | 10 gpm Leak Rate Detection Capability (Months) | 1 gpm Leak Rate Detection Capability | 10 gpm Leak Rate Detection Capability | | | |
| 1.1.6 | xLPR-2.0b_001 | 70,000 [6] | 0 | 46.4 ± 2.2 | 33.1 ± 1.7 | 9.68 ± 0.09 | 4.64 ± 0.06 | 8.07E-03 ± 2.7E-04 | 4.03E-03 ± 1.9E-04 | 1.27E-03 ± 1.1E-04 |
| 1.1.7 | xLPR-2.0d_002 | 105,000 [3] | 1.90E-05 | 46.6 ± 1.0 | 34.0 ± 0.8 | 9.52 ± 0.04 | 4.7 ± 0.017 | 8.63E-03 ± 2.9E-04 | 5.70E-03 ± 2.3E-04 | 5.33E-03 ± 2.3E-04 |
| 1.1.8 | Same as Case 1.1.0 | | | | | | | | | |
| 1.1.9 | xLPR-2.0a_003 | 105,000 [3] | 0 | 41.6 ± 2.3 | 28.9 ± 2 | 10.29 ± 0.15 | 4.81 ± 0.13 | 1.46E-03 ± 1.2E-04 | 3.05E-04 ± 5.4E-05 | 3.05E-04 ± 5.4E-05 |
| 1.1.10 | xLPR-2.0d_002 | 5,000 [5] 10-year ISI Frequency | 0 | 56.3 ± 0.4 | 39.7 ± 0.3 | 9.88 ± 0.01 | 4.63 ± 0.04 | 1.00E+00 | 1.39E-02 ± 1.7E-03 | 6.86E-03 ± 1.2E-03 |
| | | 5,000 [5] 5-year ISI Frequency | 0 | 56.3 ± 0.4 | 39.7 ± 0.3 | 9.88 ± 0.01 | 4.63 ± 0.04 | 1.00E+00 | 9.03E-04 ± 4.2E-04 | 3.30E-04 ± 2.6E-04 |
| 1.1.11 | xLPR-2.0d_002 | 5,000 [5] 10-year ISI Frequency | 0 | 56.3 ± 0.4 | 39.7 ± 0.3 | 9.88 ± 0.01 | 4.63 ± 0.04 | 1.00E+00 | 1.12E-02 ± 1.5E-03 | 5.29E-03 ± 1.0E-03 |
| | | 5,000 [5] 5-year ISI Frequency | 0 | 56.3 ± 0.4 | 39.7 ± 0.3 | 9.88 ± 0.01 | 4.63 ± 0.04 | 1.00E+00 | 6.06E-04 ± 3.5E-04 | 2.01E-04 ± 2.0E-04 |
| 1.1.12 | Abandoned | | | | | | | | | |
| 1.1.13 | Abandoned | | | | | | | | | |

| Case No. | xLPR Beta Version | Sample Size and Other Key Parameters | Mean Occurrence of Leak Rate Jump at 80 EFPY | Mean LBB Time Lapse | | Mean LBB Ratio [1] | | Probability of 1st Crack at 80 EFPY | Probability of 1st Leak at 80 EFPY | Probability of Rupture at 80 EFPY [2] |
|---|---|---|---|---|---|---|---|---|---|---|
| | | | | 1 gpm Leak Rate Detection Capability (Months) | 10 gpm Leak Rate Detection Capability (Months) | 1 gpm Leak Rate Detection Capability | 10 gpm Leak Rate Detection Capability | | | |
| 1.1.14 | xLPR-2.0a_003 | 5,000 [5] | 0 | 39 ± 0.25 | 26.8 ± 0.2 | 9.85 ± 0.01 | 4.63 ± 0.003 | 1.00E+00 | 9.65E-01 ± 2.6E-03 | 9.56E-01 ± 2.9E-03 |
| 1.1.15 | xLPR-2.0d_002 | 70,000 [6] | 0 | 14 ± 0.8 | 10.3 ± 0.7 | 9.73 ± 0.09 | 4.53 ± 0.03 | 7.80E-03 ± 2.7E-04 | 3.86E-03 ± 1.9E-04 | 1.23E-03 ± 1.1E-04 |
| 1.1.16 | xLPR-2.0d_001 | 105,000 [3] | 0 | Not Applicable | Not Applicable | Not Applicable | Not Applicable | 0.00E+00 | 0.00E+00 | 0.00E+00 |
| 1.1.17 | xLPR-2.0d_001 | 5,000 [5] | 0 | Not Applicable | Not Applicable | Not Applicable | Not Applicable | 1.00E+00 | 0.00E+00 | 0.00E+00 |
| 1.1.18 | Abandoned | | | | | | | | | |
| 1.1.19 | xLPR-2.0d_001 | 5,000 [5] Discrete Inputs | 0 | 57.0 ± 0.4 | 39.9 ± 0.3 | 10.17 ± 0.01 | 4.67 ± 0.004 | 1.00E+00 | 8.56E-01 ± 5.0E-03 | 8.15E-01 ± 5.5E-03 |
| | | 5,000 [5] Continuous Inputs | 0 | 58.4 ± 0.4 | 40.1 ± 0.3 | 10.76 ± 0.009 | 4.84 ± 0.004 | 1.00E+00 | 9.40E-01 ± 3.3E-03 | 9.12E-01 ± 4.0E-03 |
| 1.1.20 | xLPR-2.0d_002 | 105,000 [3] | 0 | 34 ± 1 | 23.6 ± 0.8 | 9.37 ± 0.04 | 4.42 ± 0.01 | 4.79E-03 ± 2.1E-04 | 3.16E-03 ± 1.7E-04 | 3.02E-03 ± 1.7E-04 |
| 1.1.21 | xLPR-2.0d_002 | 5,000 [5] | 0 | 58.1 ± 0.4 | 42.3 ± 0.3 | 9.45 ± 0.01 | 4.64 ± 0.004 | 1.00E+00 | 9.07E-01 ± 4.1E-03 | 8.80E-01 ± 4.6E-03 |

| Case No. | xLPR Beta Version | Sample Size and Other Key Parameters | Mean Occurrence of Leak Rate Jump at 80 EFPY | Mean LBB Time Lapse | | Mean LBB Ratio [1] | | Probability of 1st Crack at 80 EFPY | Probability of 1st Leak at 80 EFPY | Probability of Rupture at 80 EFPY [2] |
|---|---|---|---|---|---|---|---|---|---|---|
| | | | | 1 gpm Leak Rate Detection Capability (Months) | 10 gpm Leak Rate Detection Capability (Months) | 1 gpm Leak Rate Detection Capability | 10 gpm Leak Rate Detection Capability | | | |
| 1.1.22 | xLPR-2.0a_003 | 5,000 [5] 0.5-month Time Step | 0 | 55.53 ± 0.41 | 38.03 ± 0.28 | 9.90 ± 0.01 | 4.69 ± 0.00 | 1.00E+00 | 8.13E-01 ± 5.50E-03 | 7.70E-01 ± 5.90E-03 |
| | | 5,000 [5] 1-month Time Step | 0 | 56.18 ± 0.41 | 38.54 ± 0.29 | 10.00 ± 0.01 | 4.74 ± 0.01 | 1.00E+00 | 8.12E-01 ± 5.50E-03 | 7.68E-01 ± 5.90E-03 |
| | | 5,000 [5] 2-month Time Step | 0 | 57.52 ± 0.40 | 39.54 ± 0.28 | 10.19 ± 0.02 | 4.86 ± 0.01 | 1.00E+00 | 8.11E-01 ± 5.50E-03 | 7.67E-01 ± 5.90E-03 |
| | | 5,000 [5] 6-month Time Step | 0 | 59.04 ± 0.40 | 40.57 ± 0.29 | 9.51 ± 0.02 | 4.67 ± 0.01 | 1.00E+00 | 8.11E-01 ± 5.50E-03 | 7.65E-01 ± 6.00E-03 |
| | | 5,000 [5] 12-month Time Step | 0 | 59.01 ± 0.41 | 40.58 ± 0.30 | 8.26 ± 0.03 | 4.19 ± 0.01 | 1.00E+00 | 8.11E-01 ± 5.50E-03 | 7.65E-01 ± 6.00E-03 |
| 1.1.23 | xLPR-2.0d_002 | 20,000 [7] | 0 | Not Applicable | Not Applicable | Not Applicable | Not Applicable | 1.00E+00 | 8.04E-01 ± 5.60E-03 | 7.67E-01 ± 6.00E-03 |
| 1.2.0 | xLPR-2.0a_003 | 105,000 [3] | 0 | Not Applicable | Not Applicable | Not Applicable | Not Applicable | 0.00E+00 | 0.00E+00 | 0.00E+00 |
| 1.2.1 | xLPR-2.0a_003 | 105,000 [3] | 0 | Not Applicable | Not Applicable | Not Applicable | Not Applicable | 0.00E+00 | 0.00E+00 | 0.00E+00 |

Notes:

[1] Excludes values greater than 12 as they strongly influence the mean, except in Case 1.1.22.
[2] Excludes the effects of leak rate detection.
[3] Composite of 7 simulations each with 15,000 epistemic (outer) loop by 1 aleatory (inner) loop samples with all uncertain inputs placed on the epistemic (outer) loop.
[4] Composite of 4 simulations each with 250 epistemic (outer) loop by 100 aleatory (inner) loop samples with all uncertain inputs placed on the aleatory (inner) loop.
[5] 5000 epistemic (outer) loop by 1 aleatory (inner) loop samples with all uncertain inputs placed on the epistemic (outer) loop
[6] Composite of 7 simulations each with 10,000 epistemic (outer) loop by 1 aleatory (inner) loop samples with all uncertain inputs placed on the epistemic (outer) loop.
[7] 200 epistemic (outer) loop by 100 aleatory (inner) loop samples with input uncertainty assignments defined as reported in Section B19.

# APPENDIX B
# ANALYSIS INPUTS

## B1 Case 1.1.0

The objective of Case 1.1.0 was to assess the base likelihood of RVON weld failure caused by PWSCC initiation and growth with no ISI, mitigation, or seismic effects.

The random seeds used for the Case 1.1.0 analyses were as follows:

| Simulation Description | Replicate Simulation No. | Epistemic Random Seed | Aleatory Random Seed |
|---|---|---|---|
| 105,000-realization composite simulation using the epistemic (outer) loop | 1 | 1515 | 13118 |
| | 2 | 1974 | 713705 |
| | 3 | 2002 | 1503 |
| | 4 | 2004 | 909 |
| | 5 | 2010 | 907 |
| | 6 | 3131 | 131521 |
| | 7 | 4512 | 1685 |
| 100,000-realization composite simulation using the aleatory (inner) loop | 1 | 1974 | 713705 |
| | 2 | 2002 | 1503 |
| | 3 | 2004 | 909 |
| | 4 | 2010 | 907 |

The other inputs were developed using the Case 1, Scenario 2 input set from [25] as a template with the following modifications:

| Global ID | Name | Value / Distribution Parameters | Units | Basis |
|---|---|---|---|---|
| 0001 | Plant Operation Time | 960 | months (mon) | Equivalent to 80 EFPY, which accounts for a subsequent license renewal term |
| 0402 | Period End Time (Op Period #1) | 961 | mon | Setting for including one operating period |

| Global ID | Name | Value / Distribution Parameters | Units | Basis |
|---|---|---|---|---|
| 0403 | Input Type Choice (Op Period #1) | 2 | - | Input by stresses recommended to avoid known error in operating load calculations as described in xLPR-UM, Version 1.2, Section H.1 |
| 0405 | Period End Time (Op Period #2) | 962 | mon | Setting for including one operating period |
| 1001 | Effective Full Power Years (EFPY) | 80<br>Constant | yr | Set equal to the plant operation time. EFPY is a primary contributor to crack initiation and growth, but its impact can be considered outside of the analysis. Furthermore, it is difficult to project a different input value that would cover a subsequent license renewal term. |
| 1002<br><br>1104 | Pipe Wall Thickness<br><br>Weld Material Thickness | 0.0663<br>Constant | m | Since a specific weld is considered, the wall thickness was assumed to be constant. While the thickness may be larger in some places, it is expected that the reported thickness is a minimum through the weld. The effect of variation in wall thickness was investigated in a sensitivity study. |

| Global ID | Name | Value / Distribution Parameters | Units | Basis |
|---|---|---|---|---|
| 3102 | Operating Temperature | 320.5<br>Constant | °C | Temperature, like pressure, is a value that is quite stable in a nuclear power plant. Furthermore, only one temperature is sampled as representative for the entire power plant life. Uncertainty thus refers to the variation on the mean temperature over the specified number of plant operating years, or the duration of the applicable plant operating period. Additionally, there are many variables, such as the thermal loads, that should be correlated to the temperature but are not. For these reasons and considering that the overall estimate may be optimistic due to the asymmetrical distribution proposed for Case 1, Scenario 2, a constant temperature is considered more appropriate. The effect of variation in temperature was investigated in a sensitivity study. |
| 4001 | Earthquake Probability | 0<br>Constant | yr-1 | Case excludes seismic effects |
| 4002 | Earthquake Δ Total Membrane | 0<br>Constant | MPa | Case excludes seismic effects |
| 4003 | Earthquake Δ Inertial Bending | 0<br>Constant | MPa | Case excludes seismic effects |
| 4004 | Earthquake Δ Anchor Bending | 0<br>Constant | MPa | Case excludes seismic effects |
| 4005 | Sigma_SSa | 0<br>Constant | MPa | More realistic than the initially assumed +200 MPa that favored crack initiation |
| 4006 | Sigma_SSh | 0<br>Constant | MPa | More realistic than the initially assumed +200 MPa that favored crack initiation |
| 4121 | Membrane Stress (DW) | -0.0266<br>Constant | MPa | Derived from applicable geometry and load information in Appendix D of [25] |

| Global ID | Name | Value / Distribution Parameters | Units | Basis |
|---|---|---|---|---|
| 4122 | Maximum Bending Stress (DW) | 3.484978 Constant | MPa | Derived from applicable geometry and load information in Appendix D of [25] |
| 4123 | Membrane Stress (Thermal) | -2.39429 Constant | MPa | Derived from applicable geometry and load information in Appendix D of [25] |
| 4124 | Bending Stress (Thermal) | 143.7275 Constant | MPa | Derived from applicable geometry and load information in Appendix D of [25] |

For the supplemental deterministic LBB analysis, the inputs were as follows:

| SQUIRT4 Input Parameter | Input Value |
|---|---|
| Pipe Outside Diameter (m) | 0.869 |
| Pipe Thickness (m) | 0.0663 |
| Total Crack Length Initial Guess (m) | 0.125 |
| Bending Moment (MN-m) | 4.5935 |
| Yield Stress (MPa) | 190.1 |
| Ultimate Stress (MPa) | 435.5 |
| Collapse Stress (MPa) | 312.8 |
| Reference Stress (MPa) | 190.1 |
| Reference Strain | 0.00108 |
| Alpha | 1.858 |
| Exponent (n) | 4.0 |
| Pressure (MPa) | 15.41 |
| Temperature (°C) | 320.5 |
| Required Flow Rate (L/min) | 37.854 |
| Global Roughness (μm) | 113.9 |
| Local Roughness (μm) | 16.86 |
| Number of Turns ($m^{-1}$) | 5940 |
| Global Path Deviation | 1.009 |
| Local Path Deviation | 1.243 |

## B2 Case 1.1.1

The objective of Case 1.1.1 was to assess the sensitivity of the likelihood of RVON weld failure due to whether the crack initiation process is modeled in the analysis.

The random seeds used for the Case 1.1.1 analysis were as follows:

| Simulation Description | Epistemic Random Seed | Aleatory Random Seed |
|---|---|---|
| 5,000-realization simulation using the epistemic (outer) loop | 6128 | 369 |

The other inputs were developed using the Case 1.1.0 input set as a template with the following modifications:

| Global ID | Name | Value / Distribution Parameters | Units | Basis |
|---|---|---|---|---|
| 0501 | Crack Initiation Type Choice | 0 | - | Setting for using the initial flaw density option |
| 1209 | Number of flaws (Circumferential) | 1<br>Constant | - | Case 1.1.0 analysis showed that occurrences of 2 cracks are extremely rare and the time between 2 cracks is long enough such that only one crack is dominant |
| 1210 | Initial Flaw Full-Length (Circumferential) | Lognormal<br>(1, 4.3E-3, 2.226) | mm | Same as PWSCC initial flaw full length |
| 1211 | Multiplier Starting Full-Length (Circumferential) | 1<br>Constant | - | Same as PWSCC length multiplier |
| 1212 | Initial Flaw Depth (Circumferential) | Lognormal<br>(1, 1.5E-3, 1.419, min=5E-4, max=7.4588E-2) | mm | Same as PWSCC initial flaw depth |
| 1213 | Multiplier Starting Depth (Circumferential) | 1<br>Constant | - | Same as PWSCC depth multiplier |

| Global ID | Name | Value / Distribution Parameters | Units | Basis |
|---|---|---|---|---|
| 1214 | Number of Flaws (Axial) | 0<br>Constant | - | No axial flaws considered in this analysis |
| 0904 | Max time between 2 check – single TWC – CC | 1 | mon | Stability module called in each timestep |

## B3 Case 1.1.2

The objective of Case 1.1.2 was to assess the sensitivity of the likelihood of RVON weld failure due to severe, yet plausible, WRS.

The random seeds for Case 1.1.2 were as follows:

| Simulation Description | Replicate Simulation No. | Epistemic Random Seed | Aleatory Random Seed |
|---|---|---|---|
| 105,000-realization composite simulation using the epistemic (outer) loop | 1 | 1515 | 13118 |
| | 2 | 1974 | 713705 |
| | 3 | 2002 | 1503 |
| | 4 | 2004 | 909 |
| | 5 | 2010 | 907 |
| | 6 | 3131 | 131521 |
| | 7 | 4512 | 1685 |

The other inputs were developed using the Case 1.1.0 input set as a template with the following modifications:

| Global ID | Name | Value / Distribution Parameters | | | Units | Basis |
|---|---|---|---|---|---|---|
| - | Axial WRS pre-mitigation profile | x/t | Mean | Std. Dev. | MPa | WRS profile for nozzle like RVON and is more tensile at the inside diameter to favor crack invitation. Same standard deviation as Case 1.1.0 assumed. |
| | | 0.00 | 61.324 | 60.0 | | |
| | | 0.04 | 21.15606387 | 60.0 | | |
| | | 0.08 | -92.65432617 | 60.0 | | |
| | | 0.12 | -153.6916682 | 60.0 | | |
| | | 0.16 | -240.6042512 | 60.0 | | |
| | | 0.20 | -276.7679237 | 60.0 | | |
| | | 0.24 | -282.372931 | 60.0 | | |
| | | 0.28 | -268.8100703 | 60.0 | | |
| | | 0.32 | -248.4532662 | 60.0 | | |
| | | 0.36 | -230.4351732 | 60.0 | | |
| | | 0.40 | -204.1074 | 60.0 | | |
| | | 0.44 | -174.1062257 | 60.0 | | |
| | | 0.48 | -135.6432532 | 60.0 | | |
| | | 0.52 | -82.555698 | 60.0 | | |

| Global ID | Name | Value / Distribution Parameters | | | Units | Basis |
|---|---|---|---|---|---|---|
| | | 0.56 | -44.24388323 | 60.0 | | |
| | | 0.60 | 0.225838 | 60.0 | | |
| | | 0.64 | 50.40360806 | 60.0 | | |
| | | 0.68 | 103.1464999 | 60.0 | | |
| | | 0.72 | 183.7228583 | 60.0 | | |
| | | 0.76 | 264.2446359 | 60.0 | | |
| | | 0.80 | 306.4958349 | 60.0 | | |
| | | 0.84 | 328.2446337 | 60.0 | | |
| | | 0.88 | 322.202673 | 60.0 | | |
| | | 0.92 | 288.0755706 | 60.0 | | |
| | | 0.96 | 241.3405301 | 60.0 | | |
| | | 1.00 | 215.3525 | 60.0 | | |

## B4 Case 1.1.4

The objective of Case 1.1.4 was to assess crack initiation model uncertainty using the Weibull model for the RVON weld.

The random seeds for Case 1.1.4 were as follows:

| Simulation Description | Replicate Simulation No. | Epistemic Random Seed | Aleatory Random Seed |
|---|---|---|---|
| 105,000-realization composite simulation using the epistemic (outer) loop | 1 | 1515 | 13118 |
| | 2 | 1974 | 713705 |
| | 3 | 2002 | 1503 |
| | 4 | 2004 | 909 |
| | 5 | 2010 | 907 |
| | 6 | 3131 | 131521 |
| | 7 | 4512 | 1685 |

The other inputs were developed using the Case 1.1.0 input set as a template with the following modifications:

| Global ID | Name | Value / Distribution Parameters | Units | Basis |
|---|---|---|---|---|
| 0502 | SCC Initiation Method | 3 | - | Setting for using the Weibull model for PWSCC initiation |

## B5 Case 1.1.5

The objective of Case 1.1.5 was to assess the sensitivity of the likelihood of RVON weld failure due to SSE.

The random seeds used for the Case 1.1.5 analysis were as follows:

| Simulation Description | Epistemic Random Seed | Aleatory Random Seed |
|---|---|---|
| 5,000-realization simulation using the epistemic (outer) loop | 6128 | 369 |

The other inputs were developed using the Case 1.1.1 input set as a template with the following modifications:

| Global ID | Name | Value / Distribution Parameters | Units | Basis |
|---|---|---|---|---|
| 4001 | Earthquake probability | 1.02E-6 Constant | $yr^{-1}$ | Rock site seismic hazard curve value selected as close to the 1 x $10^{-6}$ annual frequency considered |
| 4002 | Earthquake Δ total membrane | 11.43 Constant | MPa | Corresponding earthquake membrane stress for 1.02E-6 annual frequency using the rock site seismic hazard curve |
| 4003 | Earthquake Δ inertial bending | 0 Constant | MPa | All bending stresses captured in Global ID 4004 |
| 4004 | Earthquake Δ anchor bending | 37.66 Constant | MPa | Corresponding earthquake bending stress for 1.02E-6 annual frequency using the rock site seismic hazard curve |

## B6 Case 1.1.6

The objective of Case 1.1.6 was to assess the sensitivity of the likelihood of RVON weld failure due to the inclusion of axial cracks.

The random seeds used for the Case 1.1.6 analysis were as follows:

| Simulation Description | Replicate Simulation No. | Epistemic Random Seed | Aleatory Random Seed |
|---|---|---|---|
| 70,000-realization composite simulation using the epistemic (outer) loop | 1 | 1515 | 13118 |
| | 2 | 1974 | 713705 |
| | 3 | 2002 | 1503 |
| | 4 | 2004 | 909 |
| | 5 | 2010 | 907 |
| | 6 | 3131 | 131521 |
| | 7 | 4512 | 1685 |

The other inputs were developed using the Case 1.1.0 input set as a template with the following modifications:

| Global ID | Name | Value / Distribution Parameters | Units | Basis |
|---|---|---|---|---|
| 0003 | Crack Orientation | 3 | - | Setting to include both circumferential and axial cracks |
| 0904 | Max time between 2 check – single TWC – CC | 1 | mon | Stability module called in each timestep |

## B7 Case 1.1.7

The objective of Case 1.1.7 was to assess the sensitivity of the likelihood of RVON weld failure due to the normal operating loads.

The random seeds used for the Case 1.1.7 analysis were as follows:

| Simulation Description | Replicate Simulation No. | Epistemic Random Seed | Aleatory Random Seed |
|---|---|---|---|
| 105,000-realization composite simulation using the epistemic (outer) loop | 1 | 1515 | 13118 |
| | 2 | 1974 | 713705 |
| | 3 | 2002 | 1503 |
| | 4 | 2004 | 909 |
| | 5 | 2010 | 907 |
| | 6 | 3131 | 131521 |
| | 7 | 4512 | 1685 |

The other inputs were developed using the Case 1.1.0 input set as a template with the following modifications:

| Global ID | Name | Value / Distribution Parameters | Units | Basis |
|---|---|---|---|---|
| 3101 | Operating pressure | 16<br>Constant | MPa | Bounds operating pressure dataset from licensee LBB analyses (maximum reported was 15.94 MPa) |
| 4121 | Membrane Stress (Deadweight) | 0 | MPa | All membrane stresses captured in Global ID 4123 |
| 4122 | Maximum Bending Stress (Deadweight) | 0 | MPa | All bending stresses captured in Global ID 4124 |
| 4123 | Membrane Stress (Thermal) | 3.36<br>Constant | MPa | 99$^{th}$ percentile of normal distribution fit to membrane stress dataset from licensee LBB analyses |
| 4124 | Maximum Bending Stress (Thermal) | 178<br>Constant | MPa | 99$^{th}$ percentile of lognormal distribution fit to bending stress dataset from licensee LBB analyses |

## B8 Case 1.1.9

The objective of Case 1.1.9 was to assess the impacts of MSIP on the likelihood of RVON weld failure.

The random seeds used for the Case 1.1.9 analysis were as follows:

| Simulation Description | Replicate Simulation No. | Epistemic Random Seed | Aleatory Random Seed |
|---|---|---|---|
| 105,000-realization composite simulation using the epistemic (outer) loop | 1 | 1515 | 13118 |
| | 2 | 1974 | 713705 |
| | 3 | 2002 | 1503 |
| | 4 | 2004 | 909 |
| | 5 | 2010 | 907 |
| | 6 | 3131 | 131521 |
| | 7 | 4512 | 1685 |

The other inputs were developed using the Case 1.1.0 input set as a template with the following modifications:

| Global ID | Name | Value / Distribution Parameters | Units | Basis |
|---|---|---|---|---|
| 0301 | Mitigation type choice | 1 | - | Setting for stressed-based mitigation only |
| 0305 | Stress mitigation choice | 1 | - | Setting for MSIP |
| 0306 | Stress mitigation time | 360 | mon | Equivalent to 30 years. Represents a slightly more conservative value than 27 years, which is the average based on analysis of MSIP applications using data from [33], [34], [35], [36], [37] and [38]. |
| 4353 | Axial WRS post-mitigation | Epistemic | - | Changed from constant |

| Global ID | Name | Value / Distribution Parameters | | | Units | Basis |
|---|---|---|---|---|---|---|
| - | Axial WRS post-mitigation profile | x/t | Mean | Std. Dev. | | WRS profile developed by xLPR WRS Subgroup for no-repair RVON weld with MSIP |
| | | 0.00 | -145.2293754 | 16.7 | MPa | |
| | | 0.04 | -174.4401505 | 16.7 | | |
| | | 0.08 | -194.8515862 | 16.7 | | |
| | | 0.12 | -216.7729578 | 16.7 | | |
| | | 0.16 | -222.0618726 | 16.7 | | |
| | | 0.20 | -243.7892897 | 16.7 | | |
| | | 0.24 | -254.8852946 | 16.7 | | |
| | | 0.28 | -130.411114 | 16.7 | | |
| | | 0.32 | -131.4488607 | 16.7 | | |
| | | 0.36 | -111.431656 | 16.7 | | |
| | | 0.40 | -90.63420647 | 16.7 | | |
| | | 0.44 | -78.51849419 | 16.7 | | |
| | | 0.48 | -52.83379429 | 16.7 | | |
| | | 0.52 | -34.98648635 | 16.7 | | |
| | | 0.56 | -9.146420803 | 16.7 | | |
| | | 0.60 | 7.818137834 | 16.7 | | |
| | | 0.64 | 79.99167447 | 16.7 | | |
| | | 0.68 | 113.1400283 | 16.7 | | |
| | | 0.72 | 138.5586572 | 16.7 | | |
| | | 0.76 | 160.0015609 | 16.7 | | |
| | | 0.80 | 178.8807843 | 16.7 | | |
| | | 0.84 | 195.9600291 | 16.7 | | |
| | | 0.88 | 211.6557783 | 16.7 | | |
| | | 0.92 | 226.2745379 | 16.7 | | |
| | | 0.96 | 239.9958374 | 16.7 | | |
| | | 1.00 | 252.9822128 | 16.7 | | |

## B9 Case 1.1.10

The objective of Case 1.1.10 was to assess the impacts of ISI on the likelihood of RVON weld failure.

The random seeds used for the Case 1.1.10 analyses were as follows:

| Simulation Description | Epistemic Random Seed | Aleatory Random Seed |
|---|---|---|
| 5,000-realization simulation using the epistemic (outer) loop | 6128 | 369 |

The other inputs were developed using the Case 1.1.1 input set as a template with the following modifications:

| Global ID | Name | Value / Distribution Parameters | Units | Basis |
|---|---|---|---|---|
| 0811 | Inspection schedule input type | 1 | - | Scheduled inspections based on frequency rather than by table |
| 0812 | Pre-mitigation inspection frequency | 0.1<br>and<br>0.2 | yr-1 | First analysis considered inspections every 10 years; second analysis considered inspections every 5 years. These inspection frequencies bound the American Society of Mechanical Engineers Code Case N-770-1 required volumetric examination frequencies for unmitigated butt weld components operating at hot leg temperatures less than or equal to 329 °C. |
| 0820 | Number of cracks detected | 1 | - | All cracks detected independently |

## B10 Case 1.1.11

The objective of Case 1.1.11 was to assess the impacts of ISI model parameter uncertainty for the RVON weld.

The random seeds used for the Case 1.1.11 analyses were as follows:

| Simulation Description | Epistemic Random Seed | Aleatory Random Seed |
|---|---|---|
| 5,000-realization simulation using the epistemic (outer) loop | 6128 | 369 |

The other inputs were developed using the Case 1.1.1 input set as a template with the following modifications:

| Global ID | Name | Value / Distribution Parameters | Units | Basis |
|---|---|---|---|---|
| 0811 | Inspection schedule input type | 1 | - | Scheduled inspections based on frequency rather than by table |
| 0812 | Pre-mitigation inspection frequency | 0.1<br>and<br>0.2 | yr-1 | First analysis considered inspections every 10 years; second analysis considered inspections every 5 years. These inspection frequencies bound the American Society of Mechanical Engineers Code Case N-770-1 required volumetric examination frequencies for unmitigated butt weld components operating at hot leg temperatures less than or equal to 329 °C. |
| 0820 | Number of cracks detected | 1 | - | All cracks detected independently |
| 5101 | Log reg intercept param beta_0 (circumferential) | Normal<br>(-3.31, 0.29) | - | Based on the recommendations in [39] |
| 5102 | Log reg slope param, beta_1 (circumferential) | Normal<br>(56, 13, min = 0, max = 5) | m-1 | Based on the recommendations in [39] |

| Global ID | Name | Value / Distribution Parameters | Units | Basis |
|---|---|---|---|---|
| Correlation 5101-5102 | Correlation between beta_0 and beta_1 | -0.33 | - | Based on the recommendations in [39] |

## B11 Case 1.1.14

The objective of Case 1.1.14 was to assess the impacts of hydrogen on the likelihood of RVON weld failure.

The random seeds used for the Case 1.1.14 analysis were as follows:

| Simulation Description | Epistemic Random Seed | Aleatory Random Seed |
|---|---|---|
| 5,000-realization simulation using the epistemic (outer) loop | 6128 | 369 |

The other inputs were developed using the Case 1.1.1 input set as a template with the following modifications:

| Global ID | Name | Value / Distribution Parameters | Units | Basis |
|---|---|---|---|---|
| 3002 | Unmitigated H2 level | 25 | cc/kg | Lower bound of the operating experience of PWRs as reported in [29] |

## B12 Case 1.1.15

The objective of Case 1.1.15 was to assess the impacts of the combined effects of PWSCC and fatigue for the RVON weld.

The random seeds used for the Case 1.1.15 analysis were as follows:

| Simulation Description | Replicate Simulation No. | Epistemic Random Seed | Aleatory Random Seed |
|---|---|---|---|
| 70,000-realization composite simulation using the epistemic (outer) loop | 1 | 1515 | 13118 |
| | 2 | 1974 | 713705 |
| | 3 | 2002 | 1503 |
| | 4 | 2004 | 909 |
| | 5 | 2010 | 907 |
| | 6 | 3131 | 131521 |
| | 7 | 4512 | 1685 |

The other inputs were developed using the Case 1, Scenario 10 input set from [25] as a template with the following modifications:

| Global ID | Name | Value / Distribution Parameters | Units | Basis |
|---|---|---|---|---|
| 0001 | Plant Operation Time | 960 | mon | Equivalent to 80 EFPY, which accounts for a subsequent license renewal term |
| 0301 | Mitigation Type Choice | 0 | - | Setting for no mitigation |
| 0402 | Period End Time (Op Period #1) | 961 | mon | Setting for including one operating period |
| 0403 | Input Type Choice (Op Period #1) | 2 | - | Input by stresses recommended to avoid known error in operating load calculations as described in xLPR-UM, Version 1.2, Section H.1 |
| 0405 | Period End Time (Op Period #2) | 962 | mon | Setting for including one operating period |

| Global ID | Name | Value / Distribution Parameters | Units | Basis |
|---|---|---|---|---|
| 0411 – 0411.10 | Transient Type Selection (Loads 1 – 10) | 1 | - | Setting for activating thermal transient with no stratification. All corresponding transients from Case 1, Scenario 10 included. |
| 0411.11 | Transient Type Selection (Load 11) | 3 | - | Setting for activating mechanical transient. All corresponding transients from Case 1, Scenario 10 included. |
| All uncertain variables | Data Source | Epistemic | - | Only the epistemic (outer) loop used in the simulation. |
| 1001 | Effective Full Power Years (EFPY) | 80<br>Constant | yr | Set equal to the plant operation time. Constant value chosen consistent with Case 1.1.0. |
| 1102<br><br><br>1104 | Pipe Wall Thickness<br><br>Weld Material Thickness | Normal<br>(0.0663, 0.008288, min=0.058013, max=0.074588) | m | Consistent with Case 1, Scenario 10. Minimal effect as compared to use of a constant value of 0.0663 m in Case 1.1.0, which is the associated base case for the sensitivity study. |
| 1205 | PWSCC Initial Flaw Full-Length | 0.999<br>Constant | mm | See Note 1 |
| 1207 | PWSCC Initial Flaw Depth | 0.999<br>Constant | mm | |
| 3102 | Operating Temperature | Normal<br>(320.5, 5.705, min=306.1, max=326.7) | °C | Consistent with Case 1, Scenario 10. Minimal effect as compared to use of a constant value of 320.5 °C in Case 1.1.0, which is the associated base case for the sensitivity study. |
| 4001 | Earthquake Probability | 0<br>Constant | yr-1 | Case excludes seismic effects |
| 4002 | Earthquake Δ Total Membrane | 0<br>Constant | MPa | Case excludes seismic effects |
| 4003 | Earthquake Δ Inertial Bending | 0<br>Constant | MPa | Case excludes seismic effects |

| Global ID | Name | Value / Distribution Parameters | Units | Basis |
|---|---|---|---|---|
| 4004 | Earthquake Δ Anchor Bending | 0<br>Constant | MPa | Case excludes seismic effects |
| 4005 | Sigma_SSa | 0<br>Constant | MPa | More realistic than the initially assumed +200 MPa that favored crack initiation |
| 4006 | Sigma_SSh | 0<br>Constant | MPa | More realistic than the initially assumed +200 MPa that favored crack initiation |
| 4121 | Membrane Stress (DW) | -0.0266<br>Constant | MPa | Derived from applicable geometry and load information in Appendix D of [25]. |
| 4122 | Maximum Bending Stress (DW) | 3.484978<br>Constant | MPa | Derived from applicable geometry and load information in Appendix D of [25] |
| 4123 | Membrane Stress (Thermal) | -2.39429<br>Constant | MPa | Derived from applicable geometry and load information in Appendix D of [25] |
| 4124 | Bending Stress (Thermal) | 143.7275<br>Constant | MPa | Derived from applicable geometry and load information in Appendix D of [25] |
| TIFFANY Inputs, Transient 1 | Start Month,<br>End Month,<br>Front-Back Loading,<br>Frequency,<br># of Cycles per Event,<br>Uncertainty Multiplier | 0,<br>960,<br>0.5,<br>3.33,<br>1.0,<br>Lognormal<br>(1, 0.5, 1.4142, min=0.25, max=1.0) | mon,<br>mon,<br>-,<br>1/yr,<br>-,<br>- | End month is equivalent to 80 EFPY, which accounts for a subsequent license renewal term. Remaining inputs are consistent with Case 1, Scenario 10. |
| TIFFANY Inputs, Transient 2 | Start Month,<br>End Month,<br>Front-Back Loading,<br>Frequency,<br># of Cycles per Event,<br>Uncertainty Multiplier | 0,<br>960,<br>0.5,<br>3.33,<br>1.0,<br>Lognormal<br>(1, 0.5, 1.4142, min=0.25, max=1.0) | mon,<br>mon,<br>-,<br>1/yr,<br>-,<br>- | End month is equivalent to 80 EFPY, which accounts for a subsequent license renewal term. Remaining inputs are consistent with Case 1, Scenario 10. |

| Global ID | Name | Value / Distribution Parameters | Units | Basis |
|---|---|---|---|---|
| TIFFANY Inputs, Transient 3 | Start Month,<br>End Month,<br>Front-Back Loading,<br>Frequency,<br># of Cycles per Event, Uncertainty Multiplier | 0,<br>960,<br>0.5,<br>305,<br>1.0,<br>Lognormal<br>(1, 0.5, 1.4142, min=0.25, max=1.0) | mon,<br>mon,<br>-,<br>1/yr,<br>-,<br>- | End month is equivalent to 80 EFPY, which accounts for a subsequent license renewal term. Remaining inputs are consistent with Case 1, Scenario 10. |
| TIFFANY Inputs, Transient 4 | Start Month,<br>End Month,<br>Front-Back Loading,<br>Frequency,<br># of Cycles per Event, Uncertainty Multiplier | 0,<br>960,<br>0.5,<br>305,<br>1.0,<br>Lognormal<br>(1, 0.5, 1.4142, min=0.25, max=1.0) | mon,<br>mon,<br>-,<br>1/yr,<br>-,<br>- | End month is equivalent to 80 EFPY, which accounts for a subsequent license renewal term. Remaining inputs are consistent with Case 1, Scenario 10. |
| TIFFANY Inputs, Transient 5 | Start Month,<br>End Month,<br>Front-Back Loading,<br>Frequency,<br># of Cycles per Event, Uncertainty Multiplier | 0,<br>960,<br>0.5,<br>33.33,<br>1.0,<br>Lognormal<br>(1, 0.5, 1.4142, min=0.25, max=1.0) | mon,<br>mon,<br>-,<br>1/yr,<br>-,<br>- | End month is equivalent to 80 EFPY, which accounts for a subsequent license renewal term. Remaining inputs are consistent with Case 1, Scenario 10. |
| TIFFANY Inputs, Transient 6 | Start Month,<br>End Month,<br>Front-Back Loading,<br>Frequency,<br># of Cycles per Event, Uncertainty Multiplier | 0,<br>960,<br>0.5,<br>33.33,<br>1.0,<br>Lognormal<br>(1, 0.5, 1.4142, min=0.25, max=1.0) | mon,<br>mon,<br>-,<br>1/yr,<br>-,<br>- | End month is equivalent to 80 EFPY, which accounts for a subsequent license renewal term. Remaining inputs are consistent with Case 1, Scenario 10. |

| Global ID | Name | Value / Distribution Parameters | Units | Basis |
|---|---|---|---|---|
| TIFFANY Inputs, Transient 7 | Start Month,<br>End Month,<br>Front-Back Loading,<br>Frequency,<br># of Cycles per Event, Uncertainty Multiplier | 0,<br>960,<br>0.5,<br>3.33,<br>1.0,<br>Lognormal (1, 0.5, 1.4142, min=0.25, max=1.0) | mon,<br>mon,<br>-,<br>1/yr,<br>-,<br>- | End month is equivalent to 80 EFPY, which accounts for a subsequent license renewal term. Remaining inputs are consistent with Case 1, Scenario 10. |
| TIFFANY Inputs, Transient 8 | Start Month,<br>End Month,<br>Front-Back Loading,<br>Frequency,<br># of Cycles per Event, Uncertainty Multiplier | 0,<br>960,<br>0.5,<br>1.33,<br>1.0,<br>Lognormal (1, 0.5, 1.4142, min=0.25, max=1.0) | mon,<br>mon,<br>-,<br>1/yr,<br>-,<br>- | End month is equivalent to 80 EFPY, which accounts for a subsequent license renewal term. Remaining inputs are consistent with Case 1, Scenario 10. |
| TIFFANY Inputs, Transient 9 | Start Month,<br>End Month,<br>Front-Back Loading,<br>Frequency,<br># of Cycles per Event, Uncertainty Multiplier | 0,<br>960,<br>0.5,<br>1.33,<br>1.0,<br>Lognormal (1, 0.5, 1.4142, min=0.25, max=1.0) | mon,<br>mon,<br>-,<br>1/yr,<br>-,<br>- | End month is equivalent to 80 EFPY, which accounts for a subsequent license renewal term. Remaining inputs are consistent with Case 1, Scenario 10. |
| TIFFANY Inputs, Transient 10 | Start Month,<br>End Month,<br>Front-Back Loading,<br>Frequency,<br># of Cycles per Event, Uncertainty Multiplier | 0,<br>960,<br>0.5,<br>6.67,<br>1.0,<br>Lognormal (1, 0.5, 1.4142, min=0.25, max=1.0) | mon,<br>mon,<br>-,<br>1/yr,<br>-,<br>- | End month is equivalent to 80 EFPY, which accounts for a subsequent license renewal term. Remaining inputs are consistent with Case 1, Scenario 10. |

| Global ID | Name | Value / Distribution Parameters | Units | Basis |
|---|---|---|---|---|
| TIFFANY Inputs, Transient 11 | +/- Membrane Stress,<br>+/- Bending Stress,<br>Start Month,<br>End Month,<br>Front-Back Loading,<br>Frequency,<br># of Cycles per Event,<br>Rise Time, Uncertainty Multiplier | 4.52,<br>60.61,<br>0.0,<br>960,<br>0.5,<br>0.1,<br>10,<br>1.0,<br>Lognormal (1, 0.5, 1.4142, min=0.25, max=1.0) | MPa,<br>MPa,<br>mon,<br>mon,<br>-,<br>1/yr,<br>-,<br>s,<br>- | End month is equivalent to 80 EFPY, which accounts for a subsequent license renewal term. Assumed frequency of 0.1 operating basis earthquakes per year is more conservative than the 0.000679/year frequency defined in Case 1, Scenario 10. Remaining inputs are consistent with Case 1, Scenario 10. |

Notes:

[1] After the simulation was run, typos were discovered in the definition of the PWSCC initial flaw sizes where both the initial flaw full-length and depth were set to placeholder values of a constant 0.999 mm instead of the lognormal distributions as defined in Case 1, Scenario 10. The constant values represent the 2.5$^{th}$ and 12.3$^{rd}$ percentiles of the respective lognormal distributions. As a result, the Case 1.1.15 PWSCC initial flaw sizes were smaller than in Case 1.1.0, which is the associated base case for the sensitivity study. However, the objectives of Case 1.1.15 were to (a) assess the impacts of fatigue crack initiation on the generation of new cracks, and (b) assess the impacts of fatigue crack growth on existing cracks. The typos have no effect on fatigue crack initiation. The impact of fatigue crack growth was only observed once the cracks were near to or already through-wall and starting from a smaller crack size only lengthens the time required to grow to such depths. Therefore, the inputs used have no impact on the conclusions drawn from this sensitivity study. The typos are documented here for completeness and for potential correction should the simulation be rerun in the future.

## B13 Case 1.1.16

The objective of Case 1.1.16 was to assess the likelihood of fatigue crack initiation for the RVON weld.

The random seeds used for the Case 1.1.16 analysis were as follows:

| Simulation Description | Replicate Simulation No. | Epistemic Random Seed | Aleatory Random Seed |
|---|---|---|---|
| 105,000-realization composite simulation using the epistemic (outer) loop | 1 | 1515 | 13118 |
| | 2 | 1974 | 713705 |
| | 3 | 2002 | 1503 |
| | 4 | 2004 | 909 |
| | 5 | 2010 | 907 |
| | 6 | 3131 | 131521 |
| | 7 | 4512 | 1685 |

The other inputs were developed using the Case 1.1.15 input set as a template with the following modifications:

| Global ID | Name | Value / Distribution Parameters | Units | Basis |
|---|---|---|---|---|
| 0003 | Crack Orientation | 1 | - | Setting for circumferential cracks only |
| 0501 | Crack Initiation Type Choice | 2 | - | Setting for fatigue crack initiation only |

## B14 Case 1.1.17

The objective of Case 1.1.17 was to assess the sensitivity of the likelihood of RVON weld failure due to fatigue crack growth from a large initial flaw size.

The random seeds used for the Case 1.1.17 analysis were as follows:

| Simulation Description | Epistemic Random Seed | Aleatory Random Seed |
|---|---|---|
| 5,000-realization simulation using the epistemic (outer) loop | 6128 | 369 |

The other inputs were developed using the Case 1.1.15 input set as a template with the following modifications:

| Global ID | Name | Value / Distribution Parameters | Units | Basis |
|---|---|---|---|---|
| 0501 | Crack Initiation Type Choice | 0 | - | Setting for initial flaw density option |
| 1209 | Number of Flaws (Circ) | 1<br>Constant | - | The likelihood of having two or more circumferential cracks is low enough such that it will not impact the results |
| 1210 | Initial Flaw Full-Length (Circ) | 38<br>Constant | mm | 99.9$^{th}$ percentile of lognormal distribution with a mean of 8.61 mm and a standard deviation of 4.849 mm |
| 1211 | Multiplier Starting Full-Length (Circ) | 1<br>Constant | - | Conservative value used in Global ID 1210 |
| 1212 | Initial Flaw Depth (Circ) | 3.16<br>Constant | mm | 99.9$^{th}$ percentile of lognormal distribution with a mean of 3 mm and a standard deviation of 0.05 mm |
| 1213 | Multiplier Starting Depth (Circ) | 1<br>Constant | - | Conservative value used in Global ID 1212 |
| 1214 | Number of Flaws (Axial) | 0<br>Constant | - | Axial flaws shown to not influence the results of interest in Cases 1.1.6 and 1.1.15 |

| Global ID | Name | Value / Distribution Parameters | Units | Basis |
|---|---|---|---|---|
| 1215 | Initial Flaw Full-Length (Axial) | Not modeled | - | Axial cracks shown to not influence the results of interest in Cases 1.1.6 and 1.1.15 |
| 1216 | Multiplier Starting Full-Length (Axial) | | | |
| 1217 | Initial Flaw Depth (Axial) | | | |
| 1218 | Multiplier Starting Depth (Axial) | | | |

## B15 Case 1.1.19

The objective of Case 1.1.19 was to assess the sensitivity of the likelihood of RVON weld failure due to the weld width and thickness.

The random seeds used for the Case 1.1.19 analyses were as follows:

| Simulation Description | Epistemic Random Seed | Aleatory Random Seed |
|---|---|---|
| 5,000-realization simulation using the epistemic (outer) loop | 6128 | 369 |

The other inputs were developed using the Case 1.1.1 input set as a template with the following modifications:

| Global ID | Name | Value / Distribution Parameters | Units | Basis |
|---|---|---|---|---|
| 0003 | Crack Orientation | 1 | - | Previous cases show that the inclusion of axial cracks was not necessary for this analysis |
| 1101 | Pipe Outer Diameter | Weibull (min = 0.86, slope = 0.423, mean-min = 0.0066, max = 0.891) and 0.891 Constant | m | First analysis (Case 1.1.19) considered a distribution based on least squares fit of dataset from 12 different weld geometries from licensee LBB analyses. Second analysis (Case 1.1.19a) considered largest diameter from the dataset. |
| 1102<br>1104 | Pipe Wall Thickness<br>Weld Material Thickness | Triangular (min = 0.054, mode = 0.059, max = 0.072) and 0.054 Constant | m | First analysis (Case 1.1.19) considered a distribution based on least squares fit of dataset from 12 different weld geometries from licensee LBB analyses. Second analysis (Case 1.1.19a) considered smallest thickness from the dataset. |

## B16 Case 1.1.20

The objective of Case 1.1.20 was to assess the sensitivity of the likelihood of RVON weld failure due to operating temperature.

The random seeds used for the Case 1.1.20 analysis were as follows:

| Simulation Description | Replicate Simulation No. | Epistemic Random Seed | Aleatory Random Seed |
|---|---|---|---|
| 105,000-realization composite simulation using the epistemic (outer) loop | 1 | 1515 | 13118 |
| | 2 | 1974 | 713705 |
| | 3 | 2002 | 1503 |
| | 4 | 2004 | 909 |
| | 5 | 2010 | 907 |
| | 6 | 3131 | 131521 |
| | 7 | 4512 | 1685 |

The other inputs were developed using the Case 1.1.0 input set as a template with the following modifications:

| Global ID | Name | Value / Distribution Parameters | Units | Basis |
|---|---|---|---|---|
| 3102 | Operating temperature for period #1 | 330 | °C | Bounds operating temperature dataset from Appendix G of [25] and licensee LBB analyses (maximum reported was 328 °C) |

## B17 Case 1.1.21

The objective of Case 1.1.21 was to assess the sensitivity of the likelihood of RVON weld failure due to the initial flaw dimensions.

The random seeds used for the Case 1.1.21 analysis were as follows:

| Simulation Description | Epistemic Random Seed | Aleatory Random Seed |
|---|---|---|
| 5,000-realization simulation using the epistemic (outer) loop | 6128 | 369 |

The other inputs were developed using the Case 1.1.1 input set as a template with the following modifications:

| Global ID | Name | Value / Distribution Parameters | Units | Basis |
|---|---|---|---|---|
| 1209 | Number of flaws (Circumferential) | 1<br>Constant | - | Case 1.1.0 analysis showed that occurrences of 2 cracks are extremely rare and the time between 2 cracks is long enough such that only one crack is dominant |
| 1210 | Initial Flaw Full-Length (Circ) | 0.0568<br>Constant | m | 99.9$^{th}$ percentile of the PWSCC initial flaw full-length distribution used in Case 1.1.1 |
| 1211 | Multiplier Starting Full-Length (Circ) | 1<br>Constant | - | Conservatism applied in Global ID 1210 |
| 1212 | Initial Flaw Depth (Circ) | Lognormal<br>(-6.5, 0.35) | m | Corresponds to the distribution for PWSCC initial depth used in Case 1.1.1 |
| 1213 | Multiplier Starting Depth (Circ) | 1<br>Constant | - | Uncertainty applied in Global ID 1212 |

## B18 Case 1.1.22

The objective of Case 1.1.22 was to assess the sensitivity of the likelihood of failure due to the time step for the RVON weld.

The random seeds used for the Case 1.1.22 analyses were as follows:

| Simulation Description | Epistemic Random Seed | Aleatory Random Seed |
|---|---|---|
| 5,000-realization simulation using the epistemic (outer) loop | 6128 | 369 |

The other inputs were developed using the Case 1.1.1 input set as a template with the following modifications:

| Global ID | Name | Value / Distribution Parameters | Units | Basis |
|---|---|---|---|---|
| - | Basic Time Step | 0.5,<br>1,<br>2,<br>6, and<br>12 | mon | Range of time steps including ones substantially smaller and larger than the default, 1-month time step for the purposes of the sensitivity study |

## B19 Case 1.1.23

The objective of Case 1.1.23 was to assess the impacts of separating aleatory and epistemic uncertainties for the RVON weld.

The random seeds used for the Case 1.1.23 analysis were as follows:

| Simulation Description | Epistemic Random Seed | Aleatory Random Seed |
|---|---|---|
| 20,000-realization simulation using 200 epistemic (outer) loop samples and 100 aleatory (inner) loop samples | 6128 | 369 |

The other inputs were developed using the Case 1.1.1 input set as a template with the following modifications:

| Global ID | Name | Value / Distribution Parameters | Units | Basis |
|---|---|---|---|---|
| 1102 | Pipe Wall Thickness | Epistemic | Various | Case 1, Scenario 2 from [25] |
| 1104 | Weld Material Thickness | Epistemic | | |
| 1210 | Initial Flaw Full-Length (Circ) | Aleatory | | |
| 1212 | Initial Flaw Depth (Circ) | Aleatory | | |
| 4352 | Axial WRS Pre-mitigation | Epistemic | | |
| 9002 | Surface Crack Distance Rule Modifier | Epistemic | | |
| 9003 | TW Crack Distance Rule Modifier | Epistemic | | |
| 2101 | Yield Strength, Sigy | Aleatory | | |

| Global ID | Name | Value / Distribution Parameters | Units | Basis |
|---|---|---|---|---|
| 2102 | Ultimate Strength, Sigu | Aleatory | | |
| 2105 | Elastic Modulus, E | Aleatory | | |
| 2106 | Material Init J-Resistance, Jic | Aleatory | | |
| 2107 | Material Init J-Resist Coef, C | Aleatory | | |
| 2108 | Material Init J-Resist Exponent, m | Aleatory | | |
| 2301 | Yield Strength, Sigy | Aleatory | | |
| 2302 | Ultimate Strength, Sigu | Aleatory | | |
| 2305 | Elastic Modulus, E | Aleatory | | |
| 2306 | Material Init J-Resistance, Jic | Aleatory | | |
| 2307 | Material Init J-Resist Coef, C | Aleatory | | |
| 2308 | Material Init J-Resist Exponent, m | Aleatory | | |
| 2501 | Yield Strength, Sigy | Aleatory | | |
| 2502 | Ultimate Strength, Sigu | Aleatory | | |
| 2505 | Elastic Modulus, E | Aleatory | | |
| 2506 | Material Init J-Resistance, Jic | Aleatory | | |
| 2507 | Material Init J-Resist Coef, C | Aleatory | | |
| 2508 | Material Init J-Resist Exponent, m | Aleatory | | |

| Global ID | Name | Value / Distribution Parameters | Units | Basis |
|---|---|---|---|---|
| 2591 | Activation Energy, Qg | Epistemic | | |
| 2592 | Comp-to-Comp Variab Factor, fcomp | Epistemic | | |
| 2593 | Within-Comp Variab Factor, fflaw | Aleatory | | |
| 2594 | Peak-to-Valley ECP Ratio - 1, P-1 | Epistemic | | |
| 2595 | Charact Width of Peak vs ECP, c | Epistemic | | |
| 2604 | CYS | Aleatory | | |
| 2605 | CUTS | Aleatory | | |

## B20 Case 1.2.0

The objective of Case 1.2.0 was to assess the base likelihood of RVIN weld failure caused by PWSCC initiation and growth with no ISI, mitigation, or seismic effects.

The random seeds used for the Case 1.2.0 analysis were as follows:

| Simulation Description | Replicate Simulation No. | Epistemic Random Seed | Aleatory Random Seed |
|---|---|---|---|
| 105,000-realization composite simulation using the epistemic (outer) loop | 1 | 1515 | 13118 |
| | 2 | 1974 | 713705 |
| | 3 | 2002 | 1503 |
| | 4 | 2004 | 909 |
| | 5 | 2010 | 907 |
| | 6 | 3131 | 131521 |
| | 7 | 4512 | 1685 |

The other inputs were developed using the Case 1.1.0 input set as a template with the following modifications:

| Global ID | Name | Value / Distribution Parameters | Units | Basis |
|---|---|---|---|---|
| 1101 | Pipe Outer Diameter | 0.837<br>Constant | m | Derived from applicable geometry information in Appendix D of [25] |
| 1002<br><br><br>1104 | Pipe Wall Thickness<br><br>Weld Material Thickness | 0.0837<br>Constant | m | Derived from applicable geometry information in Appendix D of [25]. Constant value chosen consistent with Case 1.1.0. |
| 3102 | Operating Temperature | 288<br>Constant | °C | Temperature for cold leg derived from applicable operating temperature information in Appendix G of [25]. Constant value chosen consistent with Case 1.1.0. |
| 3101 | Operating pressure | 15.41<br>Constant | MPa | Pressure for cold leg from NUREG/CR-2189, Vol. 3, Table 2-2 (2235 psi converted to MPa). Constant value chosen consistent with Case 1.1.0. |

| Global ID | Name | Value / Distribution Parameters | Units | Basis |
|---|---|---|---|---|
| 4121 | Membrane Stress (Deadweight) | -0.022<br>Constant | MPa | Derived from applicable geometry and load information in Appendix D of [25] |
| 4122 | Maximum Bending Stress (Deadweight) | 3.975<br>Constant | MPa | Derived from applicable geometry and load information in Appendix D of [25] |
| 4123 | Membrane Stress (Thermal) | 1.57<br>Constant | MPa | Derived from applicable geometry and load information in Appendix D of [25] |
| 4124 | Bending Stress (Thermal) | 50.015<br>Constant | MPa | Derived from applicable geometry and load information in Appendix D of [25] |

## B21 Case 1.2.1

The objective of Case 1.2.1 was to assess the impacts of the combined effects of PWSCC and fatigue for the RVIN weld.

The random seeds used for the Case 1.2.1 analysis were as follows:

| Simulation Description | Replicate Simulation No. | Epistemic Random Seed | Aleatory Random Seed |
|---|---|---|---|
| 105,000-realization composite simulation using the epistemic (outer) loop | 1 | 1515 | 13118 |
| | 2 | 1974 | 713705 |
| | 3 | 2002 | 1503 |
| | 4 | 2004 | 909 |
| | 5 | 2010 | 907 |
| | 6 | 3131 | 131521 |
| | 7 | 4512 | 1685 |

The other inputs were developed using the Case 1, Scenario 10 input set from [25] as a template with the following modifications:

| Global ID | Name | Value / Distribution Parameters | Units | Basis |
|---|---|---|---|---|
| 0001 | Plant Operation Time | 960 | mon | Equivalent to 80 EFPY, which accounts for a subsequent license renewal term |
| 0301 | Mitigation Type Choice | 0 | - | Setting for no mitigation |
| 0402 | Period End Time (Op Period #1) | 961 | mon | Setting for including one operating period |
| 0403 | Input Type Choice (Op Period #1) | 2 | - | Input by stresses recommended to avoid known error in operating load calculations as described in xLPR-UM, Version 1.2, Section H.1 |
| 0405 | Period End Time (Op Period #2) | 962 | mon | Setting for including one operating period |

| Global ID | Name | Value / Distribution Parameters | Units | Basis |
|---|---|---|---|---|
| 0411 – 0411.12 | Transient Type Selection (Loads 1 – 12) | 1 | - | Setting for activating thermal transient with no stratification. All corresponding transients from [42], Table 5-2. |
| 0904 | Max time between 2 check – single TWC – CC | 1 | mon | Stability module called in each timestep |
| All uncertain variables | Data Source | Epistemic | - | Only the epistemic (outer) loop used in the simulation. |
| 1001 | Effective Full Power Years (EFPY) | 80<br>Constant | yr | Set equal to the plant operation time. Constant value chosen consistent with Case 1.2.0. |
| 1101 | Pipe Outer Diameter | 0.837<br>Constant | m | Derived from applicable geometry information in Appendix D of [25] |
| 1002<br><br>1104 | Pipe Wall Thickness<br><br>Weld Material Thickness | 0.0837<br>Constant | m | Derived from applicable geometry information in Appendix D of [25]. Constant value chosen consistent with Case 1.2.0. |
| 3001 | Flow Rate | 17.08<br>Constant | m/s | Derived from applicable flow rate data in Appendix G of [25] and converted to m/s using the pipe outer diameter and wall thickness. |
| 3101 | Operating Pressure | 15.41<br>Constant | MPa | Pressure for cold leg from NUREG/CR-2189, Vol. 3, Table 2-2 (2235 psi converted to MPa). Constant value chosen consistent with Case 1.2.0. |

| Global ID | Name | Value / Distribution Parameters | Units | Basis |
|---|---|---|---|---|
| 3102 | Operating Temperature | 288<br>Constant | °C | Temperature for cold leg derived from applicable operating temperature information in Appendix G of [25]. Constant value chosen consistent with Case 1.2.0. |
| 3103 | Dissolved Oxygen | 999<br>Constant | ppm | See Note 1 |
| 4001 | Earthquake Probability | 0<br>Constant | yr-1 | Case excludes seismic effects |
| 4002 | Earthquake Δ Total Membrane | 0<br>Constant | MPa | Case excludes seismic effects |
| 4003 | Earthquake Δ Inertial Bending | 0<br>Constant | MPa | Case excludes seismic effects |
| 4004 | Earthquake Δ Anchor Bending | 0<br>Constant | MPa | Case excludes seismic effects |
| 4005 | Sigma_SSa | 0<br>Constant | MPa | More realistic than the initially assumed +200 MPa that favored crack initiation |
| 4006 | Sigma_SSh | 0<br>Constant | MPa | More realistic than the initially assumed +200 MPa that favored crack initiation |
| 4121 | Membrane Stress (Deadweight) | -0.022<br>Constant | MPa | Derived from applicable geometry and load information in Appendix D of [25] |
| 4122 | Maximum Bending Stress (Deadweight) | 3.975<br>Constant | MPa | Derived from applicable geometry and load information in Appendix D of [25] |
| 4123 | Membrane Stress (Thermal) | 1.57<br>Constant | MPa | Derived from applicable geometry and load information in Appendix D of [25] |

| Global ID | Name | Value / Distribution Parameters | Units | Basis |
|---|---|---|---|---|
| 4124 | Bending Stress (Thermal) | 50.015 Constant | MPa | Derived from applicable geometry and load information in Appendix D of [25] |

| | | | | | |
|---|---|---|---|---|---|
| Transient Definitions, Transient 1 | Point | Time (s) | Delta T (°C) | Delta P (Pa) | Plant heatup transient derived from information in [42], Table 5-2. |
| | 1 | 0 | -250.22 | -1.33E+07 | |
| | 2 | 16092 | -1.89 | 0 | |
| Transient Definitions, Transient 2 | Point | Time (s) | Delta T (°C) | Delta P (Pa) | Plant cooldown transient derived from information in [42], Table 5-2. |
| | 1 | 0 | -1.89 | 0 | |
| | 2 | 16092 | -250.22 | -1.33E+07 | |
| Transient Definitions, Transient 3 | Point | Time (s) | Delta T (°C) | Delta P (Pa) | Plant loading transient derived from information in [42], Table 5-2. |
| | 1 | 0 | -1.89 | 0 | |
| | 2 | 1200 | -20.22 | 0 | |
| Transient Definitions, Transient 4 | Point | Time (s) | Delta T (°C) | Delta P (Pa) | Plant unloading transient derived from information in [42], Table 5-2. |
| | 1 | 0 | -20.22 | 0 | |
| | 2 | 200 | -17.17 | 0 | |
| | 3 | 400 | -14.11 | 0 | |
| | 4 | 600 | -11.06 | 0 | |
| | 5 | 800 | -8.00 | 0 | |
| | 6 | 1000 | -4.95 | 0 | |
| | 7 | 1200 | -1.89 | 0 | |
| Transient Definitions, Transient 5 | Point | Time (s) | Delta T (°C) | Delta P (Pa) | Step load increase transient derived from information in [42], Table 5-2. |
| | 1 | 0 | -4.94 | 0 | |
| | 2 | 10 | -6.61 | -3.45E+04 | |
| | 3 | 30 | -8.50 | -2.41E+05 | |
| | 4 | 50 | -9.22 | -4.62E+05 | |
| | 5 | 100 | -9.33 | -6.62E+05 | |
| | 6 | 290 | -6.61 | 1.59E+05 | |
| | 7 | 600 | -5.44 | 0 | |
| Transient Definitions, Transient 6 | Point | Time (s) | Delta T (°C) | Delta P (Pa) | Step load decrease transient derived from information in [42], Table 5-2. |
| | 1 | 0 | -5.39 | 0 | |
| | 2 | 30 | -1.72 | 6.21E+05 | |

| Global ID | Name | Value / Distribution Parameters | | Units | Basis |
|---|---|---|---|---|---|
| | 3 | 50 | -1.17 | 5.93E+05 | |
| | 4 | 200 | -3.39 | -5.17E+05 | |
| | 5 | 290 | -4.06 | -6.27E+05 | |
| Transient Definitions, Transient 7 | Point | Time (s) | Delta T (°C) | Delta P (Pa) | Large step decrease transient derived from information in [42], Table 5-2. |
| | 1 | 0 | -5.39 | 0 | |
| | 2 | 30 | 7.68 | 8.07E+05 | |
| | 3 | 55.02 | -0.43 | -9.79E+05 | |
| | 4 | 76.02 | 2.28 | -7.93E+05 | |
| | 5 | 420 | -0.26 | -6.34E+05 | |
| | 6 | 600 | -4.48 | -6.76E+05 | |
| Transient Definitions, Transient 8 | Point | Time (s) | Delta T (°C) | Delta P (Pa) | Loss of load transient derived from information in [42], Table 5-2. |
| | 1 | 0 | -5.39 | 0 | |
| | 2 | 10 | 10.84 | 3.72E+06 | |
| | 3 | 20 | 25.28 | 2.27E+06 | |
| | 4 | 30 | 27.83 | -1.65E+06 | |
| | 5 | 80 | 7.83 | -4.16E+06 | |
| | 6 | 200 | 7.61 | -5.49E+06 | |
| Transient Definitions, Transient 9 | Point | Time (s) | Delta T (°C) | Delta P (Pa) | Loss of flow transient derived from information in [42], Table 5-2. |
| | 1 | 0 | -5.39 | 0 | |
| | 2 | 14 | -29.83 | -1.65E+05 | |
| | 3 | 30 | -9.28 | -1.34E+06 | |
| | 4 | 35 | -5.39 | -1.97E+06 | |
| | 5 | 140 | -12.06 | -2.45E+06 | |
| Transient Definitions, Transient 10 | Point | Time (s) | Delta T (°C) | Delta P (Pa) | Reactor trip transient derived from information in [42], Table 5-2. |
| | 1 | 0 | -5.39 | 0 | |
| | 2 | 5 | -1.06 | -1.35E+06 | |
| | 3 | 10 | 2.39 | -1.88E+06 | |
| | 4 | 16 | -3.17 | -2.30E+06 | |
| | 5 | 100 | -1.17 | -3.00E+06 | |

| Global ID | Name | Value / Distribution Parameters | Units | Basis |
|---|---|---|---|---|
| Transient Definitions, Transient 11 | Point / Time (s) / Delta T (°C) / Delta P (Pa) | | | Primary side hydrostatic test transient derived from information in [42], Table 5-2. |
| | 1 / 0 / -266.89 / -1.53E+07 | | | |
| | 2 / 10800 / -1.89 / 6.12E+06 | | | |
| | 3 / 21600 / -266.89 / -1.53E+07 | | | |
| Transient Definitions, Transient 12 | Point / Time (s) / Delta T (°C) / Delta P (Pa) | | | Primary leak test transient derived from information in [42], Table 5-2. |
| | 1 / 0 / -266.89 / -1.53E+07 | | | |
| | 2 / 10800 / -1.89 / 2.07E+05 | | | |
| | 3 / 21600 / -266.89 / -1.53E+07 | | | |
| TIFFANY Inputs, Transient 1 | Start Month,<br>End Month,<br>Front-Back Loading,<br>Frequency,<br># of Cycles per Event,<br>Uncertainty Multiplier | 0,<br>960,<br>0.5,<br>5.0,<br>1.0,<br>1.0 | mon,<br>mon,<br>-,<br>1/yr,<br>-,<br>- | End month is equivalent to 80 EFPY, which accounts for a subsequent license renewal term. Constant value of 1.0 for uncertainty multiplier is conservative because it represents the maximum value of the distribution as used for the transients in Case 1, Scenario 10. Remaining inputs are consistent with information in [42], Table 5-2. |
| TIFFANY Inputs, Transient 2 | Start Month,<br>End Month,<br>Front-Back Loading,<br>Frequency,<br># of Cycles per Event,<br>Uncertainty Multiplier | 0,<br>960,<br>0.5,<br>5.0,<br>1.0,<br>1.0 | mon,<br>mon,<br>-,<br>1/yr,<br>-,<br>- | End month is equivalent to 80 EFPY, which accounts for a subsequent license renewal term. Constant value of 1.0 for uncertainty multiplier is conservative because it represents the maximum value of the distribution as used for the transients in Case 1, Scenario 10. Remaining inputs are consistent with information in [42], Table 5-2. |

| Global ID | Name | Value / Distribution Parameters | Units | Basis |
|---|---|---|---|---|
| TIFFANY Inputs, Transient 3 | Start Month,<br>End Month,<br>Front-Back Loading,<br>Frequency,<br># of Cycles per Event,<br>Uncertainty Multiplier | 0,<br>960,<br>0.5,<br>362.5,<br>1.0,<br>1.0 | mon,<br>mon,<br>-,<br>1/yr,<br>-,<br>- | End month is equivalent to 80 EFPY, which accounts for a subsequent license renewal term. Constant value of 1.0 for uncertainty multiplier is conservative because it represents the maximum value of the distribution as used for the transients in Case 1, Scenario 10. Remaining inputs are consistent with information in [42], Table 5-2. |
| TIFFANY Inputs, Transient 4 | Start Month,<br>End Month,<br>Front-Back Loading,<br>Frequency,<br># of Cycles per Event,<br>Uncertainty Multiplier | 0,<br>960,<br>0.5,<br>362.5,<br>1.0,<br>1.0 | mon,<br>mon,<br>-,<br>1/yr,<br>-,<br>- | End month is equivalent to 80 EFPY, which accounts for a subsequent license renewal term. Constant value of 1.0 for uncertainty multiplier is conservative because it represents the maximum value of the distribution as used for the transients in Case 1, Scenario 10. Remaining inputs are consistent with information in [42], Table 5-2. |
| TIFFANY Inputs, Transient 5 | Start Month,<br>End Month,<br>Front-Back Loading,<br>Frequency,<br># of Cycles per Event,<br>Uncertainty Multiplier | 0,<br>960,<br>0.5,<br>50.0,<br>1.0,<br>1.0 | mon,<br>mon,<br>-,<br>1/yr,<br>-,<br>- | End month is equivalent to 80 EFPY, which accounts for a subsequent license renewal term. Constant value of 1.0 for uncertainty multiplier is conservative because it represents the maximum value of the distribution as used for the transients in Case 1, Scenario 10. Remaining inputs are consistent with information in [42], Table 5-2. |

| Global ID | Name | Value / Distribution Parameters | Units | Basis |
|---|---|---|---|---|
| TIFFANY Inputs, Transient 6 | Start Month,<br>End Month,<br>Front-Back Loading,<br>Frequency,<br># of Cycles per Event,<br>Uncertainty Multiplier | 0,<br>960,<br>0.5,<br>50.0,<br>1.0,<br>1.0 | mon,<br>mon,<br>-,<br>1/yr,<br>-,<br>- | End month is equivalent to 80 EFPY, which accounts for a subsequent license renewal term. Constant value of 1.0 for uncertainty multiplier is conservative because it represents the maximum value of the distribution as used for the transients in Case 1, Scenario 10. Remaining inputs are consistent with information in [42], Table 5-2. |
| TIFFANY Inputs, Transient 7 | Start Month,<br>End Month,<br>Front-Back Loading,<br>Frequency,<br># of Cycles per Event,<br>Uncertainty Multiplier | 0,<br>960,<br>0.5,<br>5.0,<br>1.0,<br>1.0 | mon,<br>mon,<br>-,<br>1/yr,<br>-,<br>- | End month is equivalent to 80 EFPY, which accounts for a subsequent license renewal term. Constant value of 1.0 for uncertainty multiplier is conservative because it represents the maximum value of the distribution as used for the transients in Case 1, Scenario 10. Remaining inputs are consistent with information in [42], Table 5-2. |
| TIFFANY Inputs, Transient 8 | Start Month,<br>End Month,<br>Front-Back Loading,<br>Frequency,<br># of Cycles per Event,<br>Uncertainty Multiplier | 0,<br>960,<br>0.5,<br>2.0,<br>1.0,<br>1.0 | mon,<br>mon,<br>-,<br>1/yr,<br>-,<br>- | End month is equivalent to 80 EFPY, which accounts for a subsequent license renewal term. Constant value of 1.0 for uncertainty multiplier is conservative because it represents the maximum value of the distribution as used for the transients in Case 1, Scenario 10. Remaining inputs are consistent with information in [42], Table 5-2. |

| Global ID | Name | Value / Distribution Parameters | Units | Basis |
|---|---|---|---|---|
| TIFFANY Inputs, Transient 9 | Start Month,<br>End Month,<br>Front-Back Loading,<br>Frequency,<br># of Cycles per Event,<br>Uncertainty Multiplier | 0,<br>960,<br>0.5,<br>2.0,<br>1.0,<br>1.0 | mon,<br>mon,<br>-,<br>1/yr,<br>-,<br>- | End month is equivalent to 80 EFPY, which accounts for a subsequent license renewal term. Constant value of 1.0 for uncertainty multiplier is conservative because it represents the maximum value of the distribution as used for the transients in Case 1, Scenario 10. Remaining inputs are consistent with information in [42], Table 5-2. |
| TIFFANY Inputs, Transient 10 | Start Month,<br>End Month,<br>Front-Back Loading,<br>Frequency,<br># of Cycles per Event,<br>Uncertainty Multiplier | 0,<br>960,<br>0.5,<br>10.0,<br>1.0,<br>1.0 | mon,<br>mon,<br>-,<br>1/yr,<br>-,<br>- | End month is equivalent to 80 EFPY, which accounts for a subsequent license renewal term. Constant value of 1.0 for uncertainty multiplier is conservative because it represents the maximum value of the distribution as used for the transients in Case 1, Scenario 10. Remaining inputs are consistent with information in [42], Table 5-2. |
| TIFFANY Inputs, Transient 11 | Start Month,<br>End Month,<br>Front-Back Loading,<br>Frequency,<br># of Cycles per Event,<br>Uncertainty Multiplier | 0,<br>960,<br>0.5,<br>1.38,<br>1.0,<br>1.0 | mon,<br>mon,<br>-,<br>1/yr,<br>-,<br>- | End month is equivalent to 80 EFPY, which accounts for a subsequent license renewal term. Constant value of 1.0 for uncertainty multiplier is conservative because it represents the maximum value of the distribution as used for the transients in Case 1, Scenario 10. Remaining inputs are consistent with information in [42], Table 5-2. |

| Global ID | Name | Value / Distribution Parameters | Units | Basis |
|---|---|---|---|---|
| TIFFANY Inputs, Transient 12 | Start Month,<br>End Month,<br>Front-Back Loading,<br>Frequency,<br># of Cycles per Event,<br>Uncertainty Multiplier | 0,<br>960,<br>0.5,<br>1.38,<br>1.0,<br>1.0 | mon,<br>mon,<br>-,<br>1/yr,<br>-,<br>- | End month is equivalent to 80 EFPY, which accounts for a subsequent license renewal term. Constant value of 1.0 for uncertainty multiplier is conservative because it represents the maximum value of the distribution as used for the transients in Case 1, Scenario 10. Remaining inputs are consistent with information in [42], Table 5-2. |

Notes:

[1] After the simulation was run, a typo was discovered in the definition of the dissolved oxygen concentration where a placeholder value of 999 ppm was used instead of a constant value of 40 ppb as defined in Case 1, Scenario 10. However, the dissolved oxygen concentration only affects fatigue crack initiation for carbon and low-alloy steels. Because fatigue crack initiation only was modeled in the nickel-based alloy weld metal in Case 1.2.1; this input has no impact on the conclusions drawn from this sensitivity study. The typo is documented here for completeness and for potential correction should the simulation be rerun in the future.

# APPENDIX C
# USE OF LABORATORY DATA TO DEVELOP NEW CRACK INITIATION MODEL PARAMETERS

## C1 Introduction

In the development of xLPR Version 2.0, worldwide data from both field observations and laboratory experiments were analyzed to calibrate the parameters for the three primary water stress-corrosion cracking initiation models [C-1]. However, estimates of crack initiation based on field observations contain inherent uncertainties due to the complexity of the problem. Often, the data reflect cracks of different sizes that have already initiated and grown. Estimating the time of crack initiation from such data requires working the nontrivial, inverse problem of estimating the amount of crack growth that may have occurred since initiation. Furthermore, it requires definition of the size of the crack that is considered to have initiated.

To better understand the implications of these uncertainties, the parameters for one of the three initiation models (i.e., Direct Model 1) have been recalibrated using a larger and more recent set of laboratory data with no field observations. The advantage of using only laboratory data is that it is easier to consistently define when a crack has initiated. However, a limitation is that laboratory experiments rely on extreme conditions to accelerate the crack initiation process, and there is uncertainty in scaling from those conditions to the conditions experienced by actual components inservice. The impact of using the recalibrated model parameters in the xLPR code is studied in a reference simulation. Results within the same range as those generated using the original model parameters would serve to provide confidence in the original model parameters, or the converse.

The recalibrated model parameters are based on 143 crack initiation tests as reported in Table C-1. The test data come from three different laboratories: (1) Framatome with data published by P. Scott, et al. [C-2], (2) Électricité de France (EDF) with data published by Vaillant, et al. [C-3] and Couvant, et al. [C-4], and (3) Pacific Northwest National Labs (PNNL) with data published by the NRC [C-4]. For each test, the temperature, tensile stress, time of observation, and the observation of a crack are noted. The stresses are reported as both engineering and true stresses.

**Table C-1 Laboratory dataset on Alloy 182 used for model parameter recalibration**

| Laboratory | Heat | Cracked? | Temp., °C | Initiation Time, hrs | Eng. Stress, MPa | True Stress, MPa |
|---|---|---|---|---|---|---|
| Framatome [C-2] | SOUDENEL CG5 (Lot 78801) | Yes | 325 | 2210 | 499 | 584 |
| Framatome [C-2] | SOUDENEL CG5 (Lot 78801) | Yes | 325 | 3720 | 464 | 517 |

**Table C-1 Laboratory dataset used for model parameter recalibration (continued)**

| Laboratory | Heat | Cracked? | Temp., °C | Initiation Time, hrs | Eng. Stress, MPa | True Stress, MPa |
|---|---|---|---|---|---|---|
| Framatome [C-2] | SOUDENEL CG5 (Lot 78801) | Yes | 325 | 4180 | 428 | 456 |
| Framatome [C-2] | SOUDENEL CG5 (Lot 78801) | Yes | 325 | 6460 | 466 | 521 |
| Framatome [C-2] | SOUDENEL CG5 (Lot 78801) | Yes | 325 | 10500 | 440 | 475 |
| Framatome [C-2] | SOUDENEL CG5 (Lot 78801) | Yes | 325 | 15100 | 433 | 464 |
| Framatome [C-2] | SOUDENEL CG5 (Lot 78801) | Yes | 325 | 24700 | 415 | 436 |
| Framatome [C-2] | SOUDENEL CG5 (Lot 78801) | Yes | 325 | 50400 | 407 | 424 |
| Framatome [C-2] | SOUDENEL CG5 (Lot 78801) | No | 325 | 13800 | 365 | 366 |
| Framatome [C-2] | SOUDENEL CG5 (Lot 78801) | No | 325 | 88300 | 313 | 313 |
| Framatome [C-2] | SOUDENEL CG5 (Lot 78801) | No | 325 | 7860 | 361 | 361 |
| Framatome [C-2] | SOUDENEL CG5 (Lot 78801) | No | 325 | 78000 | 368 | 370 |
| Framatome [C-2] | SOUDENEL CG5 (Lot 78801) | No | 325 | 112000 | 340 | 335 |
| Framatome [C-2] | SOUDENEL CG5 (Lot 78801) | No | 325 | 110000 | 375 | 379 |
| EDF [C-3] | D481 | Yes | 360 | 572 | 497 | 580 |
| EDF [C-3] | D545 | Yes | 325 | 2380 | 526 | 643 |
| EDF [C-3] | D545 | Yes | 325 | 2300 | 507 | 602 |
| EDF [C-3] | D545 | Yes | 325 | 2490 | 507 | 602 |
| EDF [C-3] | D545 | Yes | 325 | 3800 | 555 | 712 |

**Table C-1 Laboratory dataset used for model parameter recalibration (continued)**

| Laboratory | Heat | Cracked? | Temp., °C | Initiation Time, hrs | Eng. Stress, MPa | True Stress, MPa |
|---|---|---|---|---|---|---|
| EDF [C-3] | D545 | Yes | 325 | 3670 | 494 | 575 |
| EDF [C-3] | D545 | Yes | 325 | 4530 | 423 | 448 |
| EDF [C-3] | D545 | Yes | 325 | 7340 | 506 | 599 |
| EDF [C-3] | D545 | Yes | 325 | 7350 | 424 | 450 |
| EDF [C-3] | D545 | Yes | 325 | 12900 | 424 | 450 |
| EDF [C-3] | D545 | Yes | 325 | 13800 | 507 | 602 |
| EDF [C-3] | D545 | No | 325 | 1050 | 508 | 604 |
| EDF [C-3] | D545 | No | 325 | 2120 | 426 | 453 |
| EDF [C-3] | D545 | No | 325 | 2380 | 506 | 599 |
| EDF [C-3] | D545 | No | 325 | 2100 | 587 | 796 |
| EDF [C-3] | D545 | No | 325 | 5050 | 571 | 753 |
| EDF [C-3] | D545 | No | 325 | 6850 | 571 | 753 |
| EDF [C-3] | D545 | No | 325 | 9710 | 557 | 717 |
| EDF [C-3] | D545 | No | 325 | 7700 | 515 | 619 |
| EDF [C-3] | D545 | No | 325 | 12100 | 302 | 302 |
| EDF [C-3] | D545 | No | 325 | 10900 | 353 | 351 |
| EDF [C-3] | D545 | No | 325 | 19800 | 354 | 352 |

**Table C-1 Laboratory dataset used for model parameter recalibration (continued)**

| Laboratory | Heat | Cracked? | Temp., °C | Initiation Time, hrs | Eng. Stress, MPa | True Stress, MPa |
|---|---|---|---|---|---|---|
| EDF [C-3] | D545 | No | 325 | 8500 | 424 | 450 |
| EDF [C-3] | D545 | No | 325 | 12200 | 354 | 352 |
| EDF [C-3] | D545 | No | 325 | 10900 | 424 | 450 |
| EDF [C-3] | D545 | No | 325 | 10900 | 506 | 599 |
| EDF [C-3] | D545 | No | 325 | 19700 | 506 | 599 |
| EDF [C-3] | D545 | No | 325 | 14300 | 434 | 466 |
| EDF [C-3] | D545 | No | 325 | 19600 | 424 | 450 |
| EDF [C-3] | D545 | No | 325 | 47100 | 424 | 450 |
| EDF [C-3] | D545 | No | 325 | 46300 | 506 | 599 |
| EDF [C-3] | D545 | No | 325 | 89000 | 504 | 595 |
| EDF [C-3] | D545 | No | 325 | 95000 | 354 | 352 |
| EDF [C-3] | D545 | No | 325 | 107000 | 504 | 595 |
| EDF [C-3] | D545 | No | 325 | 110000 | 515 | 619 |
| EDF [C-3] | D545 | No | 325 | 110000 | 537 | 668 |
| EDF [C-3] | D545 | No | 325 | 111000 | 424 | 450 |
| EDF [C-3] | D545 | No | 325 | 100000 | 424 | 450 |
| EDF [C-3] | D545 | No | 325 | 91500 | 424 | 450 |

**Table C-1 Laboratory dataset used for model parameter recalibration (continued)**

| Laboratory | Heat | Cracked? | Temp., °C | Initiation Time, hrs | Eng. Stress, MPa | True Stress, MPa |
|---|---|---|---|---|---|---|
| EDF [C-3] | D545 | No | 325 | 92200 | 354 | 352 |
| EDF [C-3] | D545 | No | 325 | 98000 | 354 | 352 |
| EDF [C-3] | D545 | Yes | 325 | 229 | 574 | 760 |
| EDF [C-3] | D545 | Yes | 325 | 269 | 613 | 872 |
| EDF [C-3] | D545 | Yes | 325 | 279 | 578 | 771 |
| EDF [C-3] | D545 | Yes | 325 | 319 | 578 | 771 |
| EDF [C-3] | D545 | Yes | 325 | 406 | 497 | 581 |
| EDF [C-3] | D545 | Yes | 325 | 551 | 498 | 583 |
| EDF [C-3] | D545 | Yes | 325 | 576 | 503 | 593 |
| EDF [C-3] | D545 | Yes | 325 | 826 | 419 | 442 |
| EDF [C-3] | D545 | Yes | 325 | 728 | 525 | 641 |
| EDF [C-3] | D545 | Yes | 325 | 863 | 543 | 682 |
| EDF [C-3] | D545 | Yes | 325 | 839 | 581 | 779 |
| EDF [C-3] | D545 | Yes | 325 | 721 | 579 | 774 |
| EDF [C-3] | D545 | Yes | 325 | 1800 | 498 | 583 |
| EDF [C-3] | D545 | Yes | 325 | 3060 | 498 | 583 |
| EDF [C-3] | D545 | Yes | 325 | 2530 | 418 | 441 |

**Table C-1 Laboratory dataset used for model parameter recalibration (continued)**

| Laboratory | Heat | Cracked? | Temp., °C | Initiation Time, hrs | Eng. Stress, MPa | True Stress, MPa |
|---|---|---|---|---|---|---|
| EDF [C-3] | D545 | Yes | 325 | 3970 | 419 | 442 |
| EDF [C-3] | D545 | Yes | 325 | 9640 | 418 | 441 |
| EDF [C-3] | D545 | Yes | 325 | 32900 | 407 | 424 |
| EDF [C-3] | D545 | No | 325 | 722 | 418 | 441 |
| EDF [C-3] | D545 | No | 325 | 721 | 497 | 581 |
| EDF [C-3] | D545 | No | 325 | 4340 | 418 | 441 |
| EDF [C-3] | D545 | No | 325 | 5190 | 500 | 587 |
| EDF [C-3] | D545 | No | 325 | 70000 | 298 | 298 |
| EDF [C-3] | D545 | No | 325 | 70000 | 348 | 345 |
| EDF [C-3] | D545 | No | 325 | 160000 | 348 | 345 |
| EDF [C-3] | D545 | No | 325 | 160000 | 300 | 300 |
| EDF [C-4] | D1054 | No | 360 | 722 | 385 | 392 |
| EDF [C-4] | D1054 | No | 360 | 8626 | 390 | 400 |
| EDF [C-4] | D1054 | No | 330 | 13456 | 390 | 400 |
| EDF [C-4] | D1054 | No | 360 | 190 | 426 | 453 |
| EDF [C-4] | D1054 | No | 325 | 214 | 466 | 521 |
| EDF [C-4] | D1054 | No | 330 | 5335 | 424 | 450 |

**Table C-1 Laboratory dataset used for model parameter recalibration (continued)**

| Laboratory | Heat | Cracked? | Temp., °C | Initiation Time, hrs | Eng. Stress, MPa | True Stress, MPa |
|---|---|---|---|---|---|---|
| EDF [C-4] | D1054 | No | 360 | 12933 | 376 | 380 |
| EDF [C-4] | D1054 | Yes | 360 | 120 | 550 | 700 |
| EDF [C-4] | D1054 | Yes | 330 | 737 | 534 | 660 |
| EDF [C-4] | D1054 | Yes | 360 | 1000 | 501 | 590 |
| EDF [C-4] | D1054 | Yes | 360 | 5200 | 423 | 448 |
| EDF [C-4] | D1054 | Yes | 360 | 13365 | 352 | 350 |
| EDF [C-4] | D1054 | Yes | 350 | 23771 | 352 | 350 |
| EDF [C-4] | D1054 | No | 340 | 3240 | 390 | 400 |
| EDF [C-4] | D1054 | No | 340 | 3240 | 424 | 450 |
| PNNL [C-5] | Knolls Atomic Power Lab (KAPL) @ Yield Strength (YS) | Yes | 360 | 113 | 547 | 547 |
| PNNL [C-5] | KAPL @ YS | Yes | 360 | 30 | 552 | 552 |
| PNNL [C-5] | KAPL @ YS | Yes | 360 | 30 | 563 | 563 |
| PNNL [C-5] | KAPL @ YS | Yes | 360 | 1642 | 567 | 567 |
| PNNL [C-5] | KAPL @ YS | Yes | 360 | 1625 | 575 | 575 |
| PNNL [C-5] | KAPL @ YS | Yes | 360 | 1635 | 581 | 581 |
| PNNL [C-5] | KAPL @ YS | No | 360 | 4843 | 572 | 572 |

**Table C-1 Laboratory dataset used for model parameter recalibration (continued)**

| Laboratory | Heat | Cracked? | Temp., °C | Initiation Time, hrs | Eng. Stress, MPa | True Stress, MPa |
|---|---|---|---|---|---|---|
| PNNL [C-5] | KAPL @ YS | No | 360 | 4843 | 566 | 566 |
| PNNL [C-5] | KAPL @ YS | No | 360 | 4843 | 576 | 576 |
| PNNL [C-5] | KAPL - 90% of YS | Yes | 360 | 9205 | 505 | 505 |
| PNNL [C-5] | KAPL - 90% of YS | Yes | 360 | 9312 | 505 | 505 |
| PNNL [C-5] | KAPL - 90% of YS | Yes | 360 | 9284 | 505 | 505 |
| PNNL [C-5] | KAPL - 90% of YS | Yes | 360 | 9178 | 513 | 513 |
| PNNL [C-5] | KAPL - 90% of YS | Yes | 360 | 9312 | 513 | 513 |
| PNNL [C-5] | KAPL - 90% of YS | Yes | 360 | 500 | 513 | 513 |
| PNNL [C-5] | Studsvik @ YS | Yes | 360 | 725 | 529 | 529 |
| PNNL [C-5] | Studsvik @ YS | Yes | 360 | 30 | 532 | 532 |
| PNNL [C-5] | Studsvik @ YS | Yes | 360 | 910 | 532 | 532 |
| PNNL [C-5] | Studsvik @ YS | Yes | 360 | 2957 | 534 | 534 |
| PNNL [C-5] | Studsvik @ YS | Yes | 360 | 30 | 536 | 536 |
| PNNL [C-5] | Studsvik @ YS | Yes | 360 | 83 | 553 | 553 |
| PNNL [C-5] | Studsvik @ YS | Yes | 360 | 41 | 555 | 555 |
| PNNL [C-5] | Studsvik @ YS | Yes | 360 | 41 | 559 | 559 |
| PNNL [C-5] | Studsvik @ YS | No | 360 | 5126 | 541 | 541 |

**Table C-1 Laboratory dataset used for model parameter recalibration (continued)**

| Laboratory | Heat | Cracked? | Temp., °C | Initiation Time, hrs | Eng. Stress, MPa | True Stress, MPa |
|---|---|---|---|---|---|---|
| PNNL [C-5] | Studsvik - 90% of YS | Yes | 360 | 10437 | 465 | 465 |
| PNNL [C-5] | Studsvik - 90% of YS | Yes | 360 | 10437 | 479 | 479 |
| PNNL [C-5] | Studsvik - 90% of YS | No | 360 | 10467 | 464 | 464 |
| PNNL [C-5] | Studsvik - 90% of YS | Yes | 360 | 10437 | 465 | 465 |
| PNNL [C-5] | Studsvik - 90% of YS | Yes | 360 | 10446 | 470 | 470 |
| PNNL [C-5] | Studsvik - 90% of YS | Yes | 360 | 10264 | 466 | 466 |
| PNNL [C-5] | Phase 2B @ YS | Yes | 360 | 132 | 462 | 462 |
| PNNL [C-5] | Phase 2B @ YS | Yes | 360 | 806 | 500 | 500 |
| PNNL [C-5] | Phase 2B @ YS | Yes | 360 | 2238 | 506 | 506 |
| PNNL [C-5] | Phase 2B @ YS | Yes | 360 | 4964 | 506 | 506 |
| PNNL [C-5] | Phase 2B @ YS | Yes | 360 | 105 | 514 | 514 |
| PNNL [C-5] | Phase 2B @ YS | Yes | 360 | 409 | 514 | 514 |
| PNNL [C-5] | Phase 2B @ YS | No | 360 | 3173 | 514 | 514 |
| PNNL [C-5] | Phase 2B @ YS | No | 360 | 2971 | 467 | 467 |
| PNNL [C-5] | Flawtech @ YS | Yes | 360 | 30 | 518 | 518 |
| PNNL [C-5] | Flawtech @ YS | Yes | 360 | 30 | 518 | 518 |
| PNNL [C-5] | Flawtech @ YS | Yes | 360 | 90 | 518 | 518 |

**Table C-1 Laboratory dataset used for model parameter recalibration (continued)**

| Laboratory | Heat | Cracked? | Temp., °C | Initiation Time, hrs | Eng. Stress, MPa | True Stress, MPa |
|---|---|---|---|---|---|---|
| PNNL [C-5] | Flawtech @ YS | Yes | 360 | 79 | 525 | 525 |
| PNNL [C-5] | Flawtech @ YS | Yes | 360 | 106 | 525 | 525 |
| PNNL [C-5] | Flawtech @ YS | Yes | 360 | 113 | 525 | 525 |
| PNNL [C-5] | Flawtech @ YS | Yes | 360 | 746 | 528 | 528 |
| PNNL [C-5] | Flawtech @ YS | Yes | 360 | 825 | 528 | 528 |
| PNNL [C-5] | Flawtech @ YS | Yes | 360 | 900 | 528 | 528 |

The true stresses are higher than the engineering stresses as shown in Figure C-1. Thus, when the true stresses are used to fit the model parameters, they will lead to lower probabilities of crack initiation (i.e., equivalently longer times to crack initiation). This result may seem counterintuitive; however, it comes from the fact that the times of crack occurrence in the dataset are associated with higher stresses and thus would also require higher stresses to occur when the model is implemented in the xLPR code.

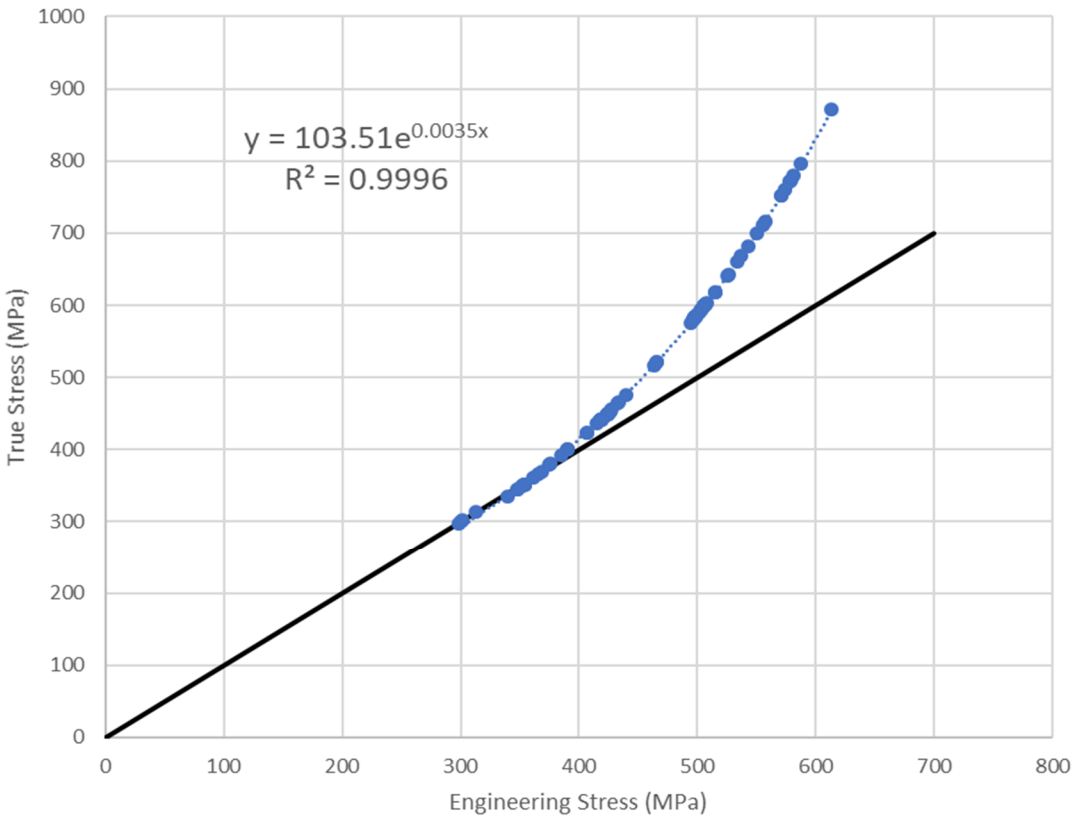


**Figure C-1 Relationship between true stress and engineering stress**

Since some of the experiments did not end with a cracked test specimen, four approaches were taken to develop datasets for recalibrating the model parameters as follows:

1. The first approach considers all specimens regardless of whether they cracked, assumes that the uncracked specimens cracked at the last observation time, and uses the engineering stresses.
2. The second approach is the same as the first but uses the true stresses instead of the engineering stresses.
3. The third approach only considers cracked specimens and uses the engineering stresses.
4. The fourth approach is the same as the third but uses the true stresses instead of the engineering stresses.

Section C2 describes the initial recalibration of the model parameters using these four approaches. However, these results needed to be corrected to support the xLPR code's spatial discretization capabilities. Section C3 discusses these corrections. Both Sections C2 and C3 include the methodology used and present results from xLPR code simulations using the recalibrated model parameters as compared to the original model parameters and laboratory

data. Section C4 summarizes the results and presents conclusions from the study. Refences are presented in Section C5.

## C2 Initial Recalibration

Section C2.1 summarizes the methodology used for the initial recalibration of the model parameters. The results of applying this methodology for all four approaches are presented in Section C2.2. Section C2.3 illustrates the effect of using of the recalibrated model parameters in an xLPR code simulation.

### C2.1 Methodology

The equation used to estimate the time of crack initiation in Direct Model 1 is as follows:

$$t_{INI} = \frac{e^{\left[\frac{Q}{R.T}\right]}}{A.\sigma^{n}} \qquad \text{Eq. 1}$$

with:

A: proportionality constant [1/EFPY-MPa$^{n}$]

Q: thermal activation energy [kJ/mol]

R: universal gas constant [kJ/K-mol]

T: temperature [K]

σ: stress at the inside diameter of the weld [MPa]

n: stress exponent [unitless]

The variables $T$ and $\sigma$ are based on the user-defined inputs for the simulation, with $A$, $Q$, $R$, and $n$ serving as model parameters that can be changed by the user; $R$ is hard-coded in the model as 8.3145 x 10$^{-3}$ kJ/mol-K. As recommended in [C-1], uncertainties in the model are accounted for through $A$, which in the xLPR code is split into two components as follows:

$A_i$: within-weld variation (i.e., spatial variability) [1/EFPY-MPa$^{n}$]

$A_{mult}$: weld-to-weld uncertainty [unitless]

Typical xLPR code input global identification numbers (IDs) along with the recommended model parameters based on laboratory data and field observations using 19 subunits are shown in Table C-2.

**Table C-2 Direct Model 1 original model parameters for 19 subunits based on laboratory data and field observations**

| Model Parameter | Typical xLPR Input Global ID | Original Direct Model 1 Parameters |
|---|---|---|
| $A_i$ | 2542 | Log-normal<br>Log-$\mu$: -4.40<br>Log-$\sigma$: 3.66 |
| $A_{mult}$ | 2543 | Log-normal<br>Log-$\mu$: 0.00<br>Log-$\sigma$: 2.89 |
| $Q$ | 2532 | 185.0 kJ/mol |
| $n$ | 2545 | 5.0 |

In the present study, a three-step process was taken to recalibrate the $A_i$ and $A_{mult}$ parameters using a larger and more recent set of laboratory data with no field observations. These steps were as follows:

1. Normalize the laboratory data to a reference stress and temperature.
2. Fit the model proportionality constant, $A$, to the normalized data.
3. Split $A$ into the weld-to-weld uncertainty component, $A_{mult}$, and the within-weld variability component, $A_i$.

Sections C2.1.1, C2.1.2, and C2.1.3 describe the details of each of step of recalibration process, respectively.

### *C2.1.1 Normalize Data*

Since laboratory experiments are subject to more extreme conditions (e.g., higher stresses and temperatures) than components inservice, the first step of the recalibration is to scale all the laboratory data to a reference stress and temperature. This scaling facilitates the creation of a cumulative distribution function (CDF) for the representative temperature and stress, which can then be set to a median value for input into the xLPR code.

Each experimentally determined stress and temperature at the time of crack initiation can be expressed as a factor applied to a reference stress or temperature as follows:

$$\sigma = k_\sigma \times \sigma_{ref} \quad \text{Eq. 2}$$

$$T = k_T \times T_{ref} \quad \text{Eq. 3}$$

with:

$k_\sigma$: ratio between the experimentally recorded stress and the reference stress

$k_T$: ratio between the experimentally recorded temperature and the reference temperature

Substituting Eq. 2 and Eq. 3 into Eq. 1 produces Eq. 4, which expresses the time of crack initiation for a reference stress and temperature as a function of the time to initiation of the current stress and temperature and other parameters:

$$t_{INI,ref} = t_{INI} \times e^{\frac{k_T - 1}{k_T} \cdot \frac{Q}{R.T_{ref}}} \times k_\sigma^n \qquad \text{Eq. 4}$$

Consistent with the approach in [C-1], the reference stress, $\sigma_{ref}$, is set to 100 MPa, and the reference temperature, $T_{ref}$, is set to 325 °C, which is equivalent to 598.15 K as used in the equation. 100 MPa represents the surface stress on the inside surface of the weld in the subunit located at top dead center when the mean value of welding residual stress is considered. It is important to note, however, that selection of the reference stress value does not impact the estimate for the distribution of $A$.

### *C2.1.2 Fit Proportionality Constant*

After the experimental data is normalized to the reference conditions, the next step is to develop a new distribution for $A$. The fitting of $A$ to the normalized data is obtained by expressing it as a function of all other parameters including time in Eq. 1 using the reference stress and temperature:

$$A = \frac{e^{\left[\frac{Q}{R \times 598.15}\right]}}{t_{INI,ref}.100^n} \qquad \text{Eq. 5}$$

The value of $A$ is estimated for all the data considered in each approach and the resulting estimates are ranked to create a distribution. This distribution of $A$ is then fit using a normal probability plot on the log-transformed estimates of $A$. The sorted results are associated with the corresponding quantiles of a standard normal distribution (where the mean is set to 0 and the standard deviation is 1). A linear fit between the original CDF on the vertical axis and the corresponding normal quantiles on the horizontal axis gives estimates of the mean $\mu$ (y-intercept) and standard deviation $\sigma$ (slope) for the log-transformed data. These estimates are the parameters of the log-normal distribution of $A$. The original fitting was not optimal when the full set of data was considered. Since only high values of $A$ can generate initiation times quick enough to be of practical interest, a second fit was developed to better match the higher quantiles of the CDF (i.e., quantiles between 0.5 and 1.0).

### *C2.1.3 Split Proportionality Constant*

The final step is to split $A$ into the weld-to-weld component, $A_{mult}$, and the within-weld component, $A_i$. The laboratory data was analyzed to determine the proportion of the total

variance of $A$ that was attributed to the weld-to-weld and within-weld variances. This analysis resulted in a total variance of 3.63, a within-weld variance of 2.28 (62.8 percent), and a weld-to-weld variance of 1.35 (37.2 percent). The field data used to develop the original model parameters exhibited a similar split; therefore, the same split derived from Section 6.5.2 of [C-1] was applied (i.e., 60 percent of the total variance attributed to the within-weld variance and 40 percent attributed to the weld-to-weld variance).

Let $\mu_A$ (mean of the log-transformed distribution) and $\sigma_A$ (standard deviation of the log-transformed distribution) be the parameters of the log-normal distribution fitted to the $A$ distribution, and let $V_A = \sigma_A^2$ be the variance of the log-transformed distribution, then:

$$A_{mult} \rightsquigarrow LN(\mu_{Amult} = 0, \sigma_{Amult} = \sqrt{0.4 \times V_A}) \quad \text{Eq. 6}$$

$$A_i \rightsquigarrow LN(\mu_{Ai} = \mu_A, \sigma_{Ai} = \sqrt{0.6 \times V_A}) \quad \text{Eq. 7}$$

Thus, $A_i \times A_{mult}$ will follow a log-normal distribution that matches the distribution of $A$.

The splitting of $A$ will not affect the probability of first crack occurrence when a single subunit is considered because the distribution of $A$ should be the same as the one derived from the observations. However, it is important to note that the choice of splitting will have some effect on the likelihood of having multiple cracks when spatial variability is considered across several subunits. In theory, a larger portion of the standard deviation applied to $A_{mult}$ equates to less variation within the weld and thus there would be a larger chance of multiple crack initiations. The impact of a different split was not considered in this study, however, because: (a) it is based on the time of first crack occurrence from laboratory data, and (b) the probability of first crack occurrence is used as a comparison.

## C2.2 Recalibrated Model Parameters

Sections C2.2.1 through C2.2.4 provide the recalibrated model parameters using the datasets from the four different approaches.

### *C2.2.1 Approach 1*

The first approach considers all specimens regardless of whether they cracked, assumes that the uncracked specimens cracked at the last observation time, and uses the engineering stresses. Implementation of the methodology presented in Section C2.1 for this approach is shown in the next set of figures. Figure C-2 applies the log-normal fit to the full distribution, whereas, Figure C-3 concentrates the fit on only the upper half of the distribution. In these figures, the left frames display the normal probability plots, which were used to (a) check whether a normal fit is appropriate in log scale, and (b) estimate the parameters of the lognormal distribution. The right frames display the resulting CDF fits. The upper half of the normal probability plot is more linear, and its slope is better represented when the fitting is concentrated on the upper quantile values of $A$ because higher values of A drive crack initiation times. As a result, this fitting will lead to a more accurate representation of the probability of crack occurrence within the first 100 years (after the data has been normalized to temperatures

and loads close to plant operating conditions). The distribution based on the second fit covers the full range of $A$ values as estimated from the experiments, but the distribution is less accurate for low values of $A$. However, this inaccuracy is not of practical concern because it corresponds with initiation times that are much longer than licensed plant operating periods (e.g., initiation times greater than 1,000 years). Such long initiation times have no impact on the xLPR code analyses.

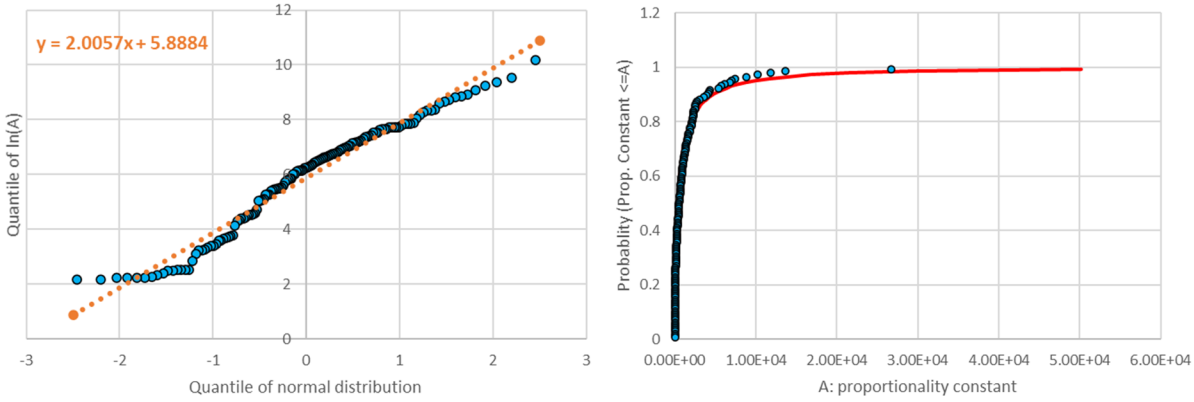


**Figure C-2 Normal probability plot (left) and original log-normal fit (right) on the full distribution based on the dataset from the first approach**

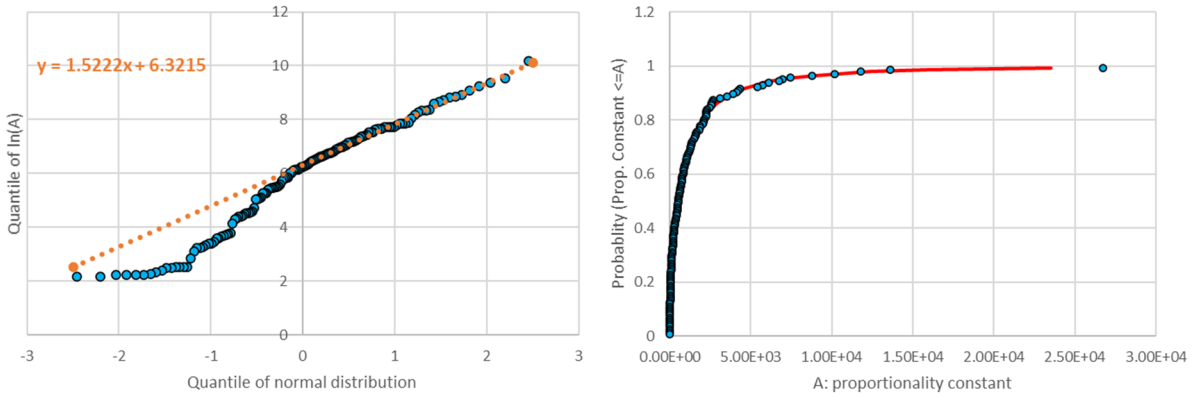


**Figure C-3 Normal probability plot (left) and updated log-normal fit (right) on only the upper half of the distribution based on the dataset from the first approach**

From the normal probability plot fit reported in Figure C-3 (left frame), the parameters for the log-normal distribution of $A$ are $\mu_A \cong 6.3215$ and $\sigma_A \cong 1.5222$, which gives the following:

$$V_A = \sigma_A^2 \cong 2.317$$

$$V_{Amult} \cong 0.4 \times V_A \cong 0.926877; \sigma_{Amult} \cong 0.963$$

$$V_{Ai} \cong 0.6 \times V_A \cong 1.3903\ ; \sigma_{Ai} \cong 1.179$$

Substituting these values into Eq. 7 and Eq. 6 splits $A$ into the weld-to-weld component, $A_{mult}$, and the within-weld component, $A_i$, as follows:

$$A_{mult} \rightsquigarrow LN(\mu: 0; \sigma: 0.963)$$

$$A_i \rightsquigarrow LN(\mu: 6.3215; \sigma: 1.179)$$

### *C2.2.2 Approach 2*

The second approach considers all specimens regardless of whether they cracked, assumes that the uncracked specimens cracked at the last observation time, and uses the true stresses. Implementation of the methodology presented in Section C2.1 for this approach is shown in the next set of figures. Figure C-4 applies the log-normal fit to the full distribution, whereas, Figure C-5 concentrates the fit on only the upper half of the distribution. As with the previous approach, the latter fit will lead to a more accurate representation of the probability of crack occurrence within the first 100 years.

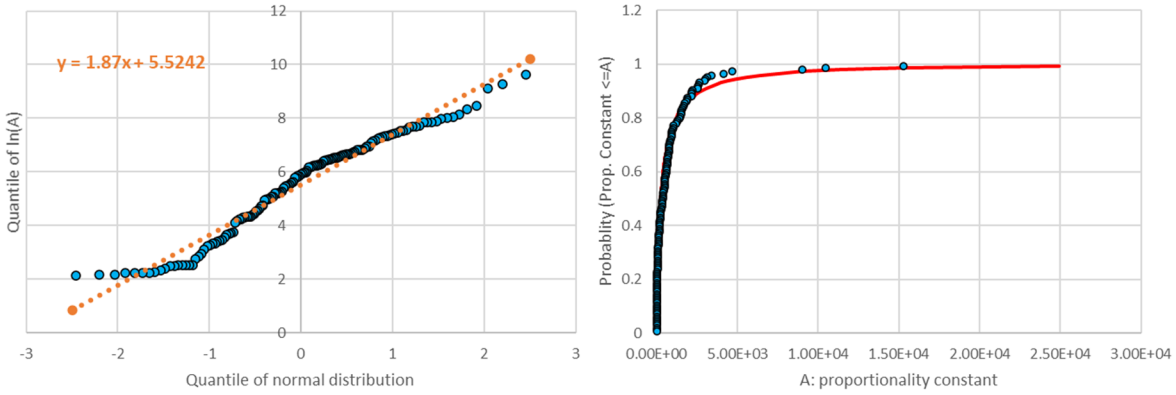


**Figure C-4 Normal probability plot (left) and original log-normal fit (right) on the full distribution based on the dataset from the second approach**

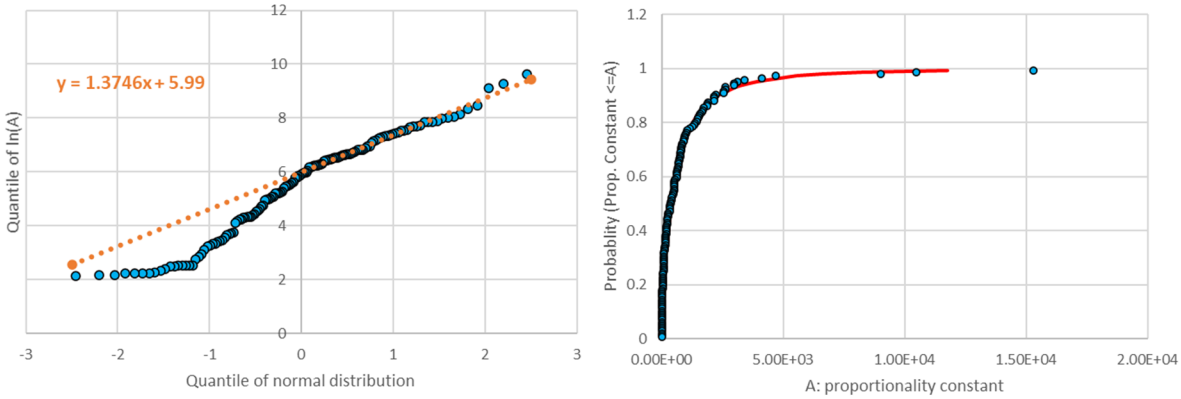


**Figure C-5 Normal probability plot (left) and updated log-normal fit (right) on only the upper half of the distribution based on the dataset from the second approach**

From the normal probability plot fit reported in Figure C-5 (left frame), the parameters for the log-normal distribution of $A$ are $\mu_A \cong 5.99$ and $\sigma_A \cong 1.374$, which gives the following:

$$V_A = \sigma_A^2 \cong 1.89$$

$$V_{Amult} \cong 0.4 \times V_A \cong 0.7559 \; ; \sigma_{Amult} \cong 0.869$$

$$V_{Ai} \cong 0.6 \times V_A \cong 1.1338 \; ; \sigma_{Ai} \cong 1.065$$

Substituting these values into Eq. 7 and Eq. 6 splits $A$ into the weld-to-weld component, $A_{mult}$, and the within-weld component, $A_i$, as follows:

$$A_{mult} \rightsquigarrow LN(\mu\colon 0; \sigma\colon 0.869)$$

$$A_i \rightsquigarrow LN(\mu\colon 5.99; \sigma\colon 1.065)$$

### *C2.2.3 Approach 3*

The third approach only considers specimens that had cracks and uses the engineering stresses. Implementation of the methodology presented in Section C2.1 for this approach is shown in the next set of figures. Figure C-6 applies the log-normal fit to the full distribution, whereas, Figure C-7 concentrates the fit on only the upper half of the distribution. As with the previous approaches, the latter fit will lead to a more accurate representation of the probability of crack occurrence within the first 100 years.

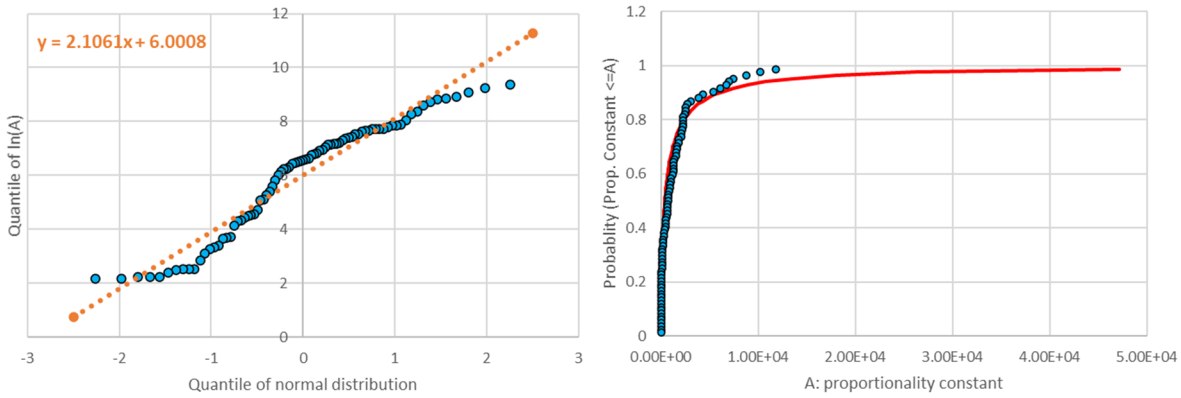


**Figure C-6 Normal probability plot (left) and original log-normal fit (right) on the full distribution based on the dataset from the third approach**

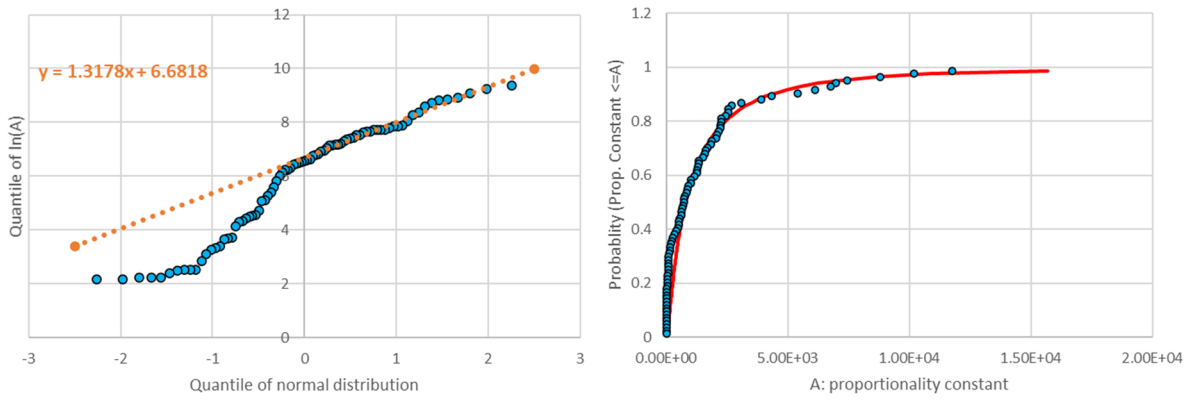


**Figure C-7 Normal probability plot (left) and updated log-normal fit (right) on only the upper half of the distribution based on the dataset from the third approach**

From the normal probability plot fit reported in Figure C-7 (left frame), the parameters for the log-normal distribution of $A$ are $\mu_A \cong 6.682$ and $\sigma_A \cong 1.318$, which gives the following:

$$V_A = \sigma_A^2 \cong 1.7367$$

$$V_{Amult} \cong 0.4 \times V_A \cong 0.6947; \sigma_{Amult} \cong 0.833$$

$$V_{Ai} \cong 0.6 \times V_A \cong 1.042; \sigma_{Ai} \cong 1.021$$

Substituting these values into Eq. 7 and Eq. 6 splits $A$ into the weld-to-weld component, $A_{mult}$, and the within-weld component, $A_i$, as follows:

$$A_{mult} \rightsquigarrow LN(\mu\colon 0; \sigma\colon 0.833)$$

$$A_i \rightsquigarrow LN(\mu\colon 6.682; \sigma\colon 1.021)$$

### *C2.2.4 Approach 4*

The fourth approach only considers specimens that had cracks and uses the true stresses. Implementation of the methodology presented in Section C2.1 for this approach is shown in the next set of figures. Figure C-8 applies the log-normal fit to the full distribution, whereas, Figure C-9 concentrates the fit on only the upper half of the distribution. As with the previous approaches, the latter fit will lead to a more accurate representation of the probability of crack occurrence within the first 100 years.

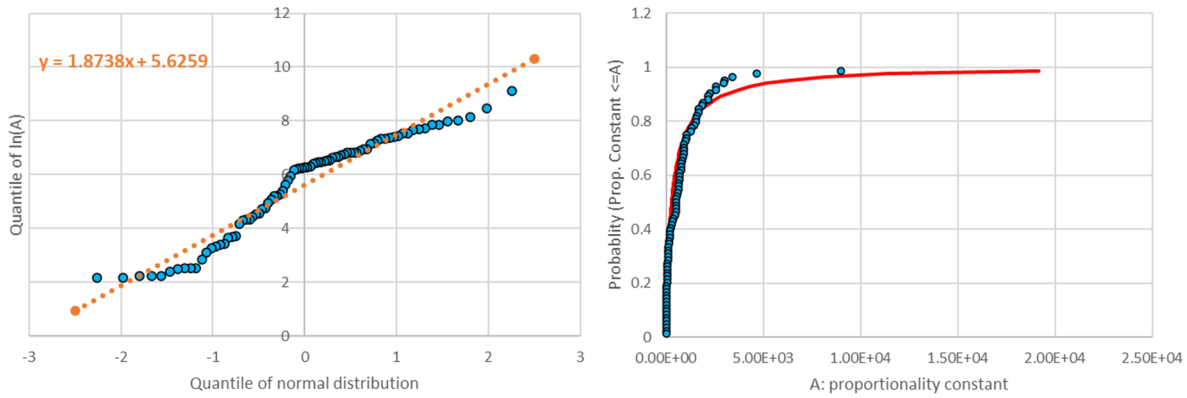


**Figure C-8 Normal probability plot (left) and original log-normal fit (right) on the full distribution based on the dataset from the fourth approach**

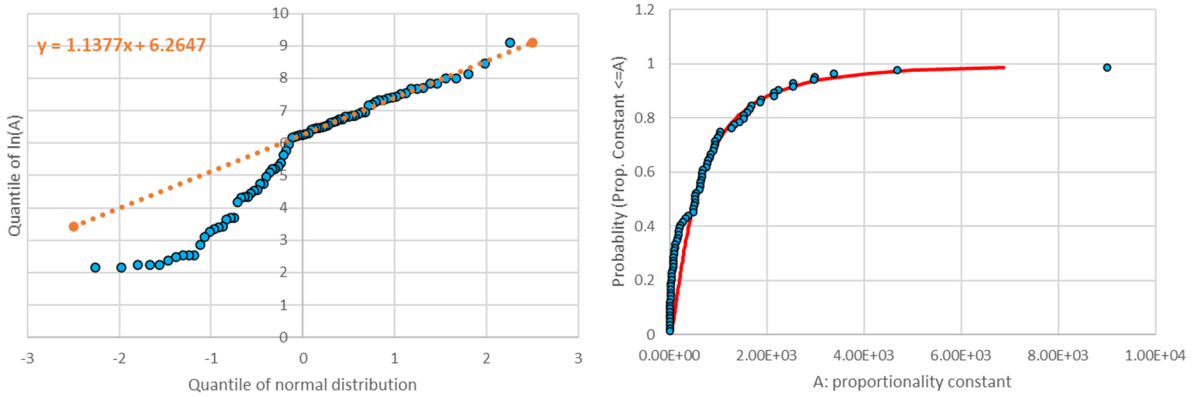


**Figure C-9 Normal probability plot (left) and updated log-normal fit (right) on only the upper half of the distribution based on the dataset from the fourth approach**

From the normal probability plot fit reported in Figure C-9 (left frame), the parameters for the log-normal distribution of $A$ are $\mu_A \cong 6.265$ and $\sigma_A \cong 1.1378$, which gives the following:

$$V_A = \sigma_A^2 \cong 1.2944$$

$$V_{Amult} \cong 0.4 \times V_A \cong 0.51777; \sigma_{Amult} \cong 0.72$$

$$V_{Ai} \cong 0.6 \times V_A \cong 0.77667; \sigma_{Ai} \cong 0.881$$

Substituting these values into Eq. 7 and Eq. 6 splits $A$ into the weld-to-weld component, $A_{mult}$, and the within-weld component, $A_i$, as follows:

$$A_{mult} \rightsquigarrow LN(\mu: 0; \sigma: 0.72)$$

$$A_i \rightsquigarrow LN(\mu: 6.265; \sigma: 0.881)$$

## C2.3 xLPR Simulation Results

Figure C-10 displays a comparison of the probability of first crack generated from the xLPR code for a Westinghouse four-loop reactor pressure vessel outlet nozzle simulation using the original model parameters as recommended in [C-1] and the recalibrated model parameters using the log-normal fit on the upper half of the distribution that were developed as presented in Section C2.2.

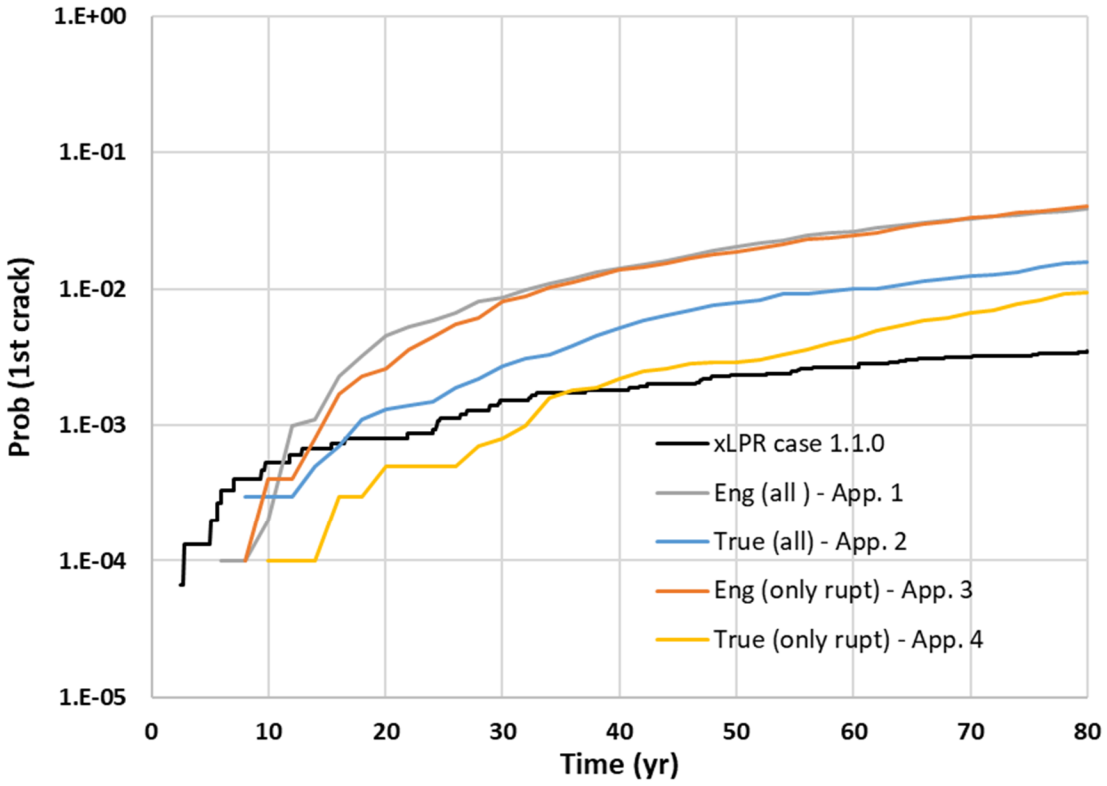


**Figure C-10 Comparison of the probability of first crack occurrence calculated in xLPR using the original and recalibrated model parameters with 19 subunits**

The results using the recalibrated model parameters are a factor of 3 to 10 higher than the results using the original model parameter recommendations. The higher values are expected considering that the weld is divided into 19 subunits in the xLPR code simulations; however, the recalibrated model parameters are based on data from only single crack initiation experiments. The proportionality constant parameters need to be adapted to the discretization used. For instance, the parameter values will be smaller if 1,000 subunits instead of 19 subunits is considered, taking into account the fact that crack initiation is tested 1,000 times versus 19 times. Regardless of the discretization, the probability of having a crack initiate should be the same for a given weld. Since the laboratory data is based on generating the first crack no matter the location, it essentially represents a single subunit. It is thus apparent that a corrective term needs to be applied to take spatial discretization of the weld into account. Development and application of such a corrective term is the focus of Section C3.

## C3 Correction for Spatial Discretization

Section C3.1 summarizes the methodology used to develop the correction factors to account for spatial discretization in the xLPR code. The results of applying this methodology for all four approaches are presented in Section C3.2. Section C3.3 illustrates the effect of using of the corrected model parameters in an xLPR code simulation.

### C3.1 Methodology

The laboratory experiments are terminated when the first crack occurs in a specimen. However, the typical xLPR code model considers spatial variability across 19 subunits in the weld, as if 19 independent locations with different stresses were considered in the laboratory. As a result, the recalibrated model parameters without any correction for spatial discretization may lead to an overestimate of the occurrence of crack when used in the xLPR code.

To correct for spatial discretization, 10,000 xLPR realizations were executed with 19 subunits using the uncorrected model parameters from Section C2.2. The earliest initiation time for each realization was then recorded and used to create a CDF. This CDF was compared to the experimental dataset considered in each of the four approaches. For each experimental data point, the corresponding quantile value from the xLPR code simulation CDF was taken and then a ratio between the two values was calculated. An average ratio was estimated from these values. The average ratio was then transformed using a natural logarithm and the corresponding value was used as the corrective term. The value is negative because, when taking the ratio, the experimental data point (numerator) tends to be lower than the quantile value estimated (denominator). The corrective term was applied to the $\mu$ values (mean of the log-transformed data) for the $A_i$ parameters reported in Section C2.2. Lastly, a new set of 10,000 xLPR code realizations was generated using the corrected model parameters and displayed as a CDF to confirm that the spatial variability was correctly addressed.

### C3.2 Corrected Model Parameters

Sections C3.2.1 through C3.2.4 provide the recalibrated model parameters corrected for spatial variability using the datasets from the four different approaches.

#### *C3.2.1 Approach 1*

Figure C-11 shows for the first approach how the corrected CDF compares with the laboratory data and 10,000 uncorrected xLPR code simulation results.

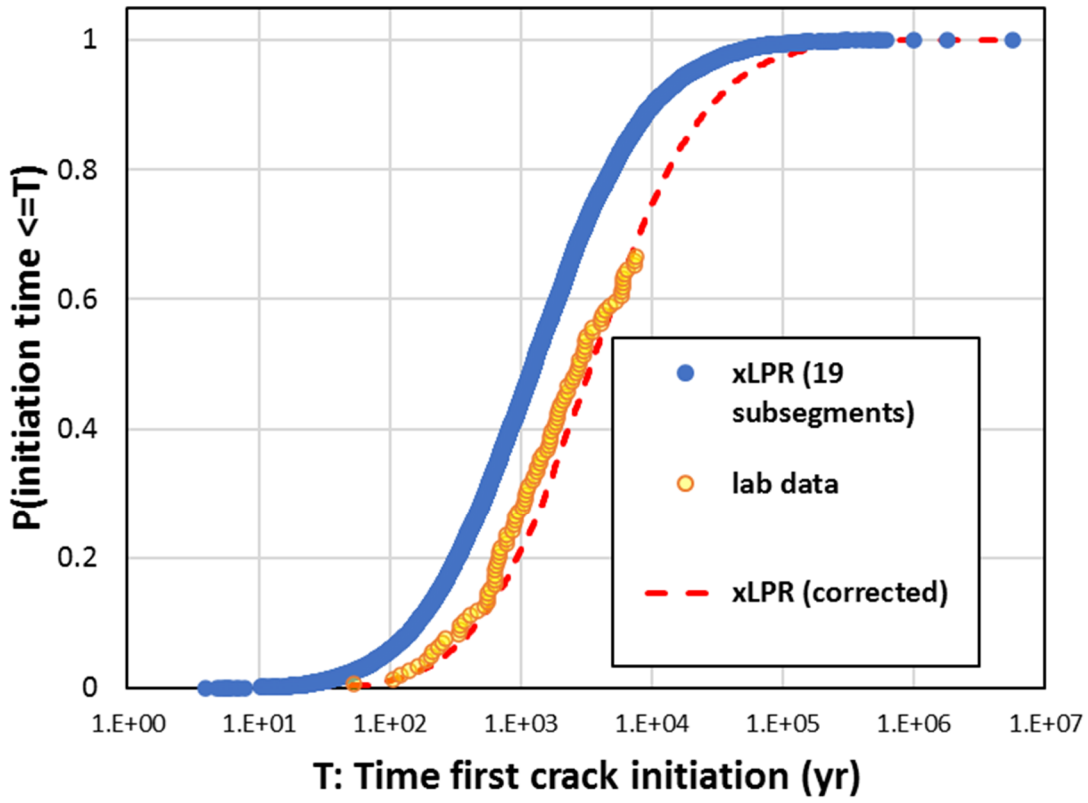


**Figure C-11 CDF of time of first crack occurrence for 19 subunits using the uncorrected (blue) and corrected (dashed red) recalibrated model parameters based on the dataset from the first approach**

The average ratio between the simulation results and laboratory data is approximately 0.34 (-1.08 in log-space). Applying this ratio as a correction factor on the parameters in Section C2.2.1 results in the following:

$$A_{mult} \rightsquigarrow LN(\mu: 0; \sigma: 0.963)$$

$$A_i \rightsquigarrow LN(\mu: 5.289; \sigma: 1.179)$$

It can be seen in Figure C-11 that sometimes the corrected CDF is below the laboratory data, which could be interpreted as a nonconservative result. However, the fitting is better for high values of $A$, which correspond to quicker initiation times (i.e., less than 100 years). Since licensed plant operating times are only up to 80 years, this is the area of most practical importance for the type of analyses performed using the xLPR code.

### *C3.2.2 Approach 2*

Figure C-12 shows for the second approach how the corrected CDF compares with the laboratory data and 10,000 uncorrected xLPR code simulation results.

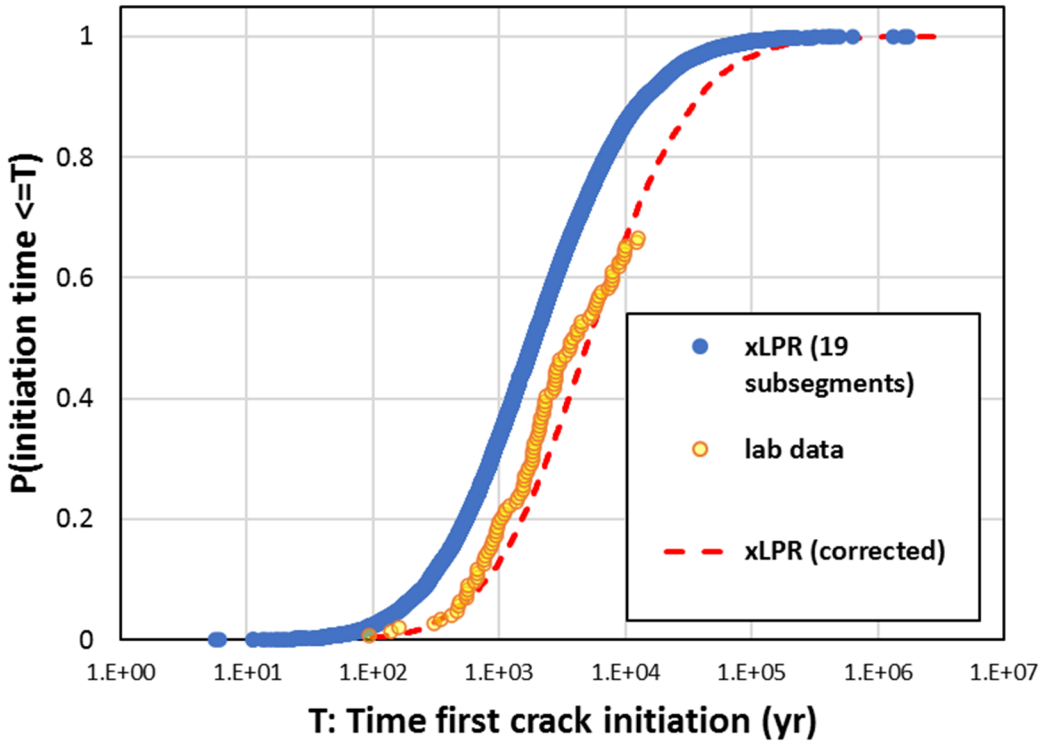


**Figure C-12 CDF of time of first crack occurrence for 19 subunits using the uncorrected (blue) and corrected (dashed red) recalibrated model parameters based on the dataset from the second approach**

The average ratio between the simulation results and laboratory data is approximately 0.38 (-0.98 in log-space). Applying this ratio as a correction factor on the parameters in Section C2.2.2 results in the following:

$$A_{mult} \rightsquigarrow LN(\mu: 0; \sigma: 0.869)$$

$$A_i \rightsquigarrow LN(\mu: 5.01; \sigma: 1.065)$$

Like the observations for the previous approach, the corrected CDF for the second approach is a better fit in the region of practical interest (i.e., high values of $A$, which correspond to quicker initiation times).

### *C3.2.3 Approach 3*

Figure C-13 shows for the third approach how the corrected CDF compares with the laboratory data and 10,000 uncorrected xLPR code simulation results.

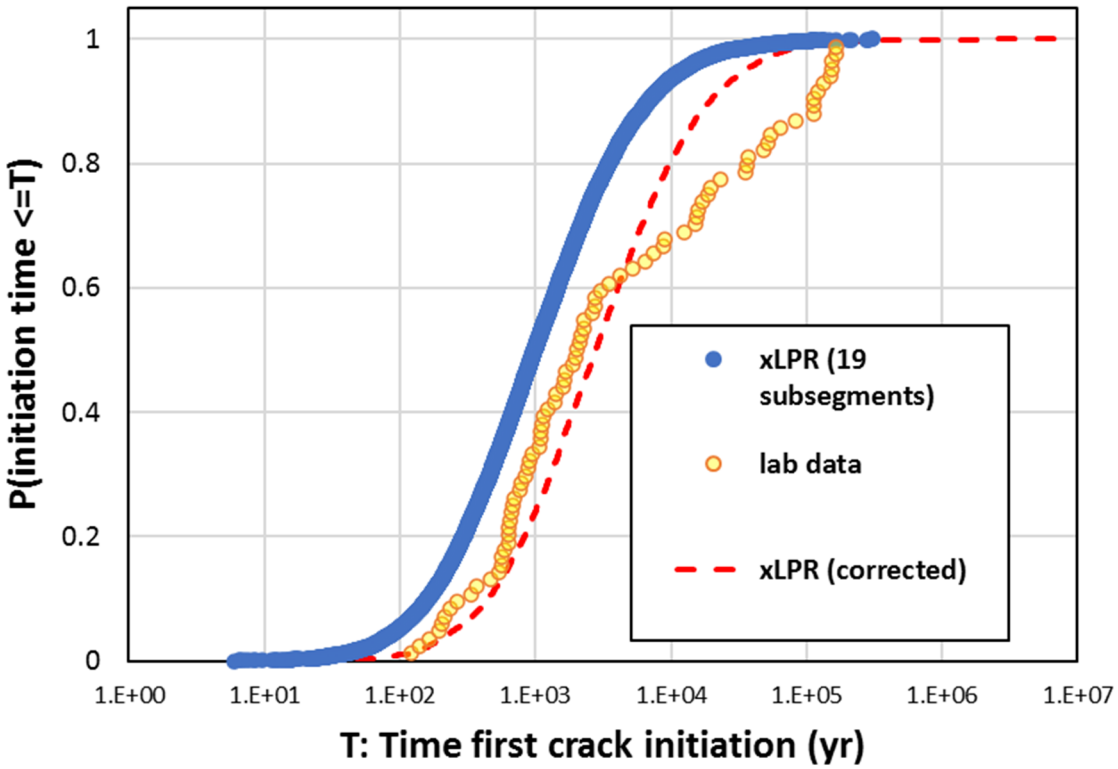


**Figure C-13 CDF of time of first crack occurrence for 19 subunits using the uncorrected (blue) and corrected (dashed red) recalibrated model parameters based on the dataset from the third approach**

The average ratio between the simulation results and laboratory data is approximately 0.36 (-1.02 in log-space). Applying this ratio as a correction factor on the parameters in Section C2.2.3 results in the following:

$$A_{mult} \rightsquigarrow LN(\mu: 0; \sigma: 0.833)$$

$$A_i \rightsquigarrow LN(\mu: 5.67; \sigma: 1.021)$$

Like the observations for the previous approaches, the corrected CDF for the third approach is a better fit in the region of practical interest (i.e., high values of $A$, which correspond to quicker initiation times).

### *C3.2.4 Approach 4*

Figure C-14 shows for the first approach how the corrected CDF compares with the laboratory data and 10,000 uncorrected xLPR code simulation results.

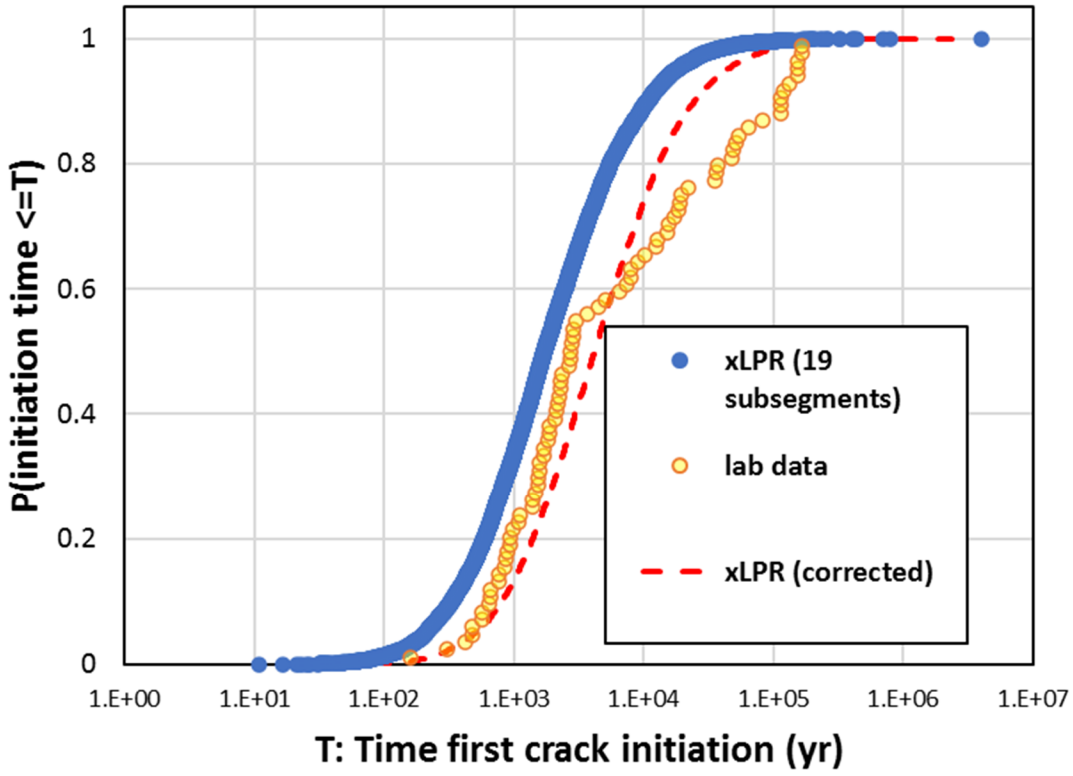


**Figure C-14 CDF of time of first crack occurrence for 19 subunits using the uncorrected (blue) and corrected (dashed red) recalibrated model parameters based on the dataset from the fourth approach**

The average ratio between the simulation results and laboratory data is approximately 0.42 (-0.87 in log-space). Applying this ratio as a correction factor on the parameters in Section C3.2.4 results in the following:

$$A_{mult} \rightsquigarrow LN(\mu: 0; \sigma: 0.720)$$

$$A_i \rightsquigarrow LN(\mu: 5.39; \sigma: 0.881)$$

Like the observations for the previous approaches, the corrected CDF for the fourth approach is a better fit in the region of practical interest (i.e., high values of A, which correspond to quicker initiation times).

### C3.3 xLPR Simulation Results

Figure C-15 displays a comparison of the probability of first crack generated from the xLPR code for a Westinghouse four-loop reactor pressure vessel outlet nozzle simulation using the original model parameters as recommended in [C-1] and the recalibrated model parameters corrected for spatial variability as presented in Section C3.2. The results using the corrected

model parameters ranged from 3 times lower to 2 times higher than the results using the original model parameter recommendations, whereas, before correction the results were 3 to 10 times higher. Thus, when spatial variability is considered, the new model parameters give results that are within the same order of magnitude as results generated using the original model parameter recommendations.

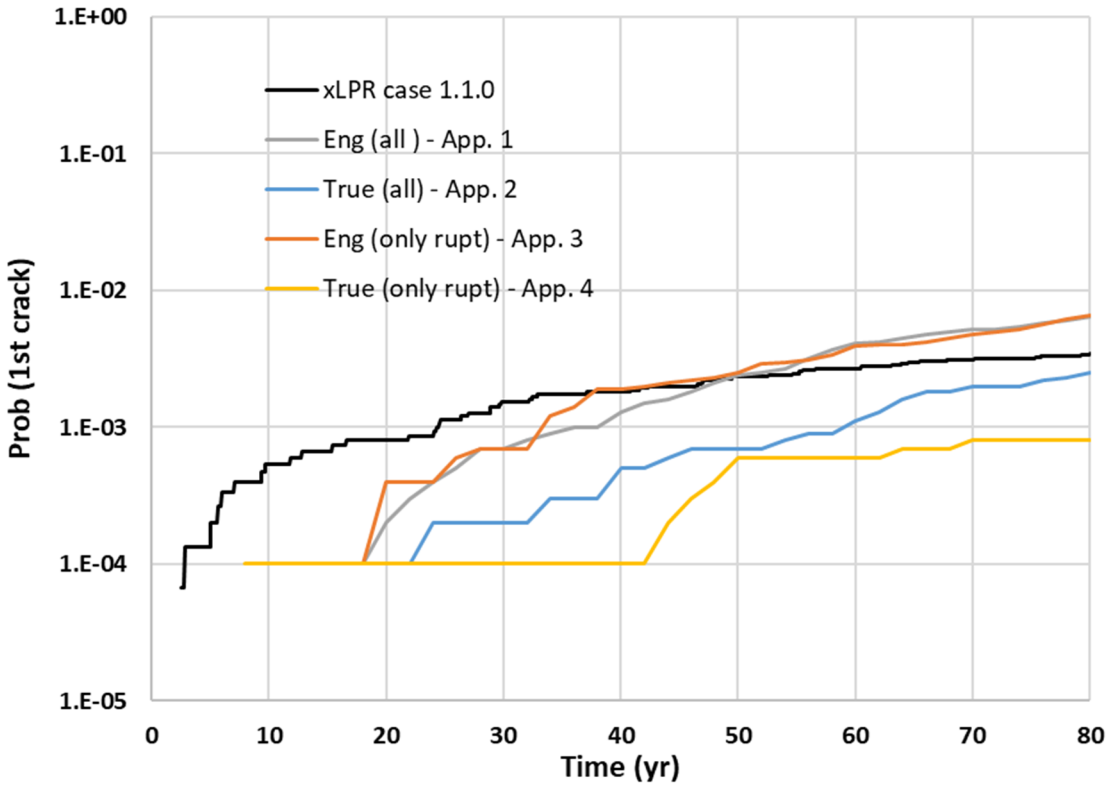


**Figure C-15 Comparison of the probability of first crack occurrence calculated in xLPR using the original and recalibrated model parameters corrected for spatial variability with 19 subunits**

## C4 Conclusion

The objective of this study was to develop new distributions for the proportionality constant $A$ for crack initiation using Direct Model 1 in the xLPR code and compare them against the original parameters recommended in [C-1]. The new model parameters were developed using a larger and more recent set of laboratory data and, unlike the original parameters, no field observations were considered. Good agreement was observed between the xLPR code simulation results generated using the original model parameters and the recalibrated model parameters after correction for spatial variability. In conclusion, it is reasonable to use laboratory data to estimate the parameters for Direct Model 1. An advantage of this approach is that it is more straightforward and uses less assumptions than the approach used to develop the original model parameters. Table C-3 presents the final xLPR code input recommendations based on the results of the study for all four of the approaches considered. The parameters for the log-normal distributions are the geometric mean and geometric standard deviation (i.e., the

exponents of $\mu$ and $\sigma$, respectively), which correspond to the parameters used by the xLPR code for a log-normal distribution.

**Table C-3 Direct Model 1 recommended model parameters for 19 subunits based on recent laboratory data**

| Model Parameter | Typical xLPR Input Global ID | Recommended Direct Model 1 Parameters | | | |
|---|---|---|---|---|---|
| | | Approach 1 | Approach 2 | Approach 3 | Approach 4 |
| $A_i$ | 2542 | Log-normal $e^{\mu} \cong e^{5.289} \cong 198$ $e^{\sigma} \cong e^{1.179} \cong 3.25$ | Log-normal $e^{\mu} \cong e^{5.01} \cong 150$ $e^{\sigma} \cong e^{1.065} \cong 2.9$ | Log-normal $e^{\mu} \cong e^{5.67} \cong 290$ $e^{\sigma} \cong e^{1.021} \cong 2.78$ | Log-normal $e^{\mu} \cong e^{5.39} \cong 219$ $e^{\sigma} \cong e^{0.881} \cong 2.41$ |
| $A_{mult}$ | 2543 | Log-normal $e^{\mu} = e^{0} = 1$ $e^{\sigma} \cong e^{0.963} \cong 2.62$ | Log-normal $e^{\mu} = e^{0} = 1$ $e^{\sigma} \cong e^{0.869} \cong 2.38$ | Log-normal $e^{\mu} = e^{0} = 1$ $e^{\sigma} \cong e^{0.833} \cong 2.42$ | Log-normal $e^{\mu} = e^{0} = 1$ $e^{\sigma} \cong e^{0.72} \cong 2.05$ |
| $Q$ | 2532 | 185.0 kJ/mol | | | |
| $n$ | 2545 | 5.0 | | | |

It is important to note that laboratory crack initiation experiments are not performed under conditions experienced by actual components in-service, and the equation used to scale the laboratory data only reflects the range of inputs for a given set of operating conditions. In addition, xLPR code analyses typically begin the crack growth calculations from an initiated crack that is on average 1.5 mm deep and 6 mm long crack based on the recommendations in [C-1]. Many of the laboratory crack initiation times are based on detecting direct current potential differences across the gauge section that occur well before the cracks reach such an "engineering" size. Due to a lack of information from the laboratory experiments on what is considered to be the initiated crack size and growth rate, it was not possible to apply any additional corrections to account for the time required for the crack to grow to the recommended initiated crack size. As a result, the recalibrated model parameters are expected to predict relatively quicker crack initiation times, an outcome that can be considered conservative.

Finally, several approaches were considered in this study to investigate the impact of excluding test specimens that did not crack and different stress estimates. Some of the experiments were still ongoing and thus the specimens had shown no crack initiation. Under the first and second approaches, all the specimens were considered, and under the third and fourth approaches, the specimens that did not initiate a crack were not considered. All the approaches are, however, conservative in that they lead to higher probabilities of crack initiation. The first and second approaches are the more conservative of the four as they assume that all the experiments initiated a crack. Additionally, two estimates of stress were used to fit the model parameters to the laboratory data. When true stresses were used (as in the second and fourth approaches), the crack initiation time was associated with higher stresses leading to an optimistic estimate of

the probability of crack occurrence. Conversely, when engineering stresses were used, the crack initiation time was associated with lower stresses, leading to a pessimistic (i.e., conservative) estimate of the probability of crack occurrence. The user should consider the most appropriate set of model parameters for the application and the bias that they may impart on the results when using them in xLPR code analyses. Sensitivity studies may also be performed to quantitatively understand the impacts of using one approach over another.

## C5 References


[C-1] K. Schmitt and G. Troyer, “xLPR Technical Report—Primary Water Stress-Corrosion Cracking Initiation Model Parameter Development, Confirmatory Analyses, and Validation, Version 2.0,” July 28, 2017, ADAMS Accession No. ML19337C202.

[C-2] P. Scott, et al., “Examination of Stress Corrosion Cracks in Alloy 182 Weld Metal After Exposure to PWR Primary Water,” in Proceedings of the 12th International Conference on Environmental Degradation of Materials in Nuclear Power System – Water Reactors,” Salt Lake City, UT, 2005.

[C-3] F. Vaillant, et al., “Environmental Behaviour and Weldability of Ni-Base Weld Metals in PWRs,” in 6th International Symposium on Contribution of Materials Investigations to Improve the Safety and Performance of LWRs: Proceedings, Fontevraud Royal Abbey, France, 2006.

[C-4] T. Couvant, et al., “Initiation of PWSCC of Weld Alloy 182,” in Proceedings of the 16th International Conference on Environmental Degradation of Materials in Nuclear Power Systems – Water Reactors, Asheville, NC, 2013.

[C-5] PNNL, PNNL-31016, "PWSCC Initiation Testing of Ni-base Alloys—Report 2," June 2021, ADAMS Accession No. ML21162A013.